



Gastrointestinal viruses and beyond: antiviral development and molecular epidemiology

Author:

Yan, Grace

Publication Date:

2023

DOI:

<https://doi.org/10.26190/unsworks/24782>

License:

<https://creativecommons.org/licenses/by/4.0/>

Link to license to see what you are allowed to do with this resource.

Downloaded from <http://hdl.handle.net/1959.4/101075> in <https://unsworks.unsw.edu.au> on 2024-05-04

Gastrointestinal viruses and beyond: antiviral development and molecular epidemiology



Grace Jia Huan Yan

A thesis in fulfilment of the requirements for the degree of
Doctor of Philosophy (Virology)

School of Biotechnology and Biomolecular Sciences

Faculty of Science

The University of New South Wales

June 2022

ORIGINALITY STATEMENT

I hereby declare that this submission is my own work and to the best of my knowledge it contains no materials previously published or written by another person, or substantial proportions of material which have been accepted for the award of any other degree or diploma at UNSW or any other educational institution, except where due acknowledgement is made in the thesis. Any contribution made to the research by others, with whom I have worked at UNSW or elsewhere, is explicitly acknowledged in the thesis. I also declare that the intellectual content of this thesis is the product of my own work, except to the extent that assistance from others in the project's design and conception or in style, presentation and linguistic expression is acknowledged.

COPYRIGHT STATEMENT

I hereby grant the University of New South Wales or its agents a non-exclusive licence to archive and to make available (including to members of the public) my thesis or dissertation in whole or part in the University libraries in all forms of media, now or here after known. I acknowledge that I retain all intellectual property rights which subsist in my thesis or dissertation, such as copyright and patent rights, subject to applicable law. I also retain the right to use all or part of my thesis or dissertation in future works (such as articles or books).

For any substantial portions of copyright material used in this thesis, written permission for use has been obtained, or the copyright material is removed from the final public version of the thesis.

AUTHENTICITY STATEMENT

I certify that the Library deposit digital copy is a direct equivalent of the final officially approved version of my thesis.

UNSW is supportive of candidates publishing their research results during their candidature as detailed in the UNSW Thesis Examination Procedure.

Publications can be used in the candidate's thesis in lieu of a Chapter provided:

- The candidate contributed **greater than 50%** of the content in the publication and are the "primary author", i.e. they were responsible primarily for the planning, execution and preparation of the work for publication.
- The candidate has obtained approval to include the publication in their thesis in lieu of a Chapter from their Supervisor and Postgraduate Coordinator.
- The publication is not subject to any obligations or contractual agreements with a third party that would constrain its inclusion in the thesis.

The candidate has declared that **their thesis contains no publications, either published or submitted for publication.**

Candidate's Declaration

I declare that I have complied with the Thesis Examination Procedure.

Table of Contents

Abstract.....	vii
Acknowledgements.....	viii
Publications during candidature.....	ix
List of Figures.....	11
List of Tables.....	12
List of Abbreviations.....	13
1 General Introduction I: Antivirals.....	14
1.1 So many viruses, not enough treatments.....	14
1.2 The difficulty with targeting viruses – emerging, re-emerging, and endemic.....	14
1.3 A brief history of antiviral treatments.....	17
1.3.1 Host targeted antivirals.....	17
1.3.2 Direct-acting antivirals.....	18
1.3.3 Targeting the RNA-dependent RNA polymerase.....	19
1.4 Are broad-spectrum NNIs possible?.....	22
1.5 Current strategies in drug discovery.....	23
1.6 Computational drug discovery.....	26
1.6.1 Ligand-based drug design.....	26
1.6.2 Structure-based drug design.....	26
2 General introduction II: Molecular epidemiology.....	28
2.1 Acute gastroenteritis.....	28
2.2 Norovirus.....	29
2.2.1 Background and history.....	29
2.2.2 Structure and genome organisation.....	30
2.2.3 Classification and nomenclature.....	32
2.2.4 Transmission.....	34
2.2.5 Clinical manifestation and pathogenesis.....	35
2.2.6 Viral replication cycle.....	36
2.2.7 Molecular epidemiology and evolution.....	37
2.2.8 Prevention and control.....	41
2.3 Adenovirus.....	42
2.3.1 Background and history.....	42
2.3.2 Classification.....	43
2.3.3 Structure and genome organisation.....	44
2.3.4 Clinical manifestation and transmission.....	45

2.3.5	Waterborne HAdV.....	46
2.3.6	Prevention and control	47
	Aims and outline of thesis.....	48
3	Materials and Methods.....	50
3.1	General molecular biology methods.....	54
3.1.1	Agarose gel electrophoresis.....	54
3.1.2	Purification of PCR products	54
3.1.3	Sanger sequencing	54
4	Development of broad-spectrum non-nucleoside inhibitors for positive-sense RNA viruses using <i>in silico</i> methods.....	55
4.1	Abstract.....	56
4.2	Introduction	57
4.2.1	The urgent need for antivirals.....	57
4.2.2	The development of early antivirals	57
4.2.3	Current strategies for antiviral development	58
4.2.4	Classes of antiviral compounds and their broad-spectrum potential	58
4.2.5	Aims.....	60
4.3	Methods.....	61
4.3.1	Multiple sequence alignment	61
4.3.2	Preparation of structures and docking	61
4.3.3	Generation of complex-based pharmacophores and virtual screening	62
4.3.4	Virtual screening	63
4.3.5	Initial antiviral compound selection.....	65
4.3.6	Selection of second set of antiviral compounds	66
4.3.7	Recombinant human norovirus GII.4 Sydney 2012 RdRp protein expression and purification.....	66
4.3.8	Recombinant Zika virus RdRp protein expression and purification.....	68
4.3.9	Human norovirus GII.4 RdRp fluorescent transcription activity assay	68
4.3.10	Fluorescent transcription activity assays for measuring calicivirus RdRp replication	69
4.3.11	Zika virus fluorescent RdRp activity assay	69
4.3.12	Measuring replicon activity.....	70
4.3.13	Examining compound inhibition of HAV and HCV G2a replication using a replicon model	71
4.3.14	Examination of compound cytotoxicity	72
4.3.15	Searching for similar compounds.....	72

4.4	Results.....	74
4.4.1	Multiple sequence alignment	74
4.4.2	Docking of NNIs and JTK-M into calicivirus RdRps: interaction with Arg392 also important for activity?	74
4.4.3	Pharmacophore generation and virtual screening using DS.....	78
4.4.4	Pharmacophore generation and virtual screening using LS	79
4.4.5	The first set of compounds: compound selection and inhibition of norovirus RdRp activity.	81
4.4.6	The second set of compounds: compound selection and inhibition of norovirus RdRp activity.	84
4.4.7	NCS-013 demonstrates cross-genera inhibition of FCV RdRp.....	89
4.4.8	Can set 1 and 2 compounds inhibit Zika virus RdRp transcription?.....	90
4.4.9	NCS-013 inhibits both HAV and HCV replicon replication.	92
4.4.10	Can NCS-013 structural analogues inhibit norovirus and Zika virus RdRp activity? 93	
4.4.11	NCS-013A inhibits of HAV replicon replication.	96
4.4.12	Potential binding configuration of NCS-013 to <i>Caliciviridae</i> RdRp	97
4.4.13	<i>In vitro</i> examination of NCS-013 binding within Site-B.....	99
4.4.14	Summary of virtual screening results	100
4.5	Discussion.....	101
4.5.1	Virtual screening in an environment lacking prior knowledge	101
4.5.2	NCS-013 inhibits <i>Caliciviridae</i> , <i>Flaviviridae</i> and <i>Picornaviridae</i> RdRp/replicon replication	103
4.5.3	Does NCS-013 bind within Site-B?	104
4.5.4	Effect of NCS-013 on other mammalian targets	106
4.5.5	Future directions and potential for further development.....	107
4.6	Concluding remarks	108
5	Molecular epidemiological surveillance of norovirus in Australia, 2018 to 2020	109
5.1	Abstract.....	110
5.2	Introduction	111
5.3	Materials and methods.....	114
5.3.1	Ethics and collection of clinical samples	114
5.3.2	Collection of wastewater samples	114
5.3.3	Viral concentration, RNA extraction and cDNA synthesis	114
5.3.4	MS2 bacteriophage process control	115
5.3.5	Amplification and sequencing of clinical specimens.....	116
5.3.6	Phylogenetic analysis of norovirus sequences.....	117

5.3.7	Quantification of norovirus RNA levels in wastewater	117
5.3.8	Capsid genotyping of norovirus in wastewater samples from Sydney and Melbourne	118
5.3.9	ORF1/2 overlap genotyping of norovirus in wastewater samples from Sydney and Melbourne	118
5.3.10	Analysis of wastewater next-generation sequencing data	119
5.4	Results	119
5.4.1	Norovirus outbreaks in NSW, Australia	120
5.4.2	Institutional gastroenteritis outbreaks reported in NSW, Australia	121
5.4.3	Institutional gastroenteritis outbreak trends were reflected by the norovirus levels detected in sewage	122
5.4.4	The increases in AGE outbreak activity in NSW were not caused by the emergence of new strains	124
5.4.5	Molecular epidemiology of GII and GIX noroviruses	127
5.4.6	Molecular epidemiology of GI noroviruses	131
5.4.7	Comparison of GII norovirus partial capsid and ORF1/2 overlap amplicon sequencing in 2018 wastewater.	132
5.4.8	Norovirus GII genotype distribution in wastewater samples, 2018-2020	134
5.4.9	Diversity of noroviruses genotypes and P-types detected	138
5.5	Discussion	139
5.6	Concluding remarks	143
6	Molecular epidemiology of adenovirus-associated gastroenteritis in Australia, 2018 to 2021	144
6.1	Abstract	145
6.2	Introduction	146
6.3	Materials and methods	149
6.3.1	Ethics and clinical specimen collection	149
6.3.2	Collection of wastewater samples	149
6.3.3	Viral concentration and extraction	150
6.3.4	Genotyping of clinical specimens	150
6.3.5	Next generation sequencing of sewage samples	151
6.3.6	NGS data analysis	151
6.4	Results	152
6.4.1	Detection of HAdV infections in clinical faecal specimens	152
6.4.2	Comparison of HAdV types detected using different diagnostic methods	152
6.4.3	Genetic diversity of HAdV in clinical specimens	153
6.4.4	Seasonality of HAdV-associated gastroenteritis	154

6.4.5	Genetic diversity of HAdV in wastewater in 2018	155
6.4.6	Comparison of genetic diversity in clinical and wastewater samples	157
6.5	Discussion.....	157
6.6	Concluding remarks	161
7	General Discussion.....	163
7.1	Broad-spectrum non-nucleoside inhibitors can be designed; <i>in silico</i> methods can aid their discovery.	164
7.1.1	Future directions.....	166
7.2	Molecular epidemiological surveillance of norovirus in Australia, 2018 to 2020	166
7.2.1	Old norovirus strains have remained in circulation in Australia.....	166
7.2.2	An interplay in herd immunity may have directed the increases in AGE outbreak activity observed in childcare centres	170
7.2.3	Future directions.....	172
7.3	A diverse range of HAdV cause gastroenteritis.	172
7.3.1	Future directions.....	174
7.4	Final remarks.....	174
8	Appendix.....	176
9	References	180

Abstract

With over 27 viral families known to infect humans, viral pathogens impose a significant global public health and economic burden. Despite this, only a small fraction of human viruses possess antiviral treatments or vaccines. Whilst antiviral development efforts are crucial to the host-pathogen arms race, so too is the molecular surveillance of these viruses to identify prevalent and virulent strains for vaccine development.

This thesis begins, in **chapter four**, with the development of broad-spectrum non-nucleoside inhibitor compounds using a complex-based pharmacophore and virtual screening approach. This virtual screen identified one compound, NCS-013, which demonstrated broad-spectrum inhibition of the transcriptional activity of human norovirus and feline calicivirus from the *Caliciviridae*, Zika virus and hepatitis C virus from the *Flaviviridae* and hepatitis A virus from the *Picornaviridae*.

The second half of the thesis focuses on molecular epidemiology of norovirus and adenovirus, two of the leading causes of viral gastroenteritis worldwide. In **chapter five**, we observed an interesting dynamic of GII.4 Sydney 2012 [P16] co-dominance in clinical samples throughout the study period. We also enhanced our sewage surveillance capabilities through the addition of partial ORF1 sequencing enabling the identification of recombinant strains. The role of non-group F adenoviruses in gastroenteritis although often reported, remains an area of controversy. In **chapter six**, we analysed sewage to complement clinical samples and better understand the diversity of adenovirus within the population, including from healthy individuals.

In summary, this thesis approached the problem of viral pathogens from both the angle of antiviral development and through understanding of population-level molecular epidemiology, which can contribute to future vaccine development efforts.

Acknowledgements

To my supervisor, **Pete**, thank you for all your advice and support over the past five years. I have learnt so much from my time in your lab – about science and life. Thank you for all the conferences and lunches, I have enjoyed hearing all your stories.

To my co-supervisor, **Renate**, thank you for taking time to answer my questions and read all my drafts. This would not have been possible without your support.

To **Emma**, thank you for always being there, for all the coffee walks and lunches, for helping me decipher those cryptic emails and comments, for always lending an ear when I need it.

To **Alice**, when I first met you, you scared me a little bit because you were always so brilliant at everything you do. As I got to know you more, I learned of your kindness, patience and generosity. Thank you for being part of this journey.

I am extremely grateful to **Sandeep**, thank you for being so incredibly generous with your time and wisdom. For going on those walks and keeping me sane, without you I am not sure how I would have written my final discussion.

To the current members of the lab, **Lewis** and **Tanu**, thank you for all the chats and for making the lab so enjoyable and fun. To past members of the lab, especially **Jen, Dan, Nat, Tulio** and **Kate**: you were there at the beginning of this journey, thank you for your time, guidance, and support. **Laurene, Jason** and **Banjo**: I wish you the best for your future endeavours.

Christine, Ryan, Hudson and **Tara**, I have thoroughly enjoyed all our various coffee breaks, walks and lunches. Thank you for your amazing kindness and for making these last few months bearable.

There are so many other people in BABS who have shown me incredible kindness over the course of my PhD. I would like to include them here, so I never forget them. **Laurence**, I am extremely grateful for all the lifts to uni during lockdown. Thank you for staying back very late when I was waiting for that sample delivery. You are one of the kindest, most generous people I am fortunate enough to know. Special thanks to the Lan lab (especially **Liam, Ada, Raisa, Michael**, and **Hiroki**), the Tree Lab (especially **Brandon, Winton** and **Julia**), the Cas-Rod Lab (especially **Karla, Izzy** and **Matt**) and the TA team (especially **Tim, Jason** and **David**).

To my lovely family and all my friends, words cannot describe how much you mean to me, so I'll keep it short. Thank you for your endless love, support and encouragement. Thank you for listening and nodding along even if you are not quite sure what I do.

I would also like to thank **Bill Rawlinson** and **Peter Huntington** from Prince of Wales hospital and **Richard Jones** and **Irena Serafimovska** from Douglas Hanley Moir pathology for their generous provision of clinical samples. Thank you also to the teams at Sydney Water and Melbourne Water for sample provision.

Publications during candidature

Research articles

Fumian TM, Tuipulotu DE, Netzler NE, Lun JH, Russo AG, **Yan GJH**, White PA. 2018. Potential therapeutic agents for feline calicivirus infection. *Viruses* DOI: 10.3390/v10080433

Lun JH, Hewitt J, **Yan GJH**, Tuipulotu DE, Rawlinson WD, White PA. 2018. Recombinant GII.P16/GII.4 Sydney 2012 was the dominant norovirus identified in Australia and New Zealand in 2017. *Viruses* DOI: 10.3390/v10100548

Russo AG, Harding EF, **Yan GJH**, Selechnik D, Ducatez S, DeVore JL, *et al.* 2021. Discovery of novel viruses associated with the invasive cane toad (*Rhinella marina*) in its native and introduced ranges. *Frontiers in Microbiology*. DOI: 10.3389/fmicb.2021.733631

Harding EF, Russo AG, **Yan GJH**, Waters PD, White PA. 2021. Ancient viral integrations in marsupials: a potential antiviral defence. *Virus Evolution*. DOI: 10.1093/ve/veab076

Harding EF, **Yan GJH**, White PA. 2021. Viral fossils in marsupial genomes: secret cellular guardians. *Microbiology Australia*. DOI: 10.1071/MA21036

Mercer LK, Harding EF, **Yan GJH**, White PA. 2022. Novel viruses discovered in the transcriptomes of agnathan fish. *Journal of Fish Diseases*. DOI: 10.1111/jfd.13602

Submitted for publication

Harding EF, Russo AG, **Yan GJH**, Mercer LK, White PA. (submitted). Revealing the uncharacterised diversity of herptile viruses. *ISME J*.

Conference Presentations (as presenting author)

Yan GJH, Lun JH, Tuipulotu DE, Morrell L, White PA. 2018. "Emergence of norovirus recombinant strain GII.P16/GII.4 Sydney 2012 in New South Wales, 2017". Poster at the Molecular Microbiology Meeting, Sydney, Australia, April 2018.

Yan GJH, Jones K, Harding EF, Lun JH, White PA. 2019. "The molecular epidemiological trends of norovirus in Australia, 2018/2019". Poster at the 7th International Calicivirus Conference, Sydney, Australia, October 2019.

Yan GJH, Jones K, Harding EF, Russo AG, White PA. 2019. "Molecular surveillance of norovirus and adenovirus in Australia 2018 – 2019". Oral at the 10th meeting of the AVS, Queenstown, New Zealand, December 2019.

Yan GJH, Harding EF, Russo AG, Jones K, White PA. 2019. "Molecular surveillance of norovirus in Australia and the benefits of social distancing measures". Online poster at the ASM, Annual Scientific Meeting, Melbourne, Australia, June 2021.

Yan GJH, Harding EF, Russo AG, White PA. “The impact of social distancing on norovirus epidemiology in New South Wales, Australia”. Online poster at the ASV annual meeting, USA, July 2021.

Yan GJH, Harding EF, Russo AG, Jones K, White PA. “Molecular surveillance of norovirus in Australia and the benefits of social distancing measures”. Poster at the School of BABS Research Symposium, Sydney, Australia, May 2022.

Yan GJH, Harding EF, Griffith R, White PA. “Development of broad-spectrum antivirals for positive-sense RNA viruses using in silico methods.” Accepted for oral at the ASM annual meeting, Sydney, Australia, July 2022.

List of Figures

Figure 1.1. Some notable human viral outbreaks in the 21st century.	16
Figure 1.2. Schematic of the human norovirus GII.4 RdRp.....	20
Figure 1.3. Schematic of HCV RdRp showing allosteric sites.	22
Figure 1.4. Flow chart of drug development pipeline using different approaches.	25
Figure 2.1. Norovirus genome organisation and capsid structure.	32
Figure 2.2. Phylogenetic classification of norovirus sequences based on full length VP1.	33
Figure 2.3. Light micrographs of jejunal mucosa biopsy specimens.....	36
Figure 2.4. Timeline of pandemic and epidemic norovirus strain emergence.	40
Figure 2.5. Human norovirus vaccine candidates.	42
Figure 2.6. Genome organisation of HAdV type C5.	44
Figure 4.1. Location of the NNI binding pocket Site-B in the calicivirus RdRp.	60
Figure 4.2. Virtual screening process.	64
Figure 4.3. Schematic representation of HAV and HCV G2a replicon constructs.....	71
Figure 4.4. Searching the chemical space for similar molecules available on catalogue.	73
Figure 4.5. Compounds used in the initial docking study.	76
Figure 4.6. Possible binding configurations of compounds JTK-109 and JTK-M on the human norovirus RdRp.....	76
Figure 4.7. Complex-based pharmacophores generated using Discovery Studio and virtual screening results.	79
Figure 4.8. Complex-based pharmacophores generated using LigandScout and virtual screening results.....	80
Figure 4.9. Inhibition of human norovirus Sydney 2012 RdRp activity by Set 1 compounds.....	84
Figure 4.10. Inhibition of human norovirus Sydney 2012 RdRp activity by Set 2 compounds... ..	89
Figure 4.11. Inhibition of FCV RdRp activity by NCS-013.	90
Figure 4.12. Screening test compounds for inhibition of Zika virus RdRp activity.	91
Figure 4.13. The effect of set 1 and 2 compounds on HAV and HCV replicons, and cells.	93
Figure 4.14. Inhibition of norovirus and Zika virus RdRp activity by NCS-013 structural analogues.	96
Figure 4.15. The effect of NCS-013 structural analogues on HAV and HCV replicons, and cells.....	97
Figure 4.16. Possible binding configurations of NCS-013 on the human norovirus RdRp.....	98
Figure 4.17. Dose dependent inhibition of wild type and mutant norovirus GII.4 Sydney 2012 RdRp activity by NCS-013.....	99
Figure 5.1. Norovirus surveillance workflow.	115
Figure 5.2. Settings and genogroup classification of norovirus strains identified from outbreaks in NSW, Australia between 2018-2020.....	120
Figure 5.3. Institutional gastroenteritis outbreaks reported in NSW, 2018-2020.....	122
Figure 5.4. Quantification of GII norovirus in Sydney wastewater 2018-2020.....	124
Figure 5.5. Norovirus genotypes detected in children aged five and under.	126
Figure 5.6. Monthly distribution of norovirus genotypes identified in NSW, Australia between 2018-2020.	128
Figure 5.7. Phylogenetic analysis of the partial polymerase (NS7, RdRp) and capsid (VP1) regions of GII noroviruses.	130
Figure 5.8. Distribution of GI norovirus genotypes identified in NSW, Australia between 2018-2020.	131

Figure 5.9. Phylogenetic analysis of the partial polymerase (RdRp) and capsid (VP1) regions of GI noroviruses.	132
Figure 5.10. Comparison of GII norovirus capsid and ORF1/2 overlap genotypic distribution in sewage samples collected from Sydney and Melbourne, 2018.	134
Figure 5.11. Major norovirus GII genotype distribution in wastewater samples collected from Sydney and Melbourne, 2018-2020.....	136
Figure 5.12. Minor norovirus GII genotype distribution in wastewater samples collected from Sydney and Melbourne, 2018-2020.....	137
Figure 5.13. Diversity of GI norovirus P-type and genotype combinations detected.	138
Figure 5.14. Diversity of GII norovirus P-type and genotype combinations detected.....	139
Figure 6.1. Diversity of HAdV detected in different age groups from 2018-2021.....	152
Figure 6.2. HAdV types found in samples identified using different diagnostic assays.....	153
Figure 6.3. Diversity of HAdV hexon types identified in clinical samples, 2018-2021.....	154
Figure 6.4. Seasonal distribution of HAdV genotypes identified in NSW, Australia between 2018-2021.	155
Figure 6.5. HAdV hexon type distribution in wastewater, 2018.....	156
Appendix Figure 8.1. Institutional gastroenteritis outbreaks reported in NSW, 2016 to 2020.....	178
Appendix Figure 8.2. Antigenic changes in the VP1 epitopes for previous GII.4 pandemic variants.....	179

List of Tables

Table 1.1. Some major milestones in the history of antiviral treatments.	17
Table 2.1. Estimated global deaths for some common aetiological agents of AGE*.	29
Table 2.2. Human adenovirus species and types.....	44
Table 2.3. Clinical manifestations of human adenovirus.....	45
Table 2.4. Some notable waterborne outbreaks of HAdV.....	46
Table 3.1. General material and reagents used in the study.....	50
Table 4.1. Crystal structures used for docking and sequence analyses.....	61
Table 4.2. Conserved motifs and residues around Site-B in calicivirus RdRps.	74
Table 4.3. Summary of predicted favourable docking interactions between antiviral compounds and conserved residues on calicivirus crystal structures.....	77
Table 4.4. First set of SPECs compounds for biological testing.	81
Table 4.5. Second set of SPECs compounds for biological testing.....	85
Table 4.6. NCS-013 structural analogues.....	94
Table 4.7. Predicted favourable docking interactions between NCS-013 and conserved residues on calicivirus crystal structures.....	98
Table 4.8. Test compounds with >25% inhibitory activity relative to negative control.	100
Table 5.1. Primers used to amplify norovirus and MS2 sequences.....	116
Table 6.1. Primers used to amplify HAdV sequences.	150
Appendix Table 8.1. MS2 cycle threshold and calculated copies.....	176
Appendix Table 8.2. Reference sequences used for mapping of NGS reads.....	176

List of Abbreviations

aa	Amino acid
HAdV	Human adenovirus
AGE	Acute gastroenteritis
bp	Base pair
COVID-19	Coronavirus disease 2019
DAA	Direct-acting antiviral
DHM	Douglass Hanley Moir
DNA	Deoxyribonucleic acid
DS	Discovery Studio
EIA	Enzyme Immunoassay
FCV	Feline calicivirus
G	Genogroup
HAV	Hepatitis A virus
HCV	Hepatitis C virus
HIV	Human immunodeficiency virus
HTA	Host targeting antiviral
HTS	High throughput screening
ICTV	International Committee on Taxonomy of Viruses
kb	Kilo base
kDa	Kilo dalton
LS	LigandScout
μ M	Micromolar
mM	Millimolar
MNV	Murine norovirus
MoH	Ministry of Health
NA	Nucleoside analogue
NGS	Next generation sequencing
NNI	Non-nucleoside inhibitor
NoV	Norovirus
NSW	New South Wales
nt	Nucleotide
ORF	Open reading frame
PCR	Polymerase chain reaction
PDB	Protein Data Bank
PoWH	Prince of Wales Hospital
qRT-PCR	Quantitative reverse transcription PCR
SARS-CoV-2	Severe acute respiratory syndrome coronavirus 2
SaV	Sapovirus
RdRp	RNA-dependent RNA polymerase
RHDV	Rabbit haemorrhagic disease virus
RMSD	Root mean square deviation
VS	Virtual screening
WWTP	Wastewater treatment plant

1 General Introduction I: Antivirals

1.1 So many viruses, not enough treatments

With 189 different families currently recognised by the International Committee on Taxonomy of Viruses (ICTV), and more than 9,100 viral species, every living organism is host to their own unique virome (1). There are at least 27 different viral families known to infect humans which encompass more than 220 virus species (1-3), causing a wide spectrum of clinical manifestations ranging from mild stomach and respiratory ailments (4, 5), to life-threatening conditions such as encephalitis and haemorrhagic fevers (6, 7). Together, viruses result in millions of deaths each year and cause debilitating disease in many others. However, approved treatments are only available for a small fraction of these viruses. These include only some members of the *Hepadnaviridae*, *Flaviviridae*, *Retroviridae*, *Pneumoviridae*, *Papillomaviridae*, *Herpesviridae*, *Orthomyxoviridae* and most recently, the *Coronaviridae* (8-13). As a result, there is an urgent need to develop antiviral treatments to target these and other clinically significant viral families.

1.2 The difficulty with targeting viruses – emerging, re-emerging, and endemic

Antiviral development is a slow and costly process, made even more challenging by its limited scalability with respect to different viruses. This is due to several factors such as the highly diverse nature of viral proteins, differences in host protein utilisation (14), high rates of evolution and formation of quasispecies (15, 16), and differences in viral tropism (17). Therefore, unlike bacterial infections which can be treated with a variety of broad-spectrum antibiotics, no such equivalent exists for viruses. Additionally, some viruses can establish persistence, thus even when antiviral treatments are available, full eradication of infection may not be possible, such as in the case of human immunodeficiency virus (HIV) (18, 19).

The public health challenge presented by viruses is further compounded by the continual emergence and re-emergence of viral pathogens such as SARS-CoV-1, SARS-CoV-2 and Ebola virus (Figure 1.1). During each of these outbreaks, the lack of effective

antiviral treatments has contributed to a significant loss of human life (Figure 1.1). Using flaviviruses as an example, the threat from endemic viruses has never subsided, aided by the expanding range and population of arthropod vectors (20). The mosquito-borne Dengue virus for example, has caused several notable outbreaks of Dengue fever in Singapore (2005) (21), India (2006) (22) and Pakistan (2006, 2011) as well as an estimated 50 to 100 million clinical cases each year (23, 24). Japanese encephalitis virus, which is similarly transmitted by an arthropod vector, causes an estimated 67,900 cases of encephalitis annually across the Asia-Pacific region (25) and has recently caused a wave of cases in Australia affecting 37 people (as of 28 April 2022) (26). Of these, 20-30% of patients die and up to 50% of survivors experience long-term neuropsychiatric impairment (27). Other viruses endemic to tropical regions of the world, such as yellow fever virus (28), chikungunya virus (29), and West Nile virus (30, 31) also contribute significantly to the global disease burden.

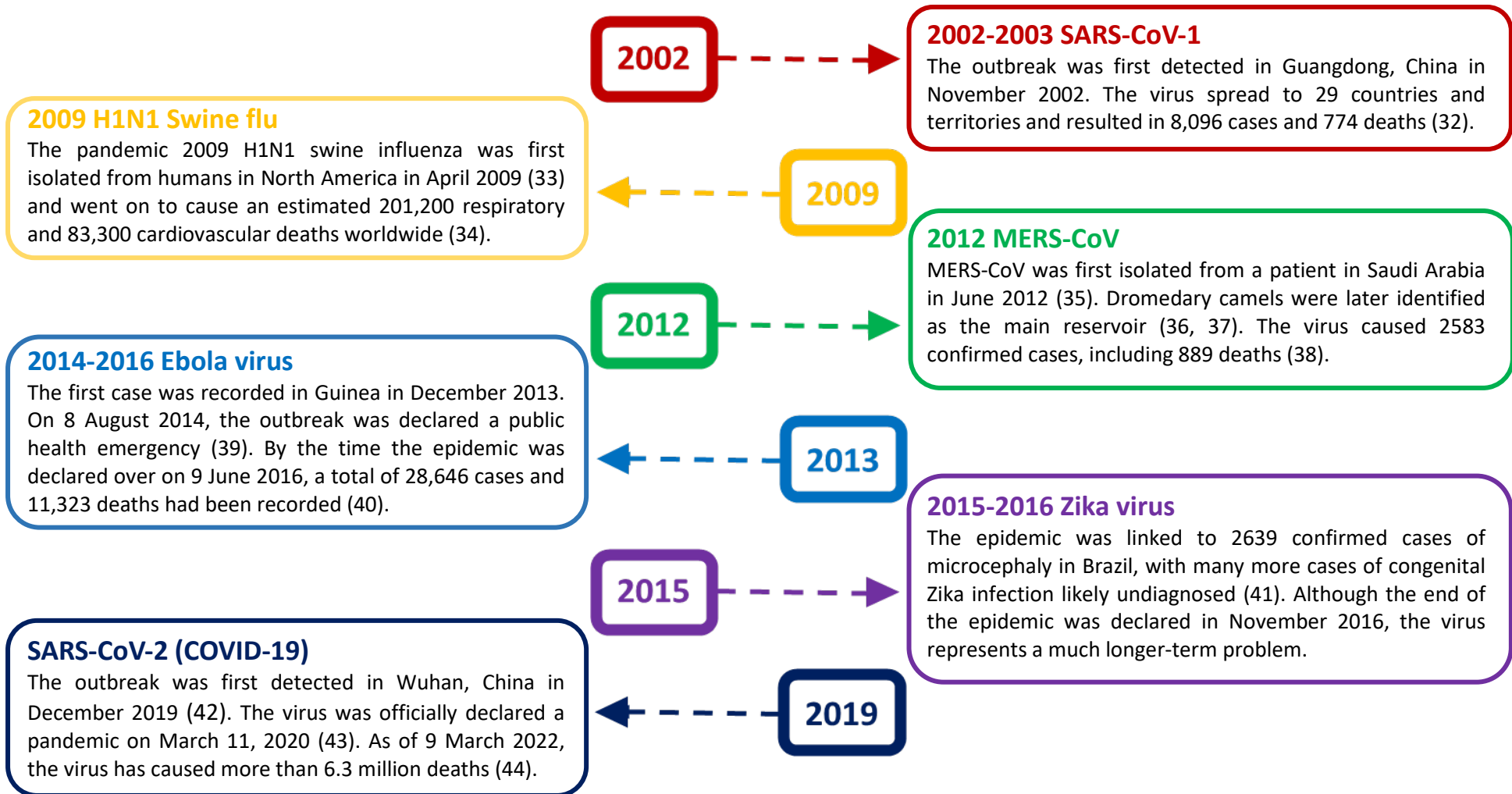


Figure 1.1. Some notable human viral outbreaks in the 21st century.

A timeline of some prominent outbreaks of emerging and re-emerging viruses that have infected humans.

1.3 A brief history of antiviral treatments

From the first studies describing viral interference and the serendipitous discovery of early antivirals, to the gradual acceptance of combination therapies and the first direct-acting antivirals (DAAs) against hepatitis C virus (HCV), antiviral development has come a long way over the past 70 years (summarised in Table 1.1). However, there is still an unmet need for antiviral therapies against both existing and newly emerging viral pathogens.

Table 1.1. Some major milestones in the history of antiviral treatments.

Year	Milestone
1957	The first description of interferon and its inhibition of virus growth (45).
1959	First synthesis of idoxuridine as a potential anticancer drug (46).
1961	Idoxuridine shown to inhibit herpes simplex virus and vaccinia virus (47).
1963	Idoxuridine, approved for the treatment of herpes simplex infections (48).
1972	Development of ribavirin, a broad-acting antiviral therapy (49).
1977	Discovery of acyclovir, a highly selective inhibitor of herpesvirus replication (50).
1980	Synthesis of recombinant interferon (51).
1983	First description of prodrug strategy to increase aqueous solubility (52).
1987	Zidovudine, approved for treatment of AIDS (53).
1989	Famciclovir – proof of oral prodrug strategy (54).
1990	Synthesis of saquinavir – the first successful, rationally designed antiviral (55).
1995	Demonstration of combination therapy to combat HIV drug resistance (56).
2011	Approval of first DAAs for treatment of HCV – boceprevir and telaprevir (57).
2013	Approval of sofosbuvir, the first interferon-free HCV treatment (58).

1.3.1 Host targeted antivirals

Host targeting antivirals (HTAs) are compounds that indirectly inhibit viral replication through interaction with host factors. This can occur through modulation of the host immune response or via antagonism of viral entry receptors and other host factors that play a role in the viral lifecycle (59). Examples of HTAs include maraviroc, a chemokine receptor type 5 antagonist approved for use against HIV infection (60), imiquimod, a TLR-7 agonist used topically for treatment of genital warts (61) and ribavirin (both a host modulator and a guanosine analogue) which was primarily used for the treatment of HCV (62), but has also been used to varying degrees of success as a broad-spectrum, last resort treatment against viral haemorrhagic fevers such as

Crimean-Congo haemorrhagic fever (63, 64), Lassa fever (65) and hantaviruses (66, 67) and more recently against SARS-CoV-2 (68).

The main advantage of HTAs is their potential for a broad-spectrum of inhibition use, since host proteins can be utilised by multiple virus families as part of their replication cycle (69, 70). For example, the serine protease TMPRSS2 is important for facilitating cell entry for a number of respiratory viruses such as parainfluenza virus (71), influenza A virus (72) and various coronaviruses (73-75); therefore, compounds that inhibit the activity of this protein could be beneficial to the treatment of these respiratory viral infections. Similarly, cleavage sites for the serine protease furin have been documented in several viral families including the *Filoviridae*, *Coronaviridae*, *Retroviridae*, *Papillomaviridae* and *Togaviridae*, among others (70), and therefore compounds that target this host protein could also have broad-spectrum antiviral activity. Additionally, since HTAs do not directly target viral proteins, they possess a comparatively higher barrier to resistance and are less influenced by genotypic and quasispecial variation (76, 77).

Disadvantages of HTAs however, may include variation in antiviral activity due to host genetic polymorphisms altering target binding affinity (78, 79). Furthermore, since host factors can play crucial and potentially uncharacterised roles in the cell, navigating potential side-effects can prove challenging. Kinases for example, have been found to play a role in the entry of a wide variety of viral families including but not limited to *Flaviviridae* (80, 81), *Poxviridae* (82), *Herpesviridae* (83), *Orthomyxoviridae* (84), *Coronaviridae* (85) and *Filoviridae* (86). However, their critical roles in the regulation of many essential cellular functions may limit their feasibility as antiviral targets. Finally, the presence of a variety of mammalian homologues, and more complex mechanisms of action can also make the transition between animal and human trials more complicated.

1.3.2 Direct-acting antivirals

Direct-acting antivirals (DAAs) are compounds that can interfere with various stages of the viral lifecycle by directly targeting viral proteins. Due to the highly specific nature of these drugs, there is typically a milder side-effect profile which has direct

positive impacts on treatment outcomes and drug adherence (87, 88). Viral proteins that have been successfully targeted using this approach include influenza matrix protein 2 (89) and neuraminidase (90, 91), cytomegalovirus terminase (92), varicella-zoster virus helicase-primase (93), HIV integrase (94), HCV NS5A (95), HIV and HCV proteases (55, 57) as well as numerous viral polymerases (50, 53, 58, 96). There are also many other viral targets in development and this includes viral kinases (97, 98), nucleoproteins (99-101), envelope proteins (102-104), methyltransferases (105-107), as well as various virus-encoded co-factors (108, 109).

One of the major obstacles to DAA design is its lengthy process, and the development of therapeutics against the aforementioned viral proteins was built upon decades of research. This is because there must be an understanding of the fundamental biology of a virus before drug development can commence. This includes, but is not limited to, the full-length viral genome sequence, development of cell culture systems for the virus, understanding of the viral life cycle as well as high-quality models of viral proteins. Therefore, although the DAA approach has led to the development of many highly effective therapeutics for HCV (110, 111) and HIV (112, 113), it may not be very feasible especially in the case of emerging viruses.

1.3.3 Targeting the RNA-dependent RNA polymerase

Viral polymerases are essential to the viral replication cycle; therefore, they are attractive targets for antiviral development. Notably, RNA-dependent RNA polymerases (RdRps), make good targets due to their conservation across RNA viruses (excluding retroviruses), well-characterised nature (compared to other viral proteins) and lack of mammalian homologues which decreases the possibility of off-target effects. RdRps form a structure resembling a closed right hand, consisting of fingers, palm, and thumb domains (Figure 1.2). There are two classes of antiviral compounds that interact with RdRps – nucleoside analogues (NAs) which interact within the active site and non-nucleoside inhibitors (NNIs) which bind allosterically.

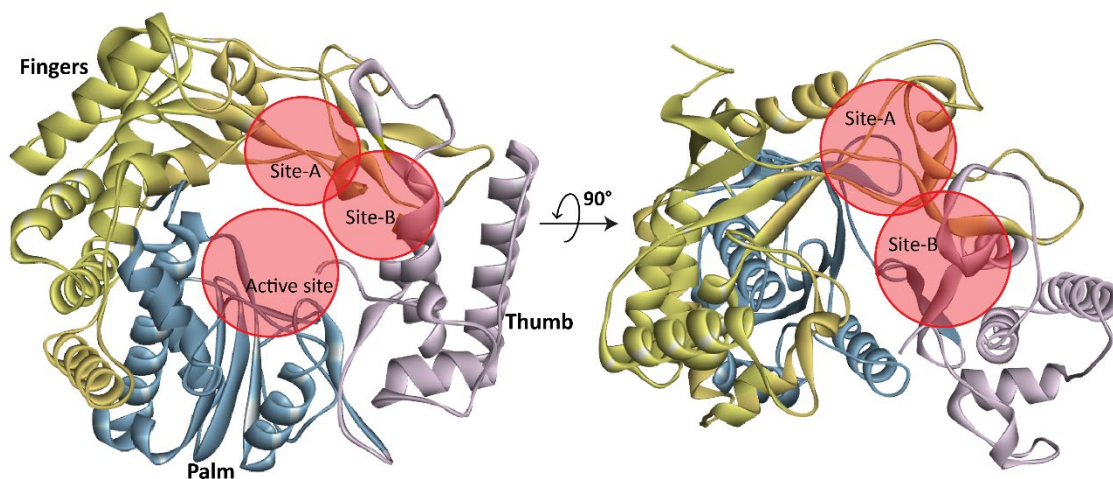


Figure 1.2. Schematic of the human norovirus GII.4 RdRp.

The human norovirus RdRp structure (PDB-ID: 4LQ9) (114) is depicted showing the fingers (yellow), palm (blue) and thumb (pink) domains. The location of the NA (active site) and two NNI (Site-A and Site-B) (114) interaction sites are also indicated. The ribbon diagram was generated using the Discovery Studio 2017 R2 software suite (Dassault Systèmes, BIOVIA Corp).

1.3.3.1 Nucleoside analogues

NAs mimic the incoming nucleoside triphosphate and inhibit replication by causing chain termination when incorporated into the growing strand of nucleic acid by the viral polymerase (50). Another less common mechanism of action for NAs is through elevating the mutation rate above an error threshold, this is known as lethal mutagenesis or error catastrophe (115, 116). Since NAs interact within the highly conserved polymerase catalytic site, they often demonstrate a broader spectrum of activity (117-120) (Figure 1.2). For this reason, the repurposing of existing NAs is a common strategy in the search for antivirals against existing and emerging viruses. Indeed, several approved NA compounds have been repurposed for use against other viral targets. For example, lamivudine, a cytidine analogue initially approved for use as an antiretroviral to manage HIV, was later repurposed as a treatment for chronic HBV infection (96, 121, 122). Similarly, favipiravir, a purine mimetic, which is licensed for use against influenza infections in Japan, has also been used off-label to treat Ebola virus (123, 124) and Lassa virus infections (125). Most recently, NAs molnupiravir and remdesivir which were initially designed to treat influenza (126) and Ebola virus disease (127), respectively, have received FDA authorisation for use against SARS-CoV-2 infection (13, 128). Furthermore, some NAs initially intended as anticancer agents

have also been successfully repurposed for use against viral diseases. However, for the same reasons why broad-spectrum activity is possible, these compounds can exhibit off-target binding to host polymerases, which may lead to undesirable effects (129-131).

1.3.3.2 *Non-nucleoside inhibitors*

NNIs bind non-competitively to allosteric sites on the viral polymerase and thereby prevent the conformational changes that are required to form an active replication complex. Due to the diverse nature of these allosteric sites, NNIs are traditionally believed to possess narrow-spectrum activity. An example of this are non-nucleoside reverse transcriptase inhibitors targeting HIV-1 which are unable to inhibit HIV-2 due to differences in binding pocket structure (132, 133).

An RdRp can possess a number of allosteric sites, the HCV RdRp for example, possesses five known allosteric sites: Thumb I, Thumb II and the overlapping Palm I, Palm II, and Palm β sites (134, 135), each targeted by different classes of compounds (Figure 1.3). The Thumb I site binds indole and benzimidazole derivatives (such as JTK-109, TMC647055 and beclabuvir which are used in **chapter four**) (136, 137). Early HCV NNIs possessed relatively low barriers to resistance as well as limited cross-genotypic coverage (138, 139). This can partly be explained by the fact that drug development efforts were initially focused against the HCV genotype 1 which commanded both the highest global prevalence (140), and also possessed the first subgenomic replicon model (141). More recently, some compounds such as the benzofurans (Palm II) have demonstrated the potential for cross-genotypic coverage (138, 142, 143). However, due to the availability of a variety of highly efficient pan-genotypic cures, further development of HCV NNIs has largely been discontinued.

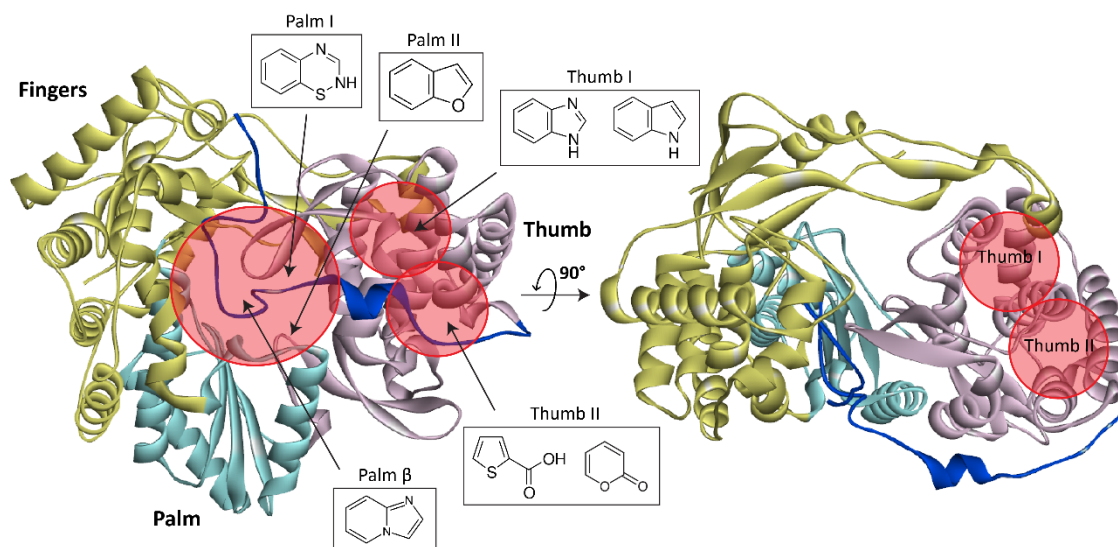


Figure 1.3. Schematic of HCV RdRp showing allosteric sites.

The HCV RdRp structure (PDB-ID: 3TYQ) (144) is depicted showing the fingers (yellow), palm (light blue), thumb (pink) and C-terminal (dark blue) domains. The locations of the five allosteric NNI binding sites are indicated. The chemical scaffolds for the classes of molecules that bind in each location are also shown. The ribbon diagram was generated using the Discovery Studio 2017 R2 software suite (Dassault Systèmes, BIOVIA Corp).

1.4 Are broad-spectrum NNIs possible?

Although NNIs have traditionally been viewed as narrow-spectrum (virus-specific or genotype-specific), recent studies repositioning DAAs have identified the cross-genera and cross-family activity of various NNI compounds. For example, FDA approved HCV Palm I inhibitor, dasabuvir, demonstrated cross-family inhibition of the hepatitis E virus (HEV) G1 replicon replication with a half-maximal effective concentration (EC_{50}) of 1.79 μM (95% CI: 1.38-2.32 μM) (145). Additionally, the same study also revealed that the RNA-binding channel targeting compound, GPC-N114 (146), originally designed against the *Picornaviridae* also displayed an EC_{50} of 1.07 μM (95% CI: 0.13-1.35 μM) against the HEV replicon (145).

Similarly, another study that repurposed existing HCV NNI compounds identified the cross-family activity of three Thumb I binders (JTK-109, TMC647055 and beclabuvir) against various members of the *Caliciviridae* (147). Additionally, this study also generated two mutant norovirus RdRps (Q414A and R419A) which were shown to confer resistance to JTK-109 inhibition. This led to the identification of the allosteric Site-B as the binding site for JTK-109 and potentially also for TMC647055 and

beclabuvir (114, 147) (Figure 1.2). These three compounds and Site-B will form the basis of the work in **chapter four**.

It is important to note however, that the broad-spectrum activity demonstrated by the named compounds are not due to the cross-family conservation of allosteric sites but rather serendipitous “off-target” binding to different and often newly described locations.

1.5 Current strategies in drug discovery

There are three main approaches that are utilised in the hit and lead identification stages of the drug discovery pipeline. These include high throughput screening (HTS), virtual screening (VS) and drug repositioning (Figure 1.4). HTS is a brute-force approach whereby massive compound libraries are screened against a target *in vitro* for the desired activity. This enables hit identification without the need for upfront knowledge about the target (148), which is very useful when the fundamental biology for a target is poorly understood. However, this approach is resource intensive with no promise of success.

An alternative to this is VS, where knowledge of the protein structure and existing ligands is used to guide the search for active molecules. This may involve high-throughput docking, where the binding orientations of a library of test compounds are predicted and scored and pharmacophore-based searching where the molecular features important for interaction are used to screen for structurally novel active compounds (149, 150). The main disadvantage of this approach is that it is heavily reliant on existing knowledge, which may not be available, especially in the case of new targets, as is the problem with emerging viral pathogens.

The final strategy is compound repositioning, which is essentially the exploration and identification of new targets for existing drugs. Since these compounds have already passed preclinical and/or clinical screening, drug repurposing can significantly reduce time and costs, such as those associated with ADMET (absorption, distribution, metabolism, excretion and toxicity) profiling (Figure 1.4). For comparison, getting a new drug to market can take 13-15 years and costs US\$2-3 billion compared to drug repositioning which is estimated to take 6.5 years and

US\$300 million on average (151). Compound repositioning, used in combination with *in vitro* and *in silico* screening approaches may offer better starting points for hit (possible active) and lead (developmental candidate) identification. Once lead compounds are identified, extensive structure-activity relationship (SAR) exploration and optimisation can then be performed to improve its pharmacokinetics and pharmacodynamics. The repurposing of HCV thumb I binders (JTK-109, TMC647055 and beclabuvir) will form the foundation of the work performed in **chapter four**.

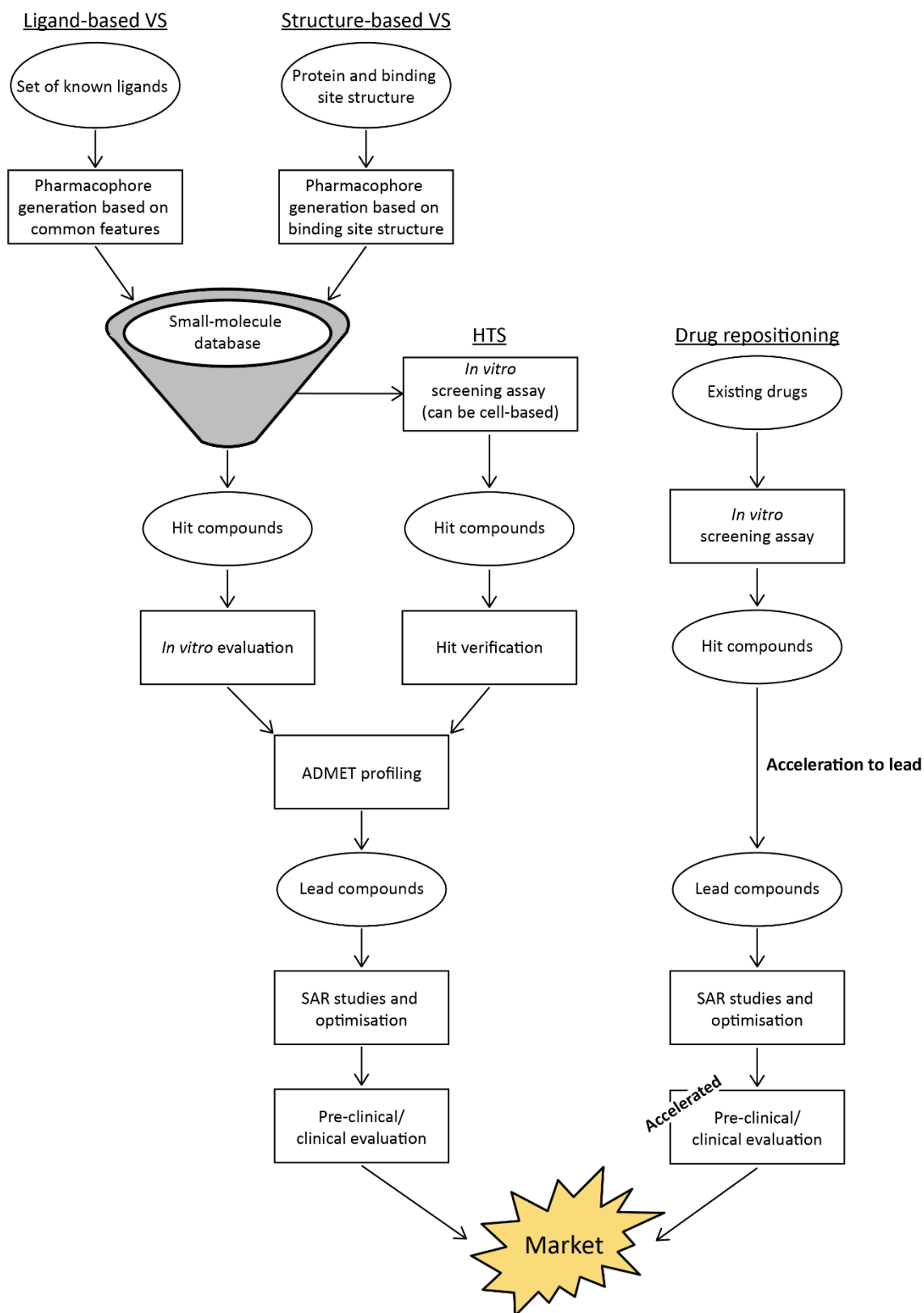


Figure 1.4. Flow chart of drug development pipeline using different approaches.

The key processes and inputs required for the different drug development approaches are shown. Ligand-based and structure-based approaches both rely on prior knowledge whilst HTS can commence even in the absence of a known target. Drug repositioning starts with existing drugs which can allow for significant acceleration of the development process.

1.6 Computational drug discovery

Computational methods such as molecular dynamics simulations, docking, ligand-based drug design and structure-based drug design are commonly used to accelerate the drug development process (152). Skilful application of these *in silico* techniques can greatly enhance the efficiency of the discovery pipeline, by decreasing the time, labour, and costs required. For example, the identification of the HIV-1 protease cleavage site between Phe-Pro on natural substrates (the HIV polyprotein) and subsequent crystallographic studies of its binding to synthetic mimetics, suggested areas for further structure-guided optimisation. This led to the development of saquinavir, a HIV protease substrate transition state mimetic; the first ever protease inhibitor approved by the FDA (55).

1.6.1 Ligand-based drug design

The ligand-based drug design approach utilises understanding of the natural substrate or other known ligands of the target protein to guide compound development (Figure 1.4). This approach relies on having a set of ligands that are known to interact at the target site. By using known inhibitors as scaffolds, pharmacophore models (spatial representations of chemical features present on a molecule predicted to be involved in binding) can be derived and used to search large 3D structural databases for compounds with conformations matching the pharmacophore. The goal of this *in silico* approach is to find structurally novel active molecules (149, 150). Additionally, further modifications of existing structures can result in compounds with more desirable properties, for example valacyclovir, the valine ester of the guanosine mimetic acyclovir possesses improved oral bioavailability (52).

1.6.2 Structure-based drug design

In contrast to ligand-based drug design, the structure-based approach is guided by knowledge of the target protein 3D structure and its binding sites (Figure 1.4). Compounds can be docked or co-crystallised in a protein structure and by investigating the interactions and residues required for binding, and optimisation of compounds can

be performed to achieve the desired activity (153, 154). Another aspect of the structure-based approach includes the use of pharmacophore models, which can be developed based on the chemical properties of a protein's binding site and used to screen 3D structural databases to uncover compounds that could potentially bind (155, 156). However, these structure-based approaches rely on having accurate models of the protein to provide the correct understanding of the binding pocket. Although these approaches can uncover structurally novel compounds, binding interactions and affinities calculated *in silico* may not translate into drug-like activities when examined *in vitro* (157, 158). This can occur due to variety of factors such as protein conformational freedom (159) and solvent effects (160).

2 General introduction II: Molecular epidemiology

2.1 Acute gastroenteritis

Acute gastroenteritis (AGE) has the second greatest burden of all infectious diseases worldwide, causing an estimated 80.9 million disability-adjusted life years (DALYs) and 1.5 million deaths in 2019 (161). AGE is also a major encumbrance on the global economy leading to a combination direct health system costs and indirect productivity losses. For example, in Belgium between 2010 and 2014, the price of AGE was estimated at an average total cost of €103 per case and represented an economic burden of approximately €1 billion per year (162), similarly in Trinidad and Tobago each case of AGE was estimated to cost up to US\$155, representing an economic burden of US\$21 million in 2009 (163). In Australia during 2016, there were an estimated 17.7 million incidences of AGE which cost the economy A\$359 million from healthcare service costs alone (164).

AGE is defined as the inflammation of the gastrointestinal tract and is characterised by the sudden onset of diarrhoeal disease. This is usually also accompanied by symptoms such as vomiting, nausea, abdominal cramps, and fever. Aetiological agents of gastroenteritis include viruses, bacteria, and parasites. Estimated number of deaths for some common causes of AGE are summarised in Table 2.1. Although improvements in sanitation and access to clean drinking water have nearly halved the number of yearly casualties over the past three decades (161), diarrhoeal diseases remain a significant global health burden.

Prior to 2006, rotavirus was the leading cause of viral gastroenteritis, resulting in an estimated 366,000 deaths in young children during 2005 (165). Unlike bacterial or parasitic gastroenteritis, rates of rotavirus infection were similar when comparing developed and developing nations (166). During this pre-vaccine era, it was estimated that by the age of five, nearly all children will have experienced an episode of rotavirus gastroenteritis, 1 in 60 would require hospitalisation and 1 in 293 would die (167, 168). Following successful implementation of the vaccine into national immunisation programs, rates of rotavirus hospitalisation have declined by an estimated 40% globally (169, 170). Benefits were even greater in high-income nations and reductions

of more than 70% were reported in Australia, Germany, and Belgium (171-174). As a result, norovirus has gradually replaced rotavirus as the most prominent agent of viral gastroenteritis in the post-vaccine era (175-178).

Table 2.1. Estimated global deaths for some common aetiological agents of AGE*.

Aetiological agent	Deaths (thousands)	Ref
Virus		
Norovirus	210.0	(179)
Rotavirus	199.2	(180)
Astrovirus	39.4	(181-183)
Adenovirus	70.2	(180)
Bacteria		
<i>Vibrio cholerae</i>	68.4	(180)
<i>Campylobacter</i> spp.	38.1	(180)
<i>Salmonella</i> spp.	90.3	(180)
Enterotoxigenic <i>Escherichia coli</i> (<i>E. coli</i>)	74.1	(180)
Enteropathogenic <i>E. coli</i>	12.0	(180)
<i>Shigella</i> spp.	164.3	(180)
<i>Clostridium difficile</i>	9.4	(180)
<i>Aeromonas</i>	67.9	(180)
Parasite		
<i>Giardia</i> spp.	35.4	(183, 184)
<i>Cryptosporidium</i> spp.	64.8	(180)
<i>Entamoeba histolytica</i>	67.9	(180)
Unknown aetiology	287.3	

* adapted from (185) which is based on GBD 2015.

2.2 Norovirus

2.2.1 Background and history

Norovirus is one of the leading aetiological agents of AGE, causing an estimated 1 in 5 incidences of AGE worldwide (186) and costing the global economy nearly US\$65 billion each year (179). Although norovirus infections typically resolve without the need for medical intervention, severe illness can occur in the immunosuppressed, elderly and in young children (187-189).

The first recorded mention of a norovirus-like illness was by Zahorsky in 1929, who described it as “hyperemesis hiemis” or “winter vomiting disease” (190). The disease was characterised by a sudden onset of diarrhoea and vomiting, and appeared to have increased activity in winter, hence its name. Zahorsky’s study was followed by

several reports of gastroenteritis outbreaks, mainly affecting children, unfortunately no aetiological agents were ever identified for these outbreaks (191-193). It was however, shown that viruses were the likely cause of these outbreaks since bacteria-free stool filtrates obtained from these community outbreaks were able to induce similar gastroenteritis symptoms in healthy adult volunteers (194).

At the end of October 1968, an outbreak of acute gastroenteritis occurred at an elementary school in Norwalk, Ohio, USA that affected 50% (n=116/232) of the staff and students (195). It was from this outbreak that the original norovirus “Norwalk virus”, would eventually be discovered. Nevertheless, all attempts at the time to cultivate the virus *in vitro* were unsuccessful and it was not until four years later, in 1972, when Albert Kapikian first observed virus-like particles under immune electron microscopy in a faecal sample collected from the 1968 Norwalk, Ohio outbreak (196). The next major breakthroughs would occur in 1990 and 1993, when Jiang, et al. would determine the sequence (197) and genome organisation (198) of the Norwalk virus genome, which facilitated further investigations into viral genetics and taxonomy. In 2002, Norwalk-like viruses were collectively recognised under the genus *Norovirus*, and the species name was norovirus (199).

2.2.2 Structure and genome organisation

Norovirus possesses an approximately 7.5 kb positive-sense, non-segmented, single-stranded RNA genome, which is encapsidated by a non-enveloped, T=3 icosahedral capsid measuring between 27-35 nm in diameter and comprised of 90 major capsid protein dimers (196, 197, 200). The norovirus genome is organised into three open reading frames (ORF1-3) (198). The 5'-terminus of the genome is covalently linked to a virus-encoded protein, VPg, whilst the 3'-terminus is polyadenylated (Figure 2.1A).

ORF1 is over 5 kb in length and encodes an approximately 200 kDa polyprotein that is post-translationally cleaved by a 3C-like protease (NS6) into six/seven (depending on whether NS1-2 is cleaved) non-structural viral proteins (NS1-7) (201) (Figure 2.1A). NS1-2 encodes the N-terminal protein which may play a role in the formation of the viral replication complex (202). The NS1-2 protein can be cleaved by

the host protease, caspase-3, to yield NS1 and NS2 (203). The secretion of NS1 has been shown to be important for murine norovirus resistance to the interferon- λ -mediated responses (204).

NS3 encodes the 40 kDa NTPase which is believed to possess both RNA helicase activity and functions to hydrolyse nucleotide triphosphates (205, 206). The NS4 region encodes for p20 (or p22) which is believed to be equivalent to the 3A protein of picornaviruses. It has similarly been shown to play a role in the induction of trans-Golgi network dismantling (202, 207), however its exact function remains to be elucidated (Figure 2.1A).

The 16 kDa VPg protein (encoded by NS5) (Figure 2.1A) which is covalently linked to the 5' end of the viral RNA genome and subgenomic RNA, acts as a primer for initiation of viral RNA synthesis (201, 208). It also plays a role in the recruitment of translation machinery (209, 210). The 19 kDa 3C-like viral protease is encoded by NS6 (Figure 2.1A) and plays a critical role of processing the ORF1 polyprotein during viral replication (201). The RdRp (encoded by NS7) is final non-structural protein of 57 kDa, and its main function is the replication of the viral genome (201).

The ORF2 region encodes the 58 kDa major capsid protein or VP1 that self-assembles to form the viral capsid (Figure 2.1A). It consists of a conserved shell (S) domain that comprises the N-terminal 225 residues which forms the interior surface of the capsid (211, 212). The S domain is followed by two protruding domains, termed P1 and P2 (Figure 2.1B), which extend towards the exterior of the capsid and are important for the stability of the capsid subunits (213). The hypervariable P2 domain is the most exposed and thus plays a pivotal role in facilitating evasion of herd immunity. This region contains several epitopes (A-G) that are antigenically important and likely involved in host cell binding (214-216).

ORF3 encodes a smaller structural protein, termed the minor capsid protein or VP2 which has a poorly defined function (Figure 2.1A). This protein has been shown to interact with the S domain of VP1 and is believed to potentially play a role in the assembly and stabilisation of virus-like particles (VLPs) (217), although it has also been shown to be non-essential for the formation of VLPs (213).

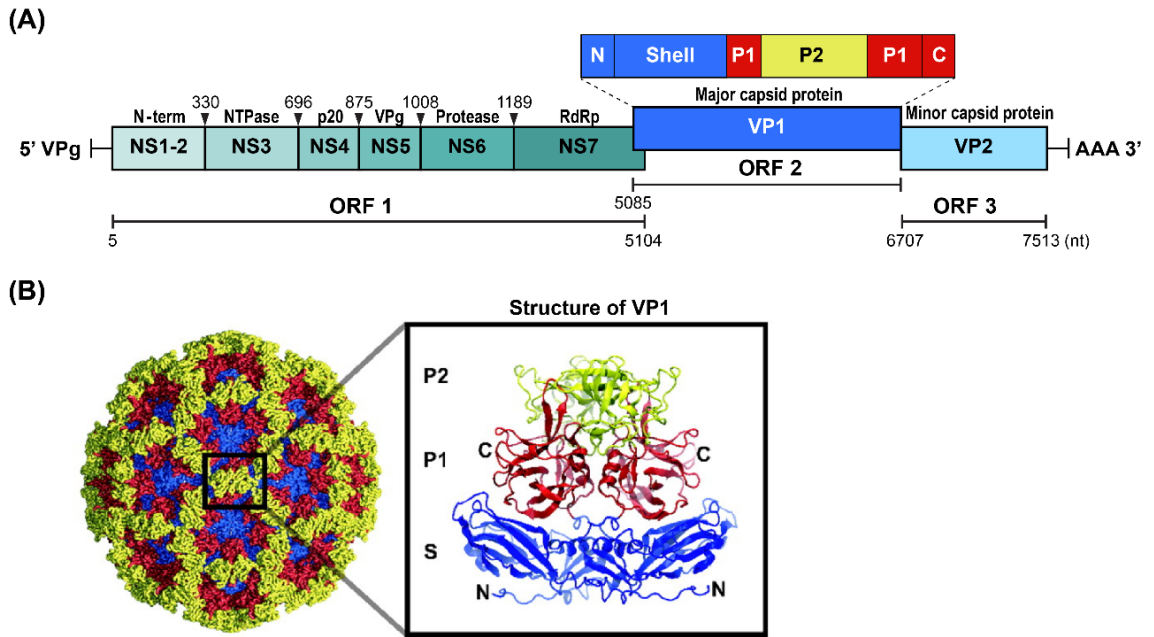


Figure 2.1. Norovirus genome organisation and capsid structure.

(A) The norovirus genome is organised into three ORFs with the nucleotide (nt) positions of the start and end of each ORF indicated below. ORF1 encodes a large polyprotein that is cleaved into six different non-structural proteins (NS1-7). The cleavage sites are indicated by the small black triangles, with the amino acid positions indicated above. ORF2 encodes the major capsid protein (VP1) whilst the minor capsid protein (VP3) is encoded by ORF3. This genome organisation is based on the human norovirus GII.4 Sydney 2012 strain (GenBank accession: JX459908). For clarity, genome is not shown to scale. (B) The T=3 capsid structure of Norwalk virus, composed of 90 VP1 subunit dimers. A ribbon representation of a VP1 dimer is shown in the box (PDB ID: 1IHM). The Shell (S), P1 and P2 domains are coloured in blue, red, and yellow, respectively. The norovirus capsid schematic was taken from (218).

2.2.3 Classification and nomenclature

Norovirus is one of eleven currently recognised genera belonging to the *Caliciviridae* family. Other members of the *Caliciviridae* include: *Lagovirus* (e.g. rabbit haemorrhagic disease virus [RHDV]), *Nebovirus*, *Recovirus*, *Sapovirus*, *Valovirus*, and *Vesivirus* (e.g. feline calicivirus [FCV]) which also infect mammalian hosts, *Bavovirus* and *Nacovirus* which infect birds as well as *Minovirus* and *Salovirus* which infect fish (219). Of these genera, only *Norovirus* and *Sapovirus* are known to infect humans, both of which cause gastroenteritis, with sapovirus infections typically milder in comparison and are largely confined to young children (220).

Norovirus was historically classified into genogroups based on the ORF2 amino acid (aa) sequence, with approximately 45% aa divergence across different genogroups (221). However, due to the frequent recombination events that occur at the ORF1/2

junction (222, 223) and to account for the emergence of novel recombinant viruses, norovirus classification has since shifted to a dual nomenclature system. The polymerase groups, or P-group, classification is based on the phylogeny of a 762 nucleotides (nt) of the RdRp encoding region (224). Under the current scheme, noroviruses may be classified into ten different genogroups (GI-GX) and two tentative non-assigned (NA) genogroups (GNA1 and GNA2) based on the aa sequence of the full-length ORF2 protein (VP1) (530-580 aa) (Figure 2.2) and eight different P-groups (GI.P-GVII.P, GX.P) and two tentative P-groups (GNA1.P and GNA2.P) based on diversity at the 3' end of the ORF1 P-region (224).

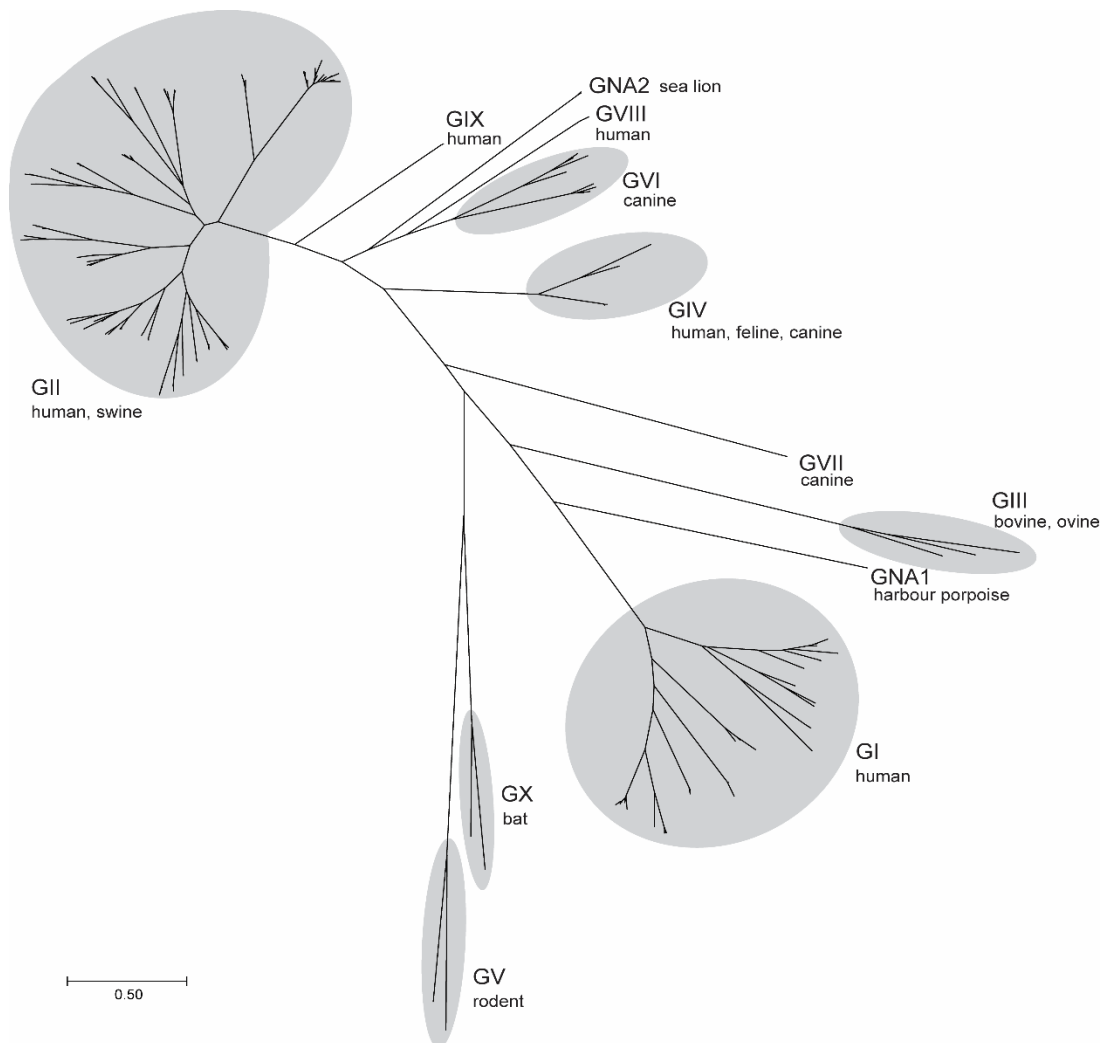


Figure 2.2. Phylogenetic classification of norovirus sequences based on full length VP1.

Noroviruses can be classified into ten genogroups and two non-assigned genogroups based on full-length VP1 amino acid sequences. Sequences were obtained from (224) and aligned using MUSCLE. A maximum-likelihood phylogenetic tree was produced using MEGA X software (225) with 500 bootstrap replicates, based on the Le Gascuel model (226). The animal hosts for each genogroup are also shown.

These groups can then be further classified into 49 different capsid genotypes and 60 different P-genotypes. Previously, a 15% amino acid divergence cut-off was used to designate new genotypes (221). However, as more sequences have become available this threshold was no longer appropriate and instead designation of genogroups and genotypes has shifted to using 2 x standard deviation criteria (224, 227). Viruses from GI, GII, GIV, GVIII and, GIX are responsible for human infections with GII associated with approximately 90% of all human norovirus infections globally (228, 229), followed by GI (~10%) (Figure 2.2). Within GII, viruses in the genotype 4 lineage (GII.4) are responsible for approximately 60-80% of all norovirus outbreaks (230-232), and have caused several epidemics and six recorded pandemics, detailed later in section 2.2.7. The term “variant” is used to define viruses within the pandemic GII.4 lineage. Historically, new variants were defined by approximately 5% amino acid divergence, evidence of epidemic activity in at least two geographically diverse regions (227, 233) and were named after the location and year of the first full-length capsid sequence deposited in the public domain (i.e., GII.4 Sydney 2012). However, since the adoption of a new norovirus nomenclature scheme (224), no novel GII.4 pandemic variants have emerged.

Currently, norovirus strains are named in the format of genogroup.genotype [P-group, P-type], whereby roman numerals are used to represent the genogroup and P-group number and Hindu-Arabic numerals used for genotype and P-type designations (224). For example, GIX.1 [GII.P15] represents virus with a genogroup IX, genotype 1 VP1 region together with a P-group II, P-type 15 polymerase region. Additionally, where genogroup and P-group follow the same designation, the P-group can be excluded. For example, GII.3 [P12] represents a virus with a genogroup II, genotype 3 capsid and a P-group II, P-type 12 polymerase.

2.2.4 Transmission

Norovirus is a highly communicable pathogen possessing a low infectious dose of approximately 10^3 virions (234), coupled with a high level of viral shedding (10^7 - 10^9 per g/faeces) during the acute, symptomatic phase of infection (235, 236). Transmission typically occurs person to person via the faecal-oral route but can also arise due to ingestion of contaminated food and water, and through exposure to

vomitus aerosols and contaminated surfaces (237, 238). Norovirus is environmentally stable and has been reported to remain infectious on surfaces for up to two weeks (239-241), or two months in groundwater (242). Furthermore, norovirus displays resistance to inactivation by commonly used disinfectants, such as ethanol and quaternary ammonium compounds when compared with other viruses (243). The combination of these factors means that outbreaks of norovirus – which commonly occur in semi-closed settings such as aged care facilities (232, 244), schools (245), hospitals (244), and cruise ships (246, 247) – can be difficult to control.

Norovirus is also frequently detected in food-related gastroenteritis incidents worldwide and is one of the most common causes of foodborne illness in the US (2009-15: 41%) (248) and Australia (2016: 14%) (249). Food-related outbreaks are commonly reported in association with contaminated shellfish, fruits and salad ingredients which typically require minimal cooking (250-253). Additionally, norovirus is resistant to acid and heating (up to 60°C for 30 minutes), which means that cooking can be insufficient for deactivating the virus (254, 255). Food-related outbreaks can also occur due to infected food handlers (256-258). As a result, food handlers with gastroenteritis are recommended to abstain from the workplace until 48 hours after their symptoms have subsided (259, 260). However, due to asymptomatic infection and prolonged shedding (235), there is still potential for these workers to contaminate the food they prepare (257, 261).

2.2.5 Clinical manifestation and pathogenesis

Norovirus has an incubation period of approximately 12 to 48 hours which is followed by illness that usually resolves within one to four days in healthy adults (262). Commonly reported symptoms of norovirus include diarrhoea, projectile vomiting, nausea, chills, abdominal cramps, and low-grade fever (5, 263). Following resolution of symptoms, patients will generally continue to shed infectious virions for up to several weeks (235, 264). Longer durations of symptoms can also occur and is typically reported among young children, the elderly and the immunosuppressed (265-267). In these vulnerable populations, more severe and persistent symptoms such as chronic diarrhoea, malnutrition, severe dehydration, and renal failure can manifest, sometimes leading to death (268, 269).

Volunteer challenge studies during the 1970s have played a significant role in our understanding of human norovirus pathogenesis. Intestinal biopsy specimens taken from volunteers who developed gastroenteritis after administration of Norwalk virus (GI.1) and Hawaii virus (GII.1) revealed intact mucosa with blunted villi, infiltration of the lamina propria by inflammatory cells and intercellular oedema (270, 271) (Figure 2.3). These challenge studies have also revealed an association between norovirus infection and transient malabsorption of carbohydrates and mild steatorrhea (272). Additionally, volunteers who developed illness also demonstrated reduced gastric motility (273). The combination of these factors causes the diarrhoea, vomiting and nausea is associated with viral gastroenteritis.

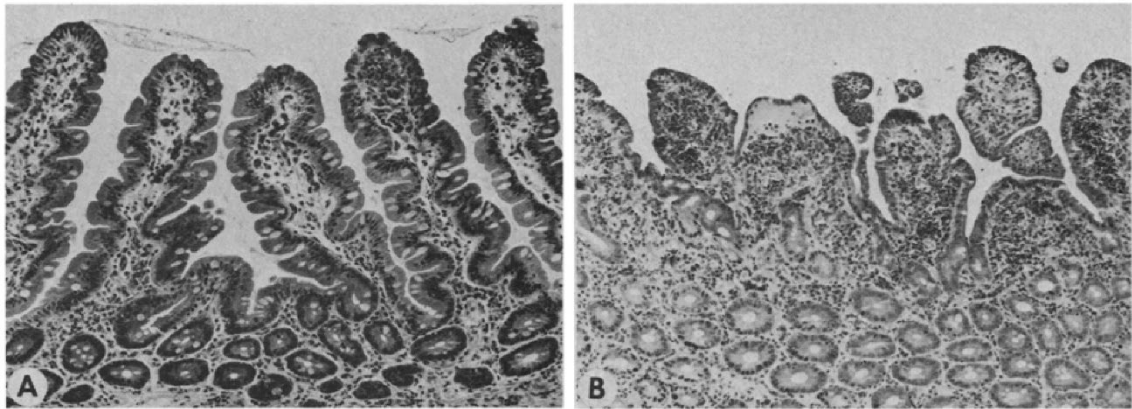


Figure 2.3. Light micrographs of jejunal mucosa biopsy specimens.

Intestinal biopsy specimens were obtained from a volunteer (A) prior to inoculation, where the villi appear normal and (B) 48 hours after inoculation with a GII.1 norovirus (Hawaii virus) after manifestation of illness, where blunting of villi can be observed. Image taken from (270).

2.2.6 Viral replication cycle

Human norovirus infection begins with the binding of the VP1 P domain to histo-blood group antigens (HBGAs) which are expressed on the surface of intestinal epithelial cells (274, 275). Additionally, it has been shown that there is viral genotypic variation in HBGA binding requirements which leads to differences in host susceptibility to norovirus infection (274, 276, 277). For example, type B individuals were found to be less susceptible to GI.3 norovirus infections (275). Similarly, individuals carrying a defective alpha-1,2-fucosyltransferase (FUT2) gene (termed “secretor-negative”) were also less susceptible to norovirus infection (278).

Following successful receptor engagement, viral entry and uncoating occurs, revealing the positive-sense RNA genome. Viral RNA translation then occurs, aided by the 5' covalently linked VPg which plays a role in the recruitment of host translation factors (209, 210). This leads to the synthesis of the ORF1 polyprotein which is post-translationally cleaved by the viral protease (NS6) into the different non-structural proteins NS1-7 (201). The newly produced RdRp (NS7) transcribes the positive-sense RNA genome into a negative-sense replication intermediate that serves as a template for both viral genome replication and the generation of subgenomic RNA. This subgenomic RNA serves as templates for the synthesis of VP1 and VP2 proteins which self-assemble around the nascent genomic RNA forming new viral particles that are released to infect more cells (211, 279).

2.2.7 Molecular epidemiology and evolution

Norovirus has a long history of causing “winter vomiting disease” outbreaks and its identification in 1972 (196) was quickly followed by several reports around the world (280-283). However, it was not until the mid-1990s that it was recognised as a cause of pandemic gastroenteritis (284). Norovirus is now the predominant agent of viral gastroenteritis worldwide – it is similarly prevalent in both developing and developed nations, circulates throughout the year, and can affect all ages (186, 244, 285). Although more than 36 human-infecting norovirus genotypes have been identified, GII.4 noroviruses remain the most prevalent and account for approximately 60-80% of all norovirus cases (229-232). The GII.4 norovirus lineage has caused six pandemics and several epidemics since the mid-1990s (Figure 2.4A).

These pandemic and epidemic variants have evolved through a combination of antigenic drift and recombination. New GII.4 variants typically demonstrate ~5% aa divergence in the VP1 region (227, 233). Most of these mutations accumulate within the epitope regions (A-G) found within the P domain of the VP1 protein (214-216). Additionally, intra- and intergenotypic recombination events during co-infection can lead to large changes in the antigenic regions enabling the virus to evade immune responses or confer selective advantages facilitating the emergence of new strains (222, 286, 287) (Figure 2.4B).

The US 1995/96 strain was the first GII.4 norovirus variant recognised as pandemic (Figure 2.4A), following its identification as the aetiological agent responsible for an increase in gastroenteritis activity worldwide, including Australia, Europe, and the US (284, 288, 289). It remained the dominant strain in circulation until it was replaced by the Farmington Hills 2002 strain (290, 291) (Figure 2.4A). Over the next decade, new GII.4 pandemic variants emerged every 2-3 years, with each rapidly replacing its predecessor (292-295). The Farmington Hills 2002 virus was replaced by the Hunter 2004 virus (Figure 2.4A), which caused major AGE outbreaks across Australia (292), Europe (296) and Asia (297).

In 2006, two new variants, Yerseke 2006a and Den Haag 2006b independently emerged (Figure 2.4A). The Yerseke 2006a emerged first, leading to an increase in gastroenteritis outbreak activity, however since this activity was largely localised to specific geographic areas, it is considered an epidemic variant (231). This virus was quickly replaced in 2007 by the Den Haag 2006b pandemic variant, which remained the most prevalent circulating strain until 2010 (293, 296, 298-300).

The New Orleans 2009 variant replaced the Den Haag 2006b virus in late 2009 and was the dominant strain in circulation during 2010 to 2012 (232, 294, 300) (Figure 2.4A). Unlike its predecessors, the New Orleans 2009 strain emerged through a combination of both antigenic drift and recombination at the ORF1/2 overlap region. This virus is believed to possess an ORF1 region derived from a Yerseke 2006a ancestor and an ORF2-3 region from the epidemic GII.4 Apeldoorn 2007 variant (286).

The most recent definitive GII.4 pandemic variant was the Sydney 2012 strain which overtook New Orleans 2009 in mid-late 2012 (295, 301) (Figure 2.4A). This virus was the most prevalent GII.4 virus in circulation until 2016 (300, 302, 303). However, despite its waning prevalence, no further antigenically novel GII.4 pandemic variants have appeared. Instead, two new recombinant viruses – GII.2 [P16] and GII.4 Sydney 2012 [P16] – have emerged (Figure 2.4B), been the two most dominant viruses, and gained prevalence, whilst the original pandemic Sydney 2012 virus has remained in circulation at lower levels (229, 303). Like its predecessor, the Sydney 2012 variant also arose from an intra-genotypic recombination event. This virus possesses a non-

structural region from the GII.4 Osaka 2007 epidemic variant and a structural region believed to be descended from an early Apeldoorn 2007 virus (286) (Figure 2.4B).

GI.4 variants have also been associated with several epidemics over the past two decades. These include Henry 2001, Japan 2001, Asia 2003, Yerseke 2006a, Apeldoorn 2007, Osaka 2007 and most recently, Melbourne 2016 (231, 304) (Figure 2.4A). Additionally, some non-GII.4 viruses have also been identified as important causes of gastroenteritis. For example, the GI.17 Kawasaki strain was a major cause of gastroenteritis activity in Asia during the 2014/15 winter season (305, 306). Other viruses such as those possessing a GI.3 capsid are frequently detected among children (307-311).

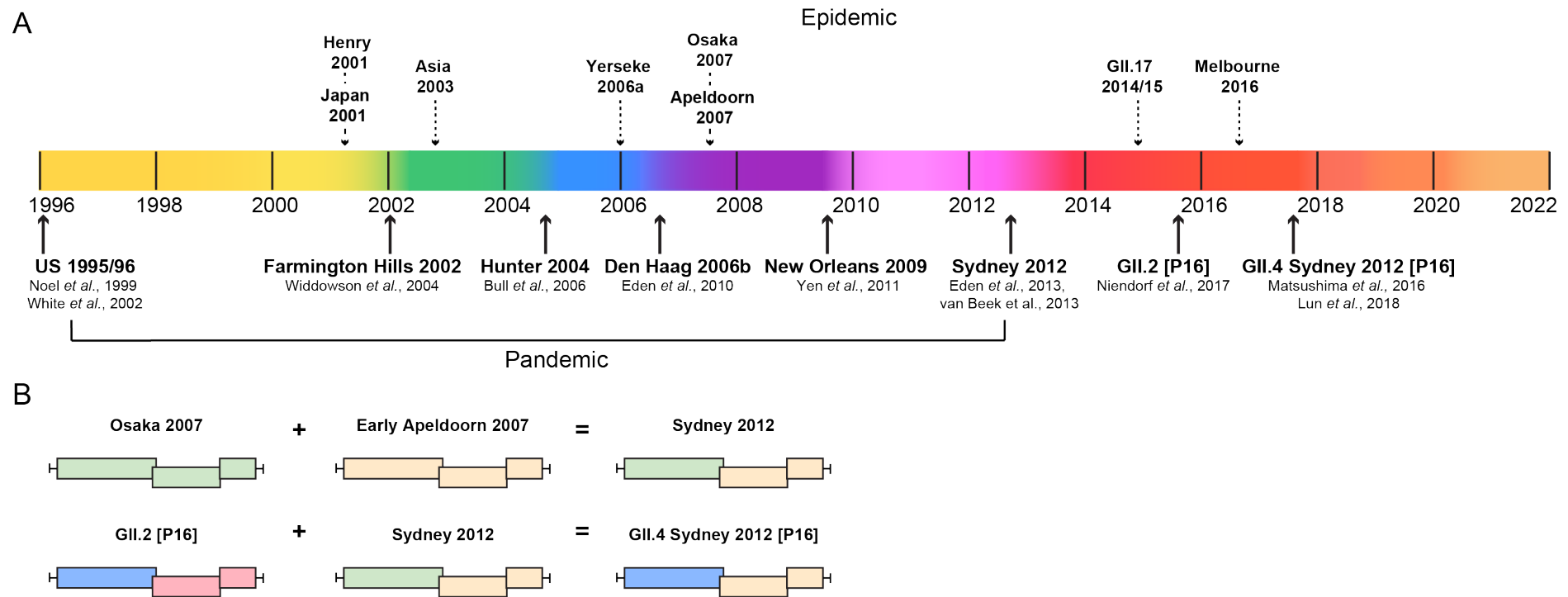


Figure 2.4. Timeline of pandemic and epidemic norovirus strain emergence.

(A) Six antigenically diverse pandemic GII.4 variants have been identified in the period between 1996 and 2014. The first pandemic variant recognised was the US1995/96 (284), followed by Farmington Hills in 2002 (291). Over the next decade, novel pandemic variants emerged every 2-3 and were identified as the Hunter 2004 (292), Den Haag 2006b (293), New Orleans 2009 (294) and Sydney 2012 (295). Since the Sydney 2012 pandemic variant, no further antigenically novel GII.4 viruses have been identified. Instead, the recombinant GII.2 [P16] and GII.4 Sydney 2012 [P16] viruses emerged (312, 313). Some epidemic strains are also shown, indicated using dashed arrows, these strains caused outbreaks in localised geographical areas (231, 304, 305). Different colours roughly denote the periods of circulation for GII.4 pandemic variants. Figure adapted from (314). (B) The pandemic Sydney 2012 variant (286) and the GII.4 Sydney 2012 [P16] strain (287) both emerged from recombination events. Colours are used to denote the non-structural and structural regions of different strains.

2.2.8 Prevention and control

There are currently no vaccines or antiviral therapies approved for the prevention and treatment of human norovirus infections (315-317). Therefore, management of norovirus outbreaks relies on the implementation of various public health strategies such as the isolation of infected patients, use of personal protective equipment, and decontamination of environmental surfaces (318, 319). Since there are no specific antiviral treatments available, disease management is primarily supportive (320, 321). This will typically include fluid and electrolyte replacement to prevent dehydration, which can occur via the oral, intravenous, or nasogastric routes (322). Additionally, ondansetron (an antiemetic) and racecadotril (an anti-diarrhoeal) may also be prescribed to reduce vomiting and diarrhoea episodes however the evidence supporting the benefits is still contended (323-326).

Although there are currently no licensed norovirus vaccines, there are several vaccine candidates in various phases of clinical and preclinical development (315, 316) which are summarised in Figure 2.5. Since human noroviruses do not grow well in cell culture (327), commonly used strategies such as inactivated particle and live-attenuated vaccines are not viable. Therefore, one current strategy is to use recombinant insect produced VLPs (328-330). Most of the vaccines currently in development possess bivalent or multivalent formulations to provide broader coverage of norovirus genotypes (331-336) (Figure 2.5). Some developmental candidates also aim to offer protection against other viruses, such as enterovirus 71 (EV71) and rotavirus (RV) (330, 336, 337). Two candidates are currently undergoing phase II clinical trials (Figure 2.5). The VLP-based bivalent GI.1 and GII.4 TAK-214 vaccine candidate developed by Takeda Pharmaceuticals International AG recently completed phase IIb trials in healthy adults, with results suggestive of potential cross-genotype protective immunity against GII.2 noroviruses (332). This vaccine was also well tolerated in children aged one to eight (338). The Longkoma vaccine developed by the Institut Pasteur of Shanghai (IPS) in collaboration with Anhui Zhifei Longcom Biopharmaceutical Co. Ltd. (Zhifei) is currently registered for phase I and phase IIa trials and is estimated to be completed on July 7, 2022 (ClinicalTrials.gov identifier: NCT04563533) (Figure 2.5).

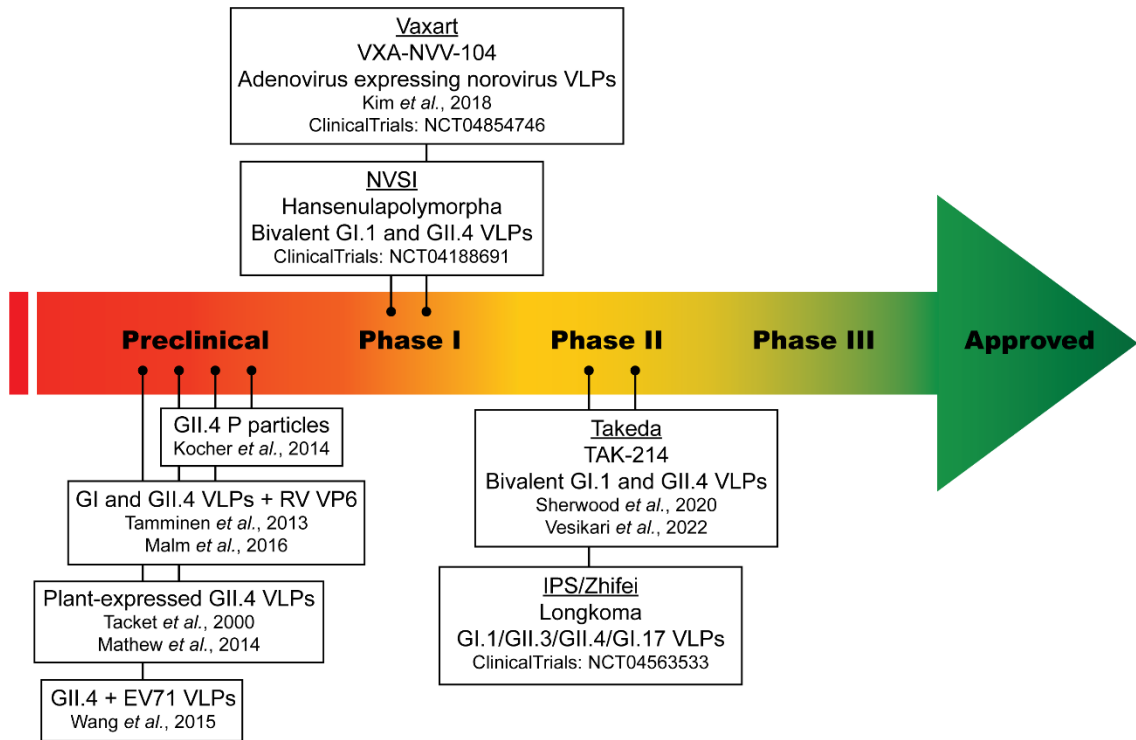


Figure 2.5. Human norovirus vaccine candidates.

Development progress for current norovirus vaccine candidates. The TAK-214 and Longkoma vaccines are currently in Phase II clinical trials (332). Two other candidates are undergoing phase I studies (331). The companies and institutions developing each vaccine candidate are shown underlined, followed by the vaccine name and components. Four other vaccines were last reported to be in the preclinical stages. Shading refers to the phase of clinical trial. Key references for each vaccine candidate are shown in text boxes. NVSI: National Vaccine and Serum Institute of China; VP6: protein in middle layer of rotavirus capsid.

2.3 Adenovirus

2.3.1 Background and history

Adenoviruses (AdVs) were named after the adenoid tissue from which they were first isolated in 1953. Wallace Rowe *et al.* (339) observed a transmissible, non-bacterial cytopathic agent during cultivation of the human adenoid cells. Since their discovery, human adenoviruses (HAdV) have become recognised as some of the most common viruses circulating in children. A 1982 study in Italian children found that 74.6% were seropositive for at least one HAdV type (340). More recent reports have observed that HAdV represent 6-20% of respiratory infections (341-345) and were detected in 11-50% of gastroenteritis-associated paediatric hospitalisations (346, 347). Worldwide, HAdV is estimated to cause one of the highest attributable incidences of diarrhoea (19.0, 95% CI 16.8–23.0) during the first two years of a child’s life (348),

resulting in an estimated 70,000 deaths annually (180). Most of these deaths occur in low-income nations. In well-resourced settings, HAdV-associated deaths are rare for immunocompetent individuals. In immunosuppressed patients however, disseminated disease can occur, for which case fatality rates can exceed 40% (349). Stringent infection containment measures are therefore essential for preventing nosocomial infection in these vulnerable patients.

2.3.2 Classification

The *Adenoviridae* family consists of six different genera and can infect a wide variety of vertebrate hosts. Currently recognised genera include *Atadenovirus* (reptiles, birds, ruminants, and marsupials) (350-353), *Aviadenovirus* (birds) (354-356), *Ichadenovirus* (fish) (357, 358), *Mastadenovirus* (mammals) (359-363), *Siadenovirus* (amphibians and birds) (364, 365), and *Testadenovirus* (turtle) (366). The *Mastadenovirus* genus, which contains more than 50 different viral species, is the only genus known to cause human infections.

Species demarcation within *Mastadenovirus* is based on a combination of the following traits: phylogenetic distance, genome organisation, nucleotide composition, oncogenicity in rodents, host range, cross-neutralisation, ability to recombine, haemagglutination, and the number of virus-associated RNA genes (367). HAdV may be grouped into seven different species (A-G), which are currently divided into 113 different proposed HAdV genotypes (<http://hadvvg.gmu.edu/>) (Table 2.2).

Historically, serological studies were used to differentiate HAdV and this resulted in the classification of the first 51 HAdV serotypes (Table 2.2). Restriction digest profiles were used to uncover genomic variation within serotypes (368, 369). As DNA sequencing and bioinformatic analysis have become more accessible, HAdV classification has shifted towards these less time consuming and resource-intensive methods (370-372). It is now known that homologous recombination plays an important role in the evolution of HAdV (373-377). Therefore, whole genome sequencing and phylogenetic analyses are critical to the designation of new HAdV types and for accurate and precise classification (376, 378-380). Presently, HAdV typing

is commonly based on sequencing of a partial hexon gene region (371, 381-383), and this is the approach that is used in **chapter six**.

Table 2.2. Human adenovirus species and types.

Species	Type
A	12, 18, 31, 61
B	3, 7, 11, 14, 16, 21, 34, 35, 50, 55, 66, 68, 76-79, 106
C	1, 2, 5, 6, 57, 89, 104, 108
D	8-10, 13, 15, 17, 19, 20, 22-30, 32, 33, 36-39, 42-49, 51, 53, 54, 56, 58-60, 62-65, 67, 69-75, 80-88, 90-103, 105, 107, 109-113
E	4
F	40, 41
G	52

2.3.3 Structure and genome organisation

AdVs possess non-segmented, double-stranded DNA genomes which are encapsidated by a non-enveloped, pseudo-T=25 icosahedral shell measuring between 70-90 nm in diameter (384, 385). The capsid is comprised of 240 hexon trimers and 12 vertex capsomers each formed by a penton base with a protruding fibre protein trimer (386-388). These fibre proteins engage with cellular receptors and play an important role in tissue tropism (389-393).

The DNA genome, which can range between 25-48 kb depending on the type, encodes for approximately 40 different proteins (367, 394). The AdV genome can be loosely organised into early (E1-E4) and late gene regions (L1-L5) (Figure 2.6). Proteins encoded by the early regions are largely non-structural and involved in the modulation of host cellular machinery, whilst the late gene products are important for virion assembly and maturation (394).

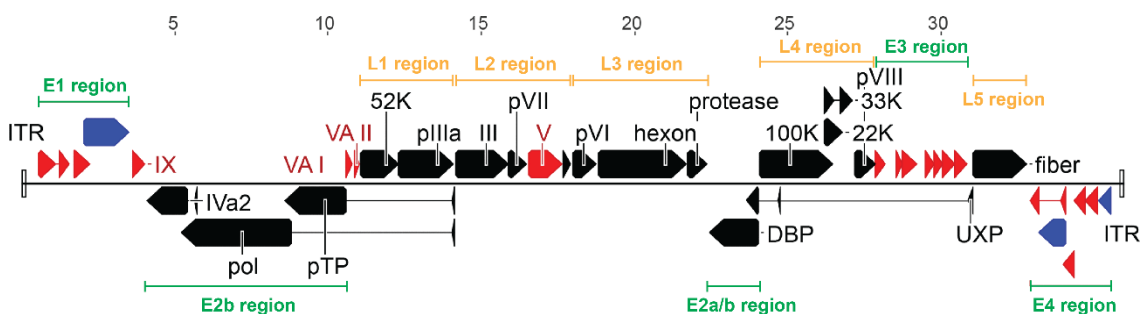


Figure 2.6. Genome organisation of HAdV type C5.

The genome for HAdV type C5 can be roughly grouped into early (E) and late (L) gene regions, which are labelled in green and yellow, respectively. Coloured arrows are used to depict the different genes that are conserved across all genera (black), present in more than one genus (blue) or found only in *Mastadenovirus* (red). The numbers at the top indicate nucleotide position in kb. Figure is adapted from (367).

2.3.4 Clinical manifestation and transmission

HAdVs are highly communicable viral pathogens; that can be shed at elevated levels in faeces (up to 10^{10} copies/g) and other bodily secretions (395), and possess a low illness-inducing dose of $\sim 10^6$ TCID₅₀ units (396). Following exposure, the incubation period can range from two days to two weeks (4, 397, 398). HAdVs can cause a wide spectrum of clinical manifestations depending on the infecting strain (Table 2.3). This can range from respiratory illness to keratoconjunctivitis to gastroenteritis but can also include rarer manifestations such as myocarditis and encephalitis (4) (Table 2.3).

The duration of illness can also vary greatly. For example, during gastroenteritis, diarrhoea can often last for up to two weeks (399), whilst for epidemic keratoconjunctivitis clinical illness typically lasts for one to three weeks (400). Depending on infecting strain and resulting symptoms, HAdV may also be transmitted through a variety of pathways such as the faecal-oral route (commonly via contaminated water) (401, 402), inhalation of aerosolised respiratory secretions (403), intranasal and intraocular inoculation (404), as well as through exposure to contaminated surfaces (405).

Table 2.3. Clinical manifestations of human adenovirus.

Target organ or system	Clinical manifestations	HAdV species or type	Ref
Gastrointestinal tract	Gastroenteritis	Species A, B, C, D, F, G	(348, 399, 406-408)
Respiratory tract	Mild respiratory illness, bronchiolitis, pneumonia, tonsillitis	Species B, C, E	(409-412)
Urinary tract	Haemorrhagic cystitis, dysuria	Species B	(413, 414)
Eye	Pharyngoconjunctival fever, epidemic keratoconjunctivitis, conjunctivitis	D8, D19, D37, B3, B7, B11, B14, Species E	(409, 415-417)
Heart	Myocarditis	C2, C5	(418, 419)
Liver	Hepatitis	C2, C5	(420)

2.3.5 Waterborne HAdV

Contaminated water has been linked to many outbreaks of gastroenteritis, pharyngoconjunctival fever and respiratory illness (421-424). A few notable, recent, waterborne HAdV outbreaks have been summarised in Table 2.4. Since both enteric and non-enteric HAdV display tropism for the gastrointestinal tract, these viruses can easily contaminate water bodies (395, 425-427). This generally occurs either via direct faecal contamination (i.e., faeces released by swimmers) or indirectly via sewage (428-430). For example, Wyn-Jones *et al.* (431) sampled recreational water sites across Europe and found adenovirus contamination in both freshwater (41.1%) and marine (27.4%) samples of which 13.6% contained viable virus. Additionally, studies have indicated that current sewage treatment practices such as UV irradiation may not be sufficient for the complete inactivation of infectious HAdV and other enteric viruses in effluents (432-434). This poses a problem for water reclamation, a process which is becoming of increasing global importance. HAdVs are also extremely stable in aquatic environments – one study found only one log reduction in viable virus titre after 160 days in surface and groundwater (435). These factors make it difficult to manage when water contamination events do occur.

Table 2.4. Some notable waterborne outbreaks of HAdV.

Aetiological agents	Location	Outbreak description	Year	Ref
F40/41. Many viruses, bacteria and parasites implicated.	Nokia, Finland	Sewage contamination of municipal drinking water supply. Estimated 8453 individuals affected with gastroenteritis.	2007	(423, 424)
B3	Hangzhou, China	Pharyngoconjunctival fever outbreak linked to swimming pool, 14.89% (134/900) of swimmers affected	2011	(436)
B7	Taiwan	Outbreak of upper respiratory tract infection linked to a swimming course; 106 patients identified.	2011	(437)
E4	Beijing, China	Pharyngoconjunctival fever outbreak linked to swimming pool, 55 patients identified.	2013	(438)

2.3.6 Prevention and control

There are currently no publicly available vaccines or antivirals for the prevention and treatment of HAdV infections. Therefore, management of HAdV outbreaks relies on implementation of effective infection containment strategies. This can include the isolation of infected patients, cohorting of personnel, and hand hygiene (439). It is also important to ensure that the cleaning of environmental surfaces is undertaken using the appropriate disinfectants, such as aldehyde and chlorine-based products (440). Since HAdV may also be transmitted through respiratory, intranasal, or intraocular inoculation, additional droplet precautions such as the use of masks and eye protection are also recommended (439, 441).

Due to a lack of specific antiviral therapies, HAdV disease management is primarily supportive. This may include rehydration therapy and the use of anti-diarrhoeal medication for AGE (322, 326), or mechanical ventilator support and intubation for severe respiratory disease (442). Management of HAdV infections in high-risk patient groups, such as solid organ transplant patients, may involve the off-label use of cidofovir and ribavirin (443, 444), although evidence for the benefits of the latter is weak (445).

An effective vaccine does exist for HAdV types E4 and B7; however, this vaccine is only available to US military personnel (446). A highly effective live-attenuated oral vaccine (E4 and B7) was first trialled in US military recruits in 1970 (447). However, the immunisation program was discontinued in early 1999 due to contract and supply issues (448). This was followed by several E4 and B7 epidemics at training centres (449-451). In March 2011, a new vaccine against HAdV types E4 and B7 was approved for use in US military personnel aged 17 to 50 (452). After reinstatement of HAdV vaccination, 100-fold declines in disease burden were observed (453).

HAdV E4 and B7 are just two of many HAdV types (Table 2.3), therefore, further efforts are required to develop vaccines and antivirals to protect against infections caused by other types. Ongoing molecular surveillance of circulating HAdV will be important for identifying targets for future vaccine and antiviral development efforts.

Aims and outline of thesis

Viral pathogens present significant public health and economic burden on society. However, very few human viruses currently possess effective antiviral therapies or vaccines. Furthermore, as exemplified by the COVID-19 pandemic, we are also faced with the threat of emerging and re-emerging viral pathogens. Therefore, current “one drug, one bug” approach is not enough to combat the ever-increasing threat. Instead, the development of broad-spectrum antivirals will be required to overcome this challenge.

However, even when antiviral therapies exist, its protection against the loss of human life can be limited. Similarly, even when effective vaccines are present, they do not offer complete immunity to infection. Instead, a combinatorial approach using both vaccines and treatments would be ideal. To develop a successful vaccine, however, it is crucial to understand viral evolution dynamics and identify prevalent and virulent strains, especially at a population level.

Therefore, this thesis aimed to address the threat of viral pathogens using both a reactive and proactive approaches. The reactive approach involved the development of broad-spectrum NNIs against positive-sense RNA viruses whereas the proactive approach included molecular surveillance of circulating strains norovirus and HAdV, two of the leading causes of gastroenteritis.

In **chapter four**, computer-aided methods were used to screen promising broad-spectrum NNIs against positive-sense RNA viruses, and initially focused on *Caliciviridae*. Two sets of complex-based pharmacophores were constructed using predicted binding configurations of JTK-109 and TMC647055 within calicivirus RdRp crystal structures. These models were then used to virtually screen approximately 200,000 commercially available structures. Selected compounds were then tested against norovirus and Zika virus RdRp, among others, to identify those with broad-spectrum inhibitory activity.

In **chapter five**, the molecular epidemiology of norovirus-associated AGE in Australia between January 2018 and December 2020 was investigated. A combination

of clinical faecal samples and monthly wastewater samples were sequenced and analysed to determine the prevalence and diversity of norovirus circulating within the community. Since the emergence of new norovirus strains is often marked by a corresponding increase in AGE activity, institutional gastroenteritis data obtained from public health authorities was also examined to investigate the potential emergence of novel strains.

In **chapter six**, a molecular epidemiological study was performed to investigate adenovirus-associated gastroenteritis in Australia over a four-year period (2018-2021). Although the role of HAdV types F40 and F41 in AGE is well recognised, the involvement of non-group F adenoviruses remains controversial. Therefore, to better understand the prevalence and role of these non-group F HAdV types in AGE, a combination of clinical sampling and next-generation sequencing of sewage samples was performed to investigate the diversity of HAdV present on a city-based population scale.

3 Materials and Methods

Methods that are used as is, in more than one research chapter are detailed here while all other methods have been described in the individual research chapters. Materials and reagents used in this thesis are listed in Table 3.1 with the details of manufacturer and source.

Table 3.1. General material and reagents used in the study.

Materials	Source and details
Bacterial Strains	
<i>E. coli</i> BL21 with Zika virus RdRp cloned into pET24a(+)	Synthesised by Alice Russo
<i>E. coli</i> T7 express with GII.4 Sydney 2012 RdRp cloned into pET26b(+)	Synthesised by Jennifer Lun
<i>Salmonella typhimurium</i> WG49	Strain UNSW103200 (ATCC 700730) from UNSW Microbiology Culture Collection
Mammalian cell lines	
Human hepatocytes (Huh7)	Gift from Dr. Mark Douglas
Viruses and replicons	
Hepatitis C virus genotype 2a replicon	Gift from John McLauchlan
Hepatitis A virus replicon	Gift from Volker Lohmann
MS2 bacteriophage	Strain UNSW103300 (ATCC 15597-B1) from UNSW Culture Collection
Antibodies	
Anti-polyhistidine-peroxidase antibody	Sigma-Aldrich (A7058)
Molecular size markers	
Colour prestained protein standard	New England BioLabs (P7712S)
Quickload purple 100 bp DNA ladder	New England BioLabs (N0551S)
Quickload purple 50 bp DNA ladder	New England BioLabs (N0556S)
1 kb Plus DNA ladder	New England BioLabs (N3200S)
Kits	
Amicon Ultra-4 centrifugal filters	Sigma-Aldrich (UFC8030)
BigDye v3.1 Terminator sequencing kit	Applied Biosystems (4337458)
CellTitre-Blue cell viability assay	Promega (G8080)
DNA Clean & Concentrator-5 Kit	Zymo Research (D4013)
HiScribe T7 High Yield RNA Synthesis Kit	New England BioLabs (E2040S)

Materials	Source and details
Immobilon Western HRP substrate kit	Millipore (P36599A)
iTaq Universal Probes One-Step kit	Bio-Rad (1725141)
iTaq Universal SYBR Green One-Step kit	Bio-Rad (1715151)
iTaq Universal SYBR Green Supermix	Bio-Rad (1725121)
KAPA HiFi HotStart ReadyMix	Roche (7958935001)
Luciferase assay system	Promega (E1500)
Monarch RNA Cleanup Kit	New England BioLabs (T2050S)
Pierce BCA Protein assay kit	Life Technologies (23225)
Platinum SuperFi II Green Master Mix	Invitrogen (12369050)
Pur-A-Lyzer Maxi dialysis kit	Sigma-Aldrich (PURX12015)
QIAamp Viral RNA kit	Qiagen (52904)
QIAprep spin plasmid miniprep kit	Qiagen (27104)
Quant-IT PicoGreen dsDNA assay kit	Life Technologies (P11496)
SuperScript III One-Step RT-PCR System with Platinum <i>Taq</i> High Fidelity DNA Polymerase	Invitrogen (12574030)
SuperScript IV VILO Master Mix	Invitrogen (11756050)
SuperScript VILO Master Mix	Invitrogen (11755050)
TGX FastCast Acrylamide Kit 10%	Bio-Rad (1610173)
Trans-IT mRNA kit	Mirus Bio (MIR2250)
Reagents	
β -mercaptoethanol	Sigma-Aldrich (M3148)
Adenosine 5' triphosphate (rATP)	Promega (P1132)
Agarose (UltraPure)	Invitrogen (16500500)
Agar powder	VWR Chemicals (20767)
Benzonase Nuclease (250 U/ μ L)	Sigma-Aldrich (E1014)
Bio-Scale Mini Profinity IMAC cartridges	Bio-Rad (7324610)
Bovine serum albumin	Sigma-Aldrich (A3059)
Bromophenol blue	Sigma-Aldrich (B8026)
Calcium chloride (CaCl ₂) solution (1M)	Amresco (E506)
CellLytic B Cell Lysis Reagent	Sigma-Aldrich (B7435)
CellLytic B Cell Lysis Reagent (10x)	Sigma-Aldrich (C8740)
Coomassie Brilliant Blue R-250 dye	Bio-Rad (1610400)
Deoxyribonucleotide triphosphates (dNTPs)	New England BioLabs (N0447S)
Dextran	Sigma-Aldrich (D9260)
DNase I	New England BioLabs (M0303S)
Dimethyl Sulfoxide (DMSO)	Sigma-Aldrich (D4540)
Diothiothreitol (DTT)	Astral Scientific (C-1029)
Disodium hydrogen phosphate (Na ₂ HPO ₄)	Sigma-Aldrich (S3264)
Ethylenediaminetetraacetic acid (EDTA)	Sigma-Aldrich (E8008)

Materials	Source and details
ExoSAP-IT PCR Product Cleanup Reagent	Applied Biosystems (78201.1.ML)
Foetal Bovine Serum (FBS)	Sigma-Aldrich (12003C)
Gel Loading Dye, Purple (6x)	New England Biolabs (B7024S)
GlutaMax Supplement	Life Technologies (35050061)
Glycerol	Sigma-Aldrich (G5516)
Glucose	Univar (A783-500G)
Guanosine 5' triphosphate (rGTP)	Promega (P1152)
Imidazole	Sigma-Aldrich (I5513)
Isopropyl-b-D-thiogalactopyranoside (IPTG)	Sigma-Aldrich (11411446001)
Kanamycin	Sigma-Aldrich (K1377)
Lysozyme	Sigma-Aldrich (L7651)
Magnesium sulfate (MgSO ₄)	Sigma-Aldrich (230391)
Manganese (II) chloride (MnCl ₂)	Sigma-Aldrich (M1787)
Methanol	Univar (A2314)
Monopotassium phosphate (KH ₂ PO ₄)	Sigma-Aldrich (P9791)
Peptone	Amresco (J849)
Polycytidylic acid (poly C)	Sigma-Aldrich (P4903)
Polyuridylic acid (poly U)	Sigma-Aldrich (P9528)
Protease inhibitor cocktail	Sigma-Aldrich (S8830)
Ribonucleotide triphosphates (rNTPs)	Promega (P1221)
RNAse A	Sigma (R4642)
RNAseZap RNase Decontamination solution	Invitrogen (AM9780)
Sodium chloride	Univar (AJA465)
Sucrose	Sigma-Aldrich (S9378)
SYBR Safe DNA Gel Stain	Invitrogen (S33102)
Triton X-100	Ajax FineChem (1552)
Trypsin-EDTA (0.5%)	Life Technologies (15400054)
Tween 20	Sigma-Aldrich (P1379)
Yeast extract	Sigma-Aldrich (70161)
Antiviral compounds	
PPNDS	Molport (MolPort-003-983-727)
BCX-4430	MedChemExpress (HY-18649A)
Various test compounds	Specs and ChemBridge
Buffers	
Bacterial lysis buffer	50 mM Tris-HCl, 20 mM NaCl, Lysozyme (100 mg/mL), Benzonase (50 U/mL), 10 mM DTT, 0.1% Triton X-100 (v/v), 2 mM MgCl ₂ , RNAse A, Protease Inhibitor, CellLytic B lysis reagent

Materials	Source and details
HEPES buffer	Life Technologies (15630106)
Phosphate buffered saline (PBS)	137 mM NaCl, 2.7 mM KCl, 10 mM Na ₂ HPO ₄ , 1.8 mM KH ₂ PO ₄
Protein equilibration buffer	50 mM Tris-HCl, 500 mM NaCl, 10 mM imidazole, 5% glycerol (v/v), 0.1% Triton X-100 (v/v)
Protein elution buffer	50 mM Tris-HCl, 500 mM NaCl, 300 mM imidazole, 5% glycerol (v/v), 0.1% Triton X-100 (v/v)
Protein dialysis buffer 1	150 mM NaCl, 5% glycerol (v/v), 0.1% Triton X-100 (v/v), 50 mM Tris-HCl and 1 mM DTT
Protein dialysis buffer 2	50 mM NaCl, 5% glycerol (v/v), 0.1% Triton X-100 (v/v), 50 mM Tris-HCl and 1 mM DTT
SDS-Page reducing buffer (2x)	125 mM Tris HCl (pH 7.5), 20% (V/V) Glycerol, 4% (w/v) SDS, 0.1% (w/v) bromophenol blue, 5% (v/v) β-mercaptoethanol
Tris-HCl (pH 7.5), (1M)	Life Technologies (15567027)
Tris/Acetate/EDTA buffer	Life Technologies (24710030)
Tris/Glycine/SDS buffer	25 mM Tris, 192 mM glycine, 20% methanol (v/v)
Media	
Dulbecco's Modified Eagle Medium (DMEM)	Life Technologies (11965118)
DMEM complete	DMEM with 10% FBS (v/v), 2 mM GlutaMax and 10 mM HEPES buffer
Luria Bertani (LB) broth	1% (w/v) NaCl, 1% (w/v) peptone, 0.5% (w/v) yeast extract
LB agar	LB broth with 1.5% agar (w/v)
Terrific broth (TB)	1.2% peptone (w/v), 2.4% yeast extract (w/v), 0.4% glycerol (w/v), 0.17 M KH ₂ PO ₄ , 0.72 M K ₂ HPO ₃
Peptone yeast glucose broth (PYGB)	1% peptone (w/v), 0.1% yeast extract (w/v), 0.8% NaCl (w/v), 2 mM CaCl ₂ , 0.1% glucose (w/v)
Peptone yeast glucose agar	PYGB with 1.4% agar (w/v)
Peptone yeast glucose semi-solid agar	PYGB with 0.7% agar (w/v), 0.5% kanamycin solution (25 mg/mL) (v/v), 12 mM MgSO ₄
Software	
Geneious Prime (v2021.1.1)	Biomatters Ltd
FinchTV	Geospiza, Inc
MEGA (version X)	https://www.megasoftware.net/
ChemDraw (v17.1)	Perkin Elmer
Discovery Studio	Dassault Systèmes, BIOVIA Corp
LigandScout	Inte:Ligand GmbH
GraphPad Prism (v9.0.0)	GraphPad Software, Inc
Rotor-Gene Q Series Software (v2.3.5)	Qiagen

3.1 General molecular biology methods

3.1.1 Agarose gel electrophoresis

Agarose gel electrophoresis was performed to visualise PCR products. PCR amplicons (4 μ l) were prepared with gel loading dye (New England Biolabs, Ipswich, MA, USA) and loaded onto 2% agarose gels (prepared as 2% w/v ultrapure agarose in 1x Tris-acetate-EDTA (TAE) buffer) and run for 35 minutes at 110V. Gels were pre-stained with SYBR Safe DNA Gel Stain (Invitrogen, Carlsbad, CA, USA) and PCR amplicons were visualised using a UV transilluminator (Gel Doc, Bio-Rad, CA, USA).

3.1.2 Purification of PCR products

Enzymatic purification of PCR products was performed to remove contaminants such as unincorporated nucleotides and primers, which would interfere with the downstream sequencing reaction. ExoSAP-IT PCR Product Cleanup Reagent (Applied Biosystems, Carlsbad, CA, USA) containing exonuclease I and shrimp alkaline phosphatase was mixed with PCR in a ratio of 1:4 (enzyme:PCR product). The reaction was incubated at 37°C for 30 minutes and then at 80°C for 15 minutes to denature the ExoSAP-IT enzymes. The purified product was then stored at -20°C until required.

3.1.3 Sanger sequencing

Reactions (20 μ l) were made up in DNase free water and contained 3.5 μ l of 5x sequencing buffer, 1 μ l of Big Dye v3.1 (Applied Biosystems, Carlsbad, CA, USA), 3.2 μ M of primer and 2 μ l of ExoSAP-IT treated PCR products (roughly 50 ng). Thermocycling conditions consisted of 25 cycles of 96°C for 10 s, 50°C for 5 s and 60°C for 4 min. This was followed by ethanol/EDTA precipitation clean-up to remove unincorporated dye-labelled terminators. Briefly, this involved the addition of 5 μ l of 125 mM of EDTA to help stabilise extension products and 60 μ l of absolute ethanol to precipitate DNA. Reactions were then incubated at room temperature for 20 min, centrifuged at 12,000 \times g for 20 min and supernatants discarded. The pellet was washed with 180 μ l of fresh 70% v/v ethanol and centrifuged again at 12,000 \times g for 15 min. The pellet was finally dried using a 90°C heat block for 5 min. The reactions were then submitted to the Ramaciotti Centre for Genomics, UNSW, Australia for sequencing on an Applied Biosystems 3730 DNA Analyser (Applied Biosystems).

4 Development of broad-spectrum non-nucleoside inhibitors for positive-sense RNA viruses using *in silico* methods.

4.1 Abstract

Viruses are a global human health burden, however, few have targeted antiviral therapies. The current “one drug, one bug” approach is unsuitable given the increasing incidence of emerging viral pathogens, instead, broad-spectrum strategies are required. Viral RdRps are attractive drug targets due to their lack of mammalian homologues and conservation across RNA viruses. For example, recent studies repurposing HCV antivirals have identified an alternative allosteric binding site (Site-B) conserved throughout *Caliciviridae* RdRps. This chapter aimed to utilise Site-B to develop broad-spectrum antivirals against *Caliciviridae*. Pharmacophore models were constructed using docking configurations of two antivirals predicted to bind within Site-B (JTK-109 and TMC647055) within calicivirus RdRp crystal structures. These models were used to virtually screen ~200,000 commercially available compounds. Resulting structures were filtered based on molecular properties to identify “drug-like” candidates and 33 “hit” compounds were selected for further study. These 33 compounds were initially tested for inhibition of human norovirus (NoV) RdRp, and one promising compound (NCS-013) was trialled against feline calicivirus (FCV) RdRp to assess cross-genera inhibition. NCS-013 inhibited both RdRps at 50 μ M (NoV: $55.9 \pm 3.8\%$, FCV: $51.3 \pm 5.4\%$). Since the pharmacophore models were based on HCV-targeting molecules, compounds were also examined against the RdRp of Zika virus (*Flaviviridae*). Additionally, eight promising candidates were trialled against replicons of HCV (*Flaviviridae*) and hepatitis A virus (HAV: *Picornaviridae*) to explore inter-family inhibition. NCS-013 demonstrated inhibition of Zika virus RdRp at 100 μ M ($58.4 \pm 22.6\%$) and HCV/HAV replicons at 10 μ M ($62.5 \pm 23.6\%$, $45.6 \pm 10.1\%$ respectively). Due to the broad-spectrum inhibition displayed by NCS-013, it was used as a scaffold for derivative searching, which identified a further 11 compounds for assessment. Of these, NCS-013A demonstrated cross-family inhibition of HAV ($58.9 \pm 17.7\%$ at 10 μ M) and Zika virus ($42.1 \pm 22.6\%$ at 50 μ M). This study identified two structures – NCS-013 and NCS-013A – with potential broad-spectrum activity. As these compounds target three viral families, they could be useful as scaffolds for future broad-spectrum antiviral discovery.

4.2 Introduction

4.2.1 The urgent need for antivirals

The risk of viral epidemics from emerging and re-emerging viruses has never been greater, as exemplified by the current coronavirus pandemic. Changing climates, poor land use practices, deforestation and ever-increasing globalisation have brought humans into closer contact with wild animals and arthropods, and as a result, the viruses that they carry. Since the start of the millennium, several major epidemics of emerging and re-emerging viruses have occurred in humans, a few examples include SARS-CoV-1, SARS-CoV-2 and MERS-CoV (*Coronaviridae*), Zika virus (*Flaviviridae*), and Marburg and Ebola viruses (*Filoviridae*). In addition, both wildlife and farmed animals have also been affected, examples include H5N1 avian influenza (454), foot and mouth disease virus in cattle (455), and African swine fever virus in pigs (456). During these human epidemics, outbreak containment in many cases has been reliant on the implementation of infection control precautions with varying degrees of success (457-462). Concomitantly, the development of antiviral agents and vaccines was undertaken to reduce the loss of human lives.

Approved antivirals exist only for a small number of human viruses including hepatitis B virus (HBV), hepatitis C virus (HCV), some human papillomaviruses, respiratory syncytial virus, some herpesviruses, human immunodeficiency virus (HIV), influenza virus, and most recently SARS-CoV-2 (8-12). Despite the urgent need for antiviral drugs to target these and other clinically significant viral families and future emerging viruses, the reality is that the drug development process has never been slower (463, 464).

4.2.2 The development of early antivirals

Since the approval of the first antiviral drug, idoxuridine, for the treatment of viral eye infections including herpes simplex keratitis, by the US Food and Drug Administration (FDA) in 1963, more than 118 antiviral drug therapies have been formally approved (10, 11, 465). Historically, a number of the early antiviral compounds were discovered serendipitously, for example the aforementioned idoxuridine was first synthesised as a potential anticancer drug (466), as was adenine

arabinoside (vidarabine) (467, 468), whilst acyclovir was originally designed to inhibit adenosine deaminases to extend the half-life of vidarabine (469, 470).

4.2.3 Current strategies for antiviral development

Modern drug discovery, however, follows a more systematic approach. There are three general approaches to the initial lead generation phase of drug discovery: 1) ligand-based, 2) structure-based and 3) high-throughput screening (HTS) (148, 153, 154). Following successful identification of promising compounds, structure-activity relationship studies can commence to improve the drug-like properties of active compounds. The ligand-based approach relies on having a database of known active/inactive compounds for quantitative structure-activity relationship studies (153). From this, the chemical features required for activity may be discerned and represented using pharmacophore models which can later be used to virtually screen compound databases (155). Alternatively, the structure-based approach utilises knowledge of the binding site and relies on the existence of high-quality protein models. In this approach, libraries of compounds may be docked into the binding site and scored based on their predicted protein-ligand interactions or pharmacophore models may be generated based on the properties of the binding site (156, 471). Due to an absence of sufficient knowledge of both existing ligands and the binding pocket itself, a combination of ligand- and structure-based methods (termed complex-based) was used in this research to develop calicivirus antivirals.

4.2.4 Classes of antiviral compounds and their broad-spectrum potential

The most important consideration when designing antivirals is the choice of target. Antiviral compounds can be broadly classified into two groups – host-targeting antivirals and direct-acting antivirals (DAAs), and this research utilised a DAA approach. DAAs work by targeting highly specific viral proteins, commonly the protease or polymerase. Major successes in suppressing HIV in infected patients and curing HCV infection within 8-12 weeks have demonstrated the enormous societal benefit and antiviral potency of this group of antivirals (110-112). By targeting viral proteins instead of the host, a reduced side-effect profile is observed, leading to better treatment outcomes and drug adherence (87, 88).

The RNA-dependent RNA polymerase (RdRp) is an attractive target for antiviral development as it is highly conserved across viral families and there are no mammalian host homologues, minimising off-target effects. There are two classes of antivirals that act on the polymerase – nucleoside analogues (NAs) which are incorporated during viral replication, causing chain termination, and non-nucleoside inhibitors (NNIs) which bind allosterically to the RdRp to prevent conformational changes that are necessary for replication (472). Although DAAs are not classically believed to exhibit broad-spectrum activity due to the highly specific nature of their viral targets, recent studies repurposing existing antivirals for use against new viral targets have indicated the potential broad-spectrum activity of several of these compounds (473-475).

Many of the more broad-spectrum antivirals are NAs (120, 476-478) and this is not surprising due to the nature of polymerase active sites, where all incoming nucleotides or NAs bind, which are surrounded by several highly conserved motifs (479). More recently however, studies examining the potential for repurposing existing antiviral compounds have shown that as well as NAs, NNIs can also display broad-spectrum activity, not only across species or genera within the same viral family (480-482), but also across different viral families (147, 483). This illustrates the potential for developing broad-spectrum NNIs to address the lack of calicivirus antivirals, a family of viruses central to this thesis. Previous work has demonstrated that HCV NNIs (thumb 1 RdRp inhibitors) JTK-109, TMC647055 and Beclabuvir also possessed broad-spectrum antiviral activity against several different calicivirus RdRps (147). The study also provided strong evidence that the binding site of these compounds is positioned within a highly conserved RdRp pocket within the thumb domain which was termed Site-B (Figure 4.1) (114, 147).

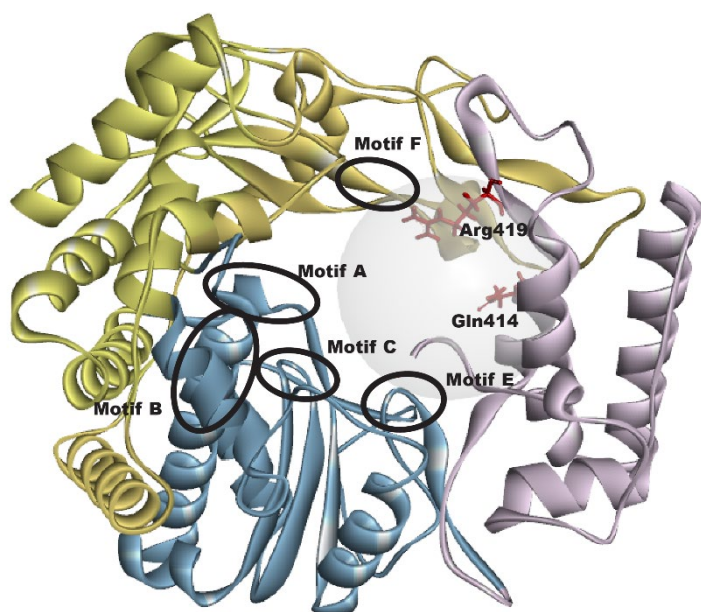


Figure 4.1. Location of the NNI binding pocket Site-B in the calicivirus RdRp.

The NNI binding pocket Site-B is represented by a grey sphere and is positioned within the thumb region. Interacting Site-B residues, Gln414 and Arg419 are represented by red sticks and labelled. The fingers (yellow), palm (blue) and thumb (pink) domains on human norovirus GII.4 RdRp (PDB-ID: 4LQ9) (114) are shown. The locations of the conserved RdRp motifs are circled. Ribbon diagram was generated using the Discovery Studio 2017 R2 software suite (Dassault Systèmes, BIOVIA Corp).

4.2.5 Aims

The overall aim of this chapter was to identify promising broad-spectrum NNIs against positive-sense RNA viruses, and initially focused on *Caliciviridae*. To achieve this aim, a series of complex-based pharmacophores were constructed using predicted binding configurations of JTK-109 and TMC647055 within calicivirus RdRp crystal structures and then used to virtually screen approximately 200,000 commercially available structures. Selected compounds were first examined for antiviral activity against human norovirus RdRp. Compounds that successfully inhibited human norovirus RdRp were also trialed against feline calicivirus to uncover cross-genera inhibition. To further identify compounds with broad-spectrum activity, all compounds in the study were also examined for inhibition of the Zika virus RdRp. Additionally, promising compounds were also examined for inhibition of HCV genotype 2a (G2a) and hepatitis A virus (HAV) replication, using a replicon model in liver Huh7 cells.

4.3 Methods

4.3.1 Multiple sequence alignment

To identify the conserved residues that form the allosteric binding pocket, Site-B, and corresponding residues across calicivirus RdRp structures, a multiple sequence alignment was performed for human norovirus, sapovirus (SaV), rabbit haemorrhagic disease virus (RHDV) and murine norovirus (MNV) (Table 4.1). The protein sequences were downloaded in the FASTA format from the relevant entry on the Protein Data Bank (PDB, www.rcsb.org) (484). The sequence alignment was conducted using Clustal Omega (<https://www.ebi.ac.uk/Tools/msa/clustalo/>) (485). The structures used in the current study are summarised in Table 4.1.

Table 4.1. Crystal structures used for docking and sequence analyses.

PDB ID	RdRp origin	Resolution (Å)	Reference
4LQ3	Human norovirus GII.4	2.60	(114)
4LQ9	Human norovirus GII.4	2.04	(114)
3UQS	Murine norovirus CW1	2.00	(486)
4O4R	Murine norovirus CW1	2.40	(487)
1KHV	Rabbit haemorrhagic disease virus	2.50	(488)
2CKW	Sapovirus	2.30	(489)

4.3.2 Preparation of structures and docking

All computational work was carried out using Discovery Studio (DS) 2017 R2 software suite (Dassault Systèmes BIOVIA Corp, CA, USA). Crystal structures for calicivirus RdRps were downloaded from the PDB (Table 4.1). Water molecules and other co-crystallised molecules were removed, and hydrogens were added. A large binding pocket was defined from residues chosen using visual inspection to encompass Site-B. Residues Lys166, Arg392, Ser410, Arg413, Gln414, Arg419 and Asn505 were chosen (residues are named and numbered by position on 4LQ9 crystal structure). Equivalent residues identified from the multiple sequence alignment were used for the other calicivirus RdRps. The ligands were sketched, appropriately protonated/deprotonated and minimised using the Smart Minimiser and the CHARMM force-field (490) in DS with default settings prior to docking. Protonation/deprotonation states were determined by checking estimated pKa using ChemDraw v17.1 (PerkinElmer).

Docking was performed using the program GOLD (Cambridge Crystallography Data Centre, UK, www.ccdc.cam.ac.uk) (491) through the DS interface (Figure 4.2). Ligands were docked using default parameters except for the number of runs (set to 100); 'Detect Cavity' and 'Early Termination' (set to 'False'); and 'Flexibility' which was fully enabled. In each instance, the pose with the highest GoldScore in the largest cluster was chosen for further analysis of receptor-ligand interactions. Clustering was performed at approximately 2Å root mean square deviation (RMSD) of heavy atoms.

4.3.3 Generation of complex-based pharmacophores and virtual screening

Pharmacophores are representations of the spatial arrangement of features necessary for ligand-receptor binding. Complex-based pharmacophore are based on the docking interactions between a ligand and receptor. Complex-based pharmacophore generations and virtual screening were performed independently using two programs, Discovery Studio and LigandScout (LS) and used to screen the publicly available SPECS database (www.specs.net). The initial virtual screening and compound selection process is summarised in Figure 4.2.

4.3.3.1 Pharmacophore generation using DS

The selected poses from the JTK-109 anion and TMC647055 dockings were used to generate complex-based pharmacophores using the 'Receptor-Ligand Pharmacophore Generation' protocol in DS. Pharmacophores were generated using default setting except 'Maximum Features' which was set to 15 and 'Minimum Interfeature Distance' which was set to 1.5Å. The pharmacophore containing all features was used in each case for further database screening.

4.3.3.2 Pharmacophore generation using LS

The selected poses from the JTK-109 anion and TMC647055 docking runs were also used to generate pharmacophores using LigandScout 4.1.10 software (Inte:Ligand GmbH) (492). The protein and docked ligand were saved separately and imported into LigandScout. The active site was defined using the same binding pocket residues, as in section 4.3.2. Both the protein and docked ligand were minimised using the 'Minimise MMFF94 Energy of Core Molecule and Side Chains' option before generating the pharmacophore using the automated pharmacophore generation procedure.

4.3.4 Virtual screening

The SPECS database (www.specs.net) containing 196,650 compounds was used for virtual screening and database preparation was previously performed by Dr Drwal (a former group member) (493). The database was then screened with the pharmacophores generated in DS and LS to identify compounds with novel scaffolds that matched the pharmacophores. To reduce the large hit-lists into a reasonable number for biological testing, the database was screened sequentially if necessary. The virtual screening process is summarised in Figure 4.2.

4.3.4.1 *Virtual screening using DS*

DS utilises the 'Catalyst' searching algorithm to perform database screening, which involves a rapid preliminary screening process followed by a rigorous atom by atom mapping of the compounds to the pharmacophore query (494). Stepwise screening of the SPECS compound database was performed using the '3D Database Search' protocol in DS for both the JTK-109 and TMC647055 set of pharmacophores previously generated in DS. Pharmacophores were used sequentially starting from the least restrictive pharmacophore (i.e., least features) to the most restrictive. This process was repeated until either all pharmacophores were utilised or until there were fewer than 100 compounds remaining. If a reduction of the number of hits below 500 was not achieved after all pharmacophores were sequentially screened, then all resulting hits were excluded from further consideration.

4.3.4.2 *Virtual screening using LS*

A stepwise approach was not possible in LS since the pharmacophores generated in LS were generally more restrictive (more features) resulting in far fewer hits, sometimes yielding none. When this occurred, the pharmacophore was modified to be less restrictive, this was repeated until the pharmacophore returned hits. As a result, database screening was performed with each pharmacophore separately and the resulting hits were combined. In instances where the number of hits found was greater than 200, the largest hit list was then compared with the second largest hit list and only the hits common to both lists were considered for further analysis.

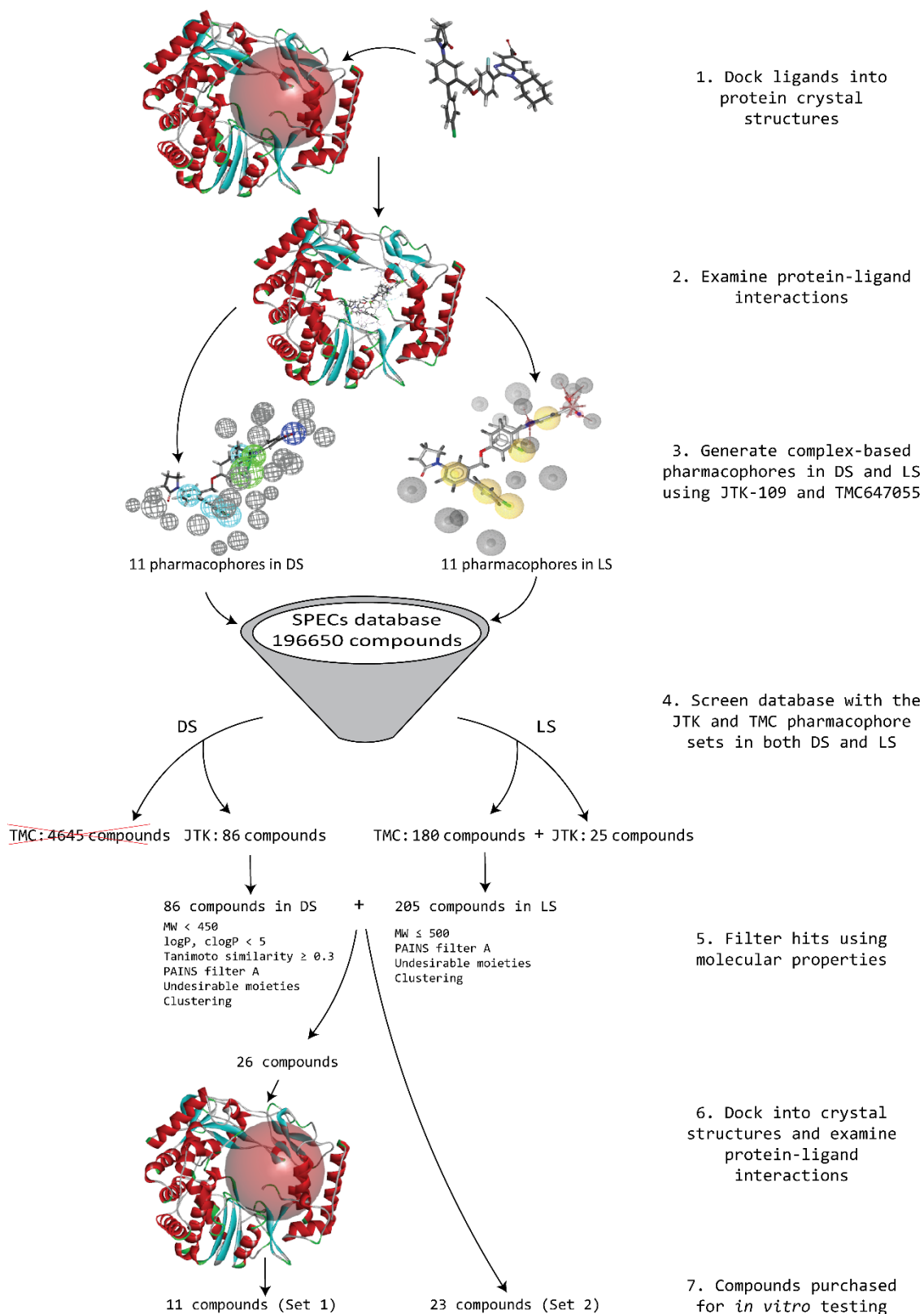


Figure 4.2. Virtual screening process.

Two sets of compounds, 34 in total were selected for *in vitro* analysis. The first set contained 11 compounds which were selected following all seven steps of the virtual screening process. The second set (n=23) was chosen using relaxed step 5 criteria and were not required to undergo step 6. The virtual screening process was as follows: Step 1) NNI compounds JTK-109

and TMC647055 were docked into six different calicivirus RdRp crystal structures (PDB IDs NoV: 4LQ3, 4LQ9; MNV: 3UQS, 4O4R; RHDV: 1KHV; RCV: 2CKW). Step 2) Predicted protein-ligand interactions were examined. Step 3) Two sets of pharmacophores were constructed from JTK-109 and TMC647055 independently using DS and LS. Step 4) The pharmacophore models were used to independently screen the SPECs compound database in both DS and LS. After sequential screening of the TMC647055 pharmacophores in DS, the number of compound hits did not reduce below 500 and so all resulting hits were excluded from further consideration and marked with a red cross. Step 5) The compound hitlists were combined, and various molecular filters applied. Step 6) Compounds were docked into the six calicivirus RdRp crystal structures and examined for interactions with Site-B residues. Step 7) Compounds were purchased for *in vitro* testing.

4.3.5 Initial antiviral compound selection

All resulting compound lists were combined into a single hitlist (n=291) and filtered using a combination of molecular properties and substructure filters (Figure 4.2). This hitlist was first clustered in LS using default settings, LS clusters compounds based on similar 3D pharmacophore features. After clustering the molecular weight (MW), partition coefficient for n-octanol/water (logP) and compound partition coefficient (ClogP) values of the compounds were checked and any compounds with MW>450 daltons (Da) or logP and ClogP>5 were excluded. The logP and ClogP values for each compound were determined using the chemical properties window in ChemDraw.

Compounds bearing some similarity to the original JTK-109 and TMC647055 were found using the “Find similar molecules by fingerprints” protocol in DS using the Tanimoto coefficient with default settings except for minimum similarity which was set to 0.30. These compounds (n=103) were then uploaded to the FAF4drugs server (<http://fafdrugs4.mti.univ-paris-diderot.fr/>) (495, 496) where they were filtered using the Pan Assay Interference Compounds (PAINS) A and undesirable substructures moieties filters. The remaining compounds were examined for clustering and in cases where more than one compound belonged to the same cluster, the compound with the lower MW was selected for molecular docking analysis.

All remaining compounds (n=26, Figure 4.2) were then appropriately protonated and minimised using the CHARMM force-field and docked into the protein structures prepared previously in section 4.3.2. Docking was first performed using default parameters (10 runs) except for ‘Detect Cavity’ and ‘Early Termination’ which

were set to 'False'. The top pose in the largest cluster was then examined for interactions with Arg392, Gln414 and Arg419 (or equivalent) across the six protein structures. Compounds making interactions across several structures were selected for more extensive docking analyses (100 runs). The top pose in the largest cluster was evaluated for interactions with the same residues and those that made interactions across several crystal structures (n=11, Figure 4.2) were purchased at $\geq 90\%$ purity for *in vitro* examination.

4.3.6 Selection of second set of antiviral compounds

Following testing of the initial set, an additional group of compounds was chosen using more relaxed criteria (Figure 4.2). Maximum compound MW was increased to 500 Da whilst logP, ClogP and Tanimoto similarity with JTK-109 and TMC647055 were no longer considered. Compounds were still uploaded to the FAF4drugs server (495, 496) and PAINS filter A and undesirable substructures moieties filters were applied. The remaining compounds were examined for clustering and in cases where more than one compound belonged to the same cluster, the compound with the lower MW was selected. To increase the scope of structures tested, compounds belonging to the same cluster as the initial set were also excluded. These compounds were not required to pass a two-step docking analysis. Finally, the remaining compounds (n=23), those that were not filtered out, were purchased at $\geq 90\%$ purity for *in vitro* testing (Figure 4.2).

4.3.7 Recombinant human norovirus GII.4 Sydney 2012 RdRp protein expression and purification

Human norovirus GII.4 Sydney 2012 RdRp (GenBank accession KT239579) was previously cloned into the expression vector pET26b+ and transformed into NEB T7 Express *Escherichia coli* (*E. coli*) (497). Overnight cultures of *E. coli* (5 mL, grown in LB broth containing 100 $\mu\text{g}/\text{mL}$ kanamycin) were diluted 1:100 in LB broth containing kanamycin and incubated at 37°C, shaking at 200 rpm until the OD₆₀₀ reached approximately 0.8. Protein expression was induced with 1 mM isopropyl β -D-1-thiogalactopyranoside (IPTG) at 20°C for 21 hours and shaking at 200 rpm. Cells were collected by centrifugation and stored at -80°C until use.

The bacterial pellet was resuspended in 1x CellLytic B buffer containing 50 mM Tris-HCl (pH 8.0), 20 mM NaCl, 2 mM MgCl₂, 200 mg/mL of lysozyme, 50U/mL of Benzonase, 2 µg/mL of RNase A solution, 10 mM DTT, 0.1% Triton-X and 1x EDTA-free protease inhibitor cocktail solution. Resuspended cells were incubated at room temperature for 30 minutes on a platform shaker at 100 rpm to allow for chemical lysis. Lysates were clarified by centrifugation at 18,400 *g* for 30 minutes at 4°C. Following centrifugation, NaCl and imidazole concentrations were adjusted to 500 mM and 10 mM respectively.

The lysate was loaded onto a Ni²⁺ column and purified with an imidazole gradient (10-300 mM) using an AKTA start dual-buffer system as described in (483) at the Recombinant Products Facility, UNSW, Sydney. The equilibration buffer contained 50 mM Tris-HCl, 500 mM NaCl, 5% glycerol (v/v), 0.1% Triton-X (v/v) and 10 mM imidazole. The elution buffer was composed of equilibration buffer with 300 mM imidazole. Presence of the norovirus RdRp in the eluate was verified by western blot analysis. Briefly, protein samples were mixed with equal volumes of sample loading buffer and resolved on a 12% SDS-PAGE gel (Bio-Rad, CA, USA). Proteins were transferred from the gel onto a nitrocellulose membrane by electrophoresis (1 hour at 110 V) in Tris/Glycine buffer containing 20% (v/v) methanol. The membrane was then blocked at room temperature for 1 hour in 5% (w/v) skim milk powder dissolved in PBS with 0.1% (v/v) Triton X-100 (PBS-T). The membrane was washed three times in PBS-T for 5 minutes each, and then incubated for 1 hour with a 1:20,000 dilution of mouse monoclonal anti-polyHistidine horseradish peroxidase antibody (Sigma-Aldrich, St. Louis, MO, USA). The membrane was washed with PBS-T again and blots were developed with Immobilon Western Chemiluminescent HRP Substrate (Merck, Darmstadt, Germany). Imaging was performed using a LAS500 Imaging System (GE Healthcare, Little Chalfont, UK).

The purified protein was then dialysed to remove imidazole using a Pur-a-lyser kit using two buffers with decreasing concentrations of NaCl (150 or 50 mM NaCl, 5% glycerol (v/v), 0.1% Triton-X (v/v), 50 mM Tris-HCl and 1 mM DTT) and concentrated using an Amicon® Ultra centrifugal filter (10 kDa cut-off, Millipore, Tokyo, Japan). All buffers used during purification and dialysis were prepared at pH 7.2. The final protein

concentration was determined using a BCA Protein assay kit (Life Technologies). The RdRp was then aliquoted and stored at -80°C.

4.3.8 Recombinant Zika virus RdRp protein expression and purification

The coding sequence of Zika virus RdRp was derived from the African reference strain MR766 (GenBank accession LC002520) and modified to remove the 29 kDa N-terminal MTase domain. This was then cloned into expression vector pET24a+ and transformed into in *E. coli* strain BL21 (498). Protein expression and purification was performed as described in section 4.3.7 except for the use of Terrific Broth as the growth media and an induction temperature of 16°C. The imidazole gradient used for purification was also different (5-500 mM) and so the imidazole concentration in the equilibration and elution buffers were adjusted accordingly.

4.3.9 Human norovirus GII.4 RdRp fluorescent transcription activity assay

Following protein purification and quantification, the activity of the purified RdRp was confirmed using a fluorescent transcription activity assay with varying amounts of RdRp (200 ng to 1600 ng). In this assay, the formation of dsRNA was quantified using a fluorescent dye PicoGreen (Life Technologies) which binds to dsRNA, as described in (499, 500). The RdRp was first incubated with test compound or 0.5% DMSO control for 10 minutes at room temperature before the addition of the remaining reaction mixture containing the RNA template, ribonucleotide triphosphates and co-factors.

Each reaction (25 µL) was performed in black-bottomed 384-well plates containing 400ng of RdRp, 20 mM Tris-HCl (pH 7.5) 250 ng poly(C), 0.25 mM rGTP, 5 mM DTT, 2.5 mM MnCl₂, 0.005% Tween 20 (v/v), 0.01% BSA (v/v). Reactions were incubated for 1 hour at 30°C followed by termination of polymerase activity with 28 mM EDTA. PicoGreen dye was then added and incubated for 5 minutes protected from light. Fluorescence was then measured using a POLARstar Omega microplate reader (BMG Labtech, Ortenberg, Germany) (excitation: 480 nm, emission: 520 nm). Heat-inactivated RdRp was used as the negative control and to provide baseline fluorescence levels for test compounds. PPNDS, a known NNI (114) was used as a

positive inhibition control. Reactions were performed in triplicate. All statistical calculations were performed using Graphpad Prism software (v9.0.0).

All compounds were dissolved in 100% DMSO at 20 mM. The first set of compounds (n=11, Figure 4.2) were tested in a preliminary screen at final concentrations of 10 µM and 100 µM. The second set of compounds (n=23) were tested in a preliminary screen at 10 µM and 50 µM. A third set of compounds (n=11, detailed later in section 4.3.15) obtained from a similarity search was also tested at fixed concentrations 10 µM and 50 µM. The percentage inhibition of RdRp activity after treatment with test compounds was calculated using the following equation:

$$\text{Percentage inhibition} = 100 - \frac{100 \times (\text{sample well} - \text{mean treatment NSA})}{\text{mean MA} - \text{mean DMSO NSA}}$$

Where NSA = non-specific activity (background fluorescence) and MA = maximal activity (DMSO control).

4.3.10 Fluorescent transcription activity assays for measuring calicivirus

RdRp replication

After compounds were examined for inhibition of the activity of human norovirus RdRp, promising hits were also trialled against the RdRp of another member of the *Caliciviridae* family. This included feline calicivirus, which belongs to a different genus *Vesivirus*. Reaction setup for transcription assays was as described in section 4.3.9. Additionally, for binding studies, promising hits were also tested against the human norovirus GII.4 Sydney 2012 Q414A and R419A mutants that were generated previously in our laboratory (147). Reaction setup for these assays was as described in section 4.3.9, except for the amount of RdRp which was increased to 800 ng per reaction. Graphpad Prism (v9.0.0) was used to plot the IC₅₀ values.

4.3.11 Zika virus fluorescent RdRp activity assay

Selected compounds were also tested for inhibition of Zika virus polymerase activity using the fluorescent transcription assay. Reactions and calculations were performed as described in section 4.3.9 except for the RNA template and ribonucleotide triphosphates concentrations which were 12 ng polyU and 66 µM rATP instead. Compounds from the first (n=11) and second set (n=23) were tested for

inhibitory activity in a preliminary screen at 10 μM and 100 μM . A third set of compounds (n=11) obtained from a similarity search was tested for inhibition of RdRp activity at fixed concentrations 10 μM and 50 μM . Heat-inactivated RdRp was used as the negative control and to provide baseline fluorescence levels for test compounds and PPNDS, a known NNI (114) was used as a positive inhibition control. Each reaction was performed in triplicate.

4.3.12 Measuring HAV and HCV G2a replicon activity

Pilot replicon activity assays were conducted to determine the optimal replicon concentration for use in inhibition assays. Viral replicons are self-replicating sub-genomic viral RNA, where the structural proteins have been deleted or replaced with a reporter gene such as firefly luciferase. Human hepatocyte Huh7 cells were maintained indefinitely in Dulbecco's Modified Eagle's Medium (DMEM) supplemented with 10% (v/v) foetal bovine serum, 2 mM Glutamax and 10 mM HEPES. Huh7 cells were seeded in 96 well plates at a density of 5,000 cells per well in 100 μL of complete DMEM and incubated for 24 hours at 37°C. Milli-Q water was added to the wells along the edge of the plate to offset the edge-effect and prevent evaporation from reaction wells.

Transfection solutions contained replicon RNA, Boost, TransIT from the TransIT RNA transfection kit (Mirus Bio LLC, Madison, WI, USA) and serum-free DMEM. The solution was incubated at room temperature for 2.5 minutes to allow the transfection complexes to form before 10 μL of transfection solution was added to each well. Wells without RNA were used to confirm successful transfection and plates were incubated at 37°C for 72 hours.

Media was then removed from each well and cells were washed with 100 μL PBS. Cell lysis buffer (50 μL) was added to each well and the plate was rocked for 10 minutes protected from light. Plates were transferred to a POLARstar Omega microplate reader where luciferase assay solution (100 μL) (Promega, Madison, WI, USA) was injected into each well and luminescence output was recorded. Each reaction was performed in quadruplicate.

4.3.13 Examining compound inhibition of HAV and HCV G2a replication using a replicon model

Compounds that displayed any dose-dependent inhibition of norovirus or Zika virus polymerase activity were also tested for antiviral activity using the HAV and HCV G2a replicons in cell culture studies. The HAV replicon based on strain HM175 18f (GenBank accession M59808) and containing a luciferase reporter gene in place of the HAV P1 domain was kindly provided by Prof. Dr. Volker Lohmann (University of Heidelberg, Germany) (Figure 4.3A) (501). The tricistronic HCV G2a replicon (tri-JFH1) containing neomycin resistance and luciferase reporter genes was kindly provided by Prof. John McLauchlan (The University of Glasgow, Scotland) (Figure 4.3B) (502).

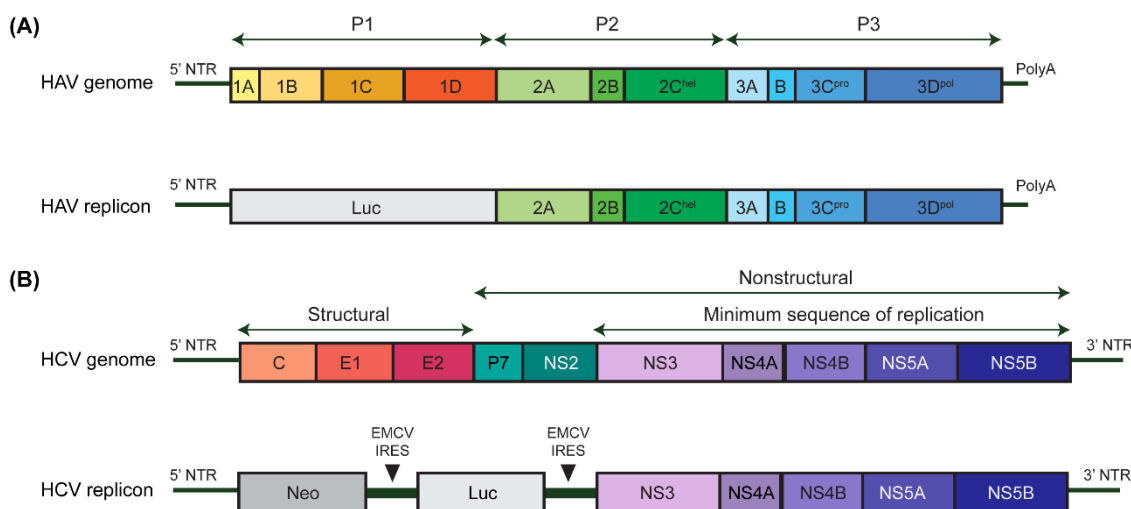


Figure 4.3. Schematic representation of HAV and HCV G2a replicon constructs.

The genome and replicon organisation are shown for (A) HAV and (B) HCV. In each instance the genome is presented above with the structure of each replicon below. The different coloured boxes represent different viral proteins, whilst the grey boxes represent reporter genes and selectable markers. For clarity, gene regions and non-translated regions are not drawn to scale. Abbreviations: IRES, internal ribosome entry site; NTR, non-translated region; Luc, luciferase; EMCV, encephalomyocarditis virus.

Huh7 cells were seeded onto plates and transfected with either HAV or HCV G2a replicon RNA as described in section 4.3.12. Compounds were prepared by dilution in complete DMEM to 30 μ M. Four hours post transfection, 50 μ L of diluted compound was added to each well (final compound concentration 10 μ M) and plates were gently rotated to facilitate mixing. Plates were then incubated at 37°C for a further 72 hours. Cells were then lysed, and bioluminescence output measured as detailed in section 4.3.12. BCX4430, an adenosine analogue with broad-spectrum

activity against a range of RNA viruses (503), was used as a positive control for inhibition. Reactions were performed in quadruplicate. All statistical calculations were performed using Graphpad Prism software (v9.0.0). The percentage inhibition of replicon activity after treatment with test compounds was calculated using the following equation:

$$\text{Percentage inhibition} = 100 - \frac{100 \times (\text{sample well} - \text{mean untransfected})}{\text{mean DMSO control}}$$

4.3.14 Examination of compound cytotoxicity

Cytotoxicity assays were performed in parallel to determine if compounds were toxic to Huh7 cells. Cells were seeded at a density of 5,000 per well onto 96 well plates and incubated at 37°C for 24 hours as described in section 4.3.12. Test compounds were prepared and added to each well as described in section 4.3.13. Maximum cell viability was determined using wells containing no additional compounds. Plates were incubated at 37°C for a further 72 hours.

Cell titre blue reagent (Promega) was prepared by diluting 1:6 in complete DMEM. Media was then removed from each well and 80 µL of cell titre blue solution was added. Plates were further incubated at 37°C for 2 hours before output was measured using the POLARstar Omega plate reader at 560 nm. Reactions were performed in quadruplicate. All statistical calculations were performed using Graphpad Prism software (v9.0.0). The percentage cell survival was calculated using the following equation:

$$\text{Percentage survival} = \frac{100 \times \text{sample well}}{\text{mean DMSO control}}$$

4.3.15 Searching for similar compounds

The most successful hit (NCS-013) was then used as a basis for further antiviral compound searching on eMolecules (<https://www.emolecules.com/>), a compound search engine containing >8 million molecules from a variety of chemical suppliers (Figure 4.4). The 2D chemical structure was used to search the chemical space for molecules with a similarity score ≥ 0.7 (Figure 4.4). Molecular property filters were also

applied ($400 \leq MW \leq 500$, $AlogP < 5$). These molecules were then uploaded to the FAF4drugs server (495, 496) and the PAINS filter A and undesirable substructure moieties filters were applied (Figure 4.4). Eleven compounds passing filters and readily available from either the SPECS or ChemBridge libraries were purchased at $\geq 90\%$ purity for testing as part of the third set (Figure 4.4).

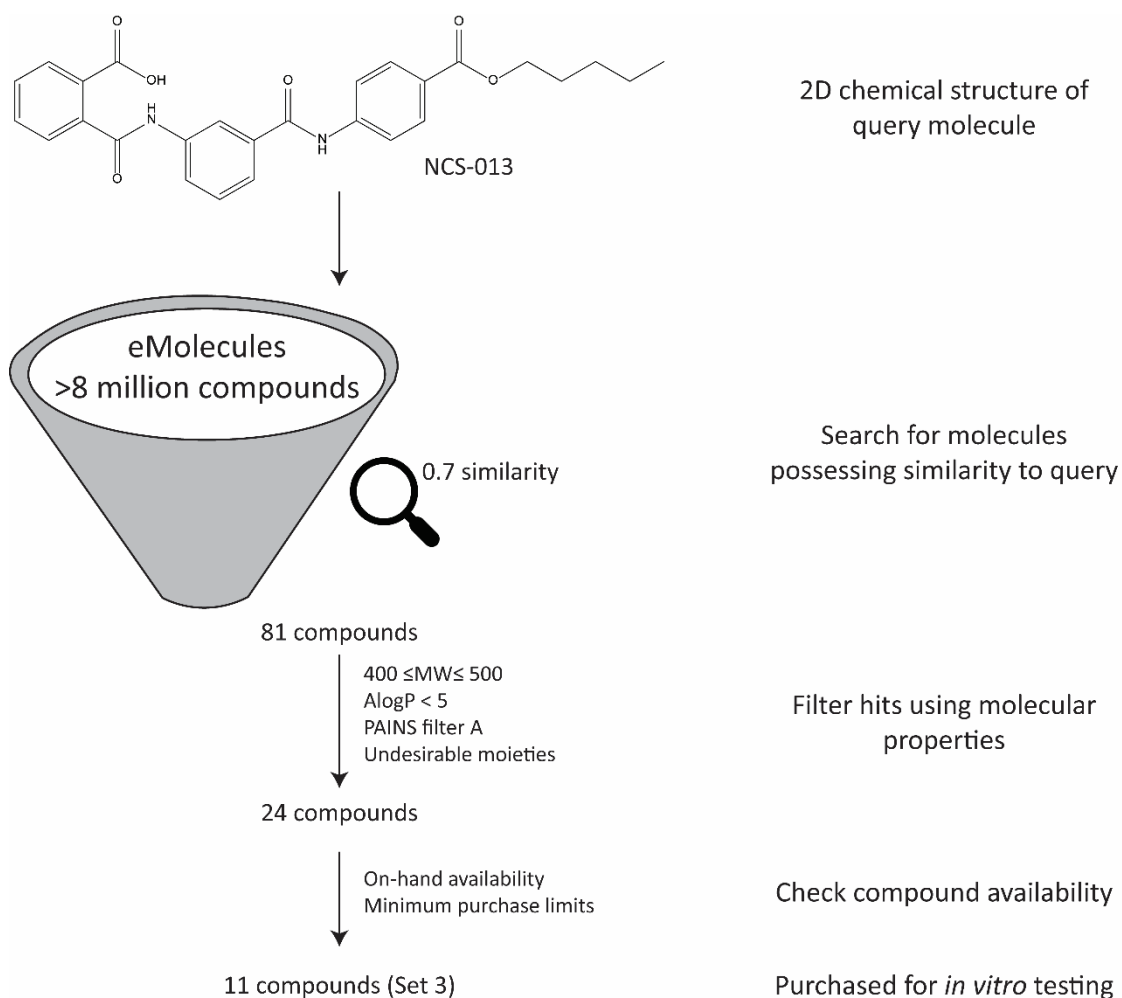


Figure 4.4. Searching the chemical space for similar molecules available on catalogue.

The 2D chemical structure of NCS-013 was used to query the eMolecules chemical search engine for similar molecules. The resulting compound list was then filtered using molecular properties and substructure filters, leaving 24 compounds remaining. Of these, 11 readily available compounds were purchased for *in vitro* examination.

4.4 Results

4.4.1 Multiple sequence alignment

Prior to docking studies, it is important to identify the equivalent binding residues that form the Site-B across different calicivirus RdRp structures (Table 4.1). To achieve this, protein sequences were aligned using Clustal Omega and key motifs were examined. All the motif regions A-F (504) were well conserved across the sequences examined, of these, motifs F, C and E are located around the Site-B pocket (Table 4.2). Additionally, non-motif Site-B residues Gln414 and Arg419 previously shown to play a role in the binding of JTK-109 (147) were also highly conserved across the calicivirus RdRps examined (Figure 4.1, Table 4.2). Amino acid and positions were based on the human norovirus RdRp crystal structure 4LQ9 (114).

Table 4.2. Conserved motifs and residues around Site-B in calicivirus RdRps.

Source virus		Motif F		Motif C		Motif E		Non motif
Norovirus	166	KDELVKT DKIY ...RLLWG	341	YGDD	390	FLRR	410	SILRQMYWTR
SaV	167	KDELRPI EKIY ...RLLWG	345	YGDD	392	FLKR	412	SITRQFYWLK
MNV	166	KDELVKP DKNK ...RLLWG	341	YGDD	390	FLRR	410	SIDRQLLWTK
RHDV	173	KDELRPL DKVK ...RLLWG	352	YGDD	401	FLKR	421	SILRQLEWSK

Amino acid codes are coloured based on conservation - red: conserved residues, blue: similar residues.

4.4.2 Docking of NNIs and JTK-M into calicivirus RdRps: interaction with Arg392 also important for activity?

This present work sought to identify important binding interactions to develop pharmacophore models and find broad-spectrum NNIs against caliciviruses. Therefore, JTK-109, TMC647055 and Beclabuvir (Figure 4.5) which have previously been demonstrated to have broad-spectrum activity against calicivirus RdRp and bind putatively within Site-B (147) were docked into the same site on calicivirus RdRp crystal structures (Table 4.3). An additional compound JTK-M (Figure 4.5), which is a smaller structural analogue of JTK-109 with negligible inhibitory activity was also investigated to compare differences in the binding modes of JTK-109 and JTK-M to identify chemical features critical to inhibitory activity (Figure 4.6, Table 4.3).

The highest scored pose in the largest cluster for each crystal structure was examined for its predicted protein-ligand interactions (six poses in total) (Table 4.3), and in particular, interactions with resistance mutations Gln414 and Arg419 (147). Although, the ligands made few interactions with Gln414, the frequency of interaction with Arg419 correlated with NNI IC₅₀ and broad-spectrum activity. JTK-109 interacted with Arg419 in five of the six poses examined, followed by TMC647055 (n=3/6) and Beclabuvir (n=2/6) (Table 4.3). Likewise, JTK-109 possesses the lowest IC₅₀ and broadest activity, followed by TMC647055 and Beclabuvir (147) (Figure 4.5). However, JTK-M, an analogue of JTK-109 which has no inhibitory activity also frequently interacted with Arg419 (n=5/6).

The ligands were also found to make interactions with residue Arg392 (Table 4.3), which is part of motif E and implicated to play a role in binding the priming nucleotide (505-507). JTK-M (n=2/6) made fewer interactions with Arg392 compared to JTK-109 (n=4/6) (Table 4.3) and occupied a much smaller area of the Site-B binding pocket (Figure 4.6). JTK-109 was also the only ligand that interacted with the adjacent motif E residue, Arg391 (n=2/6).

Although the NNIs were found to interact with similar residues of the six different crystal structures, the ligands themselves were oriented differently within the large Site-B such that different chemical groups interacted with the same protein residues. Whilst TMC647055 interacted with two residues around Site-B, by inspection, it was not positioned within Site-B of the RHDV crystal structure 1KHV using the parameters described in section 4.3.2.

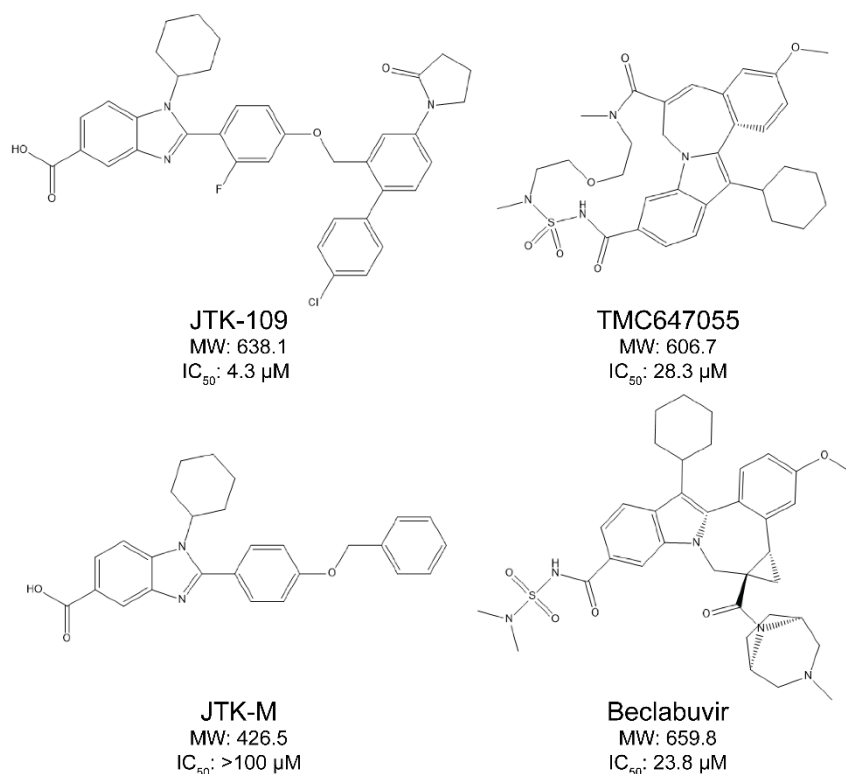


Figure 4.5. Compounds used in the initial docking study.

The chemical structure and molecular weight for each compound is shown. The compound IC₅₀ against the human norovirus GII.4 Sydney 2012 RdRp is also indicated (147).

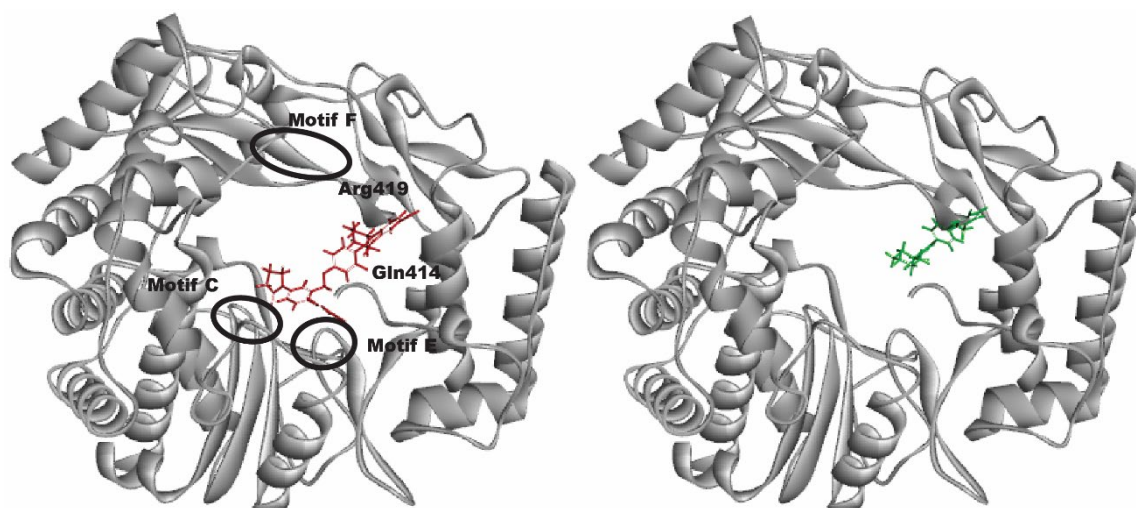


Figure 4.6. Possible binding configurations of compounds JTK-109 and JTK-M on the human norovirus RdRp.

The compounds JTK-109 (red) and JTK-M (green) were docked into Site-B on the human norovirus RdRp crystal structure (PDB ID: 4LQ9) (114). JTK-109 stretches from the Site-B pocket down towards the active site of the RdRp whereas JTK-M is positioned within Site-B only. Docking was performed using the program GOLD through the Discovery Studio interface. The binding configuration obtained from the highest scored pose in the largest cluster is shown. The locations of conserved motifs and residues around Site-B motifs are labelled.

Table 4.3. Summary of predicted favourable docking interactions between antiviral compounds and conserved residues on calicivirus crystal structures.

Compound	Motif ^a	Equiv. residue for 4LQ9	Viral RdRp					
			Norovirus		SaV	MNV		RHDV
			4LQ3	4LQ9	2CKW	3UQS	4O4R	1KHV
JTK-109	F	Lys166	X					
	F	Asp167	X					
	F	Glu168	X					
	F	Leu169		X	X	X	X	X
	F	Arg182			X		X	X
	C	Tyr341	X	X				X
	E	Leu391	X	X				
	E	Arg392	X	X		X	X	
	Non	Arg413				X		X
	Non	Gln414		X				
	Non	Arg419	X	X	X	X	X	
	Non	Arg436		X	X	X	X	X
TMC647055	F	Lys166						
	F	Asp167						
	F	Glu168						
	F	Leu169		X	X			X
	F	Arg182		X	X			X
	C	Tyr341						
	E	Leu391						
	E	Arg392	X	X	X		X	
	Non	Arg413	X	X		x		
	Non	Gln414						
	Non	Arg419	X	X			X	
	Non	Arg436					X	
Beclabuvir	F	Lys166		X	X	X		
	F	Asp167						
	F	Glu168	X				X	
	F	Leu169			X			X
	F	Arg182					X	X
	C	Tyr341		X				X
	E	Leu391						
	E	Arg392	X	X		X	X	
	Non	Arg413				X	X	X
	Non	Gln414	X					
	Non	Arg419			X			X
	Non	Arg436						
JTK-M	F	Lys166	X					
	F	Asp167	X					
	F	Glu168	X					
	F	Leu169		X	X		X	
	F	Arg182		X	X	X		X
	C	Tyr341						

Compound	Motif ^a	Equiv. residue for 4LQ9	Viral RdRp					
			Norovirus		SaV	MNV		RHDV
			4LQ3	4LQ9	2CKW	3UQS	4O4R	1KHV
E	Leu391							
E	Arg392		X		X			
Non	Arg413		X	X	X			
Non	Gln414							
Non	Arg419	X	X	X		X	X	
Non	Arg436					X		

^aLetter designates the motif, "non" refers to non-motif residues.

For clarity, coloured shading is used to indicate different motif/non-motif groups.

4.4.3 Pharmacophore generation and virtual screening using DS

Following docking of the HCV NNIs into Site-B of the six calicivirus RdRps, pharmacophores were generated using the highest scored pose in the largest cluster for each JTK-109 and TMC647055 docking, except for TMC647055 into 1KHV which failed to bind in Site-B (Figure 4.7). Beclabuvir was excluded because it had poor inhibitory activity against MNV and RHDV (IC₅₀ >100 µM) (147) and hence did not demonstrate the broad-spectrum activity desired.

Six pharmacophores for JTK-109 and five pharmacophores for TMC647055 were generated (Figure 4.7). The TMC647055 and JTK-109 pharmacophore sets were used to sequentially screen the SPECS database containing 196,650 compounds until there were less than 100 compounds remaining (Figure 4.7). Since the most restrictive pharmacophore for TMC647055 failed to reduce the number of hits below 500, this set was excluded from further consideration. Therefore, a total of 86 compounds were included for further consideration (Figure 4.7).

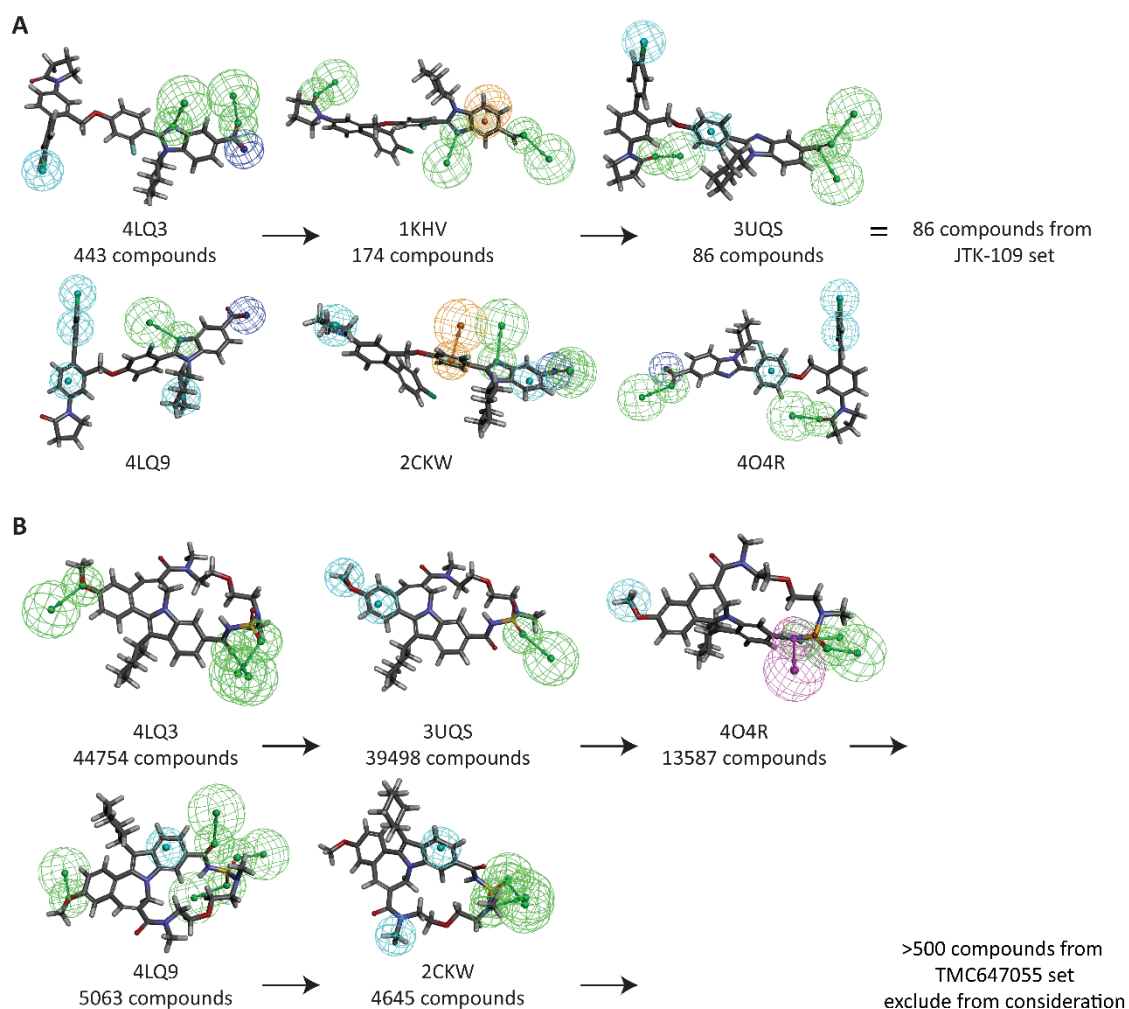


Figure 4.7. Complex-based pharmacophores generated using Discovery Studio and virtual screening results.

Pharmacophores were generated based on the highest scored docked pose in the largest cluster. The PDB ID of the crystal structures is shown below each pharmacophore. The number of compounds found using each of the pharmacophores is also shown. (A) Six pharmacophores were generated from JTK-109. (B) Five pharmacophores were generated from TMC647055. Hydrophobic features are shown as light blue, negative ionisable features in dark blue, ring aromatic (RA) features in orange, hydrogen bond donor (HBD) feature in pink and hydrogen bond acceptor (HBA) features in green. The spheres depict the location constraint of each feature. RA, HBA and HBD features are made up of two mesh spheres, the first sphere is located at the atoms which correspond to the ligand with the arrow representing a vector pointing away to a second sphere where atoms of a target can potentially form interactions with the atom of the ligand.

4.4.4 Pharmacophore generation and virtual screening using LS

The top scoring poses used in section 4.4.3 were also used to generate pharmacophores in LS. As was the case for DS, six pharmacophores for JTK-109 and

five pharmacophores for TMC647055 were generated (Figure 4.8). A total of 205 compounds were found through the LS screen (Figure 4.8). Since a stepwise approach was not possible in LS, pharmacophores were used to screen the SPECS database independently and the resulting compound lists combined. However, in the case of TMC647055:2CKW and TMC647055:3UQS, both pharmacophores were too lenient in terms of chemical features i.e., did not reduce the number of compounds <200. Therefore, only the seven compounds that were common to both pharmacophores were included for further consideration (Figure 4.8).

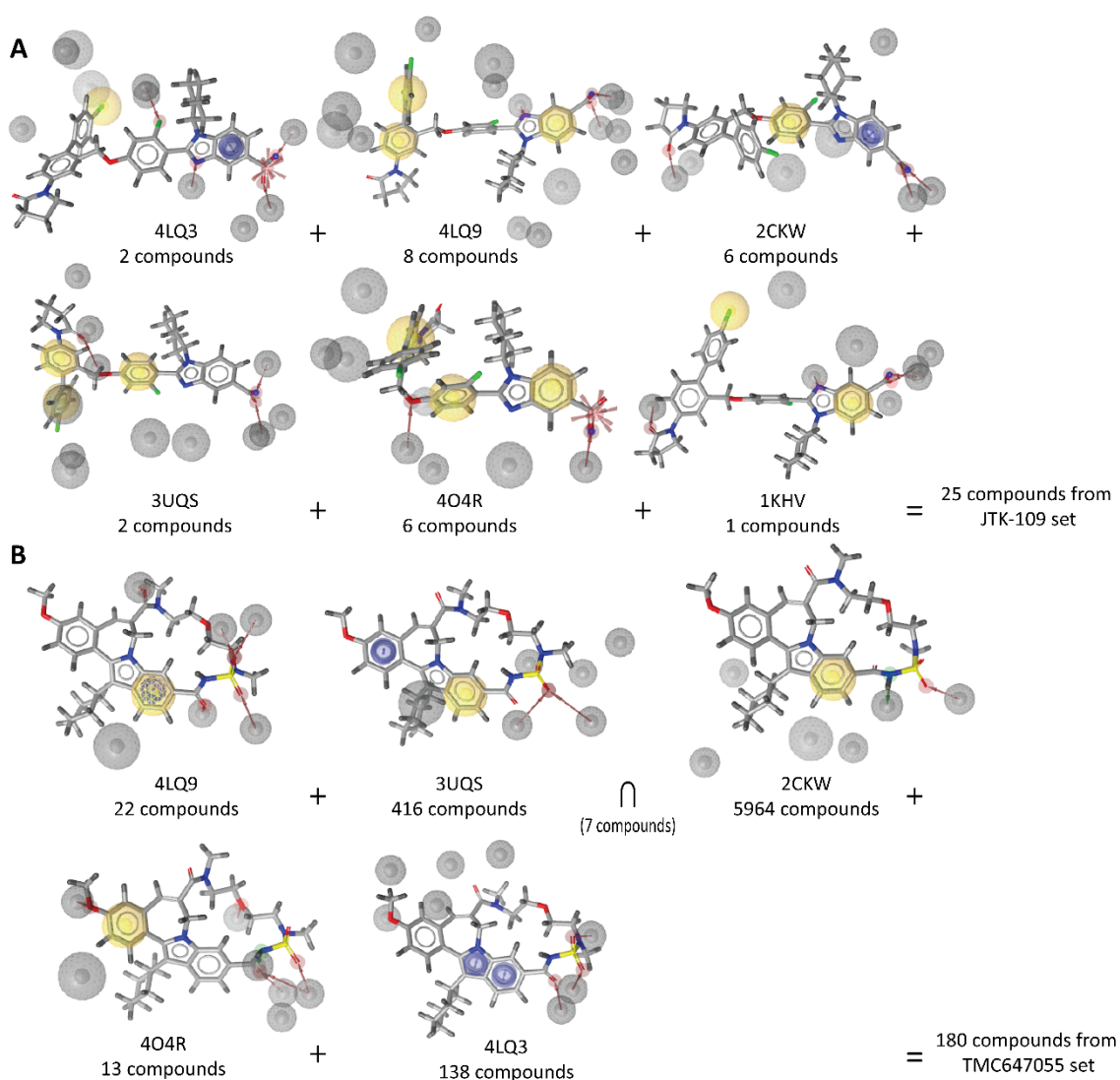


Figure 4.8. Complex-based pharmacophores generated using LigandScout and virtual screening results.

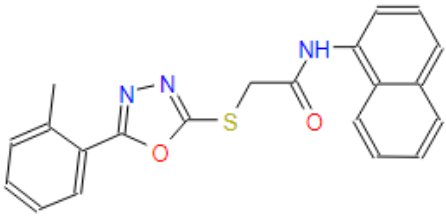
Pharmacophores were generated based on the highest scored docked pose in the largest cluster. The PDB ID of the crystal structures is shown below each pharmacophore. The number of compounds found using each of the pharmacophores is also shown. (A) Six pharmacophores were generated from JTK-109. (B) Five pharmacophores were generated from TMC647055. Hydrophobic features are shown as yellow spheres, aromatic rings are shown as dark blue rings, hydrogen bond acceptors are depicted using red arrows and small red spheres, which represent a vector pointing to the hydrogen bond acceptor depicted by the red sphere. The grey spheres represent excluded volumes where there is insufficient space for the ligand to extend.

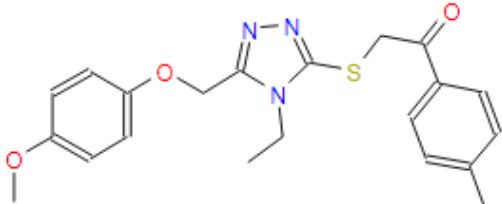
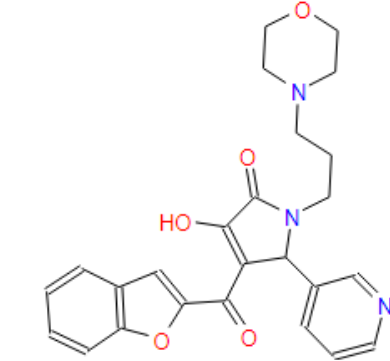
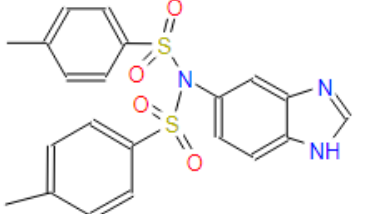
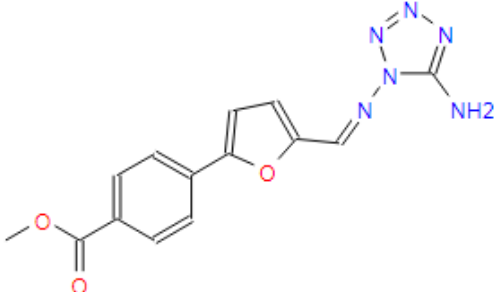
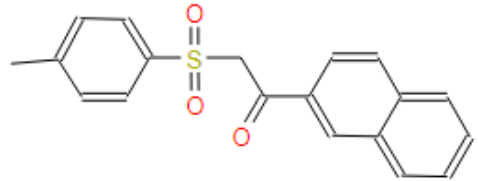
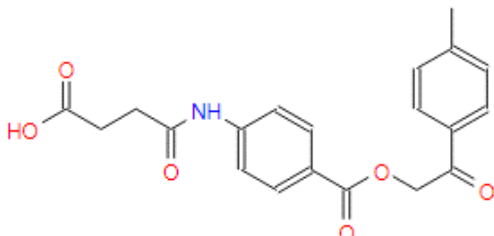
4.4.5 The first set of compounds: compound selection and inhibition of norovirus RdRp activity.

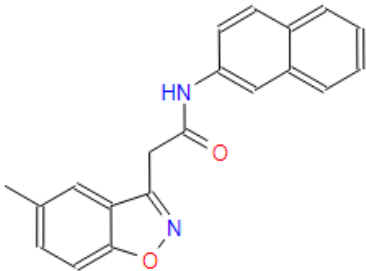
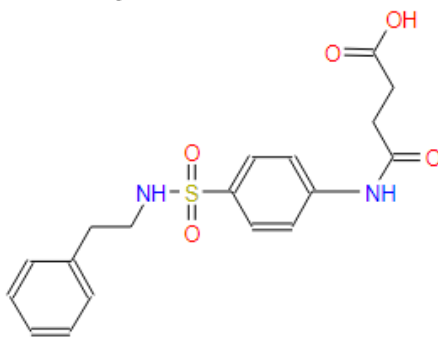
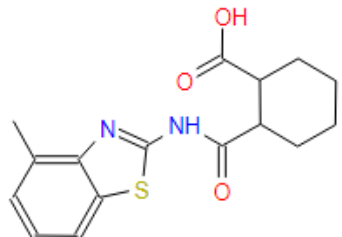
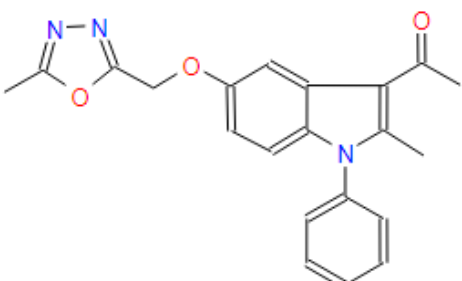
The lists of compounds found using DS and LS were combined (291 compounds) and clustered based on 3D pharmacophore features into 130 different clusters using LS (Figure 4.2). The compound list was then filtered based on molecular properties and clustering, resulting in 26 compounds remaining. These compounds underwent a two-step docking evaluation whereby receptor-ligand interactions within Site-B were examined, specifically interactions with Arg392, Gln414 and Arg419. A total of 11 compounds were chosen from this screen and purchased for *in vitro* testing and assigned IDs NCS-001 to NCS-011 (Table 4.4).

Compound antiviral activity was measured by observing its ability to inhibit synthesis of dsRNA from a poly(C) RNA template. The compounds were tested at fixed concentrations of 10 μ M and 100 μ M (Figure 4.9). The initial set of 11 compounds did not inhibit norovirus RdRp transcription relative to the positive control (Figure 4.9).

Table 4.4. First set of SPECS compounds for biological testing.

Assigned ID	Chemical structure	MW (Da)	logP/ClogP	Catalogue number
NCS-001		375.45	4.64/3.43	AG-690/40696790

Assigned ID	Chemical structure	MW (Da)	logP/ClogP	Catalogue number
NCS-002		397.50	4.62/3.51	AG-690/40752510
NCS-003		447.48	-0.74/2.73	AF-399/42016957
NCS-004		441.52	3.64/4.93	AE-848/42434526
NCS-005		312.28	ND/1.00	AN-465/14459014
NCS-006		324.39	3.66/3.58	AK-918/12232688
NCS-007		369.37	1.84/2.84	AK-918/42829285

Assigned ID	Chemical structure	MW (Da)	logP/ClogP	Catalogue number
NCS-008		316.35	3.92/3.74	AP-501/43258115
NCS-009		376.43	2.31/2.14	AN-329/42158871
NCS-010		318.39	3.76/3.68	AP-263/43419033
NCS-011		361.39	2.74/3.32	AS-768/43420232

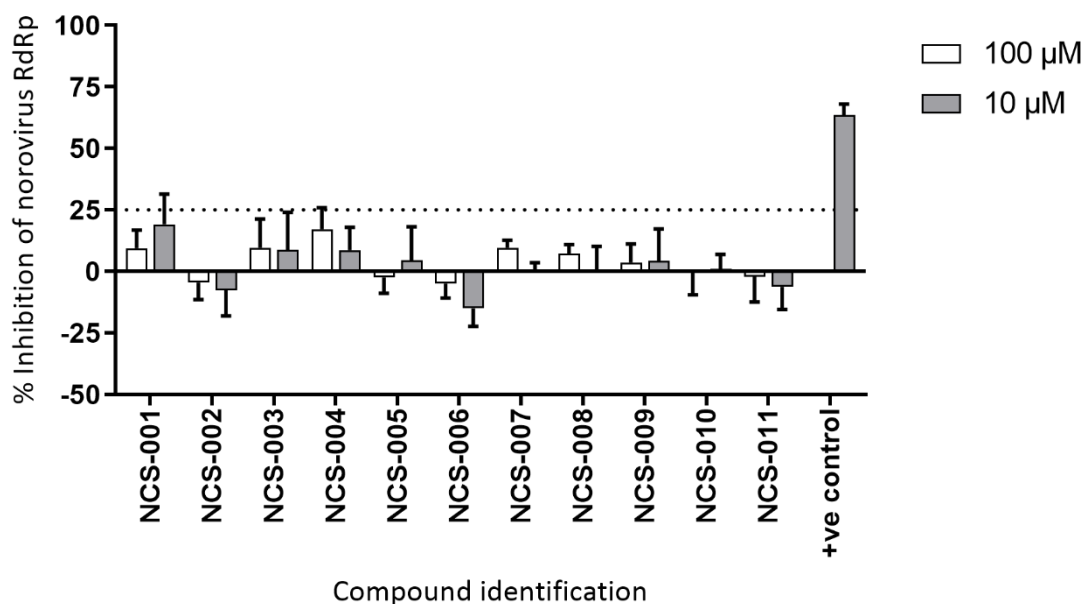


Figure 4.9. Inhibition of human norovirus Sydney 2012 RdRp activity by Set 1 compounds.

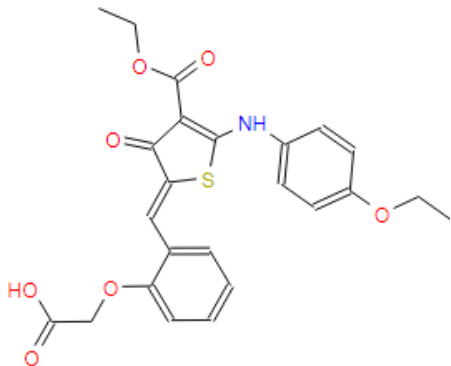
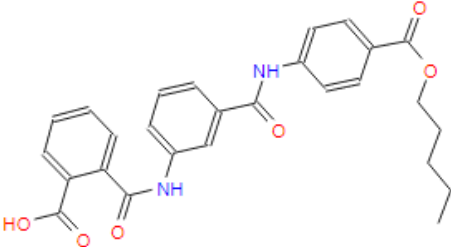
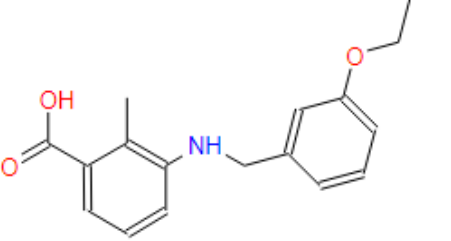
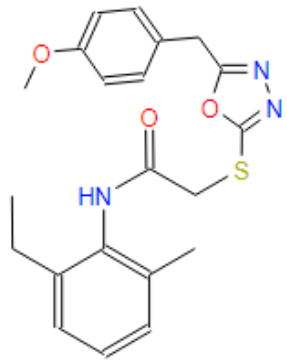
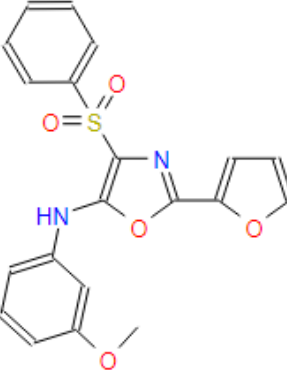
The effects of 11 compounds on norovirus RdRp activity were examined using a fluorescent activity assay at 10 μM and 100 μM . None of the compounds demonstrated dose-dependent inhibition of norovirus RdRp. The positive control was the previously reported NNI PPND5 (114) which was used at 10 μM . Results are shown as mean \pm SD from triplicate reactions.

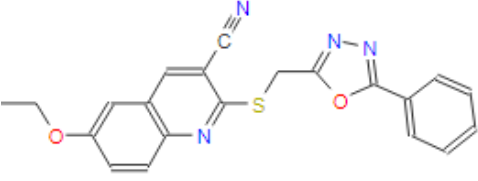
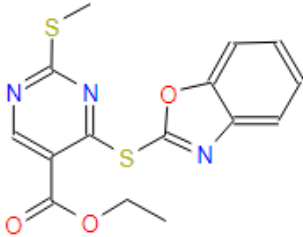
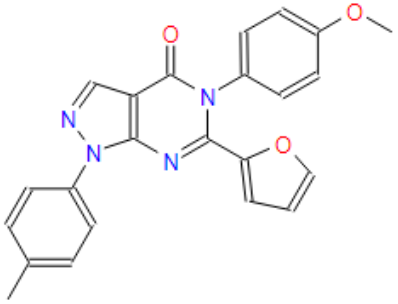
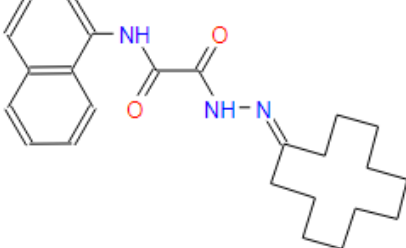
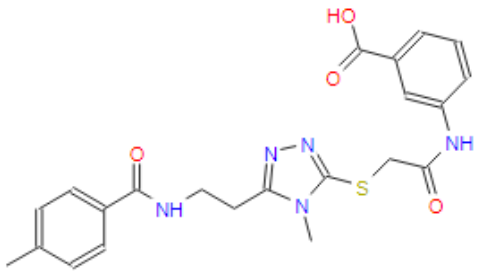
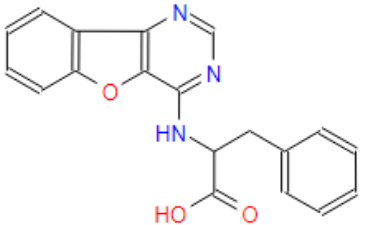
4.4.6 The second set of compounds: compound selection and inhibition of norovirus RdRp activity.

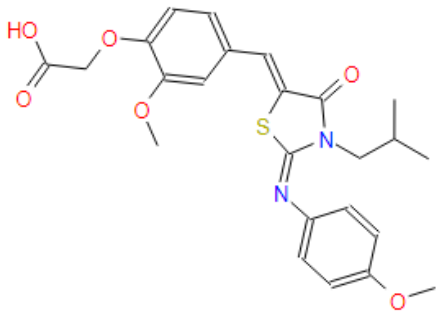
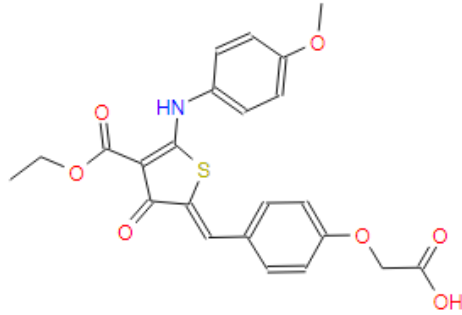
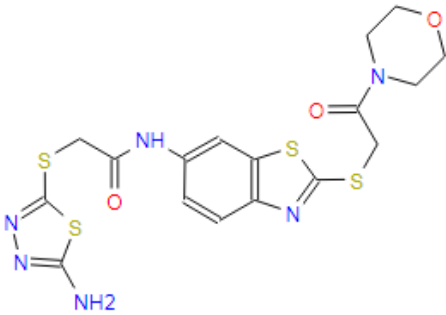
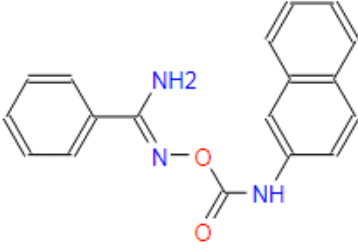
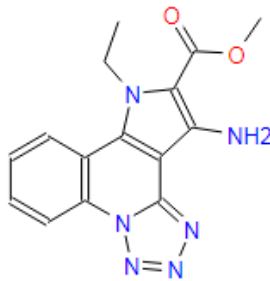
The initial set selected based on predicted chemical interactions within Site-B determined from the two-step docking analysis, however, these compounds did not demonstrate inhibitory activity against norovirus RdRp. Therefore, refinements to the virtual screening process led to the selection of a further 23 compounds (Figure 4.2). These compounds were assigned IDs NCS-012 to NCS-034 (Table 4.5).

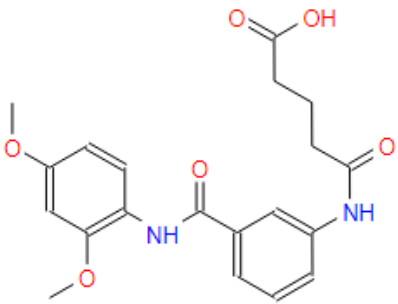
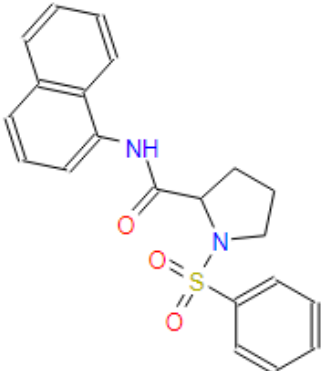
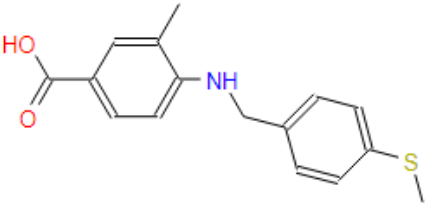
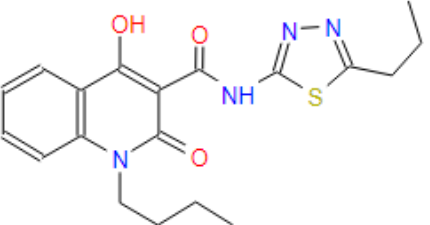
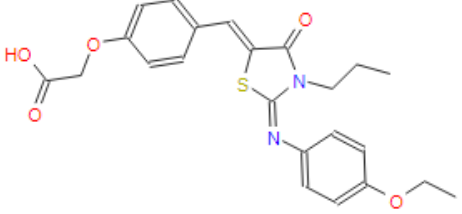
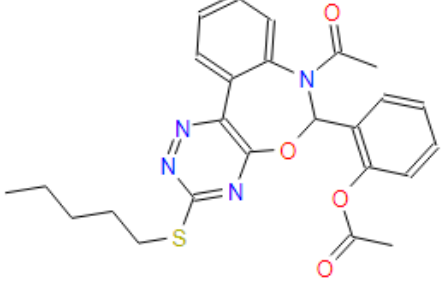
These compounds were tested at fixed concentrations of 10 μM and 50 μM (Figure 4.10). One compound (NCS-031) was completely insoluble and hence not tested. Of the remaining 22 compounds, NCS-013 displayed preliminary dose-dependent inhibition with $55.9 \pm 3.8\%$ inhibition of norovirus RdRp activity at 50 μM (Figure 4.10). This compound was sparingly aqueous soluble at concentrations above 50 μM , which made it challenging to assess its inhibitory potential.

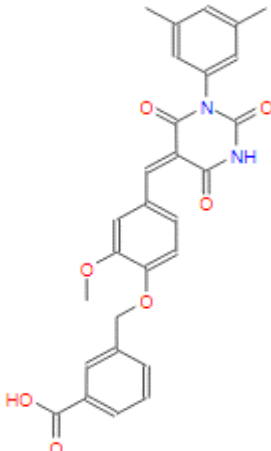
Table 4.5. Second set of SPECs compounds for biological testing.

Assigned ID	Chemical structure	MW (Da)	logP/ ClogP	Catalogue number
NCS-012		469.51	2.85/ 4.63	AN-988/ 14609101
NCS-013		474.51	4.68/ 4.82	AK-918/ 11183007
NCS-014		285.34	3.52/ 3.82	AN-465/ 43421808
NCS-015		397.50	4.79/ 1.72	AN-698/ 42115836
NCS-016		396.42	3.21/ 5.37	AF-399/ 42866018

Assigned ID	Chemical structure	MW (Da)	logP/ ClogP	Catalogue number
NCS-017		388.45	5.08/ 3.67	AG-690/ 40699155
NCS-018		347.42	3.86/ 4.13	AI-204/ 31717030
NCS-019		398.42	3.94/ 5.06	AP-064/ 43237401
NCS-020		393.53	5.64/ 6.51	AH-487/ 11381034
NCS-021		453.52	3.11/ 1.41	AR-196/ 42727049
NCS-022		333.35	2.83/ 3.85	AO-364/ 42192093

Assigned ID	Chemical structure	MW (Da)	logP/ ClogP	Catalogue number
NCS-023		470.54	3.96/ 4.74	AO-081/ 15569291
NCS-024		455.49	2.52/ 4.10	AN-988/ 14609081
NCS-025		482.63	2.97/ 1.78	AN-988/ 15131262
NCS-026		305.34	3.92/ 4.18	AG-389/ 37427001
NCS-027		310.32	ND/ 3.08	AN-514/ 37348004

Assigned ID	Chemical structure	MW (Da)	logP/ ClogP	Catalogue number
NCS-028		386.40	1.58/ 1.63	AK-918/ 40894272
NCS-029		380.47	3.30/ 4.14	AO-080/ 42479858
NCS-030		287.38	3.75/ 4.24	AN-465/ 43411544
NCS-031		386.47	3.77/ 4.44	AG-690/ 09683057
NCS-032		440.52	4.02/ 5.13	AN-989/ 40683743
NCS-033		478.57	5.66/ 5.19	AN-655/ 14768280

Assigned ID	Chemical structure	MW (Da)	logP/ ClogP	Catalogue number
NCS-034		500.50	4.49/ 4.21	AN-988/ 15130066

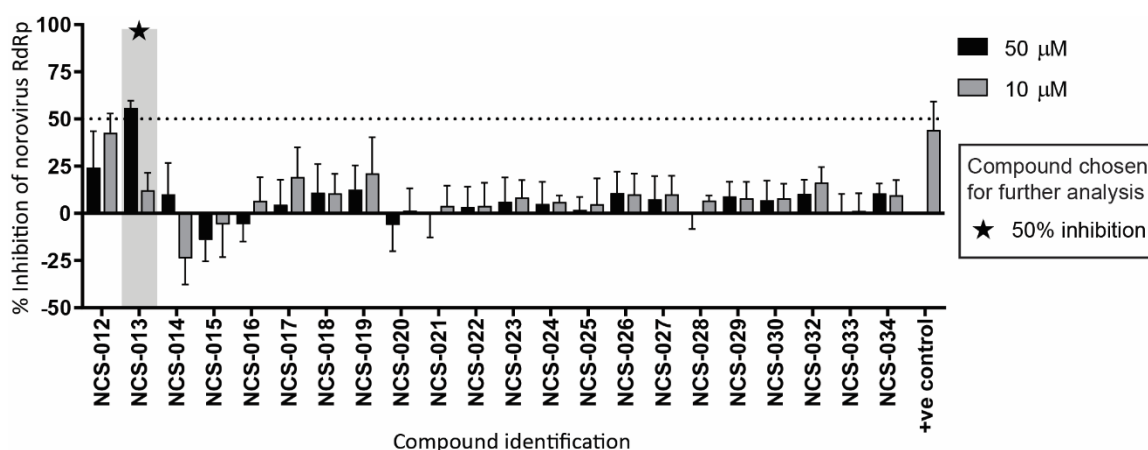


Figure 4.10. Inhibition of human norovirus Sydney 2012 RdRp activity by Set 2 compounds.

The effects of 22 compounds on norovirus RdRp activity were examined using a fluorescent activity assay at 10 µM and 50 µM. Compound NCS-013 (indicated with star) demonstrated dose-dependent inhibition of norovirus RdRp, with more than 50% inhibition at 50 µM. The positive control was the previously reported NNI PPNDS (114) which was used at 10 µM. Results are shown as mean ± SD from triplicate reactions.

4.4.7 NCS-013 demonstrates cross-genera inhibition of FCV RdRp

To further investigate the antiviral potential of NCS-013, it was examined for inhibitory activity against recombinant FCV RdRp previously synthesised in our laboratory (483). FCV is a member of the *Caliciviridae* family and belongs to the genus *Vesivirus*. NCS-013 was tested at fixed concentrations of 50 µM and 10 µM in two independent experiments. Across the two experiments, NCS-013 demonstrated 51.3 ± 5.4% inhibition of FCV RdRp activity at 50 µM (Figure 4.11).

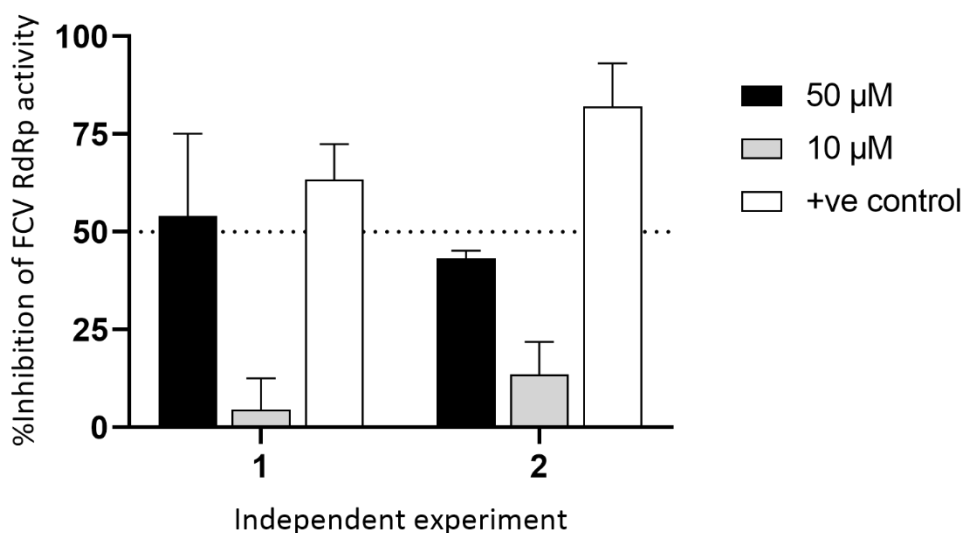


Figure 4.11. Inhibition of FCV RdRp activity by NCS-013.

The effect of test compound NCS-013 on FCV RdRp activity was examined using a fluorescent RdRp transcription assay. NCS-013 was tested at fixed concentrations of 50 μ M and 10 μ M in two independent trials. The positive control was the previously reported RdRp inhibitor PPND5 (114) which was used at 10 μ M. Results are shown as mean \pm SD from triplicate reactions.

4.4.8 Can set 1 and 2 compounds inhibit Zika virus RdRp transcription?

Since JTK-109 and TMC647055 were initially designed as NNIs of HCV (136, 508), a member of the *Flaviviridae*, the research compounds were also examined for inhibition of the Zika virus RdRp, as it is also a member of the *Flaviviridae*. Compound antiviral activity was measured by observing its ability to inhibit synthesis of dsRNA from a poly(U) RNA template. Compounds NCS-001 – NCS-034 (Table 4.4, Table 4.5) were tested for inhibitory activity at fixed concentrations of 10 μ M and 100 μ M (Figure 4.12). Eight compounds demonstrated dose-dependent inhibition of Zika virus RdRp transcription and were selected for further analysis (Figure 4.12). This included five compounds which displayed close to 50% inhibition of Zika virus RdRp activity at 100 μ M – NCS-013 (58.4 \pm 22.6%), NCS-014 (74.4 \pm 3.7%), NCS-024 (44.1 \pm 37.5%), NCS-025 (39.9 \pm 32.2%) and NCS-034 (52.6 \pm 7.9%) (Figure 4.12). Three other compounds with close to 25% inhibition of Zika virus RdRp activity were also selected – NCS-015 (30.8 \pm 25.3%), NCS-018 (32.4 \pm 9.2%) and NCS-032 (22.7 \pm 11.6%) (Figure 4.12). Although NCS-016 also demonstrated inhibitory activity (40.2 \pm 17.4%), due to aqueous solubility challenges it was excluded from further analysis.

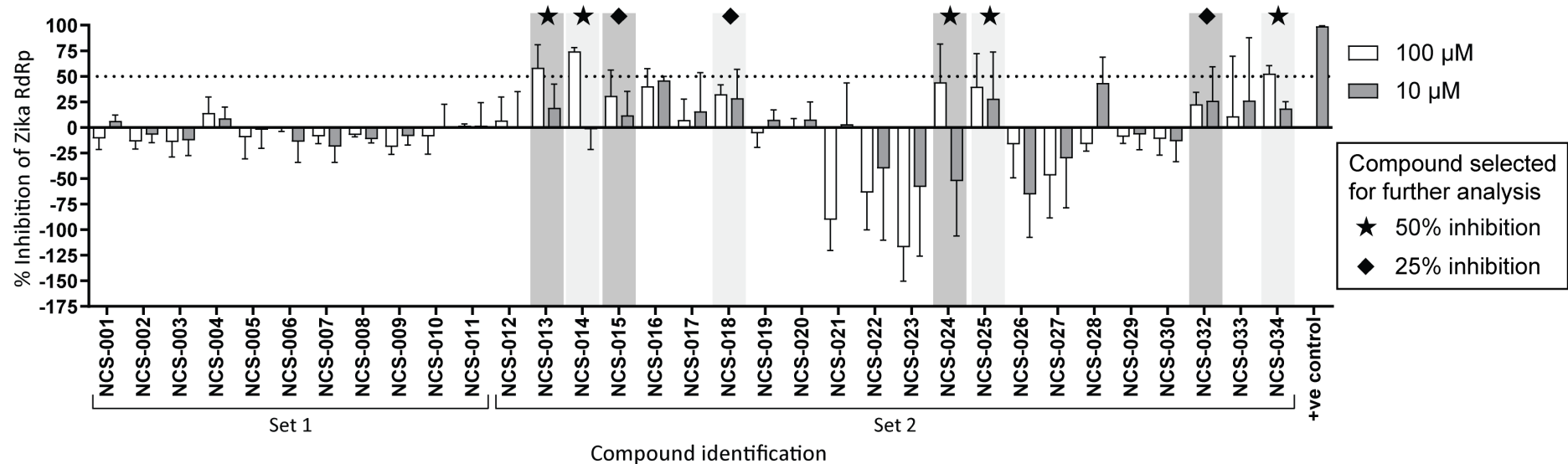


Figure 4.12. Screening test compounds for inhibition of Zika virus RdRp activity.

The effects of 33 compounds on Zika virus RdRp activity were examined using a fluorescent activity assay at 10 μM and 100 μM. Five compounds exhibited dose-dependent effects with close to 50% inhibition at 100 μM (indicated with star). Three other compounds also demonstrated some dose-dependent effects with close to 25% inhibition at 100 μM (indicated with diamond). The positive control was the previously reported RdRp inhibitor PPNS (114) which was used at 10 μM. Results are shown as mean ± SD from triplicate reactions.

4.4.9 NCS-013 inhibits both HAV and HCV replicon replication.

As the original intention of this work was to develop broad-spectrum NNIs of RNA viruses, eight compounds that displayed any level of dose-dependent inhibitory activity against either norovirus or Zika virus RdRp were selected for further studies (Figure 4.13). These compounds were examined for their ability to inhibit the replication of HAV and HCV replicons in Huh7 cells by measuring decreases in the output of the luciferase reporter gene present in the viral replicons (Figure 4.3), which is a marker of replicon replication. All compounds were tested at a fixed concentration of 10 μ M. A CellTiter-Blue cell viability assay was also performed to ascertain whether these compounds were toxic and if any decreases in luciferase output were due to changes in cell survival rather than replicon replication.

Of the eight compounds examined, one compound, NCS-013, displayed inhibitory activity against both the HCV G2a ($62.5 \pm 23.6\%$) and HAV ($45.6 \pm 10.1\%$) replicons (Figure 4.13A). A second compound, NCS-032, demonstrated inhibitory activity against the HAV replicon ($51.0 \pm 22.7\%$) (Figure 4.13A). Additionally, both compounds displayed little to no impact on cell viability (Figure 4.13B).

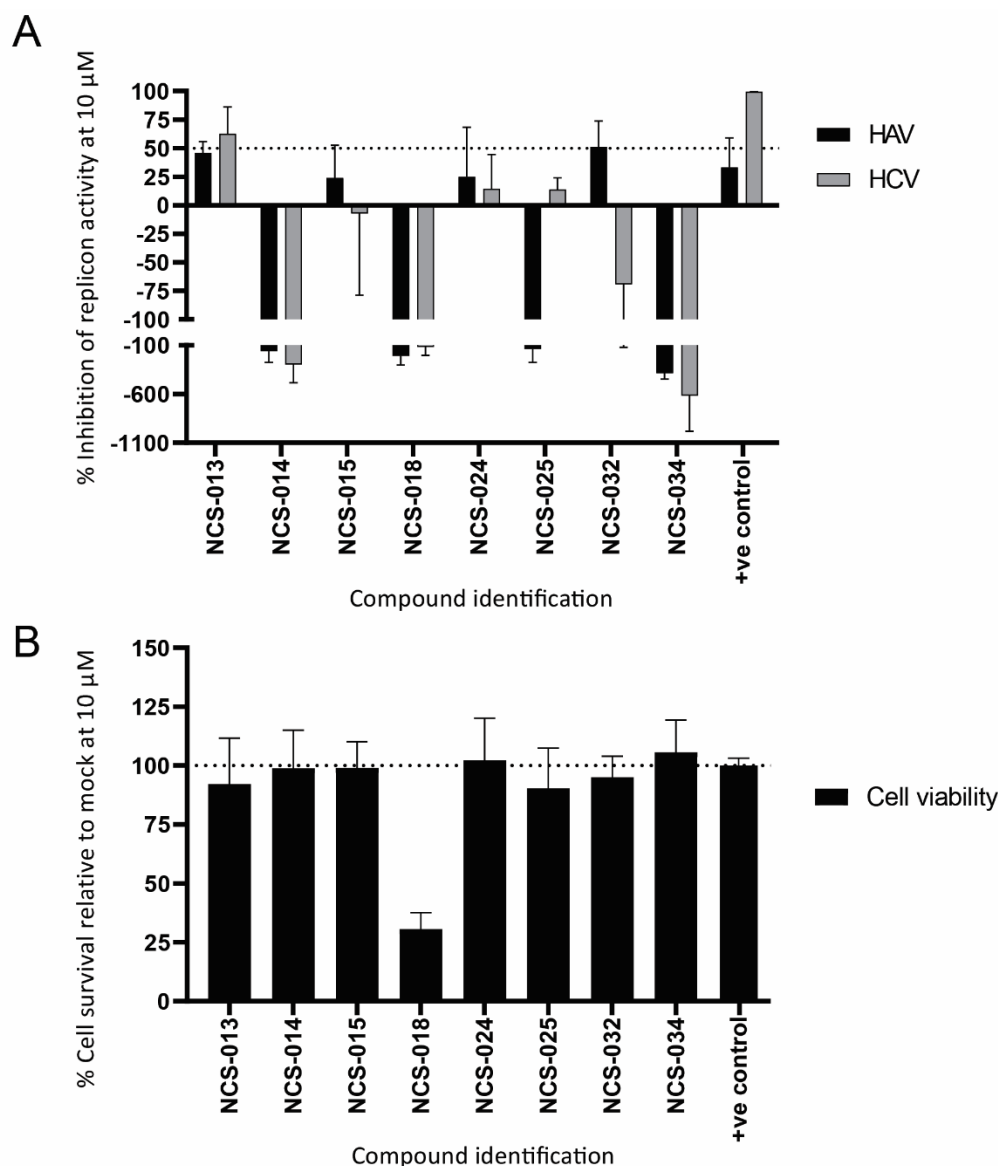


Figure 4.13. The effect of set 1 and 2 compounds on HAV and HCV replicons, and cells.

The effects of 8 compounds on HAV and HCV G2a replicon activity in Huh7 cells was examined at 10 μM using replicon cell culture with luciferase reporter output (A). The compounds were also examined at 10 μM concentrations in parallel for cellular toxicity (B). The positive control used was a previously reported broad-spectrum antiviral adenosine nucleoside analogue BCX4430 (10 μM) (503). Results are shown as mean \pm SD from quadruplicate reactions.

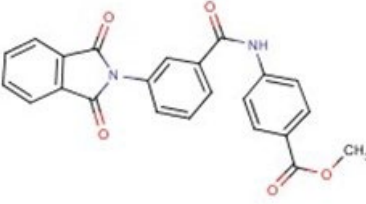
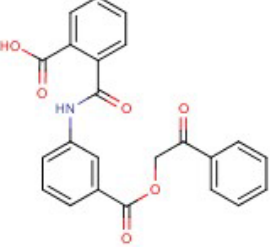
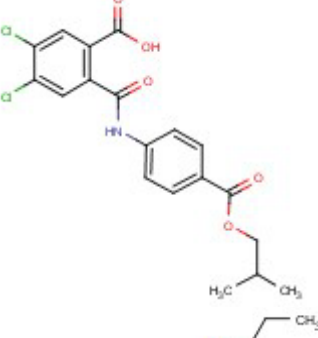
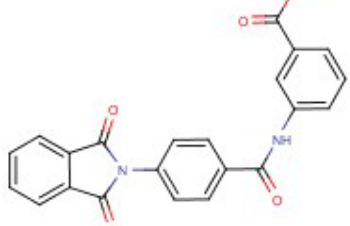
4.4.10 Can NCS-013 structural analogues inhibit norovirus and Zika virus

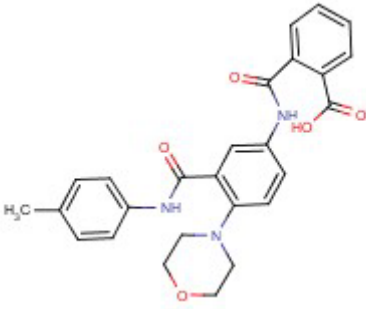
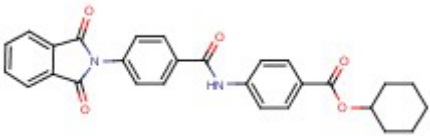
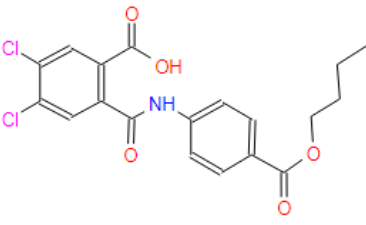
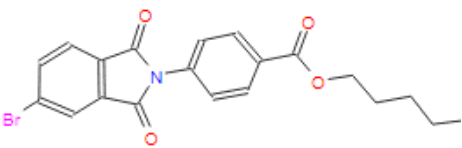
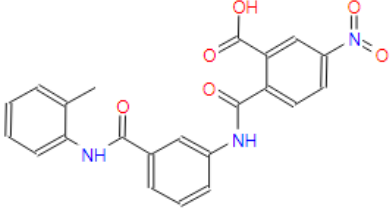
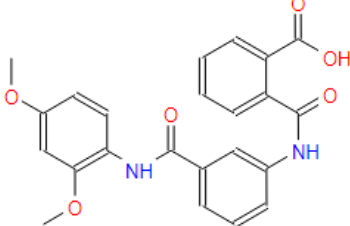
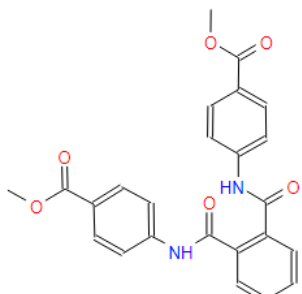
RdRp activity?

Since NCS-013 displayed broad-spectrum inhibitory activity spanning five RdRp/replicons across three viral families, it was used as a scaffold to query the eMolecules search engine for compounds with similar structure and thus potential for

similar broad-spectrum coverage (Figure 4.4). A total of 11 compounds were identified and purchased from this screen and assigned IDs NCS-013A to NCS-013K (Table 4.6). The compounds were tested for dose-dependent inhibition of norovirus and Zika virus RdRp activity at fixed concentrations of 10 μ M and 50 μ M (Figure 4.14). Three compounds demonstrated some level of inhibition of Zika virus RdRp activity at 50 μ M and were selected for further investigation in viral replicon models. These were NCS-013A ($42.1 \pm 22.6\%$), NCS-013B ($33.5 \pm 9.0\%$) and NCS-013H ($18.8 \pm 13.1\%$) (Figure 4.14B). None of the compounds displayed dose-dependent inhibition of norovirus RdRp transcription (Figure 4.14A).

Table 4.6. NCS-013 structural analogues.

Assigned ID	Chemical structure	MW (Da)	logP/ClogP	Catalogue number
NCS-013A		400.39	3.28/3.66	5581827
NCS-013B		403.39	3.14/2.86	5211029
NCS-013C		410.25	4.56/4.71	5536319
NCS-013D		428.44	4.10/4.72	6928147

Assigned ID	Chemical structure	MW (Da)	logP/ClogP	Catalogue number
NCS-013E		459.50	3.57/2.28	7161054
NCS-013F		468.51	4.82/5.69	6651341
NCS-013G		410.25	4.57/4.84	AK-918/10093064
NCS-013H		416.27	4.96/5.88	AK-918/40046982
NCS-013I		419.39	3.01/2.04	AG-690/10485033
NCS-013J		420.42	2.95/1.78	AK-918/40893922
NCS-013K		432.43	3.29/2.84	AK-968/12573227

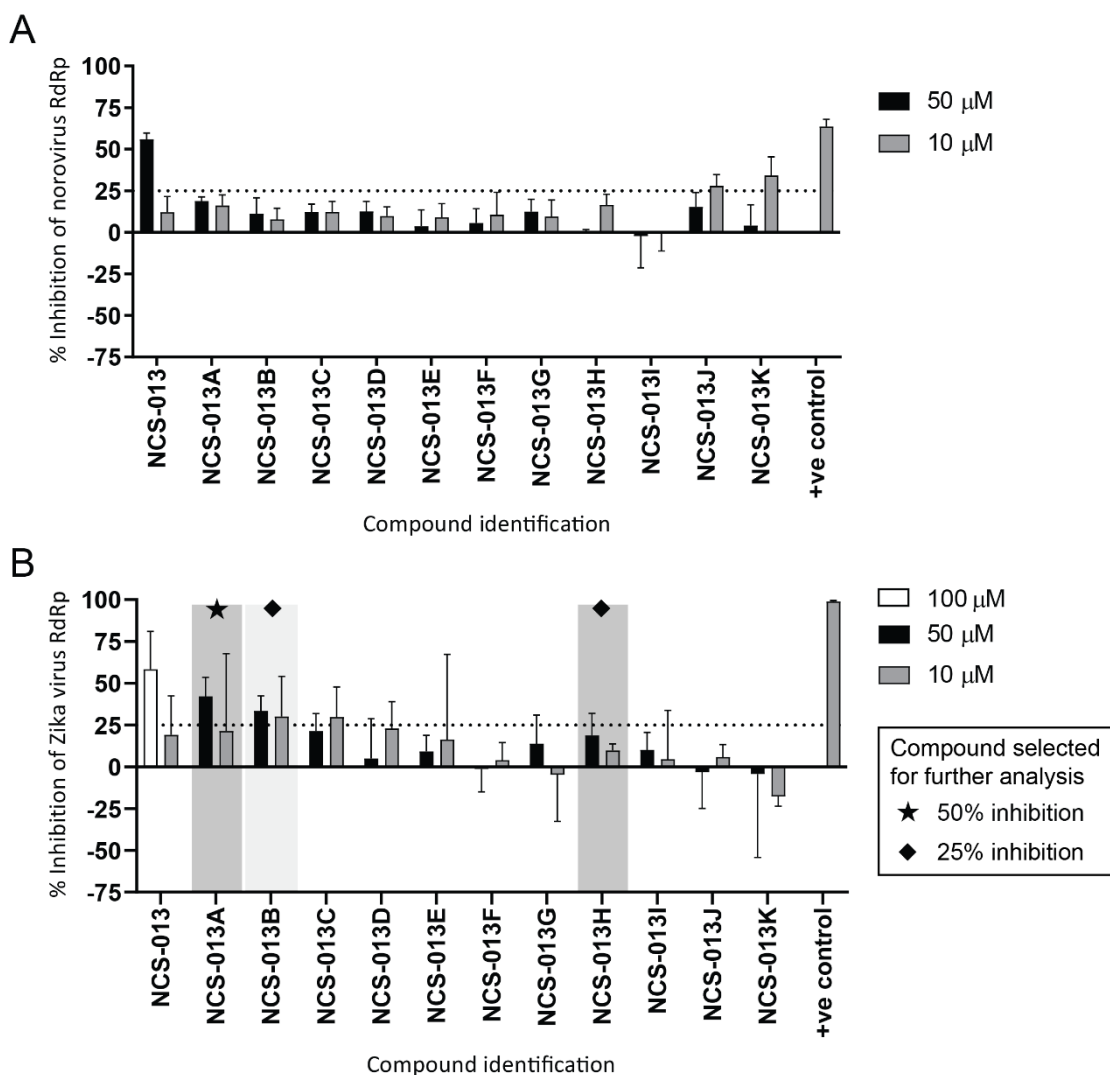


Figure 4.14. Inhibition of norovirus and Zika virus RdRp activity by NCS-013 structural analogues.

The effects of 11 compounds on (A) norovirus and (B) Zika virus RdRp activity was examined using a fluorescent transcription assay at fixed concentrations of 50 μ M and 10 μ M. The positive control was the RdRp inhibitor PPNDs (114) which was used at 10 μ M. One compound showed close to 50% inhibition of Zika virus RdRp activity at 50 μ M (indicated with star). Two other compounds displayed close to 25% inhibition at 50 μ M (diamond). None of the compounds demonstrated dose-dependent inhibition of norovirus RdRp activity. Results are shown as mean \pm SD from triplicate reactions. For comparison, the previous results for NCS-013 norovirus and Zika virus RdRp are shown.

4.4.11 NCS-013A inhibits of HAV replicon replication.

Three NCS-013 structural analogues demonstrated dose-dependent inhibition of Zika virus RdRp transcription. These compounds were then tested in mammalian cell culture against HAV and HCV replicon systems (Figure 4.15). One compound, NCS-013A, displayed low level of inhibition of the HCV G2a replicon replication (NCS-013A:

37.7 ± 23.1%) (Figure 4.15A), whilst two compounds (NCS-013A: 58.9 ± 17.7% and NCS-013H: 38.0 ± 18.8%) demonstrated inhibitory activity against the HAV replicon (Figure 4.15A). Neither of these compounds displayed negative impacts on cell viability (Figure 4.15B).

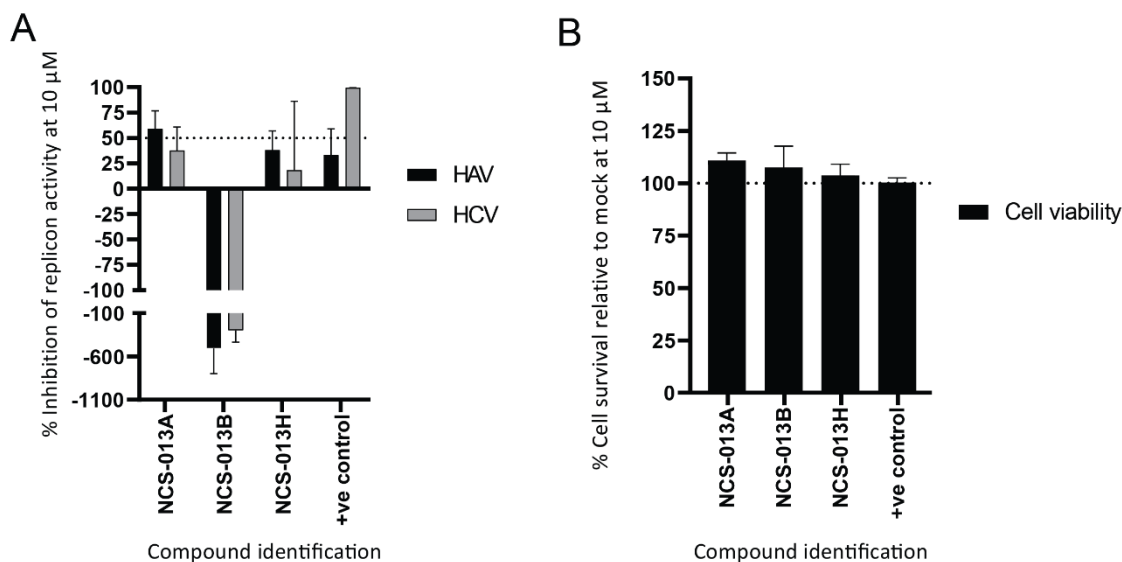


Figure 4.15. The effect of NCS-013 structural analogues on HAV and HCV replicons, and cells.

The effects of three NCS-013 structural analogues on HAV and HCV G2a replicon activity in Huh7 cells was examined at 10 μM using replicon cell culture with luciferase reporter output (A). The compounds were also examined at 10 μM concentrations in parallel for cellular toxicity (B). The positive control used was a previously reported broad-spectrum antiviral adenosine nucleoside analogue BCX4430 (10 μM) (503). Results are shown as mean ± SD from quadruplicate reactions.

4.4.12 Potential binding configuration of NCS-013 to *Caliciviridae* RdRp

Following the promising broad-spectrum antiviral activity of NCS-013, it was important to confirm that the inhibition observed was target specific and not due to assay interference. One way of confirming this is to investigate compound binding and confirm that it binds to the intended target. NCS-013 was originally discovered using pharmacophore features that were modelled from *in silico* NNI binding within Site-B (Figure 4.2). Therefore, NCS-013 was docked into Site-B of the six crystal structures as described in section 4.3.2 and predicted favourable docking interactions were investigated (Table 4.7). NCS-013 interacted with very few conserved Site-B binding pocket residues, and only interacted with Arg392 in two of the crystal structures (4LQ3 and 4O4R) (Table 4.7). For the two human norovirus RdRp structures, NCS-013 was

predicted to make favourable interactions with only two conserved binding site residues on the 4LQ3 structure and three residues on the 4LQ9 structure (Figure 4.16). There were large changes in the configuration of NCS-013 within the large Site-B binding pocket. When docked into the 4LQ3 structure, NCS-013 was positioned deeper within the protein, closer to the active site whereas on the 4LQ9 structure, the ligand bound higher up within the thumb region closer to the conserved non-motif residues (Figure 4.16).

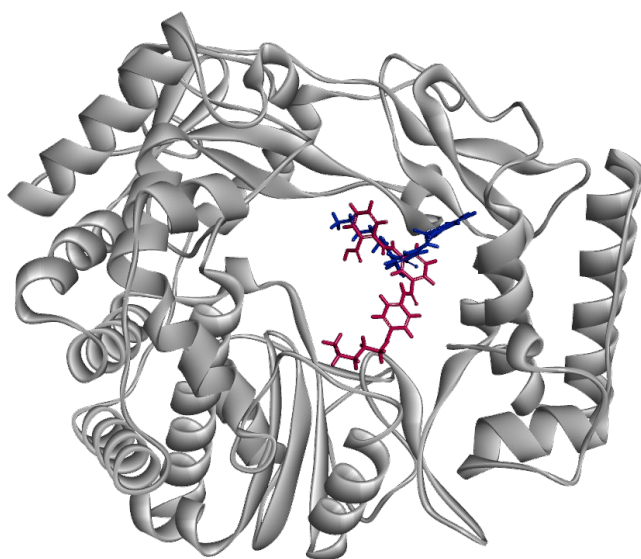


Figure 4.16. Possible binding configurations of NCS-013 on the human norovirus RdRp.

Compound NCS-013 was docked into Site-B of two human norovirus RdRp crystal structures (PDB ID: 4LQ3 and 4LQ9) (114). Docking was performed using the program GOLD through the Discovery Studio interface. The binding configuration obtained from the highest scored pose in the largest cluster for both 4LQ3 (pink) and 4LQ9 (blue) are displayed relative to the 4LQ9 protein structure. Four residues on the C terminus end were hidden for clarity.

Table 4.7. Predicted favourable docking interactions between NCS-013 and conserved residues on calicivirus crystal structures.

Compound	Motif ^a	Equiv. residue for 4LQ9	Viral RdRp					
			Norovirus		SaV	MNV		RHDV
			4LQ3	4LQ9	2CKW	3UQS	4O4R	1KHV
NCS-013	F	Lys166						
	F	Asp167						
	F	Glu168	X			X		
	F	Leu169			X		X	X
	F	Arg182		X		X		
	C	Tyr341						
	E	Leu391						

Compound	Motif ^a	Equiv. residue for 4LQ9	Viral RdRp					
			Norovirus		SaV	MNV		RHDV
			4LQ3	4LQ9	2CKW	3UQS	4O4R	1KHV
	E	Arg392	X				X	
	Non	Arg413		X	X	X	X	X
	Non	Gln414				X		
	Non	Arg419		X	X	X		
	Non	Arg436			X		X	

^aLetter designates the motif, "non" refers to non-motif residues.

For clarity, coloured shading is used to indicate different motif/non-motif groups.

4.4.13 *In vitro* examination of NCS-013 binding within Site-B

Following *in silico* examination of NCS-013 and its potential binding to the Site-B binding pocket within the RdRp, further experiments using *in vitro* fluorescent transcription assays were performed. RdRp selected for binding studies included the two Site-B norovirus RdRp mutants Q414A and R419A that were previously generated in our laboratory and shown to be resistant to the NNI JTK-109 (147). If NCS-013 achieves its inhibitory activity through interaction with Site-B, Q414 and R419 would likely be involved in its binding. In this case, the mutant RdRps would display resistance to NCS-013, as indicated by an increase in IC₅₀. Compound IC₅₀ values were established against the wild type and mutant polymerases. Less than 30% increase in IC₅₀ was observed when comparing the activity against the wild type (54.6 μM) and mutant (Q414A: 68.7 μM, R419A: 70.4 μM) RdRps (Figure 4.17).

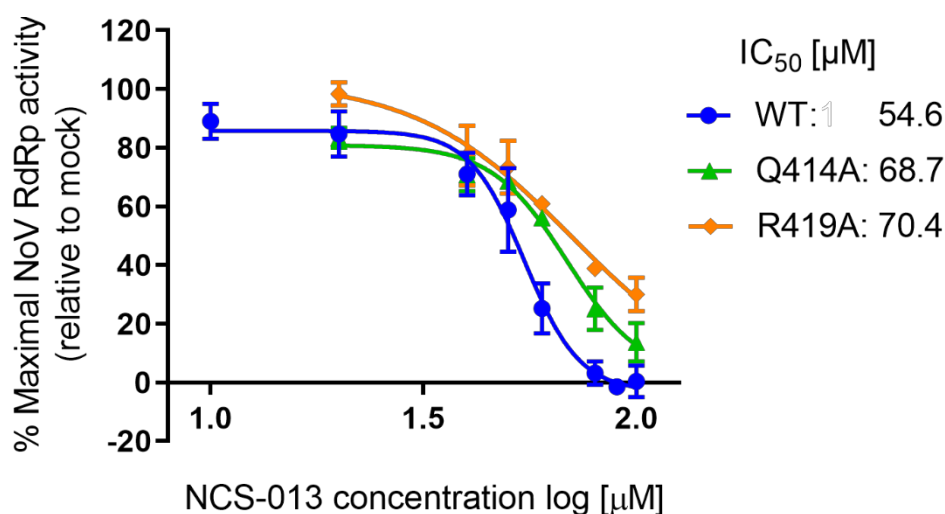


Figure 4.17. Dose dependent inhibition of wild type and mutant norovirus GII.4 Sydney 2012 RdRp activity by NCS-013.

The relative inhibitory effect of NCS-013 on the wild type (blue) was compared to the Site-B mutants Q414A (green) and R419A (orange) using a fluorescent activity assay. IC₅₀ values were calculated and are shown on the graph. The mean \pm SD from triplicate reactions is shown.

4.4.14 Summary of virtual screening results

After two rounds of virtual screening (sections 4.4.5 and 4.4.6) and one round of expanded structural analogue searching (section 4.4.10), a total of 44 compounds were investigated for inhibitory activity against norovirus and Zika virus RdRp. From this, eleven promising compounds were further assessed for inhibition of HAV and HCV replicon replication in Huh7 cells (Figure 4.13, Figure 4.15). One compound, NCS-013, demonstrated broad-spectrum inhibition of RdRp/replicon replication of five different viruses, whilst a structural homologue, NCS-13A also demonstrated some cross-family inhibition of HAV, HCV and Zika virus replication (Table 4.8). Seven other compounds also showed >25% inhibition of RdRp/replicon activity relative to the negative control (Table 4.8).

Table 4.8. Test compounds with >25% inhibitory activity relative to negative control.

Test Compound	Inhibition of RdRp activity at 50 μ M or 100 μ M			Replicon at 10 μ M	
	Norovirus ¹	FCV ¹	Zika virus ²	HAV	HCV
NCS-013	55.9 \pm 3.8%	51.3 \pm 5.4%	58.4 \pm 22.6%	45.6 \pm 10.1%	62.5 \pm 23.6%
NCS-014	None	ND	74.4 \pm 3.7%	None	None
NCS-024	None	ND	44.1 \pm 37.5%	None	None
NCS-025	None	ND	39.9 \pm 32.2%	None	None
NCS-032	None	ND	None	51.0 \pm 22.7%	None
NCS-034	None	ND	52.6 \pm 7.9%	None	None
NCS-013A	None	ND	42.1 \pm 22.6% ¹	58.9 \pm 17.7%	37.7 \pm 23.1%
NCS-013B	None	ND	33.5 \pm 9.0% ¹	None	None
NCS-013H	None	ND	None	38.0 \pm 18.8%	None

All values are displayed as mean \pm SD. ND: not determined. ¹: tested at 50 μ M. ²: tested at 100 μ M.

4.5 Discussion

There are many positive-sense RNA viruses that cause significant disease in host populations. However, progress on the development of antivirals and effective vaccines for many of these viruses remains slow. The current work aimed to use *in silico* modelling and virtual screening in combination with *in vitro* biological screening in enzyme and cell-based replicon assays to uncover drug-like compounds with broad-spectrum non-nucleoside inhibitor (NNI) activity against viruses of the *Caliciviridae* family and later expanded to include the *Flaviviridae* and *Picornaviridae*. The present work identified two compounds – NCS-013 and NCS-013A – with broad-spectrum inhibitory activity against at least two different viral families and suggests that designing NNI compounds possessing broad-spectrum antiviral activity may yet be possible.

4.5.1 Virtual screening in an environment lacking prior knowledge

Virtual screening is an attractive drug discovery method due to its capacity to screen large compound databases for a fraction of the cost compared to HTS. However, the process of constructing good-quality pharmacophores for virtual screening usually relies on extensive prior knowledge (509, 510). In the current study however, limited prior knowledge was available. From the perspective of a ligand-based approach, there are no NNIs approved for use against the *Caliciviridae*, and only a small list of NNI compounds have experimentally demonstrated antiviral activity. Furthermore, as the original intention of this study was to target the Site-B binding pocket, only compounds that bound to that site would be useful. From a structure-based perspective, only a few calicivirus RdRp crystal structures were available and of these, only two structures (PDB ID: 4LQ3 and 4O4R) were in complex with an inhibitor bound at Site-B (114, 487). Therefore, the current study utilised a combination of both ligand and structure-based knowledge to construct complex-based pharmacophores for virtual screening (Figure 4.2).

A docking approach was first used to identify interacting residues that could play an important role in the RdRp binding and inhibitory effects or lack thereof, for the compounds JTK-109, TMC647055, Beclabuvir and JTK-M (listed in order from

lowest overall IC₅₀ as per (147)). Two trends were observed, firstly compounds that made more predicted interactions with the resistance mutation Arg419 across the crystal structures also possess greater broad-spectrum activity and lower IC₅₀. However, JTK-M made the same number of interactions with Arg419 as JTK-109 and yet has no inhibitory activity (Table 4.3). This suggests that there must be additional interacting residues that are critical to the anti-transcriptional effects of JTK-109.

Closer comparison of the binding orientations of these two molecules revealed that JTK-109 made frequent interactions with motif E residue Arg392, which plays a role in binding the priming nucleotide (505, 506) as well as the adjacent motif E residue, Arg391 (Table 4.3). In contrast, interactions between JTK-M and motif E residues were less frequent. Together, the two trends suggest that Arg419 may play a role in compound binding affinity, whereas interaction with Arg392 and other motif E residues may be involved in sterically hindering transcription.

Following virtual screening, the resulting compound hitlist was filtered using various molecular property and substructure filters to improve the potential drug-likeness of compounds selected for testing (Figure 4.2). Lipinski's rule of five predicts that poor solubility and permeability is likely, when, for example, MW > 500 Da and logP > 5 (511). Therefore, hit lists were first filtered using molecular weight (<450 Da) as well as logP and ClogP (<5). Additionally, compounds containing undesirable structural elements and PAINS moieties were also excluded (512). PAINS compounds notoriously present as false positive results in many HTS assays via assay interference rather than true biological activity, therefore by removing compounds containing these PAINS moieties the possibility of encountering these problematic compounds was reduced.

The remaining compounds were also required to undergo a two-step docking assessment, examining interactions with Arg392 and the two non-motif Site-B residues Gln414 and Arg419. To maximise the diversity of the chemical space sampled during biological testing, structures within the hit lists were also clustered in LS based on 3D pharmacophore features, and only one compound from each cluster was tested.

However, after the first set of 11 compounds failed to yield any active structures able to inhibit norovirus RdRp transcription (Figure 4.9), some filtering

parameters were relaxed ($MW \leq 500$ Da, logP/ClogP and docking requirements excluded) and a second set of 23 compounds from unsampled clusters were purchased (Table 4.5).

4.5.2 NCS-013 inhibits *Caliciviridae*, *Flaviviridae* and *Picornaviridae* RdRp/replicon replication

4.5.2.1 *Caliciviridae*

Caliciviruses have been found in nearly every vertebrate group and include several human and non-human pathogenic viruses, some of which can lead to lethal consequences in their hosts (219). However, there is a lack of antiviral therapies and vaccines. Although vaccines do exist for some pathogenic non-human caliciviruses, for example RHDV and FCV, protection can be variable depending on the vaccine (513, 514), and so there is still an unmet need for the development of effective antiviral treatments. The present work identified one compound, NCS-013 which displayed cross-genera inhibition of two members of the *Caliciviridae*, human norovirus ($55.9 \pm 3.8\%$ at $50 \mu\text{M}$, Figure 4.10) and FCV ($51.3 \pm 5.4\%$ at $50 \mu\text{M}$, Figure 4.11). Although the potency of NCS-013 would require significant improvement, the identification of this compound with cross-genera activity indicates there is opportunity for development of broad-spectrum drugs to target this family of viruses.

4.5.2.2 *Flaviviridae*

Since NCS-013 was derived from a virtual screen based on HCV NNIs, it was also assessed for activity against both HCV itself and Zika virus, another member of the *Flaviviridae* family. Zika virus is a member of the genus *Flavivirus* which includes several pathogenic human viruses that are transmitted by arthropod vectors and for which there are no approved treatments. Although effective vaccines do exist for some of these viruses (such as yellow fever virus (515) and tick-borne encephalitis virus (516)), cases can still occur in endemic regions due to insufficient vaccination of the local population or unvaccinated travellers. A recent example of this was the 2016 Angola and Democratic Republic of Congo yellow fever outbreak that led to 961 confirmed cases and 137 deaths (517). Although mass vaccination and vector control strategies were eventually able to contain the outbreak, maintaining vaccine coverage

in endemic regions remains a challenge. Therefore, it is important to develop antiviral therapies for these infections. In addition to its activity against caliciviruses, NCS-013 also produced $62.5 \pm 23.6\%$ inhibition of the HCV replicon replication when examined at $10 \mu\text{M}$ in Huh7 cells (Figure 4.15). It similarly demonstrated $58.4 \pm 22.6\%$ inhibition of the Zika virus RdRp when used at $100 \mu\text{M}$ (Figure 4.12). The cross-genera and cross-family activity of NCS-013 may help inform future broad-spectrum antiviral development.

4.5.2.3 *Picornaviridae*

Members of the large *Picornaviridae* family can cause a wide spectrum of clinical manifestations in their hosts, which includes potentially life-threatening diseases such as meningitis, encephalitis, and myocarditis (518, 519). As for the *Caliciviridae* and *Flaviviridae* however, there are currently no approved antiviral agents against picornavirus infections. To further explore the broad-spectrum potential of NCS-013, it was also trialled against HAV, a member of the *Picornaviridae*. NCS-013 showed inhibition of HAV replicon replication ($45.6 \pm 10.1\%$ at $10 \mu\text{M}$) (Figure 4.15). Although this inhibitory activity was unexpected, it is nonetheless a useful starting point for the design of future HAV and picornavirus inhibitors.

4.5.3 Does NCS-013 bind within Site-B?

Following identification of NCS-013 as a potential broad-spectrum NNI in primary screening assays, an important step was to verify that the activity was the result of target-specific inhibition rather than through assay interference. Although efforts were made to decrease chances of encountering promiscuous compounds using online substructure filters (495, 496), it is nonetheless essential to confirm the mechanism of inhibition. This is especially important in the case of NCS-013 since it showed a similar level of inhibition against targets measured using the same assay method – norovirus, FCV and Zika (picogreen dye fluorescence) and HCV and HAV (luciferase bioluminescence). Additionally, all activity assays performed in the study utilised light-based detection and thus may be subject to similar interference mechanisms (520). Such verification is usually accomplished using an orthogonal assay that utilises a different reporter format to examine compound activity. Therefore, this

study attempted to confirm the compound's binding within Site-B using two different methods.

Firstly, NCS-013 was docked into the Site-B binding pocket of human norovirus, MNV, SaV and RHDV crystal structures and favourable interactions with Site-B residues were examined. Across the six crystal structures, NCS-013 made few interactions with the Site-B residues Gln414 (n=1/6) and Arg419 (n=3/6), and only interacted with motif E residue Arg392 in two of the structures (Table 4.7). More importantly, it did not simultaneously interact with both the non-motif residues and Arg392. Instead, predicted binding orientations were either positioned higher up in the structure, where they interacted with Arg419 and stretched from the thumb to the fingers domain (Figure 4.16, in blue) or were positioned deeper within the protein to interact with Arg392 (motif E) but without any interactions with Gln414 or Arg419 (Figure 4.16, in pink). Based on these predicted docking interactions, NCS-013 was judged unlikely to bind to Site-B B in the originally intended conformation. However, it is possible that the activity demonstrated by NCS-013 was caused by interactions within the large Site-B pocket via a different binding orientation or through binding to another site on the polymerase leading to its weak activity across different assays.

Since *in silico* modelling of NCS-013 was inconclusive, further attempts were made to investigate its potential binding within Site-B by comparing relative inhibitory activity using wild type and mutant RdRps *in vitro*. Mutant RdRps previously generated in our lab based on JTK-109 binding were used. The IC₅₀ of NCS-013 against the mutant RdRps was less than 30% greater than the IC₅₀ against wild type norovirus RdRp and hence the mutations did not appear to offer any significant resistance against NCS-013 (Figure 4.17). In contrast, the mutants were resistant to JTK-109 and neither reached 50% inhibition even at 100 µM (147). From this, it can be inferred that NCS-013 did not bind to Site-B in the originally intended conformation. Similarly, this result does not preclude the possibility of binding within the Site-B pocket in a different orientation or binding at a different site

4.5.4 Effect of NCS-013 on other mammalian targets

The current work is not the first time that NCS-013 has been identified in a pharmacophore based virtual screening experiment. NCS-013 was previously reported as a potent and selective agonist of peroxisome proliferator activated receptor- α (PPAR- α) (EC_{50} : 1.1 nM) and named ZINC06472206 (521). PPAR- α is expressed in tissues such as the liver, heart, skeletal muscle, kidney, and intestine (522). This receptor is a transcription factor important for the regulation of lipid metabolism. It is activated by the binding of a class of amphipathic carboxylic acids known as fibrates, which also possess pleiotropic anti-inflammatory effects (523, 524). Specifically, PPAR- α is activated in response to energy deprivation and induces fatty acid catabolism and ketogenesis (525). Activation of PPAR- α leads to a decrease in serum triglycerides and an increase in high-density lipoprotein cholesterol, making it an important pharmaceutical target for the treatment of dyslipidaemia (522). It is well established that viruses can manipulate cholesterol and triglyceride metabolism pathways to promote an environment that is optimal for their replication (526-529), making them potential drug targets for the treatment of viral infections. For example, fenofibrate, a PPAR- α agonist, has been reported to reduce mortality and improve neurological outcomes in murine models of Japanese encephalitis virus (530), it also inhibits HIV replication in cell culture models (531). A more recent study has shown that flavivirus infection leads to reduced peroxisome biogenesis and proposed that this may be a viral mechanism to hinder early antiviral signalling and thus compromise the antiviral defence (532).

In the context of the current work, the inhibitory effects of NCS-013 in viral RdRp transcription assays would not be affected by the highly potent off-target effects on PPAR- α since they were protein activity assays. However, it is possible that for the replicon replication assays performed in Huh7 hepatocyte cells, NCS-013 binding to PPAR- α may have contributed to the antiviral effects via an unknown mechanism. Future structure-activity relationship (SAR) and compound optimisation studies should therefore also consider the potential off-target effects due to potent binding of NCS-013 to PPAR- α .

4.5.5 Future directions and potential for further development

In addition to NCS-013 and NCS-013A, three other compounds (NCS-014, NCS-032 and NCS-034) also demonstrated inhibitory activity against one of the targets assessed (summarised in Table 4.8). Future work should aim to verify the antiviral activity of these compounds in orthogonal assays. In some respects, the lack of broad-spectrum activity across targets measured using the same assay system (NCS-013A, NCS-014, NCS-032 and NCS-034) could be an indication of target-derived activity rather than non-specific interference. Future confirmatory studies should also aim to use fresh, resynthesised, pure material to ensure activity is due to the compound of interest rather than impurities or degradation products.

Unfortunately, the level of inhibition demonstrated by the five active compounds, NCS-013, NCS-013A, NCS-014, NCS-032 and NCS-034 was not potent enough to justify the extensive time and resources required for SAR and optimisation studies in this instance. For comparison, pharmaceutical companies would typically identify “hit” molecules from HTS with a potency in the 100 nM – 5 μ M range to progress to the lead phase (533).

The compounds identified in this study could be useful as scaffolds for future drug discovery screening applications pending confirmation of target-derived activity. The successful identification of NCS-013A through a similarity search of catalogue available compounds, indicates that this approach could be a lower-cost strategy for early SAR analysis. This could be applied to NCS-032, for example, to search for more potent inhibitors of the HAV replicon, and potentially other picornaviruses. The mechanism of action for NCS-032 against HAV should be investigated to verify target-specific activity. Interestingly, some compounds identified in the study also appeared to have a stimulatory effect on the replicons. This could be due to compound interaction with the replicon and worth further investigation. Additionally, future work should also aim to identify the binding site of these compounds so that more targeted compound optimisation strategies may be utilised. This could be achieved through generation and sequencing of drug-resistant viruses.

4.6 Concluding remarks

This chapter explored the application of virtual screening for the development of broad-spectrum NNIs. The NNI inhibitors JTK-109 and TMC647055 were used to construct complex-based pharmacophore models for screening the SPECS compound database. Selected compounds were examined for activity *in vitro* against a variety of RdRp/replicons. This study identified two potentially broad-spectrum NNI compounds (NCS-013 and NCS-013A) as well as three other compounds with inhibitory effect against a single target (NCS-014, NCS-032, NCS-034) (summarised in Table 4.8). The current work also applied a low budget “SAR by catalogue” approach to search for additional compounds with inhibitory activity. The successful identification of NCS-013A provides some evidence for the utility of NCS-013 as a scaffold for future broad-spectrum NNI design.

5 Molecular epidemiological surveillance of norovirus in Australia, 2018 to 2020

5.1 Abstract

Norovirus causes 677 million annual cases of acute gastroenteritis globally, resulting in more than 210,000 deaths and encumbering the global economy by \$65 billion per year. Historically, antigenically novel strains have emerged from the genogroup II genotype 4 (GII.4) lineage every 3-5 years to cause pandemic gastroenteritis. As per this study, more than nine years have passed since the last pandemic variant, Sydney 2012 emerged. However, contrary to historical trends where entirely new strains emerge, the Sydney 2012 strain has been exceptional. This is because the structural region (GII.4 Sydney 2012) has extended its circulation through recombination to obtain new non-structural regions, such as from a GII.P16 virus. We investigated circulating noroviruses in Australia before and into the COVID-19 pandemic (2018-20) to identify novel recombinant strains, especially those with epidemic potential. Viral RNA was extracted from both stool (n=727) and monthly wastewater samples from three treatment plants (n=108) and amplified by RT-PCR. Amplicons from clinical samples were Sanger sequenced and data subjected to phylogenetic analysis. Amplicons from wastewater samples were sequenced on the Illumina MiSeq platform, and reads were aligned to reference sequences to determine strain prevalence. We observed the continued high prevalence of the GII.4 Sydney 2012 [P16] virus (23.0%, n=139/604), albeit co-dominant with two other strains (GII.3 [P12] (18.2%, n=110/604) and GII.2 [P16] (20.2%, n=122/604)) that have waxed and waned in prevalence. We show in this study, lockdowns reduced norovirus levels in sewage by more than 90% in May to September 2020 (1.4×10^5 genome copies/L) compared to the equivalent time periods in 2018 (1.6×10^6 gc/L) and 2019 (1.9×10^6 gc/L). The relaxation of these measures at the end of 2020 coincided with a strong resurgence in GII.2 [P16] prevalence in both clinical and wastewater samples. Wastewater surveillance successfully detected changes in GII.3 [P12] strain prevalence prior to increases in clinically detected outbreaks. Furthermore, it enabled navigation of clinical sampling gaps so that a more complete molecular epidemiological picture was obtained. The addition of ORF1/2 overlap genotyping in sewage enhanced our sentinel surveillance capabilities by facilitating the detection of recombinant viruses that may possess epidemic or pandemic potential.

5.2 Introduction

Acute gastroenteritis (AGE) is the fifth most common cause of mortality, particularly in developing countries, and is estimated to result in 1.5 million deaths each year (161). Norovirus is the leading cause of viral gastroenteritis globally and infects approximately 677 million people each year (534), costing the global economy an estimated US\$65 billion (179). Norovirus is also estimated to cause more than 210,000 deaths annually, the majority of which occur in children less than five years of age (179). Clinical symptoms of norovirus include diarrhoea, vomiting, chills, nausea, abdominal cramps, and low-grade fever (5). Although infection is generally self-limiting in healthy adults, the disease can be prolonged and debilitating in immunosuppressed patients, the elderly and in infants (187-189).

Norovirus is highly transmissible; it has a low infectious dose of $\sim 10^3$ virions (234) and patients can shed up to 10^9 genome copies/g of faeces (235). Additionally, viral shedding can last for four weeks (235, 236, 535) and virions can remain infectious in the environment for days to weeks (242). These combined traits make norovirus extremely efficient at rapidly spreading in semi-closed environments: it is the most common agent of viral gastroenteritis in aged-care facilities (232), hospitals (244), cruise ships (246, 247), and schools (245).

Norovirus is a genus of positive-sense single-stranded RNA viruses belonging to the *Caliciviridae* family. Noroviruses can be classified into ten different genogroups (GI-GX) based on amino acid diversity of full-length VP1 protein (530-580 amino acids) and eight different P-groups based on similarity within the 3' end of the RNA-dependent RNA polymerase (RdRp) region (762 nucleotides) (224). Genogroups can be further divided into 49 different capsid genotypes and 60 different P-genotypes. Viruses from GI, GII, GIV, GVIII and, GIX are associated with human infection, with GII of greatest clinical significance, accounting for more than 90% of all human norovirus infections globally (228, 229). Within GII, noroviruses belonging to genotype 4 (GII.4) lineage have historically been associated with epidemics and six recorded pandemics of viral gastroenteritis, with antigenically novel variants typically emerging every 3-5 years

(between 1996 and 2012) (summarised in section 2.2.7). The new variants circulated until they are replaced by their successor (231, 295). During circulation the dominant pandemic GII.4 variant usually accounts for around 60-80% of all norovirus infections globally (229-232).

The primary evolutionary drivers for the emergence of novel variants are both antigenic drift that leads to amino acid changes in the capsid, and recombination at the structural/non-structural boundary (ORF1/2 overlap), which enables the exchange of non-structural and structural elements of the genomes during a co-infection (223, 286). The norovirus capsid protein comprises three domains, the shell (S) domain forms the interior surface of the icosahedral shell whilst the protruding P1 and P2 domains are exposed on the surface (218). Antigenic variation usually occurs in the P2 capsid domain, facilitating viral evasion from herd immunity (216). Together with recombination, these sequence changes can lead to the emergence of epidemic and pandemic variants (229, 286, 295, 303).

Emerging in late 2012, the pandemic GII.4 [P31] Sydney 2012 variant (295) dominated the norovirus epidemiological space around the world (301, 536, 537) including, Australia and New Zealand until the end of 2015 (303). In 2016 however, the patterns of norovirus molecular epidemiology changed. Instead of the emergence of an antigenically novel GII.4 capsid variant, two daughter recombinant strains emerged, each retaining the Sydney 2012 capsid whilst acquiring different non-structural regions – [P4 New Orleans 2009] (538) and [P16], respectively (539). The recombinant GII.4 Sydney 2012 [P16] became the predominant norovirus detected in clinical samples from Australia and New Zealand in 2017 (229). The GII.4 Sydney 2012 [P16] virus was the predominant strain identified from outbreaks in Canada (536) and the US (537, 540), and has subsequently been detected around the world in Europe (312, 541, 542), South America (543, 544), Oceania (229, 303) and Asia (313, 545).

Despite its spread around the world, the recombinant GII.4 Sydney 2012 [P16] did not achieve the same level of success in Asia during 2016-2018 as compared to its pandemic predecessor. For example, as of February 2017, this strain had only been detected from a single sample in Thailand (546), whilst in Japan, a different

recombinant strain, GII.2 [P16] overtook GII.4 noroviruses in mid-2016 as the predominant cause of gastroenteritis outbreaks in children (547). Additionally, norovirus outbreak surveillance in China from late 2016 to September 2018 failed to identify any outbreaks linked to the recombinant GII.4 Sydney 2012 [P16] (245). Instead, the dominant norovirus identified during this period in Asia was again the recombinant GII.2 [P16] norovirus (546-550). This virus has also been detected in other continents around the world, including North America (536, 540), South America (544, 551) and Europe (312, 552). It was also detected in high prevalence in clinical stool specimens sampled in Australia (23.6%) and New Zealand (13.9%) during 2016 (303), and achieved greatest prevalence in January 2017 (AU = 33.3%, NZ = 37.5%) (229). In summary, the two dominant strains were GII.4 Sydney 2012 [P16] and GII.2 [P16].

To identify novel recombinants and emerging viruses with epidemic potential, ongoing surveillance of circulating noroviruses in the population is crucial. Recent publications have demonstrated wastewater is an invaluable tool for mapping the changing molecular epidemiological trends of enteric pathogens (229, 303, 553-555), which can now be done at a city-based population scale. Our group has previously identified an increasing prevalence of GII.2 noroviruses in clinical cases was also detected in sewage samples. This virus was detected from May 2016 which occurred two months before this trend could be seen in clinical samples (303). We have also detected the high prevalence of a probably mild/asymptomatic circulation of GII.17 viruses in January 2016 (68.6% of reads) as this virus was not detected in clinical samples from the same timeframe (303). Therefore, wastewater can provide invaluable insight into the true dynamics of circulating norovirus within a population, capturing both clinically important strains and genotypes associated with mild or asymptomatic infection, potentially providing an early warning of emerging strains.

Since the emergence of recombinant viruses GII.4 Sydney 2012 [P16] and GII.2 [P16] in 2016, the molecular epidemiological landscape of norovirus has changed. Instead of the circulation of a single dominant virus, there has been an interesting pattern of co-dominance. The present chapter investigated circulating noroviruses in Australia from January 2018 – December 2020, to identify novel recombinant strains, emerging strains in children, and those with epidemic potential. Wastewater samples

were used to circumvent selective biases (usually disease severity) that can occur with clinical sampling alone and to provide sentinel surveillance of potentially emerging strains.

5.3 Materials and methods

5.3.1 Ethics and collection of clinical samples

This study was approved by the University of New South Wales (UNSW) Human Research Ethics Advisory Panel (HC16828 and HC17459). All clinical samples used in this study were collected between January 2018 and December 2020. Norovirus-positive clinical stool samples were collected in New South Wales (NSW), Australia as part of routine diagnostic services or norovirus surveillance programs.

A total of 727 clinical specimens were collected from institutional gastroenteritis outbreaks and sporadic cases submitted to the Prince of Wales Hospital and Douglas Hanley Moir for routine norovirus diagnosis. We thank Peter Huntington, Richard Jones and their respective teams for provision of samples. Outbreaks were either defined by the detection of two or more norovirus-positive cases possessing the same genotype linked by time, location, or from epidemiological tracing performed by NSW public health authorities.

5.3.2 Collection of wastewater samples

Between January 2018 and December 2020, monthly 24-hour composite influent samples were collected using an autosampler from the Bondi (pop. 318,810) and Malabar (pop. 1,857,740) wastewater treatment plants (WWTP) in Sydney, Australia and from the Western WWTP (pop. 2,400,000) in Melbourne, Australia. All samples were delivered to UNSW on ice, aliquoted and stored at -80°C upon arrival.

5.3.3 Viral concentration, RNA extraction and cDNA synthesis

Clinical stool samples were prepared as 20% suspensions (v/v) in water and viral RNA extraction was performed as previously described (299, 556). Viruses in wastewater samples (10 mL) were concentrated by ultracentrifugation at 216,000 $\times g$ at 4°C for 1.5 hours and viral RNA extraction was performed using the QIAmp Viral RNA mini kit (Qiagen, Hilden, Germany) as described in (303). First-strand cDNA was then

synthesised from the extracted RNA using SuperScript VILO Master Mix (Invitrogen, Carlsbad, CA, USA) for clinical samples and using SuperScript IV VILO Master Mix (Invitrogen) for wastewater samples. Reactions were performed as per manufacturers' guidelines. The processing of clinical and wastewater specimens is summarised in Figure 5.1 below.

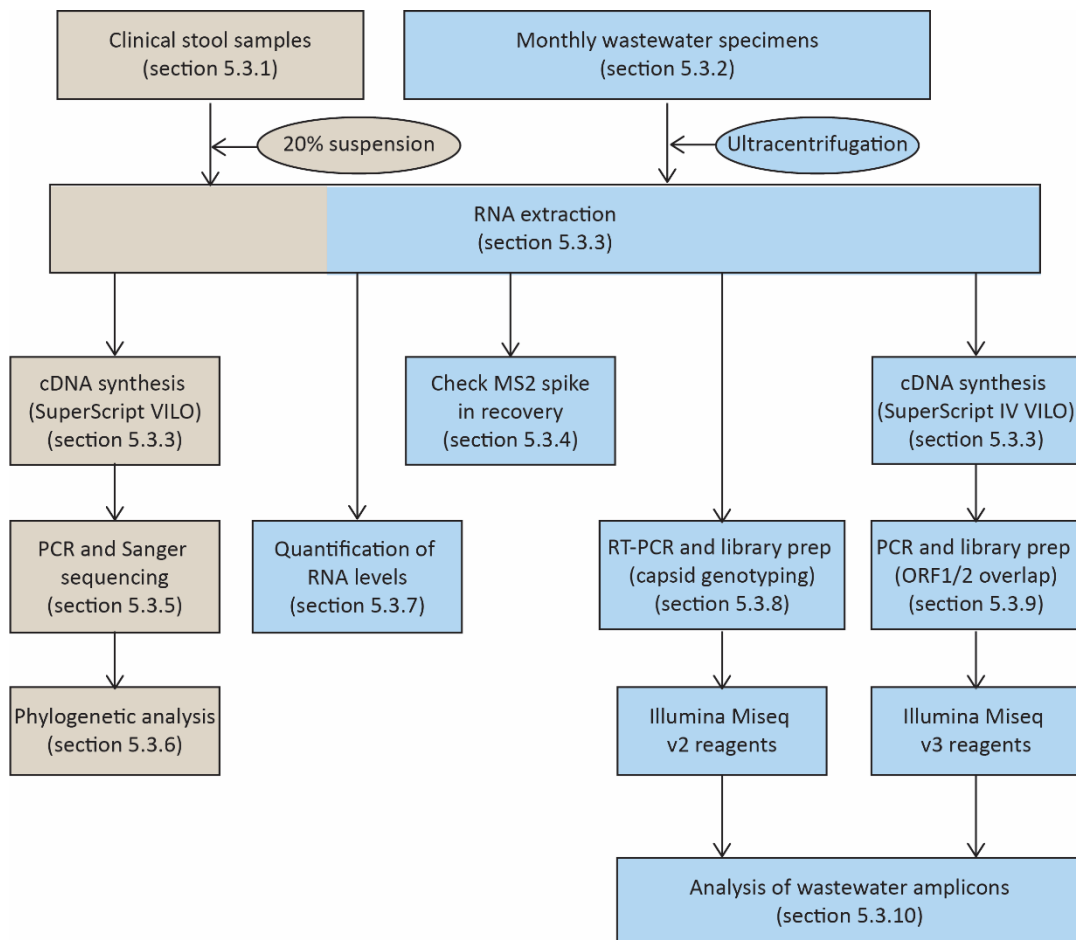


Figure 5.1. Norovirus surveillance workflow.

The main processing steps for the surveillance of norovirus from clinical (brown) and wastewater (blue) specimens are summarised. For clinical stool samples, RNA was extracted followed by cDNA synthesis, PCR, Sanger sequencing and phylogenetic analysis. For wastewater, RNA was extracted, and it was used for four different purposes. It was independently used to 1) check MS2 recovery, 2) quantify norovirus RNA levels, 3) for capsid next generation sequencing (NGS) and 4) to synthesise cDNA for ORF1/2 overlap NGS. After NGS, amplicons were then analysed.

5.3.4 MS2 bacteriophage process control

The MS2 bacteriophage was spiked in as an internal process control for the wastewater ultracentrifugation and RNA extraction as described in (303) (Figure 5.1). The MS2 bacteriophage spikes were prepared as 20 µL frozen spherical aliquots by

dropping them into liquid nitrogen. The concentration of aliquots was determined to be $1.4 \times 10^6 \pm 5.3 \times 10^5$ genome copies (gc) of viruses per 20 μ L (Appendix Table 8.1). MS2 RNA recovery was measured using the iTaq Universal SYBR Green One-Step Kit (Bio-Rad, CA, USA), 4 μ L of input RNA in each reaction (20 μ L) and the primers GV117/GV118 (Table 5.1). Cycling conditions were 50°C for 10 minutes and 95°C for 1 minute, followed by 40 cycles of 95°C for 15 seconds, 55°C for 20 seconds and 72°C for 20 seconds. Valid assays produced a cycle threshold (ct) value of 23.0 ± 0.9 in all wastewater samples (n=108).

5.3.5 Amplification and sequencing of clinical specimens

Norovirus detection was first performed on synthesised cDNA using a duplex PCR (GI primers: COG1F/G1SKR, GII primers: G2F3/G2SKR) targeting the 5' end of the capsid gene of GI and GII noroviruses (295) (Table 5.1, Figure 5.1). For the identification of recombinant strains, a PCR targeting the ORF1/ORF2 overlap region was carried out using the following primers – GI: MON432/G1SKR, GII: MON431/G2SKR (557-559) (Table 5.1). All PCR products were visualised on agarose gels to confirm size, enzymatically purified and then Sanger sequenced (methods as described in sections 3.1.1 to 3.1.3).

Table 5.1. Primers used to amplify norovirus and MS2 sequences.

Primer/probe	Sequence (5'-3') ^{a, b}	Reference
GV117	AAT CCA TTT TGG TAA CGC CGG AAC CAT AGG C	(560)
GV118	GCA CAC GGG GTG CAA TCT CAC TGG	(560)
G2F3	TTG TGA ATG AAG ATG GCG TCG A	(295, 557)
G2SKR	CCR CCN GCA TRH CCR TTR TAC AT	(295, 557)
COG1F	CGY TGG ATG CGN TTY CAT GA	(295, 557)
G1SKR	CCA ACC CAR CCA TTR TAC A	(295, 557)
MON431	TGG ACI AGR GGI CCY AAY CA	(558, 559)
MON432	TGG ACI CGY GGI CCY AAY CA	(558, 559)
G2F1	GTG GGA GGG CGA TCG CAA TCT	(557)
G2R1	TGC ATA ACC ATT RTA CAT TCT	(557)
Hep172	GGB TGG TTT GGA AAR YTG GA	(292)
T7-NV2oF	taa tac gac tca cta tag gg TGG GAG GGC GAT CGC AAT CT	This study
NV2oR	GTR AAC GCR TTY CCM GC	(222)
NV2oF2	GGA GGG CGA TCG CAA TC	This study
G2F3P	FAM-TGT GAA TGA AGA TGG CGT CGA ATG AC -ZEN/lowa Black ^c	This study

aG2F3	tcg gca gcg tca gat gtg tat aag aga cag TTG TGA ATG AAG ATG (303) GCG TCG A
aG2R1	gtc tcg tgg gct cgg aga tgt gta taa gag aca g TGC ATA ACC ATT (303) RTA CAT TCT
aMON431n	tcg gca gcg tca gat gtg tat aag aga cag TGG ACH AGR GGN CCY This study AAY CA
aG2SKR	gtc tcg tgg gct cgg aga tgt gta taa gag aca g CCR CCN GCA TRH This study CCR TTR TAC AT

^a Ambiguity code: Y, pyrimidine, (C/T); R, purine, (A/G); M, amino, (A/C); H, not G, (A/C/T); N, any base, (A/T/C/G); I, inosine, unconventional purine base.

^b Lowercase characters represent adapter or overhang sequence.

^c ZEN/Iowa Black: internal ZEN and Iowa Black double-quenched probe

5.3.6 Phylogenetic analysis of norovirus sequences

To genetically classify GI and GII noroviruses identified in this study, representative viral sequences from the different genogroups and genotypes were downloaded from GenBank. Phylogenetic analysis was conducted using the 5' end of the polymerase gene (GI: 267 nt, GII: 253 nt) and 3' end of the VP1 gene (GI: 295 nt, GII: 282 bp) (Table 5.1, Figure 5.1). The MUSCLE algorithm was used to align all sequences and maximum likelihood phylogenetic trees were constructed in MEGA X (225) using the Kimura 2-parameter (561) model and 1000 bootstrap replicates. The results were also confirmed using the Norovirus Typing Tool Version 2.0 accessed from <https://www.rivm.nl/mpf/typingtool/norovirus> (562).

5.3.7 Quantification of norovirus RNA levels in wastewater

Norovirus levels (GII) in wastewater samples were first quantified in extracted RNA by real-time RT-PCR using the pan GII primers NV2oF2/G2SKR and probe (G2F3P) targeting the 5' end of the major capsid protein gene VP1 (Table 5.1, Figure 5.1). Real-time RT-PCR was performed using the iTaq Universal Probes One-Step Kit (Bio-Rad, CA, USA) with 4 µL of input RNA in each reaction (20 µL). Cycling conditions were 50°C for 10 minutes and 95°C for 5 minutes, followed by 45 cycles of 95°C for 20 seconds, 55°C for 20 seconds and 72°C for 20 seconds. Ten-fold dilutions of synthesised GII norovirus RNA were used to generate the standard curve for quantification.

To generate the template for RNA synthesis, GII norovirus cDNA was amplified using the primers T7-NV2oF/NV2oR, containing the T7 promoter sequence (Table 5.1). T7 RNA synthesis was then performed using the HiScribe T7 High Yield RNA Synthesis

Kit (New England BioLabs, Ipswich, MA, USA), followed by RNA purification using the Monarch RNA Cleanup Kit (New England Biolabs) both as per manufacturer' guidelines.

5.3.8 Capsid genotyping of norovirus in wastewater samples from Sydney and Melbourne

To understand the molecular diversity of GII noroviruses circulating within the wider community, norovirus genotypes in wastewater were investigated. Semi-nested RT-PCR was performed on the extracted RNA to amplify the 5' end of the VP1 gene for GII norovirus and Illumina Miseq library preparation were performed as described in (303) (Figure 5.1). Briefly, one-step RT-PCR was performed using G2F1/G2R1 (Table 5.1) and SuperScript III One-Step RT-PCR System with Platinum Taq DNA Polymerase (Invitrogen, Carlsbad, CA, USA). A second round PCR was performed using the aG2F3/aG2R1 primers to attach Illumina sequencing adapters (denoted with "a" before primer name) (Table 5.1). PCR amplicons were then purified using Agencourt AMPure XP beads (Beckman Coulter, CA, USA). The next-generation sequencing (NGS) library was then prepared using Nextera XT indexes (Illumina, San Diego, CA, USA) followed by further bead purification. The KAPA Library Quantification Kit (Roche, Clifton, NJ, USA) was used for qPCR-based library quantification prior to sample normalisation and pooling. Samples were submitted to the Ramaciotti Centre for Genomics (UNSW) where fragment sizes were evaluated on a Tape Station D5000 (Agilent Technologies, Santa Clara, CA, USA) and the library was prepared with a 10% PhiX spike-in. Paired-end DNA sequencing was performed on the Illumina Miseq platform using a v2 reagents (500 cycle chemistry) and terminated at 2 x 200 bp reads.

5.3.9 ORF1/2 overlap genotyping of norovirus in wastewater samples from Sydney and Melbourne

Nested PCR was performed on the synthesised cDNA (section 5.3.3) to amplify 570 nt of the GII norovirus ORF1/2 overlap region (Figure 5.1). An initial outer PCR was performed with the Hep172/NV2oR primers (222, 292) (Table 5.1) and using the Platinum SuperFi II Green Master Mix (Invitrogen, Carlsbad, CA, USA). This was followed by an inner PCR performed with the aMON431n/aG2SKR primers (557, 559, 563) (Table 5.1) and using the KAPA HiFi HotStart ReadyMix for the inner adapter PCR

(Roche, Clifton, NJ, USA) to attach Illumina sequencing adapters. All PCRs were assembled and performed as per manufacturer' protocol. Since high-fidelity polymerases are incompatible with primers containing inosine bases due to their proofreading ability, the original MON431 primer was modified to replace inosine with the degenerate bases H and N, respectively (renamed MON431n) (Table 5.1). Libraries were then submitted to the Ramaciotti Centre for Genomics where they were purified using Agencourt AMPure XP beads and Nextera XT indexes were attached. The library was then prepared with a 10% PhiX spike-in and sequenced on the Illumina Miseq platform using Miseq v3 reagents (600 cycle chemistry) using paired-end 300 bp reads.

5.3.10 Analysis of wastewater next-generation sequencing data

The software package Geneious Prime, version 2021.1.1 (Biomatters, Auckland, New Zealand) was used to analyse the Illumina MiSeq data (Figure 5.1). The paired-end sequences were merged using the BBMerge v38.84 plug-in on a low merge-rate setting and primer sequences were removed. The reads were then mapped to a list of 66 GII reference sequences containing various combinations of P-type and genotypes downloaded from GenBank and obtain in the present study (Appendix Table 8.2). The built-in Geneious "Map to reference" tool was used, and parameters were set to medium-low sensitivity and fine tuning with up to five iterations. Mapped sequences were discarded if there were less than 10 reads that mapped to a reference sequence in a given sample. The proportion of each genotype was then calculated by dividing the total number of reads per genotype by the total number of mapped reads for that sample. To compare capsid genotypic distribution obtained from the partial capsid and ORF1/2 overlap region approaches, sequences containing different P-types were pooled if the capsid genotype was the same.

5.4 Results

This study examined the prevalence of circulating norovirus genotypes in Australia using both clinical and wastewater samples. A total of 727 clinical norovirus positive stool specimens were collected in NSW between 2018 and 2020. Of these, 538 were associated with sporadic cases with the additional 189 samples collected from 66 different outbreaks. Additionally, 108 monthly wastewater specimens were collected

from three different wastewater treatment plants, two from NSW and one from Victoria.

5.4.1 Norovirus outbreaks in NSW, Australia

A total of 66 norovirus-associated AGE outbreaks were genotyped using stool specimens collected from 189 sampled patients during the study period, 2018-2020. The scale of these outbreaks varied considerably (ranging from 2 – 131 people) and affected more than 920 patients in total. Six different outbreak settings were identified – aged care facility, cruise ship, hospital ward, private home, childcare centre, and social function (Figure 5.2A). Most outbreaks occurred in aged care facilities (40.9%, n=27/66), followed by hospital wards (36.3%, n=24/66) and then cruise ships (13.6%, n=9/66). GII noroviruses were identified in 89.3% of outbreaks (n=59/66) whilst GI viruses were identified in 9.9% (n=6/66) and the much rarer GIX in a single outbreak in a hospital ward (1.5%, n=1/66) (Figure 5.2B). Norovirus outbreaks in NSW, Australia were caused primarily by GII.4 Sydney 2012 [P16] (25.8%, n=17/66), followed by GII.3 [P12] (21.2%, n=14/66), GII.2 [P16] (18.1%, n=12/66) and GII.4 Sydney 2012 [P4 NO 2009] (12.1%, n=8/66) (Figure 5.2B).

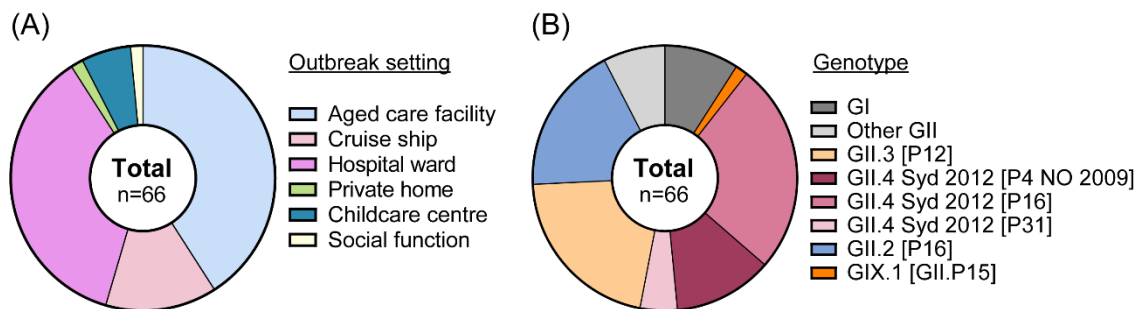


Figure 5.2. Settings and genogroup classification of norovirus strains identified from outbreaks in NSW, Australia between 2018-2020.

Sixty-six norovirus outbreaks were genotyped within the study. (A) Outbreak settings where norovirus was identified as the causative agent, with colours denoting settings, as shown in the legend. (B) Genotype identification of the norovirus strain sequenced, with colours denoting genotype. An outbreak was defined as two or more cases sharing the same genotype, linked by location and time or from epidemiological tracing performed by NSW public health authorities.

5.4.2 Institutional gastroenteritis outbreaks reported in NSW, Australia

The emergence of new norovirus strains of clinical significance is often marked by sudden increases in gastroenteritis activity. For this reason, the monthly number of institutional gastroenteritis outbreaks was also obtained from the NSW Ministry of Health (MoH), Australia to enable identification of temporal changes in gastroenteritis activity between 2018 and 2020. Since elevated levels of AGE activity were reported in 2017 due to the emergence of GII.4 Sydney 2012 [P16] (229), numbers were compared to 2016 instead.

During 2018, the number of reported gastroenteritis outbreaks (n=684) was comparable to 2016 (n=793) (303) and no remarkable increases or declines in AGE activity was observed (Figure 5.3, Appendix Figure 8.1). Between August and December 2019, a period of elevated gastroenteritis activity was observed where 731 institutional gastroenteritis outbreaks were reported across NSW to the MoH and represented a 2.0-fold and 2.8-fold increase in outbreaks compared to the same period in 2016 (n=368) (303) and 2018 (n=259), respectively (Figure 5.3). This increase in outbreaks was concentrated in childcare facilities (71.8%, n=525/731) (Figure 5.3), and during this time the GII.3 [P12] virus was prevalent among children <5 years of age (explored later in section 5.4.4).

In 2020, institutional gastroenteritis outbreaks could be separated into three periods, the pre-lockdown (January to March), lockdown (April to September) and easing (October to December 2020). During the pre-lockdown period a similar number of institutional gastroenteritis outbreaks (n=188) were reported to the MoH compared to the same period in 2016 (n=164) (303) and 2018 (n=193) (Figure 5.3). During lockdown however, a marked decrease in institutional outbreaks occurred; from April to September 2020, only 90 institutional gastroenteritis outbreaks were reported, this represented a ~4.5-fold reduction in reported gastroenteritis outbreaks compared to 2016 (n=414) and 2018 (n=392) (Figure 5.3). In November 2020 however, a sudden spike in gastroenteritis outbreaks was reported to the MoH, and this increased activity continued until the end of the study period. In these two months alone, a total of 486 institutional gastroenteritis outbreaks were detected, which is 3.9-fold and 6.8-fold

higher than in 2016 (n=126) and 2018 (n=72), respectively. This increase in outbreaks was also concentrated in childcare facilities (91.0%, n=442/486) (Figure 5.3).

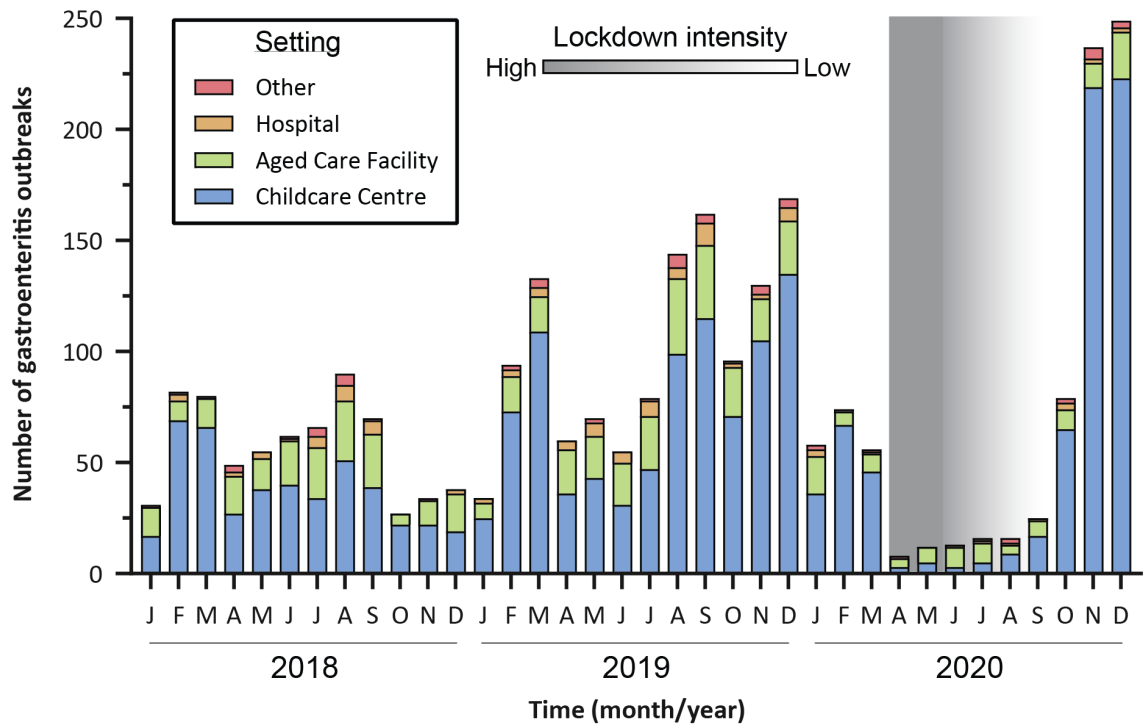


Figure 5.3. Institutional gastroenteritis outbreaks reported in NSW, 2018-2020.

The number of monthly institutional gastroenteritis outbreaks reported during 2018-2020 was obtained from the NSW Ministry of Health. The outbreak settings are categorised and represented by different colours as indicated by the legend. Lockdown intensity correlated with grey shading as shown, between April and October 2020.

5.4.3 Institutional gastroenteritis outbreak trends were reflected by the norovirus levels detected in sewage

Although institutional gastroenteritis outbreak data is useful for investigating sudden increases in gastroenteritis activity, it is heavily biased towards gastroenteritis disease in young children and the elderly due to the government mandated reporting of outbreaks in institutions including childcare centres and aged care facilities. Quantification of norovirus RNA levels within wastewater samples can offer a better way of monitoring the levels of viral activity in the community. Therefore, norovirus RNA levels were measured in monthly sewage samples collected from the large Malabar WWTP, which covers a population of 1.86 million, between 2018 and 2020.

From 2018 to 2020, norovirus levels quantified in wastewater ranged from 2.0×10^4 gc/L to 3.8×10^6 gc/L, with the higher levels typically observed during the colder months (July to October) (Figure 5.4). Changes in institutional gastroenteritis outbreak activity was also reflected by levels of norovirus detected in sewage samples collected at the corresponding timeframe. For example, during the first period of elevated institutional AGE activity between August and December 2019, norovirus viral load in wastewater also reached a peak of 3.8×10^6 gc/L sewage in August and remained at elevated levels ($>10^6$ gc/L sewage) throughout the remainder of 2019 (Figure 5.4). Similar trends were also seen for the trough period in late 2018, as norovirus levels gradually fell from seasonal winter peak of 3.3×10^6 gc/L in August down to just 2.6×10^4 gc/L in December 2018 (Figure 5.4), reflecting similar declines in institutional AGE activity reported to the MoH (Figure 5.3).

Trends seen in institutional gastroenteritis outbreaks during 2020 could also be observed in the wastewater samples. After lockdown orders were enforced on March 31, there was an immediate decrease in the levels of norovirus in the wastewater of more than 90%. As norovirus levels in April 2020 fell from 2.5×10^5 gc/L in March to below the quantitative RT-PCR detection limit (1.5×10^4 gc/L) and hence could not be measured accurately (Figure 5.4). Similarly, the number of institutional outbreaks reported in April ($n=8$), decreased by more than 85% in March ($n=56$) and remained low in subsequent months (May – September 2020) (Figure 5.3). As restrictions began to ease in June, norovirus concentrations in sewage also gradually returned to 2019 levels (1.5×10^5 gc/L) (Figure 5.4) and these trends observed in wastewater preceded similar observations from institutional reporting.

Overall, comparison of norovirus levels for the period following the lockdown termed the “socially distanced period” here, from May to September 2020 (1.4×10^5 gc/L) with the same period in 2018 (1.6×10^6 gc/L) and 2019 (1.9×10^6 gc/L), revealed an average overall decrease of more than 90% (Figure 5.4). This decline followed similar trends observed in institutional gastroenteritis outbreak activity reported by the NSW MoH (Figure 5.3).

Finally, during the second period of elevated activity (November to December 2020) norovirus levels in sewage continued to increase from August and reached their 2020 peak of 2.0×10^6 gc/L in December (Figure 5.4). This corresponded to the peak in institutional gastroenteritis outbreaks, largely seen in childcare centres, as reported by the NSW MoH (Figure 5.3).

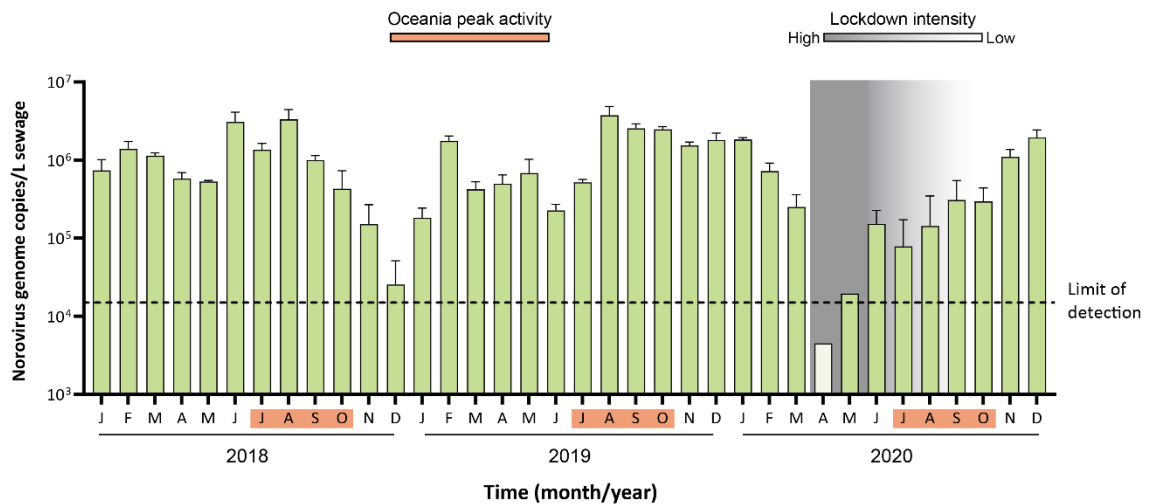


Figure 5.4. Quantification of GII norovirus in Sydney wastewater 2018-2020.

Genogroup II norovirus RNA levels were measured in monthly wastewater samples collected from the Malabar WWTP between 2018 and 2020. Periods of lockdown are indicated by grey shading, with lighter grey gradient representing easing restrictions whilst orange shading indicates the usual Oceania norovirus peak. Norovirus RNA levels in April 2020 were below assay detection limits and is represented by a pale green bar below the limit of detection. The mean and standard deviation for each sample was calculated from triplicate reactions.

5.4.4 The increases in AGE outbreak activity in NSW were not caused by the emergence of new strains

Following identification of two periods of increased institutional gastroenteritis outbreak activity in childcare facilities, between August and December 2019, and between November and December 2020, the circulating norovirus genotypes infecting children aged five and under were investigated to identify the potential emergence of new outbreak strains. Since patient samples were not available for many of the reported childcare outbreaks, genotyping data obtained from sporadic cases in children aged five and under was also included (n=267) (Figure 5.5).

Prior to the first spike in gastroenteritis activity in August 2019, the recombinant GII.3 [P12] strain represented only 20.0% of cases/outbreaks in children aged five and under (2018: n=17/85; January to July 2019: n=17/85) (Figure 5.5). The recombinant GII.4 Sydney 2012 [P16] was the predominant strain detected in children in 2018 (35.3%, n=30/85), whereas between January to July 2019, three strains were detected at similar rates (Figure 5.5). These were the GII.4 Sydney 2012 [P16] (22.4%, n=19/85), GII.4 Sydney 2012 [P31] (21.2%, n=18/85) and GII.3 [P12] (20.0%, n=17/85) (Figure 5.5). During the period of elevated activity however (August to December 2019), GII.3 [P12] prevalence increased 2.6-fold and caused 52.8% (n=28/53) of norovirus cases/outbreaks detected in children aged five and under (Figure 5.5).

Similarly, the second spike in childhood gastroenteritis activity from November to December 2020 was caused by GII.2 [P16], another existing recombinant norovirus (Figure 5.5). The strain caused 72.7% (n=16/22) of cases/outbreaks detected in children aged five and under (Figure 5.5). In comparison, GII.2 [P16] represented only 27.3% (n=6/22) of gastroenteritis incidences in children between January and October 2020, with GII.3 [P12] (n=5/22, 22.7%) and GII.4 Sydney 2012 [P16] (n=4/22, 18.2%) following close behind (Figure 5.5).

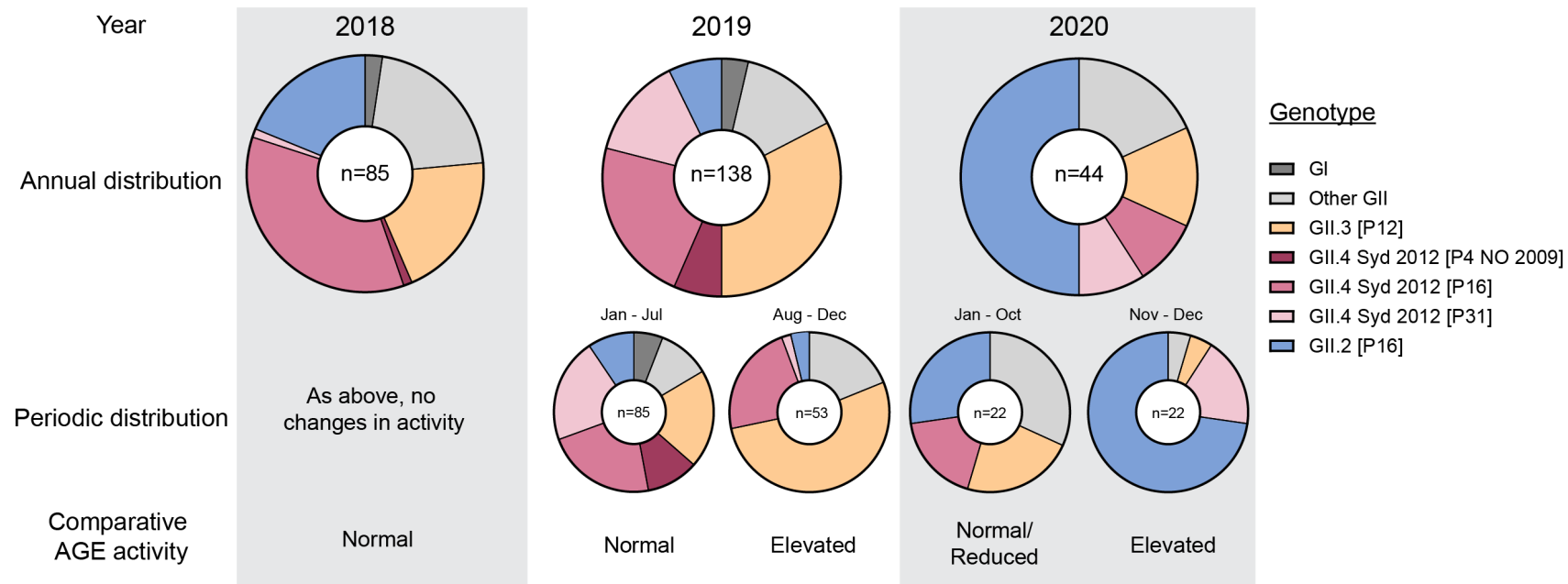


Figure 5.5. Norovirus genotypes detected in children aged five and under.

The different norovirus genotypes detected in children aged five and under were investigated for each year and split into periods of normal and elevated activity. During periods of normal activity, two or more different genotypes were co-dominant in circulation amongst children whilst during periods of elevated activity, a clear predominant strain was detected. The total number of cases/outbreaks in each period is indicated on the pie charts. Genotypes are colour-coded as indicated in the legend.

5.4.5 Molecular epidemiology of GII and GIX noroviruses

Across all age groups, GII noroviruses represented 90.6% (n=547/604) of norovirus cases/outbreaks in Australia between 2018 and 2020, whilst five cases/outbreaks (0.8%) of GIX.1 norovirus were detected (Figure 5.6). To compare the identified GII and GIX norovirus sequences obtained, representative sequences (n=100) were selected for phylogenetic tree construction (Figure 5.7).

In 2018, GII noroviruses represented 90.6% (n=183/202) of gastroenteritis cases/outbreaks sampled. The three predominant genotypes identified over the year were GII.4 Sydney 2012 [P16] (27.2%, n=55/202), GII.2 [P16] (24.3%, n= 49/202) and GII.3 [P12] (12.4%, n=25/202) (Figure 5.6).

In 2019, GII noroviruses caused 90.4% (n=265/293) of norovirus cases/outbreaks sampled. The two most dominant strains were the recombinant GII.4 Sydney 2012 [P16] (24.9%, n=73/293) and GII.3 [P12] (26.6%, n=78/293), whilst GII.2 [P16] which was prevalent in 2018 represented only 7.8% (n=23/293) of cases/outbreaks that year (Figure 5.6).

The molecular epidemiology of human norovirus in 2019 can be separated into two main periods (described in 5.4.2). During the first period (January to July 2019), the dominant strain detected was GII.4 Sydney 2012 [P16] (25.7%, n= 47/183), followed by GII.3 [P12] (13.1%, n=24/183), GII.4 Sydney 2012 [P4 NO 2009] (12.0%, n=22/183) and GII.2 [P16] (9.3%, n=17/183) (Figure 5.6). From August to December 2019 however, the predominant strains shifted, and this was associated with an increase in norovirus activity in childcare centres involving GII.3 [P12] (49.1%, n=54/110), which was the most prevalent norovirus detected, followed by GII.4 Sydney 2012 [P16] (23.6%, n=26/110), GII.7 [P7] (6.4%, n=7/110) and GII.6 [P7] (6.4%, n=7/110) (Figure 5.6).

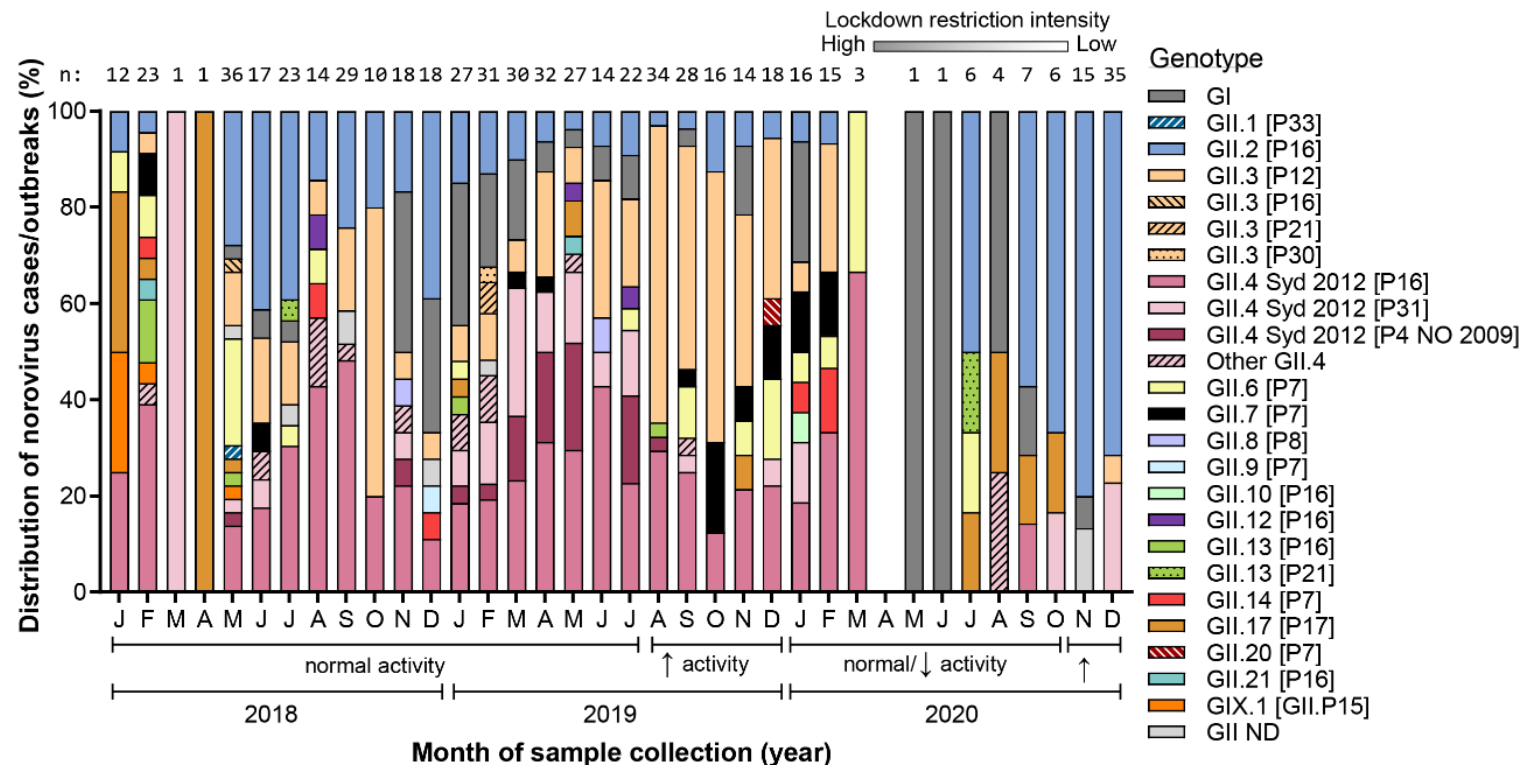


Figure 5.6. Monthly distribution of norovirus genotypes identified in NSW, Australia between 2018-2020.

A total of 547 GII norovirus cases/outbreaks were genotyped in this study. Colours represent different capsid genotypes, whilst patterns are used to denote different P-types associated with the genotypes. The total number of cases and outbreaks in each month is indicated by numbers above the graph. Each outbreak was counted as one independent event of norovirus. The GII ND (not determined) represents samples that had incomplete genotyping results where only capsid or the polymerase sequence was determined. Lockdown restriction intensity in 2020 is indicated using grey shading above the graph. The different periods of AGE activity separated into normal/reduced and elevated activity are indicated below the graph.

The molecular epidemiology of human norovirus in 2020 can be loosely separated into two main periods. The normal/reduced activity period from January to October which includes seven months of social distancing restrictions of varying intensity between April and October 2020 and the post-lockdown period from November to December during which another spike in childcare AGE activity was detected (described in 5.4.2) (Figure 5.6). Overall, GII noroviruses represented 90.8% (n=99/109) of norovirus cases/outbreaks in 2020.

Before the implementation of lockdown measures (January to March 2020), GII.4 Sydney 2012 [P16] (29.4%, n=10/34) was the predominant strain detected in NSW, followed by GII.3 [P12] (14.7%, n=5/34) (Figure 5.6). This is in stark contrast to the remainder of the year where only a single case of the recombinant GII.4 Sydney 2012 [P16] (1.3%, n= 1/75) strain was detected in September and just two cases of GII.3 [P12] (2.7%, n=2/75) were detected in December 2020 (Figure 5.6). On the other hand, GII.2 [P16], which represented only 5.9% (n=2/34) of cases/outbreaks in the first three months of the year, became the dominate strain after lockdown restrictions were introduced (65.0%, n=48/75) (Figure 5.6).

(A) 3' end of polymerase gene (253 bp)

(B) 5' end of capsid gene (285 bp)

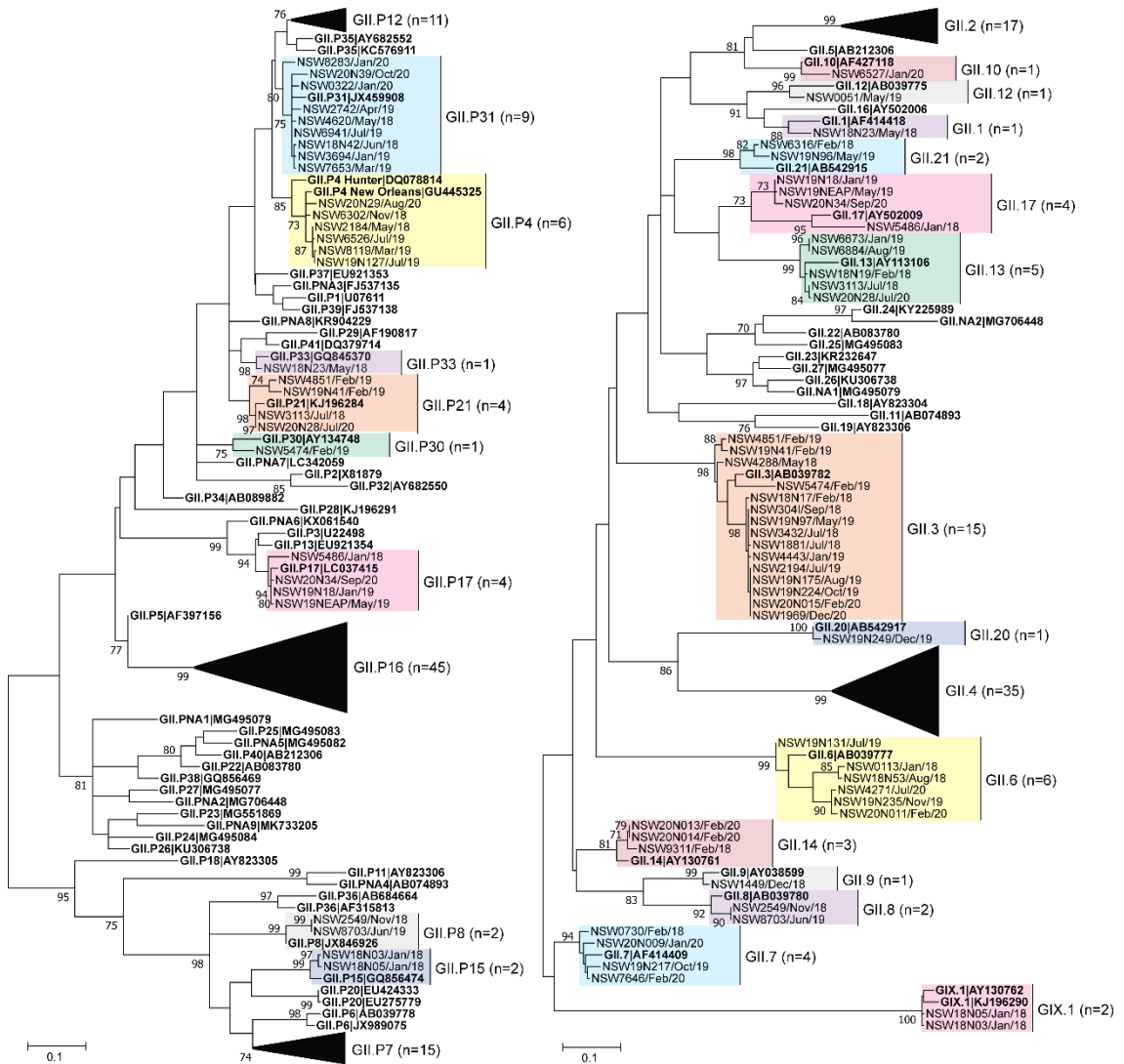


Figure 5.7. Phylogenetic analysis of the partial polymerase (NS7, RdRp) and capsid (VP1) regions of GII noroviruses.

Representative norovirus GII strains (includes GIX.1) isolated in this study (n=100/552) are shown in this phylogenetic analysis. All samples are labelled with their month and year of isolation. Reference strains were obtained from the GenBank database, labelled with their genotype and accession number. Maximum likelihood phylogeny was derived from (A) the partial 3' end of the polymerase gene (253 bp) and (B) the partial 5' end of the major capsid gene (285 bp) of GII noroviruses. Sequence alignments were performed with the MUSCLE algorithm. Maximum likelihood phylogenetic trees were produced with MEGA X (225) based on the Kimura two-parameter model (561) and 1,000 bootstrap replicates. The bootstrap percentage values are shown for values $\geq 70\%$. The scale bar indicates the number of nucleotide substitutions per site. For clarity, shading is included to distinguish between genotypes more clearly. Additionally, some genotypes have been collapsed (black triangles).

5.4.6 Molecular epidemiology of GI noroviruses

GI noroviruses represented 8.6% (n=52/604) of all norovirus cases/outbreaks identified in NSW between 2018 and 2020 (Figure 5.8). To compare the identified norovirus sequences, representative GI norovirus sequences (n=30/52) were selected for phylogenetic tree construction (Figure 5.9). The GI.4 [P4] virus was the most common (32.7%, n=17/52), followed by GI.3 [P13] (15.4%, n=8/52) and GI.3 [P3] (11.5%, n=6/52) (Figure 5.8).

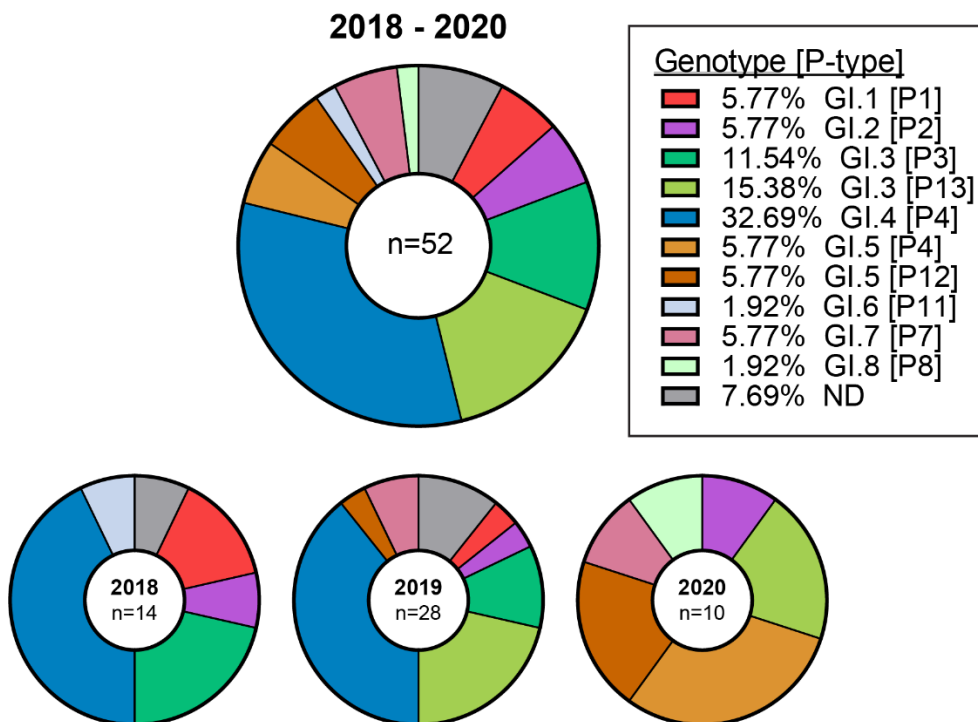


Figure 5.8. Distribution of GI norovirus genotypes identified in NSW, Australia between 2018-2020.

A total of 52 independent GI norovirus events were genotyped in this study. Different colours represent the different capsid genotype/P-type combinations. The percentage prevalence over the study period is shown. The ND represents samples that had incomplete genotyping results where only the capsid or the polymerase region was determined. Smaller pie charts represent the GI norovirus annually. Each outbreak was counted as one independent event of norovirus.

(A) 3' end of polymerase gene (264 bp)

(B) 5' end of capsid gene (297 bp)

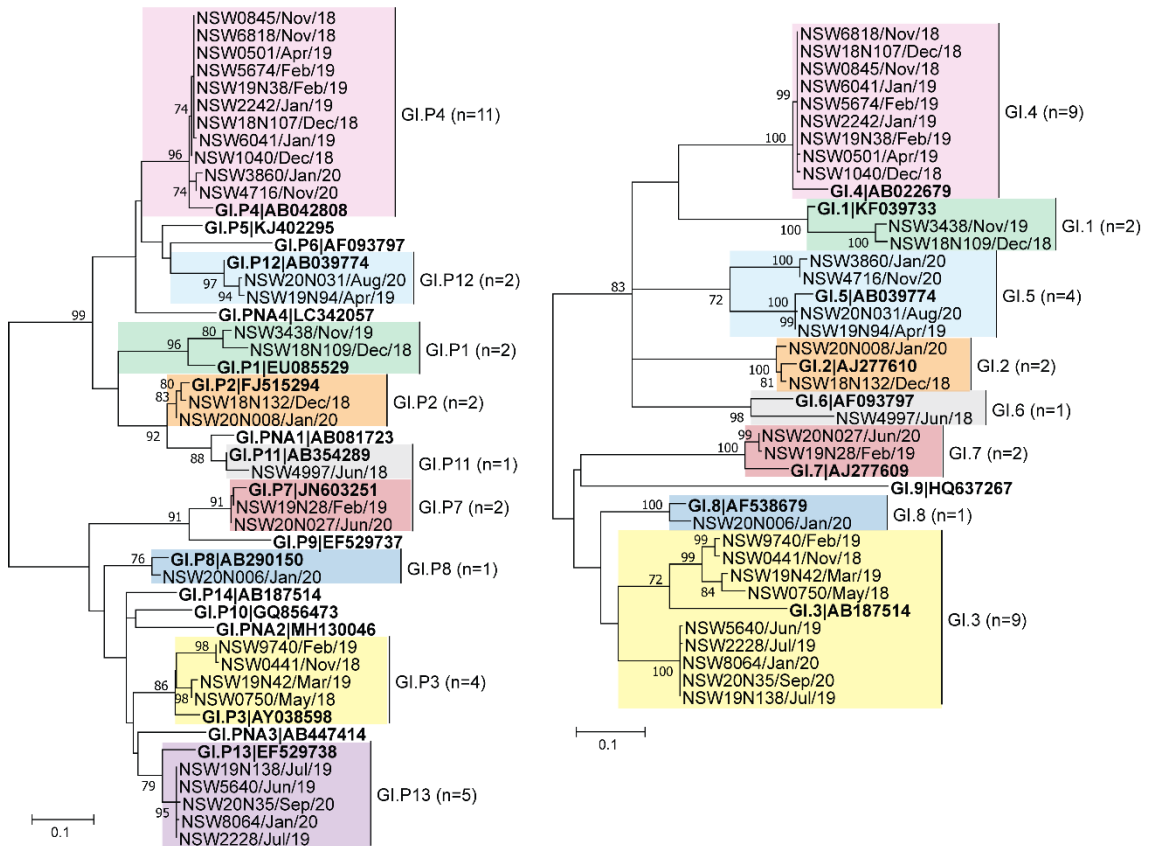


Figure 5.9. Phylogenetic analysis of the partial polymerase (RdRp) and capsid (VP1) regions of GI noroviruses.

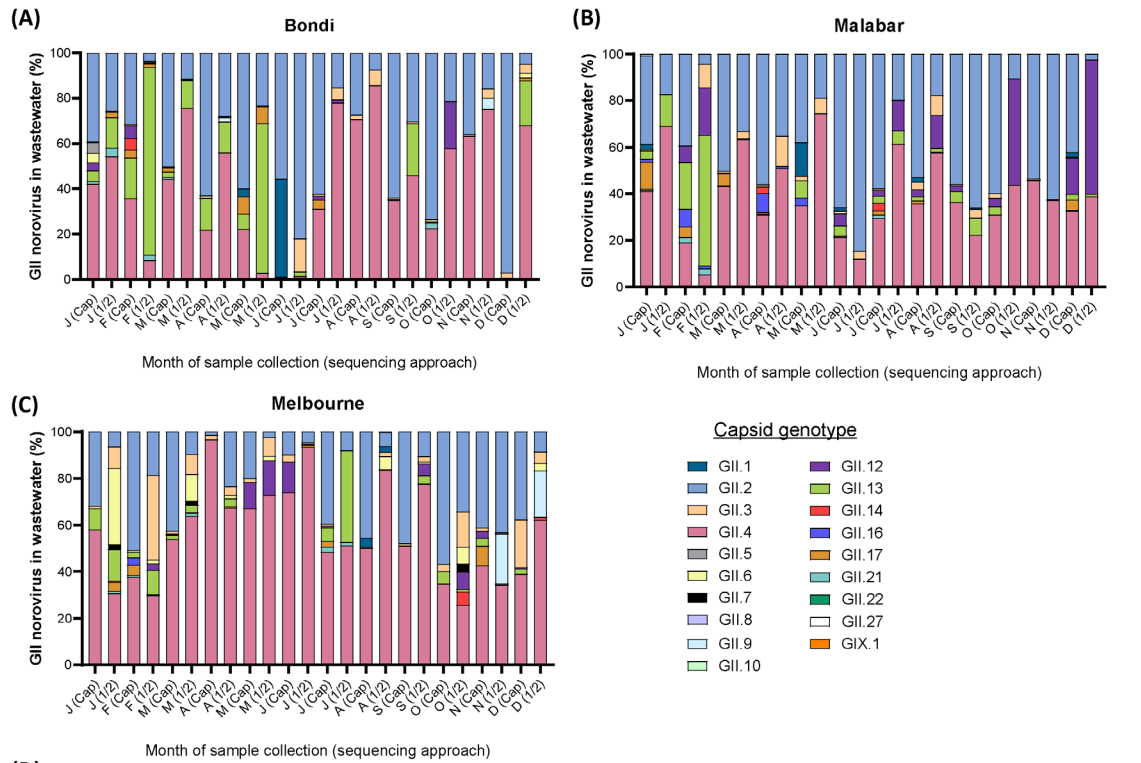
Representative norovirus GI strains isolated in this study (n=30/52) are shown in this phylogenetic analysis. All samples are labelled with their month and year of isolation. Reference strains were obtained from the GenBank database, labelled with their genotype and accession number. Maximum likelihood phylogeny derived from (A) the partial 3' end of the polymerase gene (264 bp) and (B) the partial 5' end of the major capsid gene (297 bp) of GI noroviruses. Sequence alignments were performed with the MUSCLE algorithm. Maximum likelihood phylogenetic trees were produced with MEGA X (225) based on the Kimura two-parameter model (561) and 1,000 bootstrap replicates. The bootstrap percentage values are shown for values $\geq 70\%$. The scale bar indicates the number of nucleotide substitutions per site. For clarity, shading is included to distinguish between genotypes more clearly.

5.4.7 Comparison of GII norovirus partial capsid and ORF1/2 overlap amplicon sequencing in 2018 wastewater.

This study aimed to gain a comprehensive understanding of norovirus at a population scale using NGS of amplicons generated from RNA extracted from wastewater samples. Previously, our group has used the partial capsid (Cap) amplicon for NGS norovirus genotyping of monthly wastewater samples (229, 303). However, this approach is unable to identify the presence of clinically relevant recombinant

strains due to the lack of sequencing of the RdRp region. Therefore, this chapter aimed to develop an alternative approach which utilises the ORF1/2 overlap region instead, which would enable the identification of recombinant strains and allow for better strain genotyping. RNA extracted from monthly wastewater samples in 2018 (n=36) were amplified and sequenced using both approaches and compared (Cap: 915,724 reads, ORF1/2: 2,413,260 reads) (Figure 5.10). Using the ORF1/2 approach, a greater level of sequencing depth was obtained. Using the partial capsid approach, 14 genotypes were detected, whereas using the ORF1/2 overlap amplicon, 17 different capsid genotypes were detected (Figure 5.10D).

The overall prevalence of GII.4 (Cap: 40.2%, ORF1/2: 51.1% of average monthly reads), one of the most prevalent norovirus genotypes was similar across the two different approaches (Figure 5.10). However, the other predominant genotype, GII.2, varied in prevalence across the two approaches (Cap: 47.0%, ORF1/2: 22.6% of average monthly reads). The greatest disparity was observed when comparing the prevalence of GII.1 (Cap: 7.3%, ORF1/2: 0.5% of average monthly reads) and GIX.1 (Cap: 0.5%, ORF1/2: 0.05%) which both possessed ≥ 10 -fold change in average monthly reads across the two approaches (Figure 5.10).



Genotype	GII.1	GII.2	GII.3	GII.4	GII.5	GII.6	GII.7	GII.8	GII.9	GII.10	GII.12	GII.13	GII.14	GII.16	GII.17	GII.20	GII.21	GII.22	GIX.1	Types	
Cap	x	x	x	x	x	x					x	x	x	x	x		x	x	x	14	
1/2	x	x	x	x		x	x	x	x	x	x	x	x	x	x	x	x	x	x	x	17

x: detected
 Cap: partial capsid amplicon approach
 1/2: ORF1/2 overlap amplicon approach

Figure 5.10. Comparison of GII norovirus capsid and ORF1/2 overlap genotypic distribution in sewage samples collected from Sydney and Melbourne, 2018.

The monthly norovirus genotypic distribution was determined for the (A) Bondi, (B) Malabar and (C) Melbourne WWTPs in wastewater samples using both RT-PCR methods; partial capsid method and the ORF1/2 overlap method. Amplicons were sequenced on the Miseq platform and Geneious Prime was used for the merging and mapping of reads to reference sequences. The distribution of capsid genotypes identified using the two different approaches for each sample is presented side by side with partial capsid amplicon denoted as Cap and the ORF1/2 overlap amplicon denoted as 1/2. (D) The diversity of genotypes detected using each approach is also shown. A total of 14 different capsid genotypes were detected using the partial capsid approach whilst the ORF1/2 overlap approach identified 17 genotypes.

5.4.8 Norovirus GII genotype distribution in wastewater samples, 2018-2020

The ORF1/2 overlap region (570 bp) was amplified from monthly wastewater samples collected from three WWTPs from Sydney and Melbourne and sequenced on the Illumina Miseq platform because work in section 5.4.7 showed it provides a more accurate and comprehensive genetic typing of the virus, with the added ability of determining P-type. A total of 7,314,584 filtered and successfully mapped reads were

generated from the 108 wastewater samples, with an average of 67,728 reads for each sample (range 11,489 – 166,132).

Using this new approach, GII.4 was found to be the predominant capsid genotype (53.1% of reads) across the three sites, followed by GII.2 (20.2% of reads). GII.P16 was the predominant P-type and accounted for 86.4% of reads across the three sites (Figure 5.11). The recombinant GII.4 Sydney 2012 [P16] was the predominant strain in wastewater throughout 2018 and 2019 (63.5% reads) (Figure 5.11), this trend continued until April 2020, where it dropped to less than 1% of reads that month (Figure 5.12).

The second most prevalent strain in the wastewater was the GII.2 [P16] which represented 19.7% of total reads across the three sites (Figure 5.11). The prevalence of this recombinant virus fluctuated throughout the study period. For the Bondi and Malabar sites, the GII.2 [P16] represented 25.4% of reads in 2018 but halved to just 13.0% reads in 2019. It remained in circulation in relatively low levels at Bondi (<5% reads) throughout the start of 2020, until September when it became the dominant strain detected in wastewater (Figure 5.11A). At Malabar, it represented <10% of reads during the first half of the year until August when it became the dominant strain detected in wastewater (Figure 5.11B).

For Melbourne, GII.2 [P16] represented 10.8% of reads in 2018, but its prevalence declined much sooner, representing 11.1% of reads during the first half of 2019 and just 1.4% reads in the latter half of the year, and remained at these low levels for most of 2020 (Figure 5.11C, Figure 5.12C). Although GII.2 [P16] prevalence did rise again in August 2020 in Melbourne (13.0% of reads), unlike in Sydney the recombinant GII.2 [P16] did not dominate and only reached its 2018 levels (Figure 5.11C).

Overall, 39 different genotype/P-type combinations were detected, which includes 21 minor genotypes that each represented less than <0.1% of total reads (Figure 5.12). Notable examples are GII.13 [P21], GII.14 [P7], GII.1 [P33], GIX.1 [GII.P15], GII.4 Sydney 2012 [P4 NO], GII.8 [P8] and GII.3 [P21], which were also detected in clinical stool specimens (Figure 5.11A, B; Figure 5.12A, B; Figure 5.14).

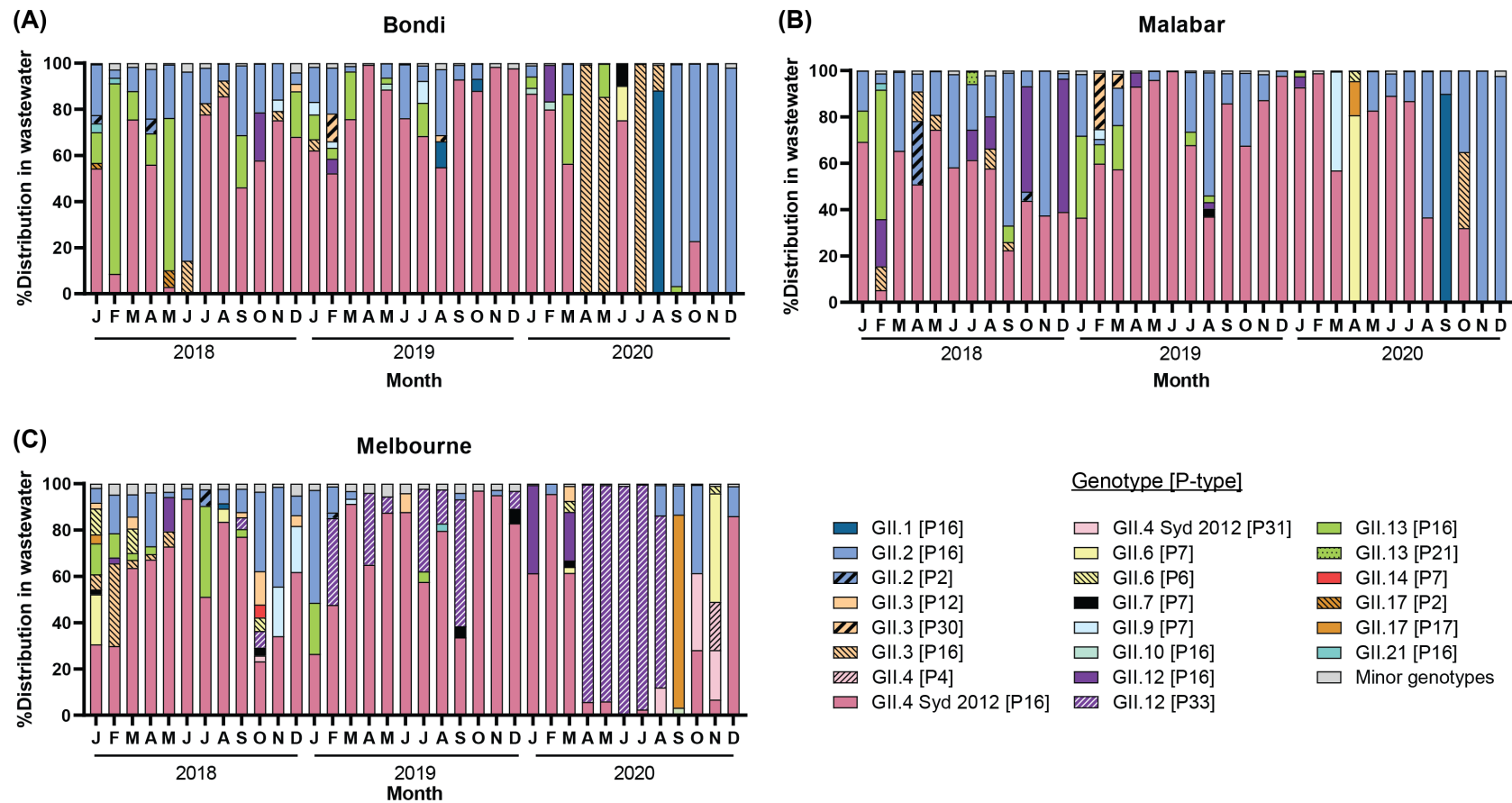


Figure 5.11. Major norovirus GII genotype distribution in wastewater samples collected from Sydney and Melbourne, 2018-2020.

The monthly genotypic distribution of major GII norovirus in wastewater between January 2018 and December 2020 was determined using ORF1/2 overlap amplicons for the (A) Bondi, (B) Malabar and (C) Melbourne WWTPs. Amplicons were sequenced on the Miseq platform and Geneious Prime was used for the merging and mapping of reads to reference sequences. For clarity, in each sample, only major genotypes ($\geq 2\%$ of reads in a given sample) are shown on the graphs, whilst minor genotypes ($< 2\%$ of reads in a given sample) have been shown combined.

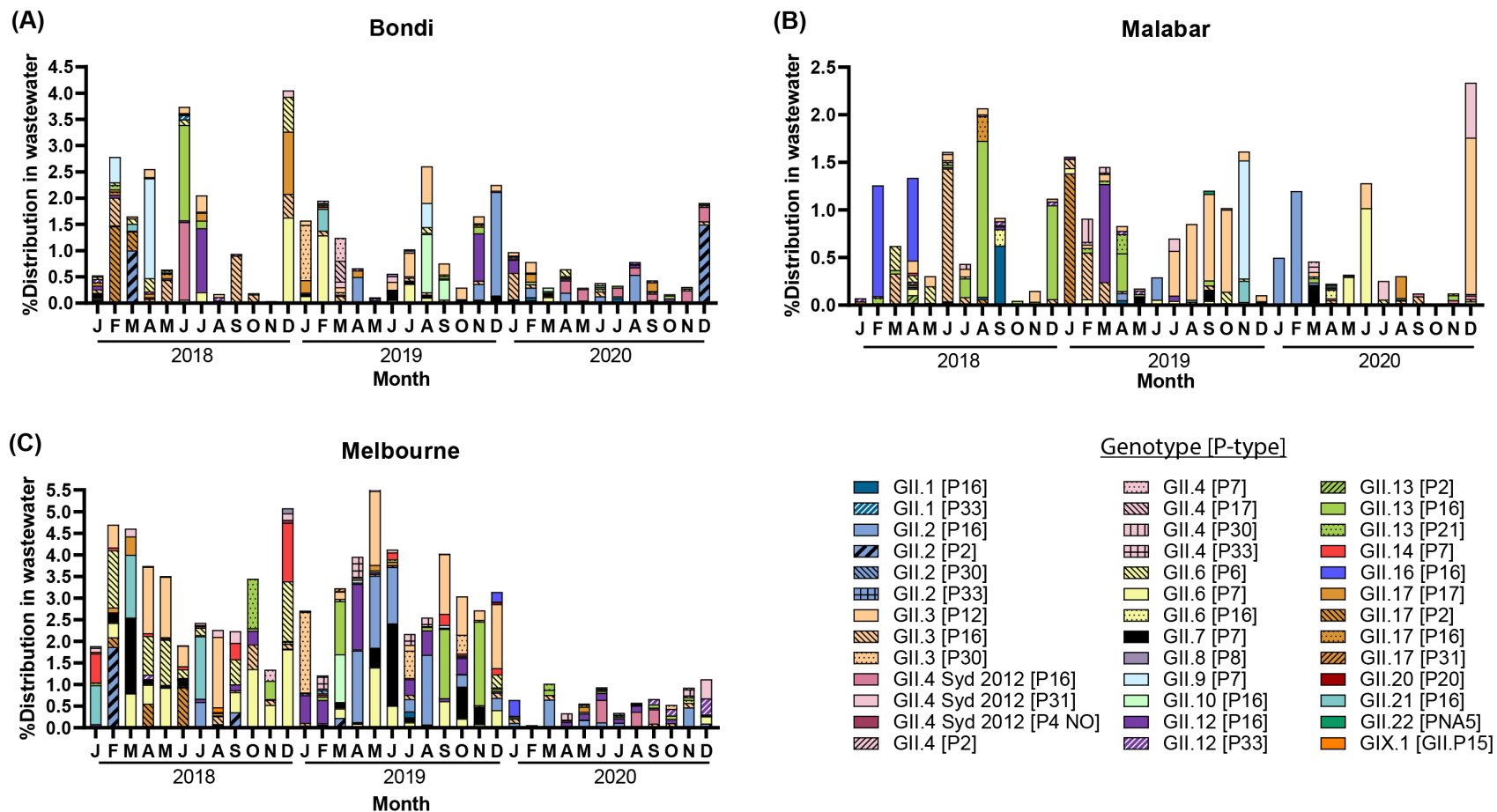


Figure 5.12. Minor norovirus GII genotype distribution in wastewater samples collected from Sydney and Melbourne, 2018-2020.

The monthly genotypic distribution of minor GII norovirus strains in wastewater between January 2018 and December 2020 was determined using ORF1/2 overlap amplicons for the (A) Bondi, (B) Malabar and (C) Melbourne WWTPs. Amplicons were sequenced on the Miseq platform and Geneious Prime was used for the merging and mapping of reads to reference sequences. For clarity, only the minor genotypes (<2% of reads in a given sample) are shown.

5.4.9 Diversity of noroviruses genotypes and P-types detected

A diverse range of human norovirus genotypes were detected from the human GI, GII and GIX genogroups in this study from clinical cases. This included eight different GI capsid genotypes and nine GI P-types (Figure 5.13), whilst 15 GII capsid genotypes, GIX.1 (formerly known as GII.15), and 11 GII P-types were identified across the time-frame sampled (Figure 5.14).

This study also examined the distribution of GII capsid genotypes and P-types in monthly wastewater samples collected from three sites in Australia to better understand the circulating norovirus within the population between 2018 and 2020. From wastewater, 17 of 26 GII capsid genotypes and GIX.1 were identified across the three sites, as well as 14 of 37 GII P-types, and the unassigned GII.PNA5 (Figure 5.14).

To infer a recombination predilection of the different norovirus polymerases, the combinations of P-type and capsid genotype were examined. Overall, the most promiscuous RdRp was the GII.P16 polymerase, which was associated with 11 different capsid genotypes (Figure 5.14). This was followed by the GII.P7 polymerase which was associated with six different capsid genotypes (Figure 5.14). Similarly, GII.4 was the most common capsid and was identified with eight different P-types. This was followed equally by GII.3, GII.2 and GII.17 which were each associated with four different P-types (Figure 5.14).

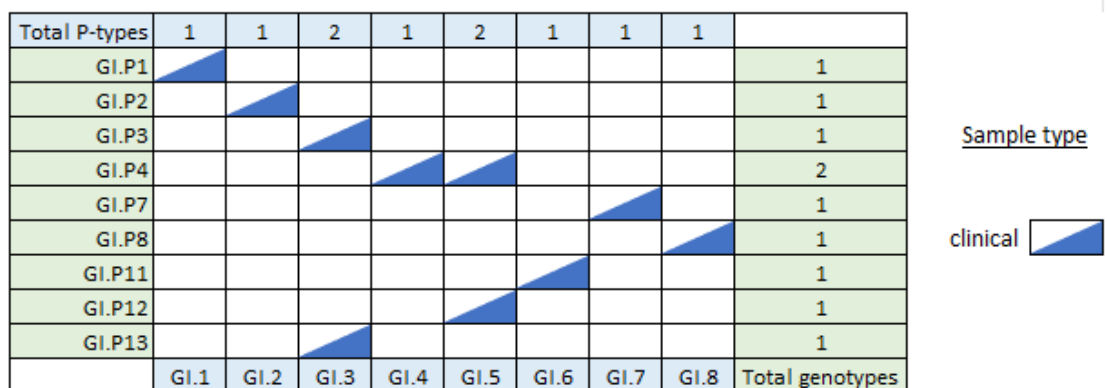


Figure 5.13. Diversity of GI norovirus P-type and genotype combinations detected.

The different combinations of GI norovirus P-type and capsid genotype identified from clinical samples. A total of eight different P-types and nine different genotypes were detected over the course of the study.



Figure 5.14. Diversity of GII norovirus P-type and genotype combinations detected.

The different combinations of GII norovirus P-type and capsid genotype identified from clinical (blue) and wastewater (orange) samples are shown. A total of 15 different P-types and 18 different genotypes were detected over the course of the study. GIX.1 (formerly GII.15) has also been included here since it is also amplified by the same GII norovirus primers. GII.PNAS refers to a temporarily designated P-type which has not been formally classified due to an insufficient number of sequences (224).

5.5 Discussion

It has been more than nine years since the last novel pandemic GII.4 variant, Sydney 2012 first emerged (295). The Sydney 2012 capsid from that particular virus has extended its dominance in the population by undergoing recombination with a GII.P16 virus to create the GII.4 Sydney 2012 [P16] virus that became the predominant strain from 2016 and 2017 in Oceania (229), USA (540), Canada (536) and Brazil (543), among others. In Asia, however, the GII.4 Sydney 2012 [P16] strain never attained the same level of prevalence, and the decline in the original Sydney 2012 variant was instead accompanied by a surge in outbreaks caused by non-GII.4 viruses, and in particular GII.2 [P16] (305, 306, 547, 550, 564, 565). Overall, however, the molecular epidemiological landscape of norovirus over the past few years has remained relatively stagnant, with no novel viruses emerging (540, 566, 567). The present chapter aimed to explore the molecular epidemiological trends of circulating norovirus strains in Australia over a three-year period from 2018 to 2020 using both clinical and wastewater specimens and compare them to trends seen globally.

Since its first detection in NSW in November 2014 (303), the GII.4 Sydney 2012 [P16] has outcompeted several epidemic noroviruses to reach its height of prevalence in 2017 (229). Although its prevalence has since declined it has remained one of the leading strains detected in the present study and represented 26.1% of clinical cases

and outbreaks between January 2018 and March 2020, when COVID-19 lockdowns began (26.1%, n=138/529) (Figure 5.6). During this 27-month period its dominance was closely contested by the recombinant GII.2 [P16] strain (2018: 24.3%, n= 49/202), which dominated in Asia (567), and the GII.3 [P12] virus (2019: 26.6%, n=78/293) (Figure 5.6), which was prevalent in childcare facility outbreaks. Although co-dominance may be observed during strain replacement such as when new GII.4 pandemic variants emerge, this is short-lived over the span of a few of months, as the novel virus usually rapidly replaces the previous strain (231, 295, 564). What was unusual in both these instances, however, was that the co-dominant virus did not replace the GII.4 Sydney 2012 [P16] virus and instead declined after a few months.

The increased prevalence of GII.3 [P12] in clinical samples in 2019 correlated with a two-fold increase in institutional gastroenteritis outbreak activity detected between August and December (Figure 5.3). These outbreaks occurred predominantly in childcare facilities (71.8%, n=525/731). The GII.3 [P12] was first detected in NSW in 2014, before emerging in 2016 to replace the GII.3 [P21] as a predominant cause of childhood gastroenteritis (229, 293, 303). Like other GII.3 viruses, it is less commonly detected in the adult population (311). Analysis of amino acid substitutions in the GII.3 VP1 gene in previous work revealed that there was a cyclical evolutionary pattern, with a tendency for key surface amino acid residues to revert to those previously used (310, 568). Since young children are more likely to be immunologically naïve, this would allow GII.3 viruses to continually infect this population despite accumulating less amino acid changes within the antigenic regions compared to GII.4 viruses for instance. Furthermore, children with gastroenteritis are more likely to present for medical advice, or at emergency departments compared to adults, creating sampling bias towards viruses in children which would partly explain its high prevalence in 2019. As children were infected with GII.3 [P12] from these outbreaks and developed immunity to the virus (569-573), the proportion of naïve individuals declined and so without a susceptible population to infect, the GII.3 [P12] subsequently declined in prevalence.

Furthermore, analysis of GII norovirus genotype distribution in wastewater revealed that GII.4 Sydney 2012 [P16] remained in circulation within the community at high levels throughout 2018, 2019 and until March 2020 (Figure 5.11). Although GII.3

[P12] represented 49.1% of detections (n=54/110) in clinical samples between August and December 2019, its prevalence in wastewater was low and represented only 0.42% of total reads during these months (Figure 5.12A, B). There are two main explanations for this, firstly, due to a lack of antigenic novelty, GII.3 [P12] is less commonly detected in older children and adults (i.e., most individuals shedding into wastewater) (310, 311). Secondly, the diaper wearing age group (0-2 years) which make up a large proportion of the AGE cases would be shedding far less frequently into sewage. Interestingly, the levels of GII.3 [P12] in Sydney wastewater in July 2019 (0.46% of reads) represented more than five-fold increase compared to June (0.08% of reads). This indicates that GII.3 [P12] circulation within the community may have increased in July (Figure 5.12A, B), one month before elevated childcare outbreaks were reported (Figure 5.3). This was congruent with our previous work, which similarly reported a rise in GII.2 abundance in 2016 wastewater two months prior to its increased detection in clinical samples (303). Together, this provides evidence for the feasibility of wastewater analysis as a sentinel surveillance platform.

The COVID-19 pandemic and subsequent infection containment measures have disrupted the epidemiology of norovirus around the world (574-578). Although norovirus circulates all year round, there are seasonal patterns with increased activity typically during the colder months of the year in temperate countries (Oceania: July to October, Northern hemisphere: December to February) (579). During the 2020/21 winter season, norovirus outbreak numbers reported by the Norovirus Sentinel Testing and Tracking (NoroSTAT) network were more than ten-fold lower than in 2019/20 (576). Likewise, in Germany, a sharp decline in the percentage of norovirus positive samples was observed in February 2020, reaching near 0% in May where it continued for the remainder of the year (577). A similar decrease in norovirus activity in 2020 was also noted in Victoria, Australia after implementation of public health measures (578).

Whilst these studies observed a decrease in laboratory confirmed norovirus cases after implementation of public health measures, this has also been in combination with a decline in testing and reporting (574-578) which can make it difficult to quantify the true effects of social distancing. The present study navigated this limitation of clinical sampling through analysis of wastewater, which was able to

continue uninterrupted throughout the COVID-19 lockdown. Through quantification of norovirus genome copies in monthly wastewater samples, this study provided conclusive evidence of the immediate decline in norovirus levels within the community in April 2020, after lockdown (below assay detection limits). This decrease was sustained throughout the socially distanced period of May to September 2020 (average: 1.4×10^5 gc/L) and represented more than 90% lower viral load compared to the same period in 2018 (1.6×10^6 gc/L) and 2019 (1.9×10^6 gc/L) (Figure 5.4).

Since its first detection in NSW in 2013 (302) and global emergence in 2016 and 2017 (312, 541, 546, 548, 549), the prevalence of the recombinant GII.2 [P16] in NSW has fluctuated (229, 303). Over the study period, the recombinant GII.2 [P16] was the second most dominant virus detected in both clinical (20.2%, $n=122/604$, Figure 5.6) and wastewater specimens (19.7% of total reads, Figure 5.11). However, prior to COVID-19 lockdown measures implemented in late March 2020, the prevalence of the GII.2 [P16] was waning, dropping from 24.3% ($n= 49/202$) of clinical samples in 2018 to just 7.8% ($n=23/293$) of norovirus events in 2019 and 5.9% ($n=2/34$) during the pre-lockdown period in 2020 (Figure 5.6). This was consistent with trends observed in NSW wastewater, where its prevalence halved from 25.4% of reads in 2018, to 13.0% reads in 2019 and further declined to just 3.6% of reads during the first three months of 2020 (Figure 5.11A, B).

The recombinant GII.2 [P16] remained in circulation throughout the lockdown period and gradually re-emerged in August 2020, as social distancing restrictions were eased, to become the most dominant genotype detected in NSW wastewater by the end of the year (98.9% of reads in November and December, Figure 5.11A, B). During this time, elevated institutional gastroenteritis activity (6.8-fold higher than 2018) was observed, primarily concentrated in childcare centres in NSW (Figure 5.3). Unlike the GII.3 [P12] virus however, GII.2 [P16] is clinically observed in a wider age group (549), as evidenced by its prevalence in wastewater during November and December 2020 (Figure 5.11A, B). Hence it was unsurprising that increases in GII.2 [P16] prevalence also corresponded to increases in GII norovirus levels measured in Sydney sewage (Figure 5.4). Although GII.2 [P16] is not a novel virus, it has demonstrated capability to

cause epidemics and has remained the leading cause of norovirus outbreaks in western China throughout 2018/19 (565, 567, 580).

More recently in Asia (2018-2020), the predominant norovirus strain identified from clinical samples may have changed without the requirement of the emergence of any new single pandemic strains. In Hong Kong, the proportion of GII.4 Sydney 2012 viruses possessing a GII.P31 non-structural region increased 2.3-fold for the 2019/20 season (65%, n=138/213) compared to the 2018/19 season (28%, n=89/314) (581). Similarly, in the north-eastern city of Tianjin, China, a study of norovirus AGE cases among hospitalised children between August 2018 and July 2020 revealed that the predominant genotype was the GII.4 Sydney 2012 [P31] (n=294/449, 65.5%), a surprising resurgence of the Sydney 2012 pandemic variant (566). Likewise, in western China, GII.4 Sydney 2012 [P31] was also the dominant norovirus detected in hospitalised children (n=79/163, 48.5%) between 2015-2019 (567). It is important to note however, that these two Chinese studies observed a discordance in strain prevalence between sporadic cases and outbreaks. This is understandable since the Sydney 2012 pandemic has been circulating in the population since late 2012 and hence most of the population should be immune. It would be interesting however, to see if similar trends of Sydney 2012 pandemic variant resurgence will occur elsewhere in the world. Only continued close monitoring of norovirus molecular epidemiology will be able to answer this question.

5.6 Concluding remarks

This chapter explored the molecular epidemiological landscape of circulating norovirus in NSW between 2018 and 2020. No novel strains of clinical significance were detected in the present study. Instead, genotyping of clinical specimens revealed an interesting dynamic of GII.4 Sydney 2012 [P16] co-dominance with GII.3 [P12] and GII.2 [P16] across the study period. Analysis of monthly wastewater samples revealed that norovirus levels within the community during lockdown were 90% lower compared to previous years. The addition of ORF1 genotyping in sewage has greatly enhanced its sentinel surveillance capabilities by facilitating the detection of recombinant viruses. This will be important for identifying emergent recombinant strains that may possess epidemic or pandemic potential.

6 Molecular epidemiology of adenovirus-associated gastroenteritis in Australia, 2018 to 2021

6.1 Abstract

Human adenoviruses (HAdV) are double-stranded DNA viruses that can cause a wide spectrum of clinical manifestations. Enteric HAdV types F40 and F41 are collectively documented as one of the most important causes of acute gastroenteritis (AGE). The role of other non-group F HAdV types in AGE, however, is controversial. This chapter explored the molecular epidemiology of adenovirus-associated gastroenteritis in NSW, Australia over a four-year period from 2018 to 2021. Thirteen different HAdV hexon types were identified from clinical faecal specimens. This included types F41 (63.8%, n=284/445), C2 (11.0%, n=49/445), C1 (10.1%, n=45/445), A31 (4.0%, 18/445), C6 (3.6%, 16/445), B3 (3.1%, n=14/445), and F40 (1.1%, n=5/445). Species D and E were only detected in three samples each, whilst types A18 and B7 were only detected in a single clinical specimen. The diversity of HAdV in monthly wastewater samples collected from three treatment plants across Sydney and Melbourne during 2018 was also investigated to explore HAdV diversity at a city-based population level. In wastewater, reads belonging to all seven species (A-G) were detected. Of these, the most prevalent was F41 (70.17%), followed by A31 (20.53%), F40 (4.07%) and A12 (3.54%). Other HAdV groups had much lower prevalence; species C represented 0.94% of reads, followed by B (0.27%), D (0.24%), E (0.10%) and G (0.02%). In the clinical samples, most species C detections (71.7%, n=81/113) occurred in AGE patients under the age of two, emphasising its aetiology in paediatric gastroenteritis. In conjunction with clinical sampling, wastewater sampling is a useful tool providing population-based surveillance of circulating HAdV and which captures a greater genetic diversity of HAdV within communities.

6.2 Introduction

Acute gastroenteritis (AGE) is a major cause of morbidity and mortality, particularly amongst young children in developing nations, where an estimated 500,000 AGE-related deaths occur each year (161). Human adenoviruses (HAdV), specifically the classically enteric serotypes F40 and F41, are well recognised as important causes of AGE worldwide. For example, the 2015 Global Burden of Disease study estimated that HAdV leads to 70,200 AGE-related deaths worldwide each year (180). Most of these deaths occur in young children, with data from the Etiology, Risk Factors, and Interactions of Enteric Infections and Malnutrition and the Consequences for Child Health and Development (MAL-ED) cohort study estimating that HAdV F40/41 has one of the highest attributable incidences of diarrhoea (19.0, 95% CI 16.8–23.0) during the first two years of a child's life (348). Although HAdV infections in healthy adults are typically self-limiting and require little medical intervention, outcomes can be severe and life-threatening in infants, young children, and the immunosuppressed (349).

HAdV are non-enveloped and icosahedral viruses belonging to the mammalian adenovirus genus *Mastadenovirus* within the *Adenoviridae* family. These viruses possess a double-stranded DNA genome of approximately 35 kb in length. There are currently 113 proposed HAdV genotypes (<http://hadvvg.gmu.edu/>), which can be classified into seven major groups or species (A-G) based on characteristics such as cross-neutralisation, phylogenetic distance, genome organisation, nucleotide composition and ability to recombine (367). HAdV were traditionally defined using cross-neutralisation studies (serotyping) up to serotype 51. Within each serotype, further genomic variation could then be distinguished based on differences in restriction digest profiles (368, 369). However, these classical approaches were both resource heavy and time intensive. Therefore, the classification of HAdV has now evolved to use nucleotide sequence-based methods (370-372). Since the discovery of HAdV type G52 (406), whole genome sequencing and phylogenetic analyses have played a crucial role in the identification and classification of novel strains, and will continue to be useful for identifying future types (376, 378-380).

HAdV can cause a wide spectrum of clinical diseases, but this is largely dependent on host factors and the infecting serotype/genotype. The species grouping can also provide a very general indication of disease and clinical symptoms. HAdV can cause upper respiratory illness (species B, C, E), keratoconjunctivitis (species B, D, E), gastroenteritis (species A, F, G) and urinary tract infections (species B), as well as rarer manifestations such as meningitis, encephalitis, and myocarditis (4). Typically, the disease manifestation determines the type of clinical specimen collected, and thus downstream diagnostic methods.

In terms of diagnosis of gastroenteritis in children, to ensure that the appropriate therapeutic and infection control measures may be initiated in a timely manner, multiplex diagnostic methodologies are useful for differentiating and identifying a wide range of enteric pathogens that may otherwise be clinically indistinguishable (582, 583). However, when diagnosing adenovirus-associated gastroenteritis, many commercial assays only test for the presence of types F40 and F41 (584-586). This can result in the under-detection of non-group F HAdV types which are associated with gastroenteritis, making it difficult to determine a more accurate number of disease incidences for the genus in general.

In recent years, there has been increasing speculation over the role of these non-F HAdV genotypes in patients of gastroenteritis (382, 383, 587-590). A Korean study conducted in 2014 to 2016 found that HAdV C2 (13.8%) and B3 (9.6%) represented the second and third most prevalent types detected in AGE patients following F41 (60.6%) (382). These results were echoed by findings reported in Thailand (2011 to 2017) where F41 (22.4%), C2 (18.2%) and B3 (15.2%) were the most common types detected in paediatric patients with AGE (383). Similarly, a high incidence of species C detection was also reported in hospitalised paediatric AGE patients in Italy (587), whilst type B3 was strongly associated with diarrhoea among infants and children with AGE in China (588). Additionally, several studies have also reported the decreased prevalence of F40 (relative to F41) (590-594), and together this indicates that updates to HAdV detection methodology are required for the accurate depiction of global adenovirus AGE disease burden.

In Australia, adenovirus-associated gastroenteritis has been a neglected area of molecular epidemiological surveillance. Prior to the work of our group in 2016 and 2017 (591), the most recent study of adenovirus-associated gastroenteritis was conducted between 1981 to 1992 (595), more than twenty years earlier. In this historical study, HAdV was found in only 3.1% of hospitalised paediatric AGE patients, however, since the enzyme immunoassay (EIA) used was limited to F40 and F41 only, any gastroenteritis caused by non-group F HAdV would have remained undetected (595). In contrast, our group found 47.5% of HAdV gastroenteritis cases (n=19/40) were associated with non-group F types in 2016/17 (591). Of these, species C was the most prevalent group and represented 35.0% of cases (n=14/40). Interestingly, wastewater analyses revealed that the most prevalent types in circulation were F41 (83.5% of reads), followed by F40 (11.0%) and A31 (3.7%) (591). The high prevalence of F40 and A31 in sewage despite extremely low clinical presence – A31 was detected in a single sample, whilst F40 was not detected at all. This demonstrates the importance of incorporating an unbiased population-based approach to complement clinical surveillance, which is inevitably biased towards the detection of disease phenotypes in vulnerable patient populations. It is important to note however, that other clinical syndromes of HAdV infection such as respiratory illness can also involve faecal shedding, thus wastewater monitoring captures all circulating HAdV rather than just AGE cases.

The need for molecular epidemiological surveillance was most recently exemplified by the sudden emergence of an acute, severe hepatitis of unknown origin. As of 26 May 2022, 650 probable cases have been reported in children across 33 countries across Europe, North and Central America and Asia (596-598). To date, the aetiology of this outbreak remains unknown, but adenovirus was detected in at least 191 patients, and HAdV type F41 was identified in 33 patients (598). However, HAdV F41 has not been reported in association with hepatitis in immunocompetent patients previously (4). Interestingly, a recent increase in HAdV detections in faecal samples among children aged 1-4 years in the UK was also observed (599). This observation would not have been possible without historical data and highlights the importance of

ongoing, molecular monitoring of pathogens within the community, particularly at a population-based scale.

The present chapter aimed to identify the HAdV genotypes associated with AGE in clinical samples and compare them to those found using wastewater surveillance. The molecular epidemiology of gastroenteritis associated HAdV genotypes in NSW, Australia was investigated using clinical faecal specimens collected over a four-year period from 2018 to 2021. Population-based surveillance using monthly sewage samples collected from three large wastewater treatment plants (WWTPs) in Sydney and Melbourne during 2018 was also performed. Although, HAdV wastewater surveillance inevitably captured more than just AGE cases, through comparison with trends seen in clinical samples, a more complete picture of the molecular epidemiology of adenovirus-associated gastroenteritis was obtained.

6.3 Materials and methods

6.3.1 Ethics and clinical specimen collection

This study was approved by the UNSW Human Research Ethics Advisory Panel (HC16828 and HC17459). Deidentified faecal specimens (n=487) were obtained from adenovirus patients with gastroenteritis symptoms in NSW, Australia between January 2018 and December 2021. Samples were collected by the Prince of Wales Hospital (PoWH) and Douglass Hanley Moir (DHM) pathology as part of routine enteric pathogen diagnostic services. We thank Peter Huntington, Richard Jones and their respective teams for provision of samples. Presence of HAdV in PoWH samples were confirmed using the multiplex PCR-based EasyScreen Enteric Viral Detection Kit (Genetic Signatures, Sydney, Australia), whereas in DHM samples confirmation was performed using the enzyme immunoassay (EIA) based RIDASCREEN Easykit ELISA Adenovirus assay (R-Biopharm, Darmstadt, Germany).

6.3.2 Collection of wastewater samples

Monthly 24-hour composite influent specimens were collected from three wastewater treatment plants (WWTPs) in Australia between January and December 2018. The Bondi and Malabar WWTPs are situated in Sydney and serve catchment populations of 318,810 and 1,857,740 respectively, whilst the Western WWTP in

Melbourne serves an estimated population of 2.4 million. Samples were delivered to UNSW on ice, aliquoted and stored at -80°C upon arrival.

6.3.3 Viral concentration and extraction

Stool samples were prepared as 20% suspensions (v/v) in water and followed by viral DNA extraction using the QIAamp Viral RNA Mini Kit (Qiagen, Hilden, Germany) as previously described (591). Viruses in clarified sewage samples (10 mL) were concentrated via ultracentrifugation at 216,000 x *g* at 4°C for 1.5 hours. Viral nucleic acid was then extracted using the QIAamp Viral RNA mini kit as described in (303).

6.3.4 Genotyping of clinical specimens

HAdV detection was performed on the extracted nucleic acid using primers (hex1deg/hex2deg) (372) which amplify a 301 bp region of the hexon gene (Table 6.1). For samples without visible amplicons, an additional nested PCR was performed using primers (nehex3deg/nehex4deg) which produce a smaller 173 bp product (Table 6.1). All PCR products were visualised on agarose gel to confirm size, enzymatically purified, then Sanger sequenced (methods as described in sections 3.1.1 to 3.1.3).

Table 6.1. Primers used to amplify HAdV sequences.

Primer	Sequence (5'-3') ^{a,b}	Ref
hex1deg	GCC SCA RTG GKC WTA CAT GCA CAT C	(372)
hex2deg	CAG CAC SCC ICG RAT GTC AAA	(372)
nehex3deg	GCC CGY GCM ACI GAI ACS TAC TTC	(372)
nehex4deg	CCY ACR GCC AGI GTR WAI CGM RCY TTG TA	(372)
anehex3deg	tcg gca gcg tca gat gtg tat aag aga cag GCC CGY GCM ACI GAI ACS TAC TTC	(591)
anehex4deg	gtc tcg tgg gct cgg aga tgt gta taa gag aca g CCY ACR GCC AGI GTR WAI CGM RCY TTG TA	(591)

^a Ambiguity code: S, strong interaction, (C/G); R, purine, (A/G); W, weak interaction, (A/T); Y, pyrimidine, (C/T); M, amino, (A/C); K, keto, (G/T); I, inosine, unconventional purine base.

^b Lowercase characters represent adapter sequences.

HAdV type was confirmed through phylogenetic analysis using reference sequences downloaded from the NCBI database. For types 1-52, the sequence accession numbers listed on the 10th ICTV report for *Adenoviridae* were used (367). For type 53 to 113, only unique hexon gene sequences recommended by the Human Adenovirus Working Group (<http://hadvwg.gmu.edu/>) were used. This is because

recombination events have resulted in the emergence of novel strains, many of which possess the same hexon region as previously characterised HAdV types (375-377).

6.3.5 Next generation sequencing of sewage samples

Nested PCR was performed on the extracted nucleic acid to amplify a region of the hexon gene and Illumina Miseq library preparation were performed as described in (591). Briefly, first round PCR was performed using the hex1deg/hex2deg primers (Table 6.1) followed by a second round PCR using the anehex3deg/anehex4deg primers, modified with Illumina sequencing adapter overhangs (denoted with “a” for adapter before the primer name) (Table 6.1). PCR products were then purified using Agencourt AMPure XP beads (Beckman Coulter, CA, USA). The next-generation sequencing (NGS) library was then prepared using Nextera XT indexes (Illumina, San Diego, CA, USA) followed by further bead purification. The KAPA Library Quantification Kit (Roche, Clifton, NJ, USA) was then used for qPCR-based library quantification prior to sample normalisation and pooling. Samples were submitted to the Ramaciotti Centre for Genomics (UNSW) where fragment sizes were evaluated on a Tape Station D5000 (Agilent Technologies, Santa Clara, CA, USA) and the library was prepared with a 10% PhiX spike-in. Paired-end DNA sequencing was performed on the Illumina Miseq platform using a v2 reagents (500 cycle chemistry) and terminated at 2 x 200 bp reads.

6.3.6 NGS data analysis

The software package Geneious Prime, version 2021.1.1 (Biomatters, Auckland, New Zealand) was used to analyse the Illumina MiSeq data. The paired-end sequences were merged using the BBMerge v38.84 plug-in on a low merge-rate setting and primer sequences were removed. The built-in Geneious “Map to reference” tool was used (parameters: medium-low sensitivity and five iterations of fine tuning) to map reads to HAdV reference sequences. Mapped sequences were discarded if there were less than 10 reads that mapped to a reference sequence in a given sample. The proportion of each group was then calculated by dividing the total number of reads per group by the total number of mapped reads for that sample.

6.4 Results

6.4.1 Detection of HAdV infections in clinical faecal specimens

Specimens tested in this study were initially positive for HAdV by either multiplex PCR or EIA. Over the course of the study, HAdV was successfully amplified and sequenced in 91.4% (n=445/487) of faecal specimens collected. The median age of HAdV AGE patients was 1.6 years. The majority (32.8%, n=146/445) of samples were collected from children aged between one and two years, followed by children in the newborns to one year old age group (24.9%, n=111/445) (Figure 6.1). Notably, species C was detected in high prevalence in samples collected from children aged two and younger and represented 31.5% of adenovirus-associated AGE in this age group (n=81/257) (Figure 6.1).

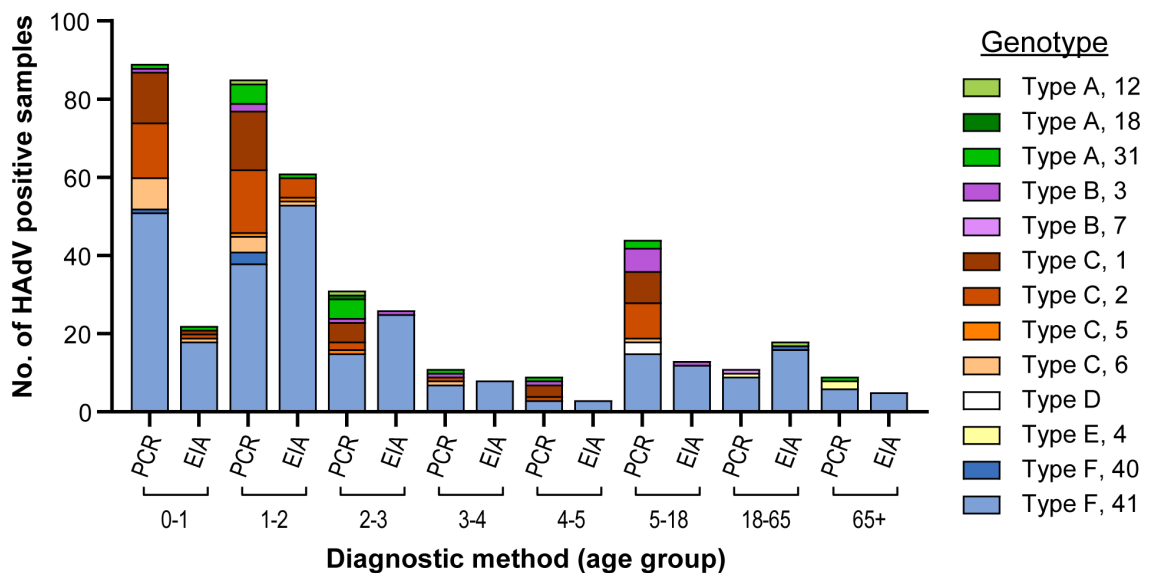


Figure 6.1. Diversity of HAdV detected in different age groups from 2018-2021.

The number of genotyped clinical faecal specimens is shown grouped by age category (in years) and diagnostic methodology (EIA or PCR). The different HAdV hexon genotypes are represented by different colours, as shown in the legend.

6.4.2 Comparison of HAdV types detected using different diagnostic methods

The initial diagnoses of adenovirus-associated gastroenteritis were obtained using two different commercial enteric pathogen diagnostic assays. Therefore, the diversity of HAdV types detected using the two different assays was compared to evaluate each method's ability at detecting a diverse range of types. Both diagnostic

kits purport to be capable of detecting HAdV types beyond the classically enteric F40/41, however, our results suggested otherwise. Of the samples collected from PoWH (multiplex PCR-based diagnostic kit), 48.8% (n=141/289) were genotyped as non-F40/41 (Figure 6.2). In comparison, only 9.6% of samples collected from DHM (n=15/156) (EIA-based diagnostic kit) were genotyped as non-F40/41 (Figure 6.2). The PCR-based diagnostic kit detected thirteen different genotypes, spanning six major groups (A-F). In contrast, the enzyme immunoassay (EIA) based kit detected only nine different serotypes, spanning four different HAdV species (A, B, C and F) (Figure 6.2).

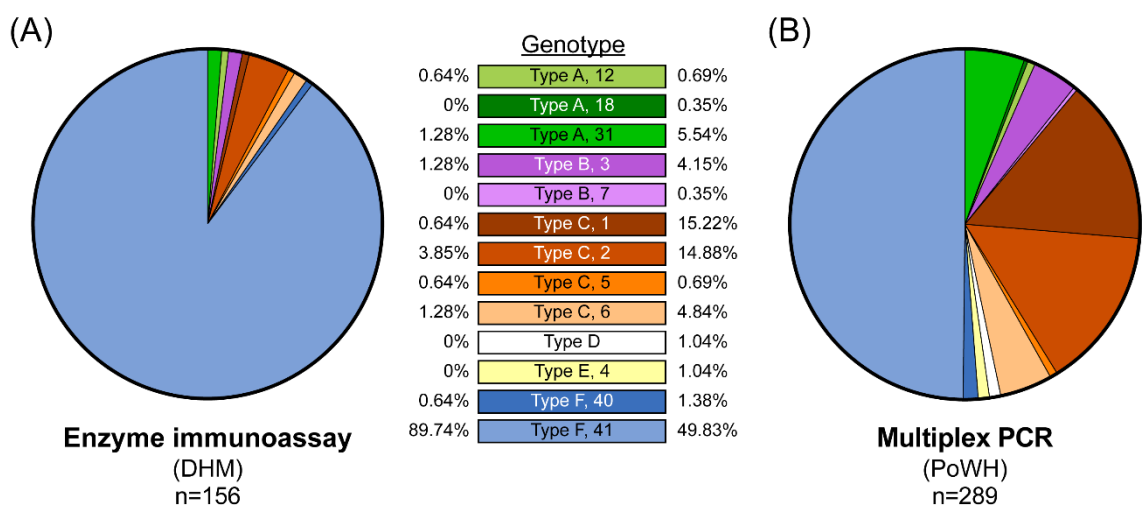


Figure 6.2. HAdV types found in samples identified using different diagnostic assays.

Faecal specimens were obtained from patients who presented with adenovirus-associated gastroenteritis that were diagnosed using either (A) enzyme immunoassay or (B) multiplex PCR based diagnostic kits. The percentage distributions of HAdV genotypes identified from samples from each diagnostic stream are shown. Genotypes are colour coded as per the figure legend.

6.4.3 Genetic diversity of HAdV in clinical specimens

Over the four-year study period, 13 different HAdV hexon genotypes were identified across six of the seven species (A-F), with species G not detected (Figure 6.3). Overall, there was little change in the yearly prevalence of different HAdV genotypes detected. The most prevalent genotype was F41 which represented 63.8% (n=284/445) of HAdV infections (Figure 6.3). Species C was the second most prevalent group and accounted for 25.4% (n=113/445) of cases over the four years (Figure 6.3). Four different genotypes were identified within species C, these were C2 (11.0%, n=49/445), C1 (10.1%, n=45/445), C5 (0.7%. n=3/445) and C6 (3.6%, n=16/445) (Figure 6.3). Other major groups A and B accounted for 4.9% (n=22/445) and 3.4% (n=15/445)

of cases, respectively, whilst groups D and E were only identified in three cases each (Figure 6.3).

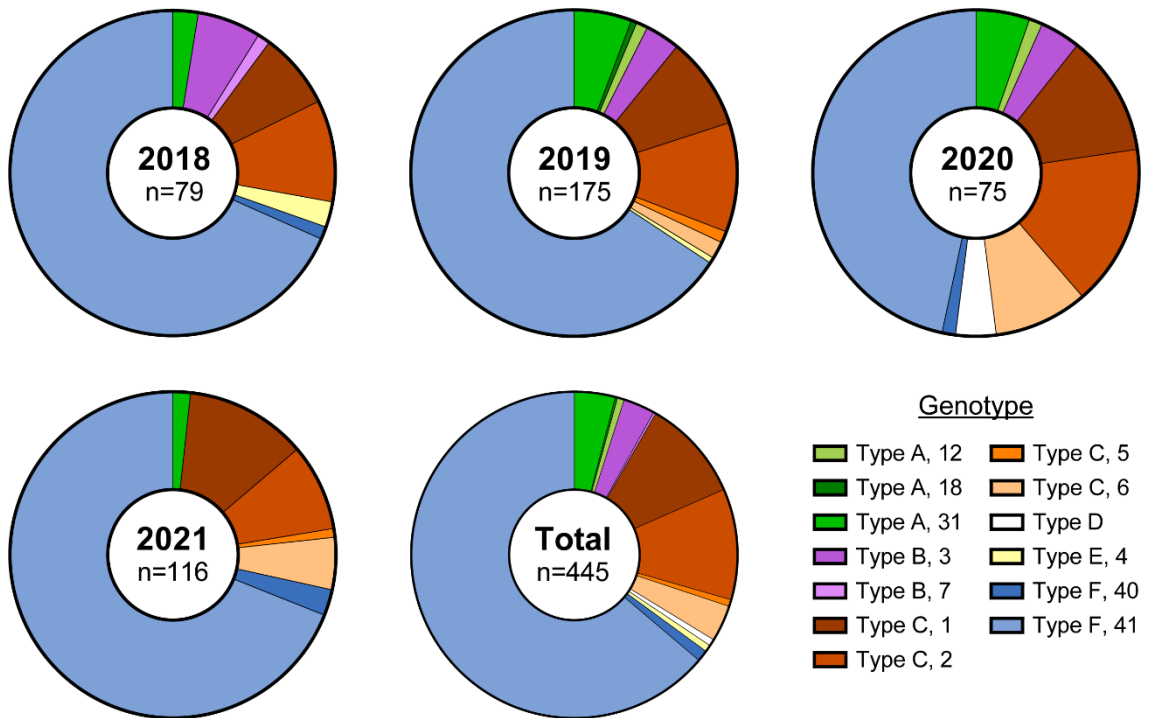


Figure 6.3. Diversity of HAdV hexon types identified in clinical samples, 2018-2021.

A total of 445 patients with adenovirus-associated gastroenteritis were investigated between January 2018 and December 2021. Phylogenetic analysis of a partial hexon gene region was used to determine the genotype which are represented by different colours as indicated in the legend.

6.4.4 Seasonality of HAdV-associated gastroenteritis

Other viruses such as norovirus (579), rotavirus (without vaccination) (600) and influenza (601) display seasonal trends, with a peak in activity typically occurring during winter/early spring in temperate regions. Therefore, the present study investigated whether any seasonal trends could be observed for HAdV-associated gastroenteritis (Figure 6.4.). Clinical sampling in 2020/21 has experienced disruptions due to COVID-19 lockdown restrictions, therefore, only seasonal activity over 2018 and 2019 was examined. Over the two-year period, no distinct seasonality was observed, with similar levels of activity detected across Winter (n=68), followed by Spring (n=66), Summer (n=61) and Autumn (n=59) (Figure 6.4.).

The genotypic distribution for the most prevalent HAdV were also compared. The most prevalent genotype, F41, represented 78.0% of cases in Autumn (n=46/59), followed by Summer (64.0%, n=39/61), Winter (63.2%, n=43/68) and Spring (62.1%, n=41/66) (Figure 6.4.). For species C, the second most prevalent group, detection prevalence in Winter (27.9%, n=19/68) and Spring (25.8%, n=17/66) were approximately 1.8-fold higher than in Summer (14.8%, n=9/61) and Autumn (15.3%, n=9/59) (Figure 6.4.).

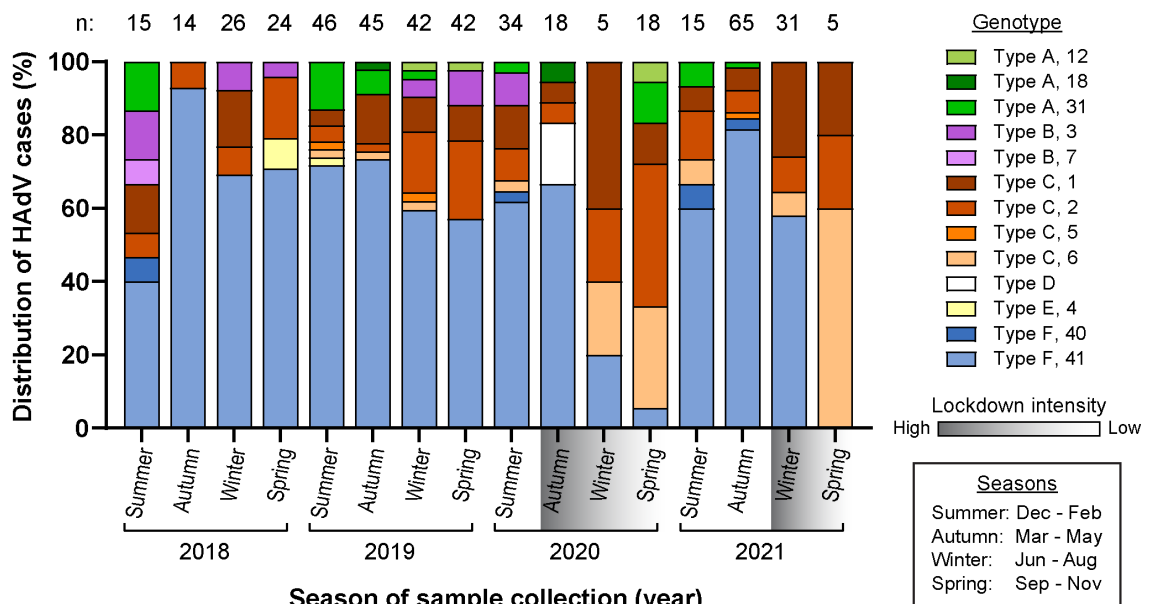


Figure 6.4. Seasonal distribution of HAdV genotypes identified in NSW, Australia between 2018-2021.

A total of 445 patients with adenovirus-associated gastroenteritis were investigated between January 2018 and December 2021. Phylogenetic analysis of a partial hexon gene region was used to determine the genotype which are represented by different colours as indicated in the legend. The total number of cases in each seasonal quarter is indicated by numbers above the graph. Each seasonal year was designated to commence in December in line with the beginning of summer for the Southern Hemisphere. Periods with lockdown and its intensity are indicated by grey shading below the graph.

6.4.5 Genetic diversity of HAdV in wastewater in 2018

This study aimed to gain a more comprehensive understanding of HAdV at a population scale using NGS of amplicons generated from DNA extracted from wastewater samples. A partial hexon gene region (173 bp) was amplified from monthly wastewater samples collected from three sites (Bondi, Malabar, and Melbourne) in 2018 and sequenced on the Illumina Miseq platform. A total of 2,868,917 filtered and

successfully mapped reads were generated from 36 wastewater samples, with an average of 79,692 reads for each sample (range 3,095 – 302,674).

All seven species of HAdV (A-G) were detected over the course of the year. Of these, species F was the most prevalent and accounted for 74.24% of total reads (Figure 6.5). Specifically, F41 represented 70.17% of total reads whilst F40 represented 4.07% (Figure 6.5). F41 accounted for an average of 73.79% of monthly reads in Bondi (ranging from 23.25% to 99.49% per month), 65.06% in Malabar (ranging from 32.49% to 96.02%), and 76.60% in Melbourne (ranging from 39.62% to 99.77%) (Figure 6.5A, B, C). The second most prevalent group was species A (24.19% of reads). Two genotypes from species A were detected, A31 and A12, which represented 20.53% and 3.54% of reads, respectively. The levels of the other major groups were much lower, species C represented 0.94% of reads, followed by B (0.27%), D (0.24%), E (0.10%) and lastly species G which accounted for only 0.02% of total reads (Figure 6.5D).

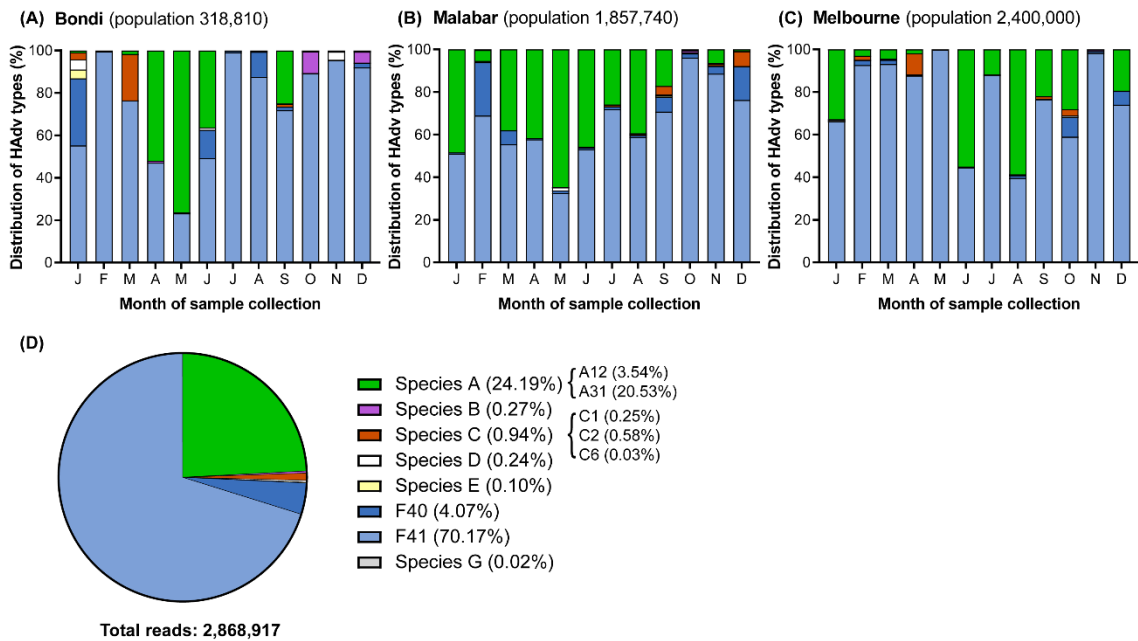


Figure 6.5. HAdV hexon type distribution in wastewater, 2018.

The monthly distribution of HAdV in wastewater collected in 2018 was determined using partial hexon amplicons for the (A) Bondi, (B) Malabar and (C) Melbourne WWTPs. Amplicons were sequenced on the Miseq platform and Geneious Prime was used for the merging and mapping of reads to reference sequences. (D) The total distribution of reads is across the year. The total number of reads is shown below the pie chart, as well as the relative prevalence of each group. For clarity, reads from different genotypes within non-F groups were grouped by species in the graph.

6.4.6 Comparison of genetic diversity in clinical and wastewater samples

Genotypic diversity and prevalence of HAdV found in clinical and wastewater samples were then compared to investigate correlation. F41 was the most prevalent genotype detected in both clinical (63.8%, n=284/445) and wastewater samples (70.17% of total reads) (Figure 6.3, Figure 6.5). A disparity, however, was observed for the second most prevalent group identified. Species C was the second most prevalent group detected in patients of adenovirus-associated gastroenteritis (25.4%, n=113/445), whilst species A was the second most dominant group in sewage (24.19% of reads) (Figure 6.3, Figure 6.5). In wastewater, F40 was the third most prevalent genotype, and accounted for 4.07% of total reads. In contrast, F40 was found in only five cases (1.1%, n=5/445) over the four-year study period (Figure 6.3). In clinical specimens, species C was detected more frequently during Winter and Spring (Figure 6.4), however no such trend was observed in sewage (Figure 6.4, Figure 6.5). Additionally, species G was detected in wastewater only (Figure 6.5).

6.5 Discussion

Enteric HAdV types F40 and F41 are significant contributors to the global diarrhoeal disease burden, particularly among young children in developing nations (161, 602). As a result, epidemiological studies of AGE have frequently focused on F40/41 to the exclusion of all other HAdV types (602-605). This has inevitably resulted in the under-detection of non-group F HAdV and thus contributed to the current poor understanding of the role of these viruses in diarrhoeal disease. This study explored the role of enteric and non-enteric HAdV types in AGE in NSW, Australia using clinical faecal specimens collected over a four-year period (2018-2021). Monthly wastewater samples collected from three WWTPs during 2018 were also analysed to provide population-based representation of circulating HAdV within the community.

Historically, HAdV types F40 and F41 were both frequently isolated from paediatric AGE patients (606, 607). However, since the early 1980s, the decline of F40 alongside the concomitant dominance of F41 has been observed, firstly in Australia (595) and the Netherlands (608), followed by Canada (609) and the UK (610, 611) and finally in Japan (612). This change in F40 and F41 ratio was likely due to a shift in F41

variant frequency, and several studies have noted antigenic changes in circulating F41 strains occurring around a similar time (608, 609, 611). In the twenty years since, HAdV type F41 has maintained its dominance over F40 (590, 592-594), and recently, our group has reported an absence of F40 in clinical AGE specimens collected in NSW, Australia during 2016 and 2017 (591). Congruent with prior studies, the present work also found HAdV type F41 to be the most common cause of HAdV associated AGE (63.8%, n=284/445), whilst F40 was detected in only 1.1% of adenovirus-associated gastroenteritis cases (n=5/445) (Figure 6.3). F41 was also the leading HAdV type detected in wastewater samples (70.17% of total reads) (Figure 6.5). This was consistent with our previous work, where F41 represented 83.5% of all wastewater amplicon NGS reads (591). Similar observations of F41 prevalence in sewage have also been reported in Italy (613) and Luxembourg during 2013 (428), in Spain during 2013 and 2016 (614, 615) and in French Polynesia (616). Despite its low levels in clinical AGE cases, F40 was the third most prevalent HAdV type found in wastewater specimens in 2018 (4.07% of total reads) (Figure 6.5D). This was not unexpected, considering our previous study found F40 to represent 11.0% of all reads in 2016-17 (591).

The second most prevalent type detected in wastewater was A31 which accounted 20.53% of reads (up from 3.7% in 2016-17 (591)) (Figure 6.5D). This contrasted with its low detection rates in AGE where it represented 4.0% of clinical cases (n=18/445) across the four-year period and just 2.5% of cases in 2018 (n=2/79) (Figure 6.3). However, the high abundance of A31 in sewage although unexpected, was conceivable considering A31 has been identified as an important cause of gastroenteritis in children (408, 617-619). Nonetheless, it is important to note that HAdV genotypes causing other clinical infections are also shed in stool or other bodily fluids into sewage. A similar trend was observed for HAdV type A12, which was not detected from clinical samples during 2018 yet represented 3.54% of total sewage reads (Figure 6.3, Figure 6.5D). As with A31, HAdV type A12 has also been reported in association with paediatric gastroenteritis (407, 620). Both A31 and A12 have similarly been found in high prevalence in wastewater collected in Luxembourg in 2013 (428), Spain in 2016 (615) and in French Polynesia (616). This suggests that A31 and A12 could cause milder or asymptomatic infection, leading to its underrepresentation in

clinical samples. However, a case-control study comparing the frequencies of different HAdV types and their attribution to paediatric AGE found that non-group F HAdV strains have a low attribution to AGE with detection in asymptomatic children (619) and so wastewater surveillance was likely capturing a high proportion of group A HAdV shedding that was caused by other clinical syndromes.

The second most prevalent group detected clinically, was species C, which represented 25.4% (n=113/445) of AGE cases typed (Figure 6.3). Furthermore, most of these cases occurred in children aged two and younger (71.7%, n=81/113) (Figure 6.1). Species C is typically associated with respiratory illness (4); however, an increasing number of studies have reported an association between this group and paediatric gastroenteritis (382, 383, 587, 621). Recently, a case-control study showed that species C HAdV (specifically C1, C2, C5 and C6) had 51.7% attribution to AGE (95% CI, 11.5-73.4%) due to detection among the control cohort (619). Nevertheless, even accounting for the low attribution to AGE, species C represented very large proportion AGE cases typed. In contrast, group C HAdV accounted for less than 1% of reads in sewage in 2018 (Figure 6.5D). There are several possible explanations for this. Firstly, most of these patients were within a diaper wearing age group (0-2 years) (71.7%, n=81/113) (Figure 6.1), and these children are less likely to contribute to sewage. Secondly, the faecal viral load for non-group F HAdV is typically lower, so there would be less shedding into wastewater overall (619). Additionally, species C can establish persistent infections in the gastrointestinal tract, which can result in prolonged shedding in faeces (425, 622, 623). Therefore, the possibility also exists that a small number of detections may have occurred due to prolonged low-level shedding after recovery from a previous infection.

Other non-group F HAdV detected clinically include species B (3.4%, n=15/445), D (n=3/445) and E (n=3/445) (Figure 6.3), which are commonly associated with upper respiratory illness or keratoconjunctivitis (4). As with species C HAdV, several studies have also detected these viruses in AGE patients (382, 383, 589, 590), with one case-control study finding a positive correlation between type B3 and diarrhoea (588). Consistent with observations in clinical specimens, these viruses were detected in very low levels in wastewater (<0.3% of total reads each) (Figure 6.5D).

Interestingly, there was a stark contrast between the genetic diversity detected by the two diagnostic kits (PCR-based EasyScreen versus EIA-based RIDASCREEN). Since our adenovirus-associated gastroenteritis samples were initially identified using different commercial diagnostic kits, we compared the genetic diversity represented in each set of samples. It is important that commercial diagnostic panels used for pathogen detection can accurately detect a diverse range of HAdV types since ongoing surveillance is crucial for detecting molecular epidemiological changes should novel, severe strains emerge, as exemplified by the current outbreak of acute, severe hepatitis (596). The present study found that PCR-based detection identified a higher number of non-group F cases (PCR: 48.8% vs EIA: 9.6%) (Figure 6.2). The most likely explanation for this is that the antibodies used in the RIDASCREEN kit were less sensitive for detecting non-group F viruses, resulting in an under-detection of these HAdV in stool samples and hence their lack on inclusion in this study. Indeed, it is widely recognised that PCR-based methods are more sensitive compared to EIA (624-627).

In light of the current outbreak of acute, severe hepatitis (596-598), it is important to also consider the more severe clinical manifestations that may be caused by HAdV types found in this study. In addition to respiratory tract infections and gastroenteritis, HAdV types C1, C2, C5, B3 and B7 have been reported to cause severe hepatitis and liver failure in immunocompromised patients (420, 628-630). Species B and C HAdV have also been associated with disseminated disease which can lead to hepatitis (631-635). Disseminated disease typically occurs in immunodeficient patients, however, it has also been reported in patients who were considered immunocompetent (631). Although there have been a few documented cases of HAdV-associated severe hepatitis in immunocompetent patients, these case reports failed to determine the infecting HAdV type (636-638). So far, HAdV identification in patients with acute, severe hepatitis has been performed using a variety of partial hexon typing approaches and no standardised protocol has been recommended (639). HAdV are known to evolve through recombination, and species A-D all contain new members that have emerged through recombination (375-377, 618). Indeed, a recent study comparing the genomes of HAdV strains associated with severe and mild

infections found that the incidence of recombination events was higher in severe cases (640). Therefore, it is possible that a novel recombinant HAdV has emerged to cause this hepatitis outbreak. This new virus could consist of an F41 hexon and different penton and fibre proteins leading to its hepatotropism (389-391, 641). Whole genome sequencing of the virus is currently underway (639), and this information will hopefully provide further insights into the virus. These sequencing efforts are also vital for designing strain-specific primers for a sewage-based assay. Wastewater monitoring as described here, can provide an early warning tool to detect this strain even before cases arise in the community, as was demonstrated recently for SARS-CoV-2 (642, 643).

This study is not without limitations. All clinical samples used in the study were fully deidentified. Therefore, we were unaware of any patient comorbidities or their immune functionality. Clinical history was also unavailable, so the study cannot exclude the possibility of patients also displaying respiratory symptoms in addition to gastroenteritis or detecting prolonged shedding following a past infection. For future studies, it would be useful if full clinical history, including symptom severity and patient characteristics were also obtained so that further epidemiological links may be drawn. Additionally for wastewater, since HAdV genotypes causing other clinical infections are also shed in stool, the prevalence of a genotype in wastewater would reflect more than just AGE cases within the community.

6.6 Concluding remarks

This chapter explored the molecular epidemiology of adenovirus-associated gastroenteritis in NSW, Australia over a period of four years. Aided by wastewater analyses, the prevalence of circulating HAdV types within the community was also investigated in 2018. Although species A HAdV represented only a small proportion of genotyped cases (<5%), it represented nearly a quarter of reads within wastewater. This suggests that it is less virulent compared to other groups, leading to an underestimation of its prevalence if only clinical samples are used. We also observed a high prevalence of species C HAdV in young children with gastroenteritis (<2 years of age). Even accounting for a 51.7% attribution to AGE (619), it is nonetheless an important aetiological agent of paediatric gastroenteritis and should be monitored.

The integration of both clinical and wastewater specimens is a useful combination to provide a better understanding of circulating HAdV within the population.

7 General Discussion

Viral pathogens pose a significant global health and economic burden. To minimise the loss of human life, we rely on pharmaceutical interventions such as vaccines and antivirals. However, the reality is that effective antivirals and vaccines simply do not exist for most human viral pathogens, including those explored in this thesis – namely norovirus, human adenovirus (HAdV), Zika virus, hepatitis A virus (HAV; lacks antivirals) and hepatitis C virus (HCV; lacks a vaccine). Collectively, these viruses account for an estimated death toll exceeding 287,000 each year and billions of dollars' worth of healthcare costs and productivity losses (179, 180, 644). Furthermore, even when an effective vaccine or antiviral therapy exists, the protection provided can be limited. For example, even though a highly effective yellow fever virus vaccine is available, vaccine coverage is weak in poorly resourced regions where yellow fever is prevalent (645, 646). Thus, when outbreaks do occur in these regions, the lack of effective antiviral treatments has contributed to the loss of human life, and this was exemplified by the 2016 Angola and Democratic Republic of Congo yellow fever outbreak (517). Conversely, even when highly effective therapies are available, full eradication of infection may not be possible, such as in the case of human immunodeficiency virus (HIV) (18, 19).

This work aimed to address the threat of viral pathogens using a two-pronged approach that began with the development of broad-spectrum non-nucleoside inhibitors (NNIs) against RNA viruses (**chapter four**). Later, the holistic surveillance of circulating noroviruses (**chapter five**) and HAdV (**chapter six**) in Australia was conducted using both clinical and wastewater specimens. The significance of key findings from broad-spectrum NNI development and future directions are discussed in section 7.1 below. The significance of key findings from the molecular epidemiological surveillance of norovirus and adenovirus are discussed in sections 7.2 and 7.3, respectively. Section 7.4 presents the overall conclusion of this work.

7.1 Broad-spectrum non-nucleoside inhibitors can be designed; *in silico* methods can aid their discovery.

In chapter four, a unique combination of strategies (compound repositioning, complex-based pharmacophores, virtual screening and “structure-activity relationship (SAR) by catalogue”) was employed to navigate insufficient prior knowledge (lack of existing compounds and high-quality protein structures) and develop NNI compounds. This work resulted in the initial identification of four active compounds – NCS-014, NCS-032, NCS-034 and NCS-013. Of these, the first three displayed narrow-spectrum inhibition against one target each. The fourth compound, NCS-013, displayed broad-spectrum inhibition of RNA-dependent RNA polymerase (RdRp)/replicon replication for five different viruses (human norovirus, feline calicivirus, Zika virus, HCV, and HAV). These five viruses span three positive-strand RNA virus families (*Caliciviridae*, *Flaviviridae*, and *Picornaviridae*), and except for HCV, none of these viruses have approved antiviral therapies (11). Thus, the broad-spectrum and cross-family activity of NCS-013 identified in this work, suggests that this compound could also have antiviral effects against other viruses from these three families.

As NCS-013 has broad-spectrum potential, it was used as a scaffold for similarity searching of available compounds (termed “SAR by catalogue”). This led to the identification of a fifth compound, NCS-013A, which similarly exhibited cross-family inhibition of the Zika virus RdRp and the HCV and HAV replicons. The successful use of NCS-013 as a scaffold suggests it could provide a viable starting point for future drug discovery efforts.

The concept for broad-spectrum antivirals is not new, however, the development of such compounds is challenging due to the highly diverse nature of viruses in terms of structure, machinery and in their replication strategies (647). Therefore, recent efforts have focused on targeting host proteins required for viral replication or modulating host immune responses to viral infection (section 1.3.1). The alternative is to target viral proteins essential for replication as these are more likely to be conserved. Several broad-spectrum virus-targeting molecules have been described; however, the broad-spectrum action of these compounds was identified due to

serendipitous “off-target” effects rather than by design (elaborated in sections 1.3.3 and 1.4). To the best of our knowledge, this study represents the first attempt to develop NNI compounds with cross-family activity and the successful identification of NCS-013A suggests that broad-spectrum NNIs can be rationally designed.

Drug discovery has traditionally been an extremely resource-intensive process, and this creates barriers to entry for entities outside of big pharmaceutical companies. However, advancements in hardware computing power and software intelligence, and an increasing number of publicly available protein sequences, structures and other biological datasets have made it possible to use computational techniques to aid drug discovery. In this work, a variety of low-cost methods were used to develop broad-spectrum NNI compounds, demonstrating that the initial stages of drug discovery do not have to be expensive and inaccessible. Firstly, drug repositioning was used in combination with complex-based pharmacophores and virtual screening of the SPECS compound database as a low-budget alternative (software licenses and server costs only, with some software available free-of-charge) to high-throughput screening (HTS). For comparison, equivalent HTS of the SPECS compound database could cost US\$200,000 (based on US\$1 per compound estimates and excluding setup costs) (648); these economies of scale are only achievable for large entities. Secondly, the eMolecules chemical search engine was used as an alternative to contracting a medicinal chemist. The identification of NCS-013A in this work using an “SAR by catalogue” approach highlights its feasibility as a low-budget alternative for early hit expansion and SAR analyses.

Finally, from the 44 compounds that were assessed using *in vitro* assays, this work achieved a hit rate of 4.5% ($n=2/44$) for potentially broad-spectrum compounds. In comparison, it is not uncommon for HTS to achieve hit rates less than 1% (649), and a previous HTS screen for norovirus NNIs performed by our group yielded a primary hit rate of only 0.18% (500). This work showed that computer-aided methods can greatly increase the hit rate for a fraction of the cost, streamlining the drug discovery process.

7.1.1 Future directions

The two NNI compounds (NCS-013 and NCS-013A) can be validated for their broad-spectrum activity as follows. Firstly, the target-specific antiviral activity of these structures can be verified by using freshly synthesised, pure material in orthogonal assays (650, 651), such as a gel-shift assay (147). Additional hit expansion and SAR analysis can also be performed using the “SAR by catalogue” approach and these compounds examined *in vitro* against a variety of RdRp targets to search for more potent structures. This will be also useful for both computational binding site prediction and for guiding compound SAR optimisation. Docking studies and molecular dynamics simulations can then be performed using these compounds to investigate the ligand-protein interactions. Crystal structures are already available for many flavivirus [such as HCV (144), Zika virus (652), Dengue virus (653), bovine viral diarrhoea virus (654) and yellow fever virus (655)] and picornavirus virus RdRp [foot-and-mouth disease virus (656), enterovirus A71 (657), human rhinovirus (658) and poliovirus (659)], and promising compounds should be modelled in these structures. For viruses without any available structures (such as HAV), tools such as AlphaFold 2 (a machine learning based structure prediction tool) (660) could be used to generate protein models from available sequence data. Additionally, direct target verification via cell culture (where available) should also be performed, alongside sequencing of drug-resistant mutants to better assess the longer-term utility (barrier to resistance) of potential compounds. Once a sufficiently potent structure (100 nM – 5 µM range) (533) with verified activity has been obtained, ADMET (absorption, distribution, metabolism, excretion and toxicity) evaluations can be performed followed by thorough SAR exploration to optimise drug properties. The compound can then be progressed to clinical trials and eventually enter the market as a broad-spectrum antiviral therapeutic.

7.2 Molecular epidemiological surveillance of norovirus in Australia, 2018 to 2020

7.2.1 Old norovirus strains have remained in circulation in Australia

In order to design a successful norovirus vaccine, it is critical to understand the molecular epidemiology of circulating norovirus genotypes. Careful consideration must

be undertaken to ensure that the strains incorporated in the vaccine can induce broad protective immunity against a wide range of clinically relevant noroviruses. These vaccines would also require regular updates to account for viral evolution and thus evasion of herd immunity. Therefore, it is crucial to undertake continued molecular epidemiological surveillance of circulating norovirus strains around the world, as this work will inform vaccine development efforts.

In chapter five, circulating noroviruses in Australia before and during the COVID-19 pandemic (2018-20) were investigated in clinical faecal specimens (from norovirus acute gastroenteritis (AGE) patients in NSW) and monthly wastewater samples (from Malabar and Bondi treatment plants in Sydney and the Western treatment plant in Melbourne). This work found that the GII.4 Sydney 2012 capsid was the dominant capsid detected in clinical samples and three viruses that possessed a GII.4 Sydney 2012 capsid (with a GII.P16, GII.P4 New Orleans, or GII.P31 non-structural region) collectively represented 34.2% (n=207/604) of clinical samples. Although this GII.4 Sydney 2012 capsid has remained the dominant capsid detected, its prevalence was substantially lower than the 60-80% reported previously for GII.4 noroviruses (230-232). One reason for this observation is that the capsid has now been in circulation for more than nine years, which would have resulted in high population herd immunity. Antigenic changes within the viral capsid are important for facilitating evasion of herd immunity and thus the emergence of novel GII.4 pandemic variants every 3-5 years (216, 661) (elaborated in section 2.2.7). Therefore, it is unusual that the GII.4 Sydney 2012 capsid has remained prevalent for so long.

Of the three non-structural regions that the Sydney 2012 capsid has been associated with, GII.P4 New Orleans (4.1%, n=25/604) was the non-structural region from the preceding pandemic variant which circulated between 2009 and 2012 (232, 294, 300) whilst GII.P31 (7.1%, n=43/604) is the original non-structural region of the Sydney 2012 pandemic variant (Figure 5.6). Due to the lack of antigenic novelty in these viruses, it is unsurprising that neither of these strains circulated with high prevalence during the study period. The GII.P16 polymerase, similarly, has also been in circulation for several years now. It emerged epidemically in 2016 as the recombinant GII.2 [P16] virus (303) and it is believed that this virus donated its non-structural region

to create the GII.4 Sydney 2012 [P16] virus (287). This GII.4 Sydney 2012 [P16] virus then became the dominant norovirus in Australia (56.8%) and New Zealand (42.9%) during 2017 (229), despite accumulating few changes within the VP1 blockade epitopes (A-G) (214, 216). In our previous study, comparison of GII.4 Sydney 2012 capsid sequences from GII.P16 and GII.P31 viruses revealed only one novel antigenic change, this occurred in residue 373 of epitope A (R→H) (229). All other changes detected were reversions to residues found in previous pandemic variants (Appendix Figure 8.2).

Antigenic reversion is commonly observed in RNA viruses (662-667), however its mechanisms and benefits are not well understood. Some studies have shown that reversion occurs when an immune escape mutation decreases viral fitness, and thus when naïve hosts are infected there is a rapid reversion to previous high-fitness variants (662, 668). In other instances, such as in GII.3 noroviruses, the propensity for antigenic reversion in VP1 gene and thus lack of novelty is believed to be one of the reasons why this genotype is associated with paediatric infections, as this population is more likely to be immunologically naïve (310, 568). Therefore, antigenic drift alone cannot explain the success of the GII.4 Sydney 2012 [P16] virus which has circulated since 2016.

Instead, the non-structural region must also play a fundamental role in viral fitness enabling its persistent circulation in the population either through direct evasion of herd immunity or by altering replication rates and infectivity. For example, the VP1 amino acid sequence of the re-emerged GII.2 [P16] strain was almost identical (≤ 2 amino acid changes) to some previously detected GII.2 [P2] and pre-2016 GII.2 [P16] strains (287). Comparison of polymerases from the post-2002 GII.4 pandemic lineage to pre-2002 polymerases revealed that a single point mutation on residue 291 altered kinetic activity (669). Furthermore, acquisition of a polymerase with reduced replication fidelity and/or increased kinetic activity can improve transmissibility (670). This has been observed in both pandemic GII.4 strains (669) and is speculated to have contributed to the epidemic emergence of GII.17 [P17] (671) and GII.2 [P16] (287).

Another old strain that has remained in circulation was GII.2 [P16] which emerged in Australia and New Zealand in mid-2016 and was responsible for 18.2% of

all sporadic and outbreak cases (303). The same study found that GII.2 noroviruses were dominant in wastewater from August to December 2016 (303). GII.2 noroviruses declined in prevalence in both clinical and wastewater samples in 2017 as they were replaced by the GII.4 Sydney 2012 [P16] virus (229). The decreased circulation of this recombinant strain throughout 2018 and 2019 until its re-emergence in August 2020 were described in this thesis (Figure 5.6, Figure 5.11). Mechanisms of its re-emergence warrant further investigation, particularly into any changes in the VP1 or polymerase amino acid sequence. Since the viral polymerase is a popular target for direct-acting antivirals, examining norovirus polymerase evolution will also be useful for drug development efforts.

Recently, between 2018 to 2020, norovirus molecular epidemiology in Asia may have begun changing again, with a potential re-emergence of the Sydney 2012 pandemic variant (GII.4 Sydney 2012 [P31]) in paediatric AGE patients (566, 567, 581, 672). Although this virus has been in circulation in China and Hong Kong since late 2012 (311, 673), its prevalence had decreased in the wake of the epidemic emergence of GII.17 [P17] and GII.2 [P16] during the winters of 2014/15 and 2016/17, respectively (245, 549, 564, 581, 674). VP1 sequence analysis of Chinese outbreak strains identified three novel antigenic changes in epitopes A (residue 368), E (residue 414) and G (residue 355) (compared to pandemic GII.4 prototype sequences shown in Appendix Figure 8.2) (672). Further investigation into the VP1 amino acid sequences of strains that possess a GII.4 Sydney 2012 capsid will be useful for understanding why these viruses have circulated within the community for such an extended period.

Work in this thesis showed that several old strains (GII.4 Sydney 2012 [P16], GII.2 [P16], GII.4 Sydney 2012 [P4 New Orleans] and GII.4 Sydney 2012 [P31]) have remained in circulation in the community longer than the expected timeframe. This is unusual and could pose important implications for vaccine development strategies if future norovirus evolution and molecular epidemiology no longer follow the same historical trends.

7.2.2 An interplay in herd immunity may have directed the increases in AGE outbreak activity observed in childcare centres

When novel strains of norovirus emerge, this is typically followed by a sudden increase in AGE outbreak activity. Therefore, in chapter five, the number of monthly institutional outbreaks was tracked (Figure 5.3) and any periods of elevated activity were investigated. Two periods of epidemic activity were identified, and these occurred between August and December 2019 (GII.3 [P12]) and in November and December 2020 (GII.2 [P16]) (Figure 5.5). These outbreaks were not caused by the emergence of any new strains but rather existing noroviruses that had remained in circulation.

GII.3 noroviruses are important causes of sporadic AGE, particularly among children (307-309). The GII.3 [P12] virus emerged in NSW in 2016, replacing GII.3 [P21] as a prevalent cause of childhood gastroenteritis (229, 293, 303). However, despite acquiring a new non-structural region, prior to the current work, GII.3 [P12] has not been associated with large-scale outbreaks or epidemics (229, 303, 675, 676). One explanation for this could be the consecutive emergence of the GII.2 [P16] and GII.4 Sydney 2012 [P16] recombinants in NSW that occurred shortly afterwards (229, 303). Compared to GII.3 [P12], these strains possessed greater novelty, a better polymerase, and in the case of GII.4 Sydney 2012 [P16], also bound to a broader range of histo-blood group antigens (HBGA) types and thus would have a larger pool of susceptible hosts (215, 677). These two viruses probably outcompeted GII.3 [P12], suppressing its circulation before population immunity was reached. Similar trends have been reported in Jiangsu, China where decreases in GII.3 [P12] detection rate in children correlated with the epidemic emergence of GII.17 [P17] and GII.2 [P16] in 2014 and 2016, respectively (675). Therefore, the epidemic emergence of GII.3 [P12] in children during late 2019 (Figure 5.3, Figure 5.5) could be due to the interplay between rising population immunity to GII.2 [P16] and GII.4 Sydney 2012 coupled with immunological naivety to GII.3 [P12]. Then, as herd immunity was reached, the prevalence of GII.3 [P12] returned to “normal”.

A similar interplay may have contributed to the epidemic re-emergence of GII.2 [P16] during November and December 2020 (Figure 5.3, Figure 5.5). Despite causing

epidemics in Asia (546-550), in NSW, the virus was quickly outcompeted by the more virulent GII.4 Sydney 2012 [P16] and has been declining in prevalence since 2017 (229), and almost disappeared from clinical circulation in 2019. Then, throughout the majority of 2020, it was further suppressed by COVID-19 lockdown measures which included the closing of schools and childcare centres (Figure 5.3). Like GII.3, GII.2 is considered a “static” capsid genotype as it has changed very little over the past few decades and was similarly associated with paediatric gastroenteritis (287, 678). Interestingly, “static” genotypes such as GII.2, GII.3, and GII.6 were found to cause outbreaks of AGE in childcare centres and schools, with the dominant genotype shifting every season (570). This is suggestive of population immunity influencing endemic norovirus circulation. Therefore, I hypothesise that the appearance of several novel viruses in 2016 (303) and the subsequent competition may have disrupted the normal circulation dynamics of these strains within the community, leading to their pronounced resurgence once these competitive pressures eased. Future studies could examine this hypothesis by investigating the dominant genotypes in young children from historical stool collections.

The work in chapter five also found that despite subdued levels of institutional AGE outbreak activity for most of 2020 as a direct result of COVID-19 lockdowns, due to the large spike in outbreaks recorded in childcare facilities during November and December 2020, the yearly total (n=843) remained comparable to previous years (Appendix Figure 8.1). This shows that when population immunity is not maintained via either natural infection or vaccination, the declines are unsustainable and a rapid increase in cases is inevitable to correct for these deviations. Similar trends were seen in paediatric enterovirus D68 infections in Europe, which were very low during lockdown, however, once restrictions were relaxed, historically high levels were detected (679). Likewise, increases in respiratory syncytial virus (RSV) activity following relaxation of non-pharmaceutical public health measures have also been reported around the world (680, 681), with similar warnings issued for influenza (682, 683). These rapid corrections could pose consequences for patient outcomes and quality-of-care if health systems become overloaded. However, ongoing infectious disease surveillance, such as the work in this thesis, can help mitigate some of these burdens

by supplying historical data that can support the prediction of such trends, facilitating greater government and health system preparedness.

7.2.3 Future directions

Future studies should sequence the full-length VP1 gene from strains that possess a GII.4 Sydney 2012 capsid detected in the present work, to examine whether these novel antigenic changes can also be found in Australia. If they are present, this may provide some explanation into the prolonged circulation of these viruses within the community. The full-length polymerase gene from prevalent strains should also be sequenced to explore amino acid changes, such as those around residue 291 that may affect kinetic activity or replication fidelity (287, 669, 670). Additionally, the effects of these mutations may be explored using recombinant polymerases in replication kinetics or fidelity assays as performed by Bull *et al.* (669). If these mutations decrease polymerase fidelity or increase replication kinetics, this could increase viral fitness and explain why certain strains have remained in circulation for so long.

7.3 A diverse range of HAdV cause gastroenteritis.

HAdVs are one of the leading aetiological agents of childhood infections causing 6-20% of respiratory infections (341-345) and 11-50% of AGE-related hospitalisations (346, 347). Globally, enteric HAdV causes an estimated 70,200 diarrhoeal disease-related deaths each year (180), other types can result in large outbreaks of acute respiratory illness in military recruits (E4, B7, B14) (449-451), or epidemic keratoconjunctivitis (D8, D19, D37) (4). Despite this, there are currently no publicly available vaccines or antivirals approved for the prevention or treatment of HAdV infections. In order to design effective vaccines, it is essential to understand the molecular epidemiology of HAdV to ensure that the strains incorporated in the vaccine will protect against a broad range of clinically relevant strains. Although group F HAdV are recognised as one of the leading causes of AGE, the importance of non-group F HAdV is still unclear.

In chapter six, the molecular epidemiology of adenovirus-associated gastroenteritis in NSW (2018-2021) was investigated. This work found that non-group F HAdV caused 35.1% of all adenovirus-associated AGE cases (n=156/445) (Figure 6.3).

The two most prevalent non-F HAdV types were C2 (11.0%, n=49/445) and C1 (10.1%, n=45/445) from species C (Figure 6.3), which has traditionally been associated with paediatric respiratory illness (4, 341, 343, 345). This work found that species C HAdV also represented 31.5% (n=81/257) of adenovirus-associated AGE in children aged two or younger (Figure 6.1). This study highlights the importance of this group as a common cause of paediatric gastroenteritis. Thus, future surveillance projects should include tests that detect all HAdV and perform genotyping to gain better understanding of their contribution to global disease burden. This knowledge will guide the formulation of future vaccines and identify targets for antiviral development.

Understanding of HAdV molecular epidemiology is vital because these viruses are also used as gene delivery vectors for vaccination (684-687) and pre-existing neutralising antibodies can have consequences for vaccine efficacy (688, 689). HAdV type C5 for example, is a popular choice for adenoviral gene delivery (690-693), however this virus is also extremely common in the population. Xiang *et al.* reported the presence of neutralising antibodies in a large proportion of adults in the USA (34.0%), Thailand (76.5%), Cameroon (55.8%), Nigeria (89.0%), and Côte d'Ivoire (95.8%) (694). Recent efforts to use HAdV C5 as a delivery platform for a COVID-19 vaccine have found that pre-existing immunity diminished both T-cell and antibody-mediated responses to vaccination (691, 692). Therefore, adenoviral vectors may need to shift towards the use of rare human serotypes or those derived from non-human primates instead. One of the problems with using these serotypes, however, is that seroprevalence can also vary between different geographical regions (694, 695). Thus, it is essential that holistic molecular surveillance of circulating HAdV is performed on a global scale, to correctly identify rare types, facilitating the development of more effective vaccines. Another problem encountered when using AdV vaccines was the rare but severe side-effects that were noted in the large-scale use of the AstraZeneca Adv-based COVID-19 vaccine which will likely provide a major hurdle to the future development of HAdV vaccines. The work performed in this thesis is crucial as it provides an Australian perspective on HAdV circulation within the population. Such molecular epidemiological surveillance should be consistent and ongoing so that any changes in prevalence may be identified, particularly in the case of rare strains.

7.3.1 Future directions

In April 2022, an acute, severe hepatitis of unknown origin emerged suddenly, and has since been reported (as of 26 May 2022) in 650 children across 33 countries including the UK, USA, Netherlands, Italy, Spain, Israel, and Japan, (596, 598). HAdV and type F41 in particular, have been proposed as a potential aetiology agents due to their high detection rates in patient samples (596). Additional circumstantial evidence for an adenoviral cause includes the significant increase in HAdV infections in the UK, where the majority of cases have been identified (599). Although F41 has not been associated with hepatitis in the past, HAdV are known to evolve through recombination (375-377, 618, 640). Therefore, it is possible that a novel recombinant HAdV possessing an F41 hexon and different penton and fibre proteins has caused this outbreak of acute, severe hepatitis.

This recent outbreak of hepatitis is a reminder of the importance of continued surveillance of HAdV within the community. Thorough molecular monitoring (whole-genome sequencing) and virus cultivation studies would be required to assess whether HAdV is the cause of this acute, severe hepatitis outbreak. Furthermore, molecular epidemiological surveillance should be expanded to include typing of other major components of the viral capsid such as the penton and fibre genes which determine tissue tropism (389-391, 641). This will facilitate the detection of novel recombinant strains that may emerge in the population. Molecular typing data should also be linked to severity and range of clinical symptoms as this would enable identification of epidemiological connections. This will be useful for detecting emerging strains of clinical significance.

7.4 Final remarks

The goal of this thesis has been to address the threat of viral pathogens through providing groundwork for future antiviral and vaccine development. The work of this thesis has contributed to development of broad-spectrum non-nucleoside inhibitors of RNA viruses. The molecular surveillance of norovirus and HAdV in the population conducted will be essential for identifying appropriate targets for future vaccine and therapeutic development. This study has expanded sewage surveillance capabilities to

include the detection of recombinant noroviruses. The level of genomic detail retrieved from wastewater samples in this thesis showcases the utility of wastewater as a surveillance tool for other similarly enterically shed pathogens within the community. As the role of the non-structural region becomes increasingly important to norovirus viral fitness, this will enhance our ability to detect recombinant viruses with epidemic or pandemic potential. This thesis also demonstrates the importance of non-group F HAdV in gastroenteritis and the urgent need to continue molecular monitoring of all HAdV strains. Such holistic ongoing global surveillance will be vital to development of effective adenoviral vector vaccines.

8 Appendix

Appendix Table 8.1. MS2 cycle threshold and calculated copies.

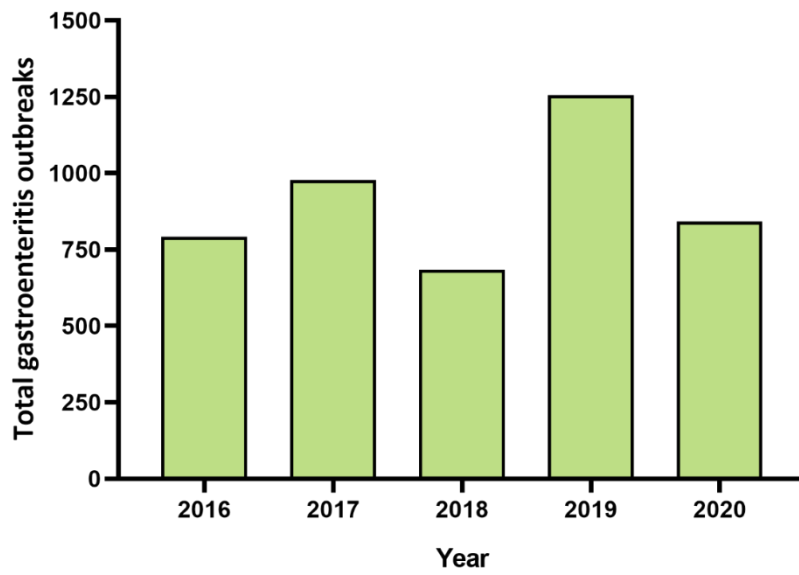
Test	Cycle threshold	Calculated copies ^a
1	21.29	934,590
1 (diluted 1 in 10)	24.46	1,257,400
2	21.42	862,580
2 (diluted 1 in 10)	24.33	1,358,350
3	21.76	695,265
3 (diluted 1 in 10)	24.94	945,250
4	21.60	772,830
4 (diluted 1 in 10)	24.48	1,239,900
5	21.08	1,076,470
5 (diluted 1 in 10)	24.04	1,632,050
6	20.97	1,142,025
7	19.81	2,388,345
8	20.64	1,411,680
9	20.43	1,617,000
10	20.15	1,927,740
11	21.09	1,062,240
12	20.30	1,747,665
13	20.15	1,920,495
14	20.20	1,860,600
15	20.09	2,000,340
16	20.74	1,321,515
17	19.69	2,583,270
18	21.88	642,225

^aCopies in original frozen spherical aliquot.

Appendix Table 8.2. Reference sequences used for mapping of NGS reads.

P-type-genotype	Accession number
GII.PNA9-GII.27	MK733205.1
GII.PNA5-GII.22	MG495082.1
GII.PNA4-GII.11	AB074893.1
GII.PNA2-GII.NA2	MG706448.1
GII.PNA1-GII.NA1	MG495079.1
GII.P41-GII.13	DQ379714.1
GII.P40-GII.5	AB212306.1
GII.P38-GII.25	GQ856469.1
GII.P33-GII.12	KJ710246.1
GII.P33-GII.4	Sequence from current study
GII.P33-GII.1	JN797508.1
GII.P31-GII.17	KT589391.1
GII.P31-GII.4 Sydney	JX459908.1
GII.P31-GII.4 Osaka	AB434770.1
GII.P31-GII.2	LC209439.1
GII.P30-GII.4	Sequence from current study
GII.P30-GII.3	MT492039.1
GII.P30-GII.2	AY134748.1
GII.P29-GII.3	AF190817.1

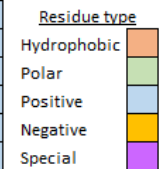
GII.P27-GII.27	MG495078.1
GII.P26-GII.26	MF352142.1
GII.P25-GII.25	MG495083.1
GII.P24-GII.24	MG495084.1
GII.P23-GII.23	MG551869.1
GII.P22-GII.22	AB083780.1
GII.P21-GII.21	KJ196284.1
GII.P21-GII.13	MH702263.1
GII.P21-GII.3	MG892954.3
GII.P20-GII.20	EU424333.1
GII.P18-GII.18	AY823304.1
GII.P17-GII.17	LC037415.1
GII.P17-GII.4	Sequence from current study
GII.P16-GII.21	Sequence from current study
GII.P16-GII.17	KJ196286.1
GII.P16-GII.13	MG892908.3
GII.P16-GII.12	MK754447.1
GII.P16-GII.10	MT501827.1
GII.P16-GII.6	Sequence from current study
GII.P16-GII.4 Sydney	LC153121.1
GII.P16-GII.3	MK280951.1
GII.P16-GII.2	KY865306.1
GII.P16-GII.1	MK483908.2
GII.P15-GIX .1	KJ196290.1
GII.P12-GII.13	KJ196276.1
GII.P12-GII.12	KJ196299.1
GII.P12-GII.10	AF504671.2
GII.P12-GII.4 Asia	AB220922.1
GII.P12-GII.3	KY905334.1
GII.P11-GII.19	AY823306.1
GII.P11-GII.11	AB126320.1
GII.P8-GII.8	AB039780.1
GII.P7-GII.14	GU017903.2
GII.P7-GII.9	AY038599.2
GII.P7-GII.7	MH218692.1
GII.P7-GII.6	AB039777.1
GII.P7-GII.4	Sequence from current study
GII.P6-GII.6	JX989075.1
GII.P4 NO-GII.4 Sydney	KF386146.1
GII.P3-GII.3	AB039782.1
GII.P2-GII.21	Sequence from current study
GII.P2-GII.17	Sequence from current study
GII.P2-GII.13	Sequence from current study
GII.P2-GII.4	Sequence from current study
GII.P2-GII.2	X81879.1
GII.P1-GII.1	U07611.2
GII.P16-GII.16	AY502010



Appendix Figure 8.1. Institutional gastroenteritis outbreaks reported in NSW, 2016 to 2020.

The total number of yearly institutional gastroenteritis outbreaks reported to the NSW Ministry of Health between 2016 and 2020. Monthly institutional outbreaks from 2016 and 2017 were previously published in (303) and (229), respectively.

	F	A	A	A	A	A	H	H	F	B	C	C	C	G	G	G	G	G	G	A	A	A	C	C	C	C	B	D	D	D	D	D	F	E	E	E	E	E
Strain ID	234	294	295	296	297	298	309	310	327	333	339	340	341	352	355	356	357	359	364	368	372	373	375	376	377	378	382	393	394	395	396	397	404	407	411	412	413	414
AY032605_MD145_1987	V	V	G	S	H	D	S	N	V	L	R	A	D	S	S	V	H	T	S	T	N	N	F	Q	T	G	K	D	-	H	H	Q	V	N	R	T	G	H
AY741811_US95_96	V	A	G	S	H	D	N	N	V	M	R	E	D	S	S	V	H	T	S	T	N	N	F	Q	T	G	K	N	-	N	H	Q	V	N	R	T	G	H
AY502023_Farmington_Hills_2002	V	A	G	T	H	N	N	N	V	M	R	G	D	S	D	V	H	T	S	N	N	N	F	E	T	G	K	N	G	T	H	Q	V	S	R	T	G	H
DQ078814_Hunter_2004	V	A	G	T	Q	N	N	N	V	V	R	R	D	S	S	V	H	T	S	S	S	N	F	E	T	G	R	S	T	T	H	Q	V	D	R	D	S	H
EF126965_Den_Haag_2006	V	A	G	S	R	N	N	N	V	V	K	G	D	Y	S	A	P	T	S	S	E	N	F	E	T	H	K	S	T	T	H	R	V	S	R	N	V	H
GU445325_New_Orleans_2009	V	P	G	S	R	N	N	S	V	V	R	T	N	Y	S	A	D	S	R	A	D	N	F	E	T	N	K	S	T	T	P	R	V	S	R	N	I	H
JX459908_Sydney_2012_P31	V	T	G	S	R	N	N	D	V	V	R	T	D	Y	S	A	D	A	R	E	D	R	F	E	A	N	K	G	T	T	H	R	V	S	R	N	T	H
LC175468_Sydney_2012_P16	V	T	G	S	R	N	N	N	V	M	R	T	D	Y	S	A	D	A	R	E	D	H	F	E	A	N	K	S	T	T	H	R	V	S	R	N	T	H



Appendix Figure 8.2. Antigenic changes in the VP1 epitopes for previous GII.4 pandemic variants.

Full-length capsid sequences of pre-pandemic and pandemic lineage GII.4 noroviruses were compared to identify antigenic variations. The Strain ID includes the GenBank accession number and variant name. Amino acid residues are coloured by based on side chain properties. Antigenic epitopes A-H are labelled using coloured boxes at the top. Amino acid positions are also indicated.

9 References

1. Walker PJ, Siddell SG, Lefkowitz EJ, Mushegian AR, Adriaenssens EM, *et al.* 2021. Changes to virus taxonomy and to the International Code of Virus Classification and Nomenclature ratified by the International Committee on Taxonomy of Viruses (2021). *Arch Virol* **166**:2633.
2. Siegel RD. 2018. 201 - Classification of Human Viruses, p 1044-1048.e1. In Long SS, Prober CG, Fischer M (ed), Principles and Practice of Pediatric Infectious Diseases (Fifth Edition). Elsevier.
3. Woolhouse M, Scott F, Hudson Z, Howey R, Chase-Topping M. 2012. Human viruses: discovery and emergence. *Philosophical transactions of the Royal Society of London Series B, Biological sciences* **367**:2864.
4. Lynch JP, 3rd, Kajon AE. 2016. Adenovirus: Epidemiology, Global Spread of Novel Serotypes, and Advances in Treatment and Prevention. *Semin Respir Crit Care Med* **37**:586.
5. Rockx B, De Wit M, Vennema H, Vinjé J, De Bruin E, *et al.* 2002. Natural history of human calicivirus infection: a prospective cohort study. *Clin Infect Dis* **35**:246.
6. Bray M. 2005. Pathogenesis of viral hemorrhagic fever. *Curr Opin Immunol* **17**:399.
7. Kennedy PGE. 2004. Viral encephalitis: causes, differential diagnosis, and management. *J Neurol Neurosurg Psychiatry* **75**:i10.
8. Ianevski A, Zusinaite E, Kuivanen S, Strand M, Lysvand H, *et al.* 2018. Novel activities of safe-in-human broad-spectrum antiviral agents. *Antiviral Res* **154**:174.
9. Debing Y, Neyts J, Delang L. 2015. The future of antivirals: broad-spectrum inhibitors. *Curr Opin Infect Dis* **28**:596.
10. De Clercq E, Li G. 2016. Approved Antiviral Drugs over the Past 50 Years. *Clin Microbiol Rev* **29**:695.
11. Tompa DR, Immanuel A, Srikanth S, Kadirvel S. 2021. Trends and strategies to combat viral infections: A review on FDA approved antiviral drugs. *Int J Biol Macromol* **172**:524.
12. U.S. Food and Drug Administration. 2021. Coronavirus (COVID-19) update: FDA authorizes first oral antiviral for treatment of COVID-19. 22 Dec 2021.
13. U.S. Food and Drug Administration. 2021. FDA Approves First Treatment for COVID-19. 22 Oct 2021.
14. Laureti M, Narayanan D, Rodriguez-Andres J, Fazakerley JK, Kedzierski L. 2018. Flavivirus receptors: Diversity, identity, and cell entry. *Front Immunol* **9**.
15. Chen L, Zhang Q, Yu DM, Wan MB, Zhang XX. 2009. Early changes of hepatitis B virus quasispecies during lamivudine treatment and the correlation with antiviral efficacy. *J Hepatol* **50**:895.
16. Raj VS, Hundie GB, Schürch AC, Smits SL, Pas SD, *et al.* 2017. Identification of HCV Resistant Variants against Direct Acting Antivirals in Plasma and Liver of Treatment Naïve Patients. *Sci Rep* **7**:4688.
17. Hirsch MS, Günthard HF, Schapiro JM, Vézinet FB, Clotet B, *et al.* 2008. Antiretroviral Drug Resistance Testing in Adult HIV-1 Infection: 2008 Recommendations of an International AIDS Society-USA Panel. *Clin Infect Dis* **47**:266.
18. Nassal M. 2015. HBV cccDNA: viral persistence reservoir and key obstacle for a cure of chronic hepatitis B. *Gut* **64**:1972.
19. Ndung'u T, McCune JM, Deeks SG. 2019. Why and where an HIV cure is needed and how it might be achieved. *Nature* **576**:397.
20. Kilpatrick AM, Randolph SE. 2012. Drivers, dynamics, and control of emerging vector-borne zoonotic diseases. *Lancet* **380**:1946.
21. Koh BK, Ng LC, Kita Y, Tang CS, Ang LW, *et al.* 2008. The 2005 dengue epidemic in Singapore: epidemiology, prevention and control. *Ann Acad Med Singap* **37**:538.

22. Bharaj P, Chahar HS, Pandey A, Diddi K, Dar L, *et al.* 2008. Concurrent infections by all four dengue virus serotypes during an outbreak of dengue in 2006 in Delhi, India. *Virology* **5**:1.
23. Bhatt S, Gething PW, Brady OJ, Messina JP, Farlow AW, *et al.* 2013. The global distribution and burden of dengue. *Nature* **496**:504.
24. Stanaway JD, Shepard DS, Undurraga EA, Halasa YA, Coffeng LE, *et al.* 2016. The global burden of dengue: an analysis from the Global Burden of Disease Study 2013. *Lancet Infect Dis* **16**:712.
25. Campbell GL, Hills SL, Fischer M, Jacobson JA, Hoke CH, *et al.* 2011. Estimated global incidence of Japanese encephalitis: a systematic review. *Bull World Health Organ* **89**:766.
26. World Health Organisation. 2022. Japanese encephalitis - Australia. 28 Apr 2022.
27. Fischer M, Hills S, Staples E, Johnson B, Yaich M, *et al.* 2008. Japanese encephalitis prevention and control: advances, challenges, and new initiatives. In (ed), *Emerging infections*.
28. Gaythorpe KAM, Hamlet A, Jean K, Garkauskas Ramos D, Cibrelus L, *et al.* 2021. The global burden of yellow fever. *eLife* **10**:e64670.
29. Labeaud AD, Bashir F, King CH. 2011. Measuring the burden of arboviral diseases: the spectrum of morbidity and mortality from four prevalent infections. *Popul Health Metr* **9**:1.
30. Bakonyi T, Haussig JM. 2020. West Nile virus keeps on moving up in Europe. *Euro Surveill* **25**:2001938.
31. Hadfield J, Brito AF, Swetnam DM, Vogels CBF, Tokarz RE, *et al.* 2019. Twenty years of West Nile virus spread and evolution in the Americas visualized by Nextstrain. *PLoS Pathog* **15**:e1008042.
32. World Health Organisation. 2015. Summary of probable SARS cases with onset of illness from 1 November 2002 to 31 July 2003. 24 Jul 2015.
33. Garten RJ, Davis CT, Russell CA, Shu B, Lindstrom S, *et al.* 2009. Antigenic and Genetic Characteristics of Swine-Origin 2009 A(H1N1) Influenza Viruses Circulating in Humans. *Science* **325**:197.
34. Dawood FS, Iuliano AD, Reed C, Meltzer MI, Shay DK, *et al.* 2012. Estimated global mortality associated with the first 12 months of 2009 pandemic influenza A H1N1 virus circulation: a modelling study. *Lancet Infect Dis* **12**:687.
35. Zaki AM, van Boheemen S, Bestebroer TM, Osterhaus ADME, Fouchier RAM. 2012. Isolation of a Novel Coronavirus from a Man with Pneumonia in Saudi Arabia. *N Engl J Med* **367**:1814.
36. Azhar EI, El-Kafrawy SA, Farraj SA, Hassan AM, Al-Saeed MS, *et al.* 2014. Evidence for camel-to-human transmission of MERS coronavirus. *N Engl J Med* **370**:2499.
37. Reusken CB, Haagmans BL, Müller MA, Gutierrez C, Godeke GJ, *et al.* 2013. Middle East respiratory syndrome coronavirus neutralising serum antibodies in dromedary camels: a comparative serological study. *Lancet Infect Dis* **13**:859.
38. World Health Organisation. 2021. MERS situation update. World Health Organisation, Geneva.
39. Briand S, Bertherat E, Cox P, Formenty P, Kieny MP, *et al.* 2014. The International Ebola Emergency. *N Engl J Med* **371**:1180.
40. World Health Organisation. 2021. Ebola virus disease. World Health Organisation, Geneva. 23 Feb 2021.
41. Peiter PC, Pereira RdS, Nunes Moreira MC, Nascimento M, Tavares MdFL, *et al.* 2020. Zika epidemic and microcephaly in Brazil: Challenges for access to health care and promotion in three epidemic areas. *PLoS One* **15**:e0235010.
42. Zhu N, Zhang D, Wang W, Li X, Yang B, *et al.* 2020. A Novel Coronavirus from Patients with Pneumonia in China, 2019. *N Engl J Med* **382**:727.

43. World Health Organisation. 2020. WHO media briefing on COVID-19. 11 Mar 2020.
44. World Health Organisation. 2022. WHO Coronavirus (COVID-19) Dashboard, on World Health Organisation. <https://covid19.who.int/> Accessed 07/06/2021.
45. Isaacs A, Lindenmann J, Andrewes CH. 1957. Virus interference. I. The interferon. *Proceedings of the Royal Society of London Series B - Biological Sciences* **147**:258.
46. Prusoff WH. 1959. Synthesis and biological activities of iododeoxyuridine, an analog of thymidine. *Biochim Biophys Acta* **32**:295.
47. Herrmann EC. 1961. Plaque Inhibition Test for Detection of Specific Inhibitors of DNA Containing Viruses. *Proc Soc Exp Biol Med* **107**:142.
48. Prusoff WH. 1967. Recent advances in chemotherapy of viral diseases. *Pharmacol Rev* **19**:209.
49. Witkowski J, Robins RK, Sidwell RW, Simon LN. 1972. Design, synthesis, and broad spectrum antiviral activity of 1- β -D-ribofuranosyl-1, 2, 4-triazole-3-carboxamide and related nucleosides. *J Med Chem* **15**:1150.
50. Elion GB, Furman PA, Fyfe JA, Miranda Pd, Beauchamp L, *et al.* 1977. Selectivity of action of an antiherpetic agent, 9-(2-hydroxyethoxymethyl)guanine. *Proceedings of the National Academy of Sciences* **74**:5716.
51. Nagata S, Taira H, Hall A, Johnsrud L, Streuli M, *et al.* 1980. Synthesis in *E. coli* of a polypeptide with human leukocyte interferon activity. *Nature* **284**:316.
52. Colla L, De Clercq E, Busson R, Vanderhaeghe H. 1983. Synthesis and antiviral activity of water-soluble esters of acyclovir [9-[(2-hydroxyethoxy)methyl]guanine]. *J Med Chem* **26**:602.
53. Brook I. 1987. Approval of Zidovudine (AZT) for Acquired Immunodeficiency Syndrome: A Challenge to the Medical and Pharmaceutical Communities. *JAMA* **258**:1517.
54. Vere Hodge RA, Sutton D, Boyd MR, Harnden MR, Jarvest RL. 1989. Selection of an oral prodrug (BRL 42810; famciclovir) for the antiherpesvirus agent BRL 39123 [9-(4-hydroxy-3-hydroxymethylbut-1-yl)guanine; penciclovir]. *Antimicrob Agents Chemother* **33**:1765.
55. Roberts NA, Martin JA, Kinchington D, Broadhurst AV, Craig JC, *et al.* 1990. Rational design of peptide-based HIV proteinase inhibitors. *Science* **248**:358.
56. Larder BA, Kemp SD, Harrigan PR. 1995. Potential mechanism for sustained antiretroviral efficacy of AZT-3TC combination therapy. *Science* **269**:696.
57. Traynor K. 2011. Two drugs approved for chronic hepatitis C infection. *Am J Health Syst Pharm* **68**:1176.
58. U.S. Food and Drug Administration. 2013. FDA approves Sovaldi for chronic hepatitis C. 6 Dec 2013.
59. Ji X, Li Z. 2020. Medicinal chemistry strategies toward host targeting antiviral agents. *Med Res Rev* **40**:1519.
60. Sayana S, Khanlou H. 2009. Maraviroc: a new CCR5 antagonist. *Expert Rev Anti Infect Ther* **7**:9.
61. Edwards L, Ferenczy A, Eron L, Baker D, Owens ML, *et al.* 1998. Self-administered Topical 5% Imiquimod Cream for External Anogenital Warts. *Arch Dermatol* **134**:25.
62. Paeshuyse J, Dallmeier K, Neyts J. 2011. Ribavirin for the treatment of chronic hepatitis C virus infection: a review of the proposed mechanisms of action. *Curr Opin Virol* **1**:590.
63. Negrodo A, de la Calle-Prieto F, Palencia-Herrejón E, Mora-Rillo M, Astray-Mochales J, *et al.* 2017. Autochthonous Crimean–Congo Hemorrhagic Fever in Spain. *N Engl J Med* **377**:154.
64. Espy N, Pérez-Sautu U, Ramírez de Arellano E, Negrodo A, Wiley MR, *et al.* 2018. Ribavirin Had Demonstrable Effects on the Crimean-Congo Hemorrhagic Fever Virus (CCHFV) Population and Load in a Patient With CCHF Infection. *J Infect Dis* **217**:1952.

65. Eberhardt KA, Mischlinger J, Jordan S, Groger M, Günther S, *et al.* 2019. Ribavirin for the treatment of Lassa fever: A systematic review and meta-analysis. *Int J Infect Dis* **87**:15.
66. Rusnak JM, Byrne WR, Chung KN, Gibbs PH, Kim TT, *et al.* 2009. Experience with intravenous ribavirin in the treatment of hemorrhagic fever with renal syndrome in Korea. *Antiviral Res* **81**:68.
67. Huggins JW, Hsiang CM, Cosgriff TM, Guang MY, Smith JI, *et al.* 1991. Prospective, Double-Blind, Concurrent, Placebo-Controlled Clinical Trial of Intravenous Ribavirin Therapy of Hemorrhagic Fever with Renal Syndrome. *J Infect Dis* **164**:1119.
68. Hung IFN, Lung KC, Tso EYK, Liu R, Chung TWH, *et al.* 2020. Triple combination of interferon beta-1b, lopinavir-ritonavir, and ribavirin in the treatment of patients admitted to hospital with COVID-19: an open-label, randomised, phase 2 trial. *Lancet* **395**:1695.
69. Schor S, Einav S. 2017. Repurposing of Kinase Inhibitors as Broad-Spectrum Antiviral Drugs. *DNA Cell Biol* **37**:63.
70. Tian S, Huang Q, Fang Y, Wu J. 2011. FurinDB: A Database of 20-Residue Furin Cleavage Site Motifs, Substrates and Their Associated Drugs. *Int J Mol Sci* **12**:1060.
71. Abe M, Tahara M, Sakai K, Yamaguchi H, Kanou K, *et al.* 2013. TMPRSS2 Is an Activating Protease for Respiratory Parainfluenza Viruses. *J Virol* **87**:11930.
72. Sakai K, Ami Y, Tahara M, Kubota T, Anraku M, *et al.* 2014. The Host Protease TMPRSS2 Plays a Major Role in *In Vivo* Replication of Emerging H7N9 and Seasonal Influenza Viruses. *J Virol* **88**:5608.
73. Hoffmann M, Kleine-Weber H, Schroeder S, Krüger N, Herrler T, *et al.* 2020. SARS-CoV-2 Cell Entry Depends on ACE2 and TMPRSS2 and Is Blocked by a Clinically Proven Protease Inhibitor. *Cell* **181**:271.
74. Shirato K, Kawase M, Matsuyama S. 2013. Middle East respiratory syndrome coronavirus infection mediated by the transmembrane serine protease TMPRSS2. *J Virol* **87**:12552.
75. Bertram S, Dijkman R, Habjan M, Heurich A, Gierer S, *et al.* 2013. TMPRSS2 activates the human coronavirus 229E for cathepsin-independent host cell entry and is expressed in viral target cells in the respiratory epithelium. *J Virol* **87**:6150.
76. Puyang X, Poulin DL, Mathy JE, Anderson LJ, Ma S, *et al.* 2010. Mechanism of Resistance of Hepatitis C Virus Replicons to Structurally Distinct Cyclophilin Inhibitors. *Antimicrob Agents Chemother* **54**:1981.
77. Lanford RE, Hildebrandt-Eriksen ES, Petri A, Persson R, Lindow M, *et al.* 2010. Therapeutic Silencing of MicroRNA-122 in Primates with Chronic Hepatitis C Virus Infection. *Science* **327**:198.
78. King JK, Yeh SH, Lin MW, Liu CJ, Lai MY, *et al.* 2002. Genetic polymorphisms in interferon pathway and response to interferon treatment in hepatitis B patients: A pilot study. *Hepatology* **36**:1416.
79. Kim K, Johnson JA, Derendorf H. 2004. Differences in Drug Pharmacokinetics Between East Asians and Caucasians and the Role of Genetic Polymorphisms. *The Journal of Clinical Pharmacology* **44**:1083.
80. Neveu G, Ziv-Av A, Barouch-Bentov R, Berkerman E, Mulholland J, *et al.* 2015. AP-2-associated protein kinase 1 and cyclin G-associated kinase regulate hepatitis C virus entry and are potential drug targets. *J Virol* **89**:4387.
81. Clark Margaret J, Miduturu C, Schmidt Aaron G, Zhu X, Pitts Jared D, *et al.* 2016. GNF-2 Inhibits Dengue Virus by Targeting Abl Kinases and the Viral E Protein. *Cell Chemical Biology* **23**:443.
82. Langhammer S, Koban R, Yue C, Ellerbrok H. 2011. Inhibition of poxvirus spreading by the anti-tumor drug Gefitinib (Iressa™). *Antiviral Res* **89**:64.

83. Schleiss M, Eickhoff J, Auerochs S, Leis M, Abele S, *et al.* 2008. Protein kinase inhibitors of the quinazoline class exert anti-cytomegaloviral activity *in vitro* and *in vivo*. *Antiviral Res* **79**:49.
84. Perwitasari O, Yan X, O'Donnell J, Johnson S, Tripp RA. 2015. Repurposing Kinase Inhibitors as Antiviral Agents to Control Influenza A Virus Replication. *Assay Drug Dev Technol* **13**:638.
85. Coleman CM, Sisk JM, Mingo RM, Nelson EA, White JM, *et al.* 2016. Abelson Kinase Inhibitors Are Potent Inhibitors of Severe Acute Respiratory Syndrome Coronavirus and Middle East Respiratory Syndrome Coronavirus Fusion. *J Virol* **90**:8924.
86. Nelson EA, Dyall J, Hoenen T, Barnes AB, Zhou H, *et al.* 2017. The phosphatidylinositol-3-phosphate 5-kinase inhibitor apilimod blocks filoviral entry and infection. *PLoS Negl Trop Dis* **11**:e0005540.
87. Younossi ZM, Stepanova M, Henry L, Nader F, Younossi Y, *et al.* 2016. Adherence to treatment of chronic hepatitis C: from interferon containing regimens to interferon and ribavirin free regimens. *Medicine* **95**:e4151.
88. Read P, Lothian R, Chronister K, Gilliver R, Kearley J, *et al.* 2017. Delivering direct acting antiviral therapy for hepatitis C to highly marginalised and current drug injecting populations in a targeted primary health care setting. *International Journal of Drug Policy* **47**:209.
89. Hay AJ, Wolstenholme AJ, Skehel JJ, Smith MH. 1985. The molecular basis of the specific anti-influenza action of amantadine. *The EMBO Journal* **4**:3021.
90. Birnkrant D, Cox E. 2009. The Emergency Use Authorization of Peramivir for Treatment of 2009 H1N1 Influenza. *N Engl J Med* **361**:2204.
91. Hayden FG, Osterhaus ADME, Treanor JJ, Fleming DM, Aoki FY, *et al.* 1997. Efficacy and Safety of the Neuraminidase Inhibitor Zanamivir in the Treatment of Influenzavirus Infections. *N Engl J Med* **337**:874.
92. Kim ES. 2018. Letermovir: First Global Approval. *Drugs* **78**:147.
93. Kawashima M, Nemoto O, Honda M, Watanabe D, Nakayama J, *et al.* 2017. Amenamevir, a novel helicase–primase inhibitor, for treatment of herpes zoster: A randomized, double-blind, valaciclovir-controlled phase 3 study. *The Journal of Dermatology* **44**:1219.
94. Grinsztejn B, Nguyen BY, Katlama C, Gatell JM, Lazzarin A, *et al.* 2007. Safety and efficacy of the HIV-1 integrase inhibitor raltegravir (MK-0518) in treatment-experienced patients with multidrug-resistant virus: a phase II randomised controlled trial. *Lancet* **369**:1261.
95. Belema M, Meanwell NA. 2014. Discovery of Daclatasvir, a Pan-Genotypic Hepatitis C Virus NS5A Replication Complex Inhibitor with Potent Clinical Effect. *J Med Chem* **57**:5057.
96. Ault A. 1998. FDA approves two new hepatitis therapies. *Lancet* **352**:1996.
97. Biron Karen K, Harvey Robert J, Chamberlain Stanley C, Good Steven S, Smith Albert A, *et al.* 2002. Potent and Selective Inhibition of Human Cytomegalovirus Replication by 1263W94, a Benzimidazole l-Riboside with a Unique Mode of Action. *Antimicrob Agents Chemother* **46**:2365.
98. James SH, Hartline CB, Harden EA, Driebe EM, Schupp JM, *et al.* 2011. Cyclopropavir Inhibits the Normal Function of the Human Cytomegalovirus UL97 Kinase. *Antimicrob Agents Chemother* **55**:4682.
99. Lejal N, Tarus B, Bouguyon E, Chenavas S, Bertho N, *et al.* 2013. Structure-Based Discovery of the Novel Antiviral Properties of Naproxen against the Nucleoprotein of Influenza A Virus. *Antimicrob Agents Chemother* **57**:2231.
100. Rhodin MHJ, McAllister NV, Castillo J, Noton SL, Fearn R, *et al.* 2021. EDP-938, a novel nucleoprotein inhibitor of respiratory syncytial virus, demonstrates potent antiviral activities *in vitro* and in a non-human primate model. *PLoS Pathog* **17**:e1009428.

101. Aceti DJ, Ahmed H, Westler WM, Wu C, Dashti H, *et al.* 2020. Fragment screening targeting Ebola virus nucleoprotein C-terminal domain identifies lead candidates. *Antiviral Res* **180**:104822.
102. Rebensburg S, Helfer M, Schneider M, Koppensteiner H, Eberle J, *et al.* 2016. Potent *in vitro* antiviral activity of *Cistus incanus* extract against HIV and Filoviruses targets viral envelope proteins. *Sci Rep* **6**:20394.
103. de Wispelaere M, Lian W, Potisopon S, Li PC, Jang J, *et al.* 2018. Inhibition of Flaviviruses by Targeting a Conserved Pocket on the Viral Envelope Protein. *Cell Chemical Biology* **25**:1006.
104. Ho YJ, Wang YM, Lu JW, Wu TY, Lin LI, *et al.* 2015. Suramin Inhibits Chikungunya Virus Entry and Transmission. *PLoS One* **10**:e0133511.
105. Chung KY, Dong H, Chao AT, Shi P-Y, Lescar J, *et al.* 2010. Higher catalytic efficiency of N-7-methylation is responsible for processive N-7 and 2'-O methyltransferase activity in dengue virus. *Virology* **402**:52.
106. Benmansour F, Trist I, Coutard B, Decroly E, Querat G, *et al.* 2017. Discovery of novel dengue virus NS5 methyltransferase non-nucleoside inhibitors by fragment-based drug design. *Eur J Med Chem* **125**:865.
107. Basu S, Mak T, Ulferts R, Wu M, Deegan T, *et al.* 2021. Identifying SARS-CoV-2 antiviral compounds by screening for small molecule inhibitors of Nsp14 RNA cap methyltransferase. *Biochem J* **478**:2481.
108. Brown CS, Lee MS, Leung DW, Wang T, Xu W, *et al.* 2014. *In Silico* Derived Small Molecules Bind the Filovirus VP35 Protein and Inhibit Its Polymerase Cofactor Activity. *J Mol Biol* **426**:2045.
109. Yang CC, Hsieh YC, Lee SJ, Wu SH, Liao CL, *et al.* 2011. Novel Dengue Virus-Specific NS2B/NS3 Protease Inhibitor, BP2109, Discovered by a High-Throughput Screening Assay. *Antimicrob Agents Chemother* **55**:229.
110. Thompson AJ. 2016. Australian recommendations for the management of hepatitis C virus infection: a consensus statement. *Med J Aust* **204**:268.
111. Razavi H, Sanchez Gonzalez Y, Yuen C, Cornberg M. 2020. Global timing of hepatitis C virus elimination in high-income countries. *Liver Int* **40**:522.
112. World Health Organisation. 2013. Global update on HIV treatment 2013: results, impact and opportunities. World Health Organisation, Geneva.
113. Saag MS, Gandhi RT, Hoy JF, Landovitz RJ, Thompson MA, *et al.* 2020. Antiretroviral Drugs for Treatment and Prevention of HIV Infection in Adults: 2020 Recommendations of the International Antiviral Society–USA Panel. *JAMA* **324**:1651.
114. Tarantino D, Pezzullo M, Mastrangelo E, Croci R, Rohayem J, *et al.* 2014. Naphthalene-sulfonate inhibitors of human norovirus RNA-dependent RNA-polymerase. *Antiviral Res* **102**:23.
115. Crotty S, Cameron CE, Andino R. 2001. RNA virus error catastrophe: direct molecular test by using ribavirin. *Proceedings of the National Academy of Sciences* **98**:6895.
116. Loeb LA, Essigmann JM, Kazazi F, Zhang J, Rose KD, *et al.* 1999. Lethal mutagenesis of HIV with mutagenic nucleoside analogs. *Proceedings of the National Academy of Sciences* **96**:1492.
117. Warren TK, Wells J, Panchal RG, Stuthman KS, Garza NL, *et al.* 2014. Protection against filovirus diseases by a novel broad-spectrum nucleoside analogue BCX4430. *Nature* **508**:402.
118. Furuta Y, Takahashi K, Shiraki K, Sakamoto K, Smee DF, *et al.* 2009. T-705 (favipiravir) and related compounds: Novel broad-spectrum inhibitors of RNA viral infections. *Antiviral Res* **82**:95.
119. Yin Z, Chen YL, Schul W, Wang QY, Gu F, *et al.* 2009. An adenosine nucleoside inhibitor of dengue virus. *Proceedings of the National Academy of Sciences* **106**:20435.

120. Enosi Tuipulotu D, Fumian TM, Netzler NE, Mackenzie JM, White PA. 2019. The Adenosine Analogue NITD008 has Potent Antiviral Activity against Human and Animal Caliciviruses. *Viruses* **11**:496.
121. Ohta Y, Shinkai I. 1997. New drugs—reports of new drugs recently approved by the FDA lamivudine. *Bioorg Med Chem* **5**:639.
122. Lai CL, Chien RN, Leung NWY, Chang TT, Guan R, *et al.* 1998. A One-Year Trial of Lamivudine for Chronic Hepatitis B. *N Engl J Med* **339**:61.
123. Bai C-Q, Mu J-S, Kargbo D, Song Y-B, Niu W-K, *et al.* 2016. Clinical and Virological Characteristics of Ebola Virus Disease Patients Treated With Favipiravir (T-705)—Sierra Leone, 2014. *Clin Infect Dis* **63**:1288.
124. Sissoko D, Laouenan C, Folkesson E, M'Lebing A-B, Beavogui A-H, *et al.* 2016. Experimental Treatment with Favipiravir for Ebola Virus Disease (the JIKI Trial): A Historically Controlled, Single-Arm Proof-of-Concept Trial in Guinea. *PLoS Med* **13**:e1001967.
125. Raabe VN, Kann G, Ribner BS, Morales A, Varkey JB, *et al.* 2017. Favipiravir and Ribavirin Treatment of Epidemiologically Linked Cases of Lassa Fever. *Clin Infect Dis* **65**:855.
126. Yoon JJ, Toots M, Lee S, Lee ME, Ludeke B, *et al.* 2018. Orally Efficacious Broad-Spectrum Ribonucleoside Analog Inhibitor of Influenza and Respiratory Syncytial Viruses. *Antimicrob Agents Chemother* **62**:e00766.
127. Mulangu S, Dodd LE, Davey RT, Tshiani Mbaya O, Proschan M, *et al.* 2019. A randomized, controlled trial of Ebola virus disease therapeutics. *N Engl J Med* **381**:2293.
128. U.S. Food and Drug Administration. 2021. Coronavirus (COVID-19) Update: FDA Authorizes Additional Oral Antiviral for Treatment of COVID-19 in Certain Adults. 23 Dec 2021.
129. Johnson AA, Ray AS, Hanes J, Suo Z, Colacino JM, *et al.* 2001. Toxicity of Antiviral Nucleoside Analogs and the Human Mitochondrial DNA Polymerase. *J Biol Chem* **276**:40847.
130. Arnold JJ, Sharma SD, Feng JY, Ray AS, Smidansky ED, *et al.* 2012. Sensitivity of Mitochondrial Transcription and Resistance of RNA Polymerase II Dependent Nuclear Transcription to Antiviral Ribonucleosides. *PLoS Pathog* **8**:e1003030.
131. Feng Joy Y, Xu Y, Barauskas O, Perry Jason K, Ahmadyar S, *et al.* 2016. Role of Mitochondrial RNA Polymerase in the Toxicity of Nucleotide Inhibitors of Hepatitis C Virus. *Antimicrob Agents Chemother* **60**:806.
132. Witvrouw M, Pannecouque C, Switzer WM, Folks TM, Clercq ED, *et al.* 2004. Susceptibility of HIV-2, Siv and Shiv to Various Anti-HIV-1 Compounds: Implications for Treatment and Postexposure Prophylaxis. *Antivir Ther* **9**:57.
133. Ren J, Bird LE, Chamberlain PP, Stewart-Jones GB, Stuart DI, *et al.* 2002. Structure of HIV-2 reverse transcriptase at 2.35-Å resolution and the mechanism of resistance to non-nucleoside inhibitors. *Proceedings of the National Academy of Sciences* **99**:14410.
134. Eltahla AA, Luciani F, White PA, Lloyd AR, Bull RA. 2015. Inhibitors of the Hepatitis C Virus Polymerase; Mode of Action and Resistance. *Viruses* **7**:5206.
135. Mittal L, Kumari A, Suri C, Bhattacharya S, Asthana S. 2020. Insights into structural dynamics of allosteric binding sites in HCV RNA-dependent RNA polymerase. *J Biomol Struct Dyn* **38**:1612.
136. Hirashima S, Suzuki T, Ishida T, Noji S, Yata S, *et al.* 2006. Benzimidazole Derivatives Bearing Substituted Biphenyls as Hepatitis C Virus NS5B RNA-Dependent RNA Polymerase Inhibitors: Structure–Activity Relationship Studies and Identification of a Potent and Highly Selective Inhibitor JTK-109. *J Med Chem* **49**:4721.

137. Zhao F, Liu N, Zhan P, Jiang X, Liu X. 2015. Discovery of HCV NS5B thumb site I inhibitors: Core-refining from benzimidazole to indole scaffold. *Eur J Med Chem* **94**:218.
138. Eltahla Auda A, Tay E, Douglas Mark W, White Peter A. 2014. Cross-Genotypic Examination of Hepatitis C Virus Polymerase Inhibitors Reveals a Novel Mechanism of Action for Thumb Binders. *Antimicrob Agents Chemother* **58**:7215.
139. Herlihy Kileen J, Graham Joanne P, Kumpf R, Patick Amy K, Duggal R, *et al.* 2008. Development of Intergenotypic Chimeric Replicons To Determine the Broad-Spectrum Antiviral Activities of Hepatitis C Virus Polymerase Inhibitors. *Antimicrob Agents Chemother* **52**:3523.
140. Mohd Hanafiah K, Groeger J, Flaxman AD, Wiersma ST. 2013. Global epidemiology of hepatitis C virus infection: New estimates of age-specific antibody to HCV seroprevalence. *Hepatology* **57**:1333.
141. Lohmann V, Körner F, Koch J, Herian U, Theilmann L, *et al.* 1999. Replication of subgenomic hepatitis C virus RNAs in a hepatoma cell line. *Science* **285**:110.
142. Xiao D, Dai X, Liu H, He S, Shi ZC, *et al.* 2020. Multi-step parallel synthesis enabled optimization of benzofuran derivatives as pan-genotypic non-nucleoside inhibitors of HCV NS5B. *Bioorg Med Chem Lett* **30**:127004.
143. Zhong M, Peng E, Huang N, Huang Q, Huq A, *et al.* 2018. Discovery of novel potent HCV NS5B polymerase non-nucleoside inhibitors bearing a fused benzofuran scaffold. *Bioorg Med Chem Lett* **28**:963.
144. Chen KX, Lesburg CA, Vibulbhan B, Yang W, Chan TY, *et al.* 2012. A Novel Class of Highly Potent Irreversible Hepatitis C Virus NS5B Polymerase Inhibitors. *J Med Chem* **55**:2089.
145. Netzler Natalie E, Enosi Tuipulotu D, Vasudevan Subhash G, Mackenzie Jason M, White Peter A. 2019. Antiviral candidates for treating hepatitis E virus infection. *Antimicrob Agents Chemother* **63**:e00003.
146. van der Linden L, Vives-Adrián L, Selisko B, Ferrer-Orta C, Liu X, *et al.* 2015. The RNA Template Channel of the RNA-Dependent RNA Polymerase as a Target for Development of Antiviral Therapy of Multiple Genera within a Virus Family. *PLoS Pathog* **11**:e1004733.
147. Netzler NE, Tuipulotu DE, Eltahla AA, Lun JH, Ferla S, *et al.* 2017. Broad-spectrum non-nucleoside inhibitors for caliciviruses. *Antiviral Res* **146**:65.
148. Macarron R, Banks MN, Bojanic D, Burns DJ, Cirovic DA, *et al.* 2011. Impact of high-throughput screening in biomedical research. *Nat Rev Drug Discov* **10**:188.
149. Böhm HJ, Flohr A, Stahl M. 2004. Scaffold hopping. *Drug Discov Today: Technol* **1**:217.
150. Ripphausen P, Nisius B, Bajorath J. 2011. State-of-the-art in ligand-based virtual screening. *Drug Discov Today* **16**:372.
151. Nosengo N. 2016. Can you teach old drugs new tricks? *Nature* **534**:314.
152. Sabe VT, Ntombela T, Jhamba LA, Maguire GEM, Govender T, *et al.* 2021. Current trends in computer aided drug design and a highlight of drugs discovered via computational techniques: A review. *Eur J Med Chem* **224**:113705.
153. Macalino SJY, Gosu V, Hong S, Choi S. 2015. Role of computer-aided drug design in modern drug discovery. *Arch Pharm Res* **38**:1686.
154. Menéndez-Arias L, Gago F. 2013. Antiviral Agents: Structural Basis of Action and Rational Design, p 599-630. *In* Mateu MG (ed), *Structure and Physics of Viruses: An Integrated Textbook*. Springer Netherlands, Dordrecht.
155. Yang SY. 2010. Pharmacophore modeling and applications in drug discovery: challenges and recent advances. *Drug Discov Today* **15**:444.
156. Tran-Nguyen VK, Da Silva F, Bret G, Rognan D. 2019. All in One: Cavity Detection, Druggability Estimate, Cavity-Based Pharmacophore Perception, and Virtual Screening. *J Chem Inf Model* **59**:573.

157. Plewczynski D, Łaźniewski M, Augustyniak R, Ginalski K. 2011. Can we trust docking results? Evaluation of seven commonly used programs on PDBbind database. *J Comput Chem* **32**:742.
158. Genheden S, Ryde U. 2015. The MM/PBSA and MM/GBSA methods to estimate ligand-binding affinities. *Expert Opinion on Drug Discovery* **10**:449.
159. Sherman W, Day T, Jacobson MP, Friesner RA, Farid R. 2006. Novel Procedure for Modeling Ligand/Receptor Induced Fit Effects. *J Med Chem* **49**:534.
160. Li Z, Lazaridis T. 2007. Water at biomolecular binding interfaces. *Phys Chem Chem Phys* **9**:573.
161. Vos T, Lim SS, Abbafati C, Abbas KM, Abbasi M, *et al.* 2020. Global burden of 369 diseases and injuries in 204 countries and territories, 1990-2019: a systematic analysis for the Global Burden of Disease Study 2019. *Lancet* **396**:1204.
162. Papadopoulos T, Klamer S, Jacquinet S, Catry B, Litzroth A, *et al.* 2019. The health and economic impact of acute gastroenteritis in Belgium, 2010–2014. *Epidemiol Infect* **147**:e146.
163. Lakhan C, Badrie N, Ramsubhag A, Sundaraneedi K, Indar L. 2013. Burden and Impact of Acute Gastroenteritis and Foodborne Pathogens in Trinidad and Tobago. *J Health Popul Nutr* **31**:S30.
164. Barker SF, Zomer E, O’Toole J, Sinclair M, Gibney K, *et al.* 2018. Cost of gastroenteritis in Australia: A healthcare perspective. *PLoS One* **13**:e0195759.
165. Tate JE, Burton AH, Boschi-Pinto C, Parashar UD, for the World Health Organization–Coordinated Global Rotavirus Surveillance N, *et al.* 2016. Global, Regional, and National Estimates of Rotavirus Mortality in Children <5 Years of Age, 2000–2013. *Clin Infect Dis* **62**:S96.
166. de Zoysa I, Feachem RG. 1985. Interventions for the control of diarrhoeal diseases among young children: rotavirus and cholera immunization. *Bull World Health Organ* **63**:569.
167. Parashar UD, Hummelman EG, Bresee JS, Miller MA, Glass RI. 2003. Global illness and deaths caused by rotavirus disease in children. *Emerg Infect Dis* **9**:565.
168. Pediatric REC. 2006. The paediatric burden of rotavirus disease in Europe. *Epidemiol Infect* **134**:908.
169. Burnett E, Jonesteller CL, Tate JE, Yen C, Parashar UD. 2017. Global Impact of Rotavirus Vaccination on Childhood Hospitalizations and Mortality From Diarrhea. *J Infect Dis* **215**:1666.
170. Aliabadi N, Antoni S, Mwenda JM, Weldegebriel G, Biey JNM, *et al.* 2019. Global impact of rotavirus vaccine introduction on rotavirus hospitalisations among children under 5 years of age, 2008-2016: findings from the Global Rotavirus Surveillance Network. *Lancet Glob Health* **7**:e893.
171. Buttery JP, Lambert SB, Grimwood K, Nissen MD, Field EJ, *et al.* 2011. Reduction in Rotavirus-associated Acute Gastroenteritis Following Introduction of Rotavirus Vaccine Into Australia's National Childhood Vaccine Schedule. *Pediatr Infect Dis J* **30**.
172. Dey A, Wang H, Menzies R, Macartney K. 2012. Changes in hospitalisations for acute gastroenteritis in Australia after the national rotavirus vaccination program. *Med J Aust* **197**:453.
173. Marquis A, Koch J. 2020. Impact of Routine Rotavirus Vaccination in Germany: Evaluation Five Years After Its Introduction. *Pediatr Infect Dis J* **39**.
174. Sabbe M, Berger N, Blommaert A, Ogunjimi B, Grammens T, *et al.* 2016. Sustained low rotavirus activity and hospitalisation rates in the post-vaccination era in Belgium, 2007 to 2014. *Euro Surveill* **21**:30273.
175. Hassan F, Kanwar N, Harrison CJ, Halasa NB, Chappell JD, *et al.* 2018. Viral Etiology of Acute Gastroenteritis in <2-Year-Old US Children in the Post–Rotavirus Vaccine Era. *Journal of the Pediatric Infectious Diseases Society* **8**:414.

176. Kim A, Chang JY, Shin S, Yi H, Moon JS, *et al.* 2017. Epidemiology and Factors Related to Clinical Severity of Acute Gastroenteritis in Hospitalized Children after the Introduction of Rotavirus Vaccination. *jkms* **32**:465.
177. Platts-Mills JA, Babji S, Bodhidatta L, Gratz J, Haque R, *et al.* 2015. Pathogen-specific burdens of community diarrhoea in developing countries: a multisite birth cohort study (MAL-ED). *Lancet Glob health* **3**:e564.
178. Fletcher S, Van Hal S, Andresen D, McLaws M-L, Stark D, *et al.* 2013. Gastrointestinal pathogen distribution in symptomatic children in Sydney, Australia. *J Epidemiol Glob Health* **3**:11.
179. Bartsch SM, Lopman BA, Ozawa S, Hall AJ, Lee BY. 2016. Global Economic Burden of Norovirus Gastroenteritis. *PLoS One* **11**:e0151219.
180. Wang H, Naghavi M, Allen C, Barber RM, Bhutta ZA, *et al.* 2016. Global, regional, and national life expectancy, all-cause mortality, and cause-specific mortality for 249 causes of death, 1980–2015: a systematic analysis for the Global Burden of Disease Study 2015. *Lancet* **388**:1459.
181. Elyan D, Wasfy M, El Mohammady H, Hassan K, Monestersky J, *et al.* 2014. Non-bacterial etiologies of diarrheal diseases in Afghanistan. *Trans R Soc Trop Med Hyg* **108**:461.
182. Higgins G, Schepetiuk S, Ratcliff R. 2012. Aetiological importance of viruses causing acute gastroenteritis in humans. *Microbiol Aust* **33**:49.
183. Lanata CF, Fischer Walker CL, Olascoaga AC, Torres CX, Aryee MJ, *et al.* 2013. Global causes of diarrheal disease mortality in children <5 years of age: a systematic review. *PLoS One* **8**:e72788.
184. Fischer Walker CL, Sack D, Black RE. 2010. Etiology of diarrhea in older children, adolescents and adults: a systematic review. *PLoS Negl Trop Dis* **4**:e768.
185. Hessling M, Feiertag J, Hoenes K. 2017. Pathogens provoking most deaths worldwide: A review. *Heal Sci Commun Biosci Biotech Res Comm* **10**:1.
186. Ahmed SM, Hall AJ, Robinson AE, Verhoef L, Premkumar P, *et al.* 2014. Global prevalence of norovirus in cases of gastroenteritis: a systematic review and meta-analysis. *Lancet Infect Dis* **14**:725.
187. Ludwig A, Adams O, Laws HJ, Schrotten H, Tenenbaum T. 2008. Quantitative detection of norovirus excretion in pediatric patients with cancer and prolonged gastroenteritis and shedding of norovirus. *J Med Virol* **80**:1461.
188. Boillat Blanco N, Kuonen R, Bellini C, Manuel O, Estrade C, *et al.* 2011. Chronic norovirus gastroenteritis in a double hematopoietic stem cell and lung transplant recipient. *Transpl Infect Dis* **13**:213.
189. Roos-Weil D, Ambert-Balay K, Lanternier F, Mamzer-Bruneel MF, Nochy D, *et al.* 2011. Impact of Norovirus/Sapovirus-Related Diarrhea in Renal Transplant Recipients Hospitalized for Diarrhea. *Transplantation* **92**:61.
190. Zahorsky J. 1929. Hyperemesis hiemis or the winter vomiting disease. *Arch Pediatr* **46**:391.
191. Miller R, Raven M. 1936. Epidemic Nausea and Vomiting. *Br Med J* **1**:1242.
192. Gray JD. 1939. Epidemic Nausea and Vomiting. *Br Med J* **1**:209.
193. Reimann HA, Hodges JH, Price AH. 1945. Epidemic diarrhea, nausea and vomiting of unknown cause. *J Am Med Assoc* **127**:1.
194. Gordon I, Ingraham HS, Korn RF. 1947. Transmission of epidemic gastroenteritis to human volunteers by oral administration of fecal filtrates. *J Exp Med* **86**:409.
195. Adler JL, Zickl R. 1969. Winter Vomiting Disease. *J Infect Dis* **119**:668.
196. Kapikian AZ, Wyatt RG, Dolin R, Thornhill TS, Kalica AR, *et al.* 1972. Visualization by immune electron microscopy of a 27-nm particle associated with acute infectious nonbacterial gastroenteritis. *J Virol* **10**:1075.

197. Jiang X, Graham DY, Wang K, Estes MK. 1990. Norwalk virus genome cloning and characterization. *Science* **250**:1580.
198. Jiang X, Wang M, Wang K, Estes MK. 1993. Sequence and genomic organization of Norwalk virus. *Virology* **195**:51.
199. Mayo MA. 2002. A summary of taxonomic changes recently approved by ICTV. *Arch Virol* **147**:1655.
200. Prasad BV, Rothnagel R, Jiang X, Estes MK. 1994. Three-dimensional structure of baculovirus-expressed Norwalk virus capsids. *J Virol* **68**:5117.
201. Belliot G, Sosnovtsev SV, Mitra T, Hammer C, Garfield M, *et al.* 2003. *In vitro* proteolytic processing of the MD145 norovirus ORF1 nonstructural polyprotein yields stable precursors and products similar to those detected in calicivirus-infected cells. *J Virol* **77**:10957.
202. Hyde JL, Mackenzie JM. 2010. Subcellular localization of the MNV-1 ORF1 proteins and their potential roles in the formation of the MNV-1 replication complex. *Virology* **406**:138.
203. Robinson BA, Van Winkle JA, McCune BT, Peters AM, Nice TJ. 2019. Caspase-mediated cleavage of murine norovirus NS1/2 potentiates apoptosis and is required for persistent infection of intestinal epithelial cells. *PLoS Pathog* **15**:e1007940.
204. Lee S, Liu H, Wilen CB, Sychev ZE, Desai C, *et al.* 2019. A Secreted Viral Nonstructural Protein Determines Intestinal Norovirus Pathogenesis. *Cell Host Microbe* **25**:845.
205. Pfister T, Wimmer E. 2001. Polypeptide p41 of a Norwalk-Like Virus Is a Nucleic Acid-Independent Nucleoside Triphosphatase. *J Virol* **75**:1611.
206. Li TF, Hosmillo M, Schwanke H, Shu T, Wang Z, *et al.* 2018. Human norovirus NS3 has RNA helicase and chaperoning activities. *J Virol* **92**:e01606.
207. Sharp TM, Guix S, Katayama K, Crawford SE, Estes MK. 2010. Inhibition of Cellular Protein Secretion by Norwalk Virus Nonstructural Protein p22 Requires a Mimic of an Endoplasmic Reticulum Export Signal. *PLoS One* **5**:e13130.
208. Belliot G, Sosnovtsev SV, Chang K-O, McPhie P, Green KY. 2008. Nucleotidylylation of the VPg protein of a human norovirus by its proteinase-polymerase precursor protein. *Virology* **374**:33.
209. Daughenbaugh KF, Fraser CS, Hershey JWB, Hardy ME. 2003. The genome-linked protein VPg of the Norwalk virus binds eIF3, suggesting its role in translation initiation complex recruitment. *The EMBO Journal* **22**:2852.
210. Hosmillo M, Lu J, McAllaster MR, Eaglesham JB, Wang X, *et al.* 2019. Noroviruses subvert the core stress granule component G3BP1 to promote viral VPg-dependent translation. *eLife* **8**:e46681.
211. Jiang X, Wang M, Graham DY, Estes MK. 1992. Expression, self-assembly, and antigenicity of the Norwalk virus capsid protein. *J Virol* **66**:6527.
212. Prasad BVV, Hardy Michele E, Dokland T, Bella J, Rossmann Michael G, *et al.* 1999. X-ray Crystallographic Structure of the Norwalk Virus Capsid. *Science* **286**:287.
213. Bertolotti-Ciarlet A, White Laura J, Chen R, Prasad BVV, Estes Mary K. 2002. Structural Requirements for the Assembly of Norwalk Virus-Like Particles. *J Virol* **76**:4044.
214. Tohma K, Lepore Cara J, Gao Y, Ford-Siltz Lauren A, Parra Gabriel I, *et al.* 2019. Population Genomics of GII.4 Noroviruses Reveal Complex Diversification and New Antigenic Sites Involved in the Emergence of Pandemic Strains. *mBio* **10**:e02202.
215. Lindesmith LC, Donaldson EF, LoBue AD, Cannon JL, Zheng DP, *et al.* 2008. Mechanisms of GII.4 Norovirus Persistence in Human Populations. *PLoS Med* **5**:e31.
216. Lindesmith LC, Beltramello M, Donaldson EF, Corti D, Swanstrom J, *et al.* 2012. Immunogenetic Mechanisms Driving Norovirus GII.4 Antigenic Variation. *PLoS Pathog* **8**:e1002705.
217. Vongpunswad S, Venkataram Prasad BV, Estes Mary K. 2013. Norwalk Virus Minor Capsid Protein VP2 Associates within the VP1 Shell Domain. *J Virol* **87**:4818.

218. Choi JM, Hutson AM, Estes MK, Prasad BVV. 2008. Atomic resolution structural characterization of recognition of histo-blood group antigens by Norwalk virus. *Proc Natl Acad Sci U S A* **105**:9175.
219. Vinjé J, Estes MK, Esteves P, Green KY, Katayama K, *et al.* 2019. ICTV Virus Taxonomy Profile: *Caliciviridae*. *J Gen Virol* **100**:1469.
220. Pang XL, Honma S, Nakata S, Vesikari T. 2000. Human Caliciviruses in Acute Gastroenteritis of Young Children in the Community. *J Infect Dis* **181**:S288.
221. Zheng DP, Ando T, Fankhauser RL, Beard RS, Glass RI, *et al.* 2006. Norovirus classification and proposed strain nomenclature. *Virology* **346**:312.
222. Bull RA, Hansman GS, Clancy LE, Tanaka MM, Rawlinson WD, *et al.* 2005. Norovirus recombination in ORF1/ORF2 overlap. *Emerg Infect Dis* **11**:1079.
223. Bull RA, Tanaka MM, White PA. 2007. Norovirus recombination. *J Gen Virol* **88**:3347.
224. Chhabra P, de Graaf M, Parra GI, Chan MC-W, Green K, *et al.* 2019. Updated classification of norovirus genogroups and genotypes. *J Gen Virol* **100**:1393.
225. Kumar S, Stecher G, Li M, Knyaz C, Tamura K. 2018. MEGA X: Molecular evolutionary genetics analysis across computing platforms. *Mol Biol Evol* **35**:1547.
226. Le SQ, Gascuel O. 2008. An Improved General Amino Acid Replacement Matrix. *Mol Biol Evol* **25**:1307.
227. Kroneman A, Vega E, Vennema H, Vinjé J, White PA, *et al.* 2013. Proposal for a unified norovirus nomenclature and genotyping. *Arch Virol* **158**:2059.
228. Pang XL, Joensuu J, Vesikari T. 1999. Human calicivirus-associated sporadic gastroenteritis in Finnish children less than two years of age followed prospectively during a rotavirus vaccine trial. *Pediatr Infect Dis J* **18**:420.
229. Lun JH, Hewitt J, Yan GJH, Enosi Tuipulotu D, Rawlinson WD, *et al.* 2018. Recombinant GII.P16/GII.4 Sydney 2012 Was the Dominant Norovirus Identified in Australia and New Zealand in 2017. *Viruses* **10**:548.
230. Kroneman A, Verhoef L, Harris J, Vennema H, Duizer E, *et al.* 2008. Analysis of integrated virological and epidemiological reports of norovirus outbreaks collected within the foodborne viruses in Europe network from 1 July 2001 to 30 June 2006. *J Clin Microbiol* **46**:2959.
231. Siebenga JJ, Vennema H, Zheng DP, Vinjé J, Lee BE, *et al.* 2009. Norovirus Illness Is a Global Problem: Emergence and Spread of Norovirus GII.4 Variants, 2001–2007. *J Infect Dis* **200**:802.
232. Vega E, Barclay L, Gregoricus N, Shirley SH, Lee D, *et al.* 2014. Genotypic and Epidemiologic Trends of Norovirus Outbreaks in the United States, 2009 to 2013. *J Clin Microbiol* **52**:147.
233. Zheng DP, Widdowson MA, Glass RI, Vinjé J. 2010. Molecular Epidemiology of Genogroup II-Genotype 4 Noroviruses in the United States between 1994 and 2006. *J Clin Microbiol* **48**:168.
234. Teunis PFM, Moe CL, Liu P, E. Miller S, Lindesmith L, *et al.* 2008. Norwalk virus: How infectious is it? *J Med Virol* **80**:1468.
235. Atmar RL, Opekun AR, Gilger MA, Estes MK, Crawford SE, *et al.* 2008. Norwalk virus shedding after experimental human infection. *Emerg Infect Dis* **14**:1553.
236. Tu ETV, Bull RA, Kim MJ, Mclver CJ, Heron L, *et al.* 2008. Norovirus excretion in an aged-care setting. *J Clin Microbiol* **46**:2119.
237. Estes MK, Prasad BVV, Atmar RL. 2006. Noroviruses everywhere: has something changed? *Curr Opin Infect Dis* **19**.
238. Lopman B, Gastañaduy P, Park GW, Hall AJ, Parashar UD, *et al.* 2012. Environmental transmission of norovirus gastroenteritis. *Curr Opin Virol* **2**:96.
239. Evans MR, Meldrum R, Lane W, Gardner D, Ribeiro CD, *et al.* 2002. An outbreak of viral gastroenteritis following environmental contamination at a concert hall. *Epidemiol Infect* **129**:355.

240. Thornley CN, Emslie NA, Sprott TW, Greening GE, Rapana JP. 2011. Recurring Norovirus Transmission on an Airplane. *Clin Infect Dis* **53**:515.
241. Cheesbrough J, Barkess-Jones L, Brown D. 1997. Possible prolonged environmental survival of small round structured viruses. *J Hosp Infect* **4**:325.
242. Seitz SR, Leon JS, Schwab KJ, Lyon GM, Dowd M, *et al.* 2011. Norovirus Infectivity in Humans and Persistence in Water. *Appl Environ Microbiol* **77**:6884.
243. Tung G, Macinga D, Arbogast J, Jaykus LA. 2013. Efficacy of commonly used disinfectants for inactivation of human noroviruses and their surrogates. *J Food Prot* **76**:1210.
244. Lopman BA, Adak GK, Reacher MH, Brown DWG. 2003. Two epidemiologic patterns of norovirus outbreaks: surveillance in England and Wales, 1992-2000. *Emerg Infect Dis* **9**:71.
245. Jin M, Wu S, Kong X, Xie H, Fu J, *et al.* 2020. Norovirus Outbreak Surveillance, China, 2016–2018. *Emerg Infect Dis* **26**:437.
246. Morillo SG, Luchs A, Cilli A, do Carmo Sampaio Tavares Timenetsky M. 2012. Rapid Detection of Norovirus in Naturally Contaminated Food: Foodborne Gastroenteritis Outbreak on a Cruise Ship in Brazil, 2010. *Food Environ Virol* **4**:124.
247. Vivancos R, Keenan A, Sopwith W, Smith K, Quigley C, *et al.* 2010. Norovirus outbreak in a cruise ship sailing around the British Isles: Investigation and multi-agency management of an international outbreak. *J Infect* **60**:478.
248. Dewey-Mattia D, Manikonda K, Hall AJ, Wise ME, Crowe SJ. 2018. Surveillance for Foodborne Disease Outbreaks - United States, 2009–2015. *MMWR Morb Mortal Wkly Rep* **67**:1.
249. Bell R, Draper A, Fearnley E, Franklin N, Glasgow K, *et al.* 2021. Monitoring the incidence and causes of disease potentially transmitted by food in Australia: Annual report of the OzFoodNet network, 2016. *Commun Dis Intell* **45**.
250. Westrell T, Dusch V, Ethelberg S, Harris J, Hjertqvist M, *et al.* 2010. Norovirus outbreaks linked to oyster consumption in the United Kingdom, Norway, France, Sweden and Denmark, 2010. *Euro Surveill* **15**:19524.
251. Müller L, Rasmussen LD, Jensen T, Schultz AC, Kjelsø C, *et al.* 2016. Series of Norovirus Outbreaks Caused by Consumption of Green Coral Lettuce, Denmark, April 2016. *PLoS Curr* **8**.
252. Maunula L, Roivainen M, Keränen M, Mäkelä S, Söderberg K, *et al.* 2009. Detection of human norovirus from frozen raspberries in a cluster of gastroenteritis outbreaks. *Euro Surveill* **14**:19435.
253. Le Guyader Françoise S, Bon F, DeMedici D, Parnaudeau S, Bertone A, *et al.* 2006. Detection of Multiple Noroviruses Associated with an International Gastroenteritis Outbreak Linked to Oyster Consumption. *J Clin Microbiol* **44**:3878.
254. Dolin R, Blacklow NR, DuPont H, Buscho RF, Wyatt RG, *et al.* 1972. Biological Properties of Norwalk Agent of Acute Infectious Nonbacterial Gastroenteritis. *Proc Soc Exp Biol Med* **140**:578.
255. McDonnell S, Kirkland KB, Hlady WG, Aristeguieta C, Hopkins RS, *et al.* 1997. Failure of cooking to prevent shellfish-associated viral gastroenteritis. *Arch Intern Med* **157**:111.
256. Schmid D, Stüger HP, Lederer I, Pichler AM, Kainz-Arnfelder G, *et al.* 2007. A Foodborne Norovirus Outbreak Due To Manually Prepared Salad, Austria 2006. *Infection* **35**:232.
257. Yu JH, Kim NY, Koh YJ, Lee HJ. 2010. Epidemiology of Foodborne Norovirus Outbreak in Incheon, Korea. *J Korean Med Sci* **25**:1128.
258. Hardstaff JL, Clough HE, Lutje V, McIntyre KM, Harris JP, *et al.* 2018. Foodborne and Food-Handler Norovirus Outbreaks: A Systematic Review. *Foodborne Pathog Dis* **15**:589.

259. Food Standards Agency. 2009. Food handlers: fitness to work. <https://www.food.gov.uk/sites/default/files/media/document/fitnesstoworkguide.pdf> Accessed 25/05/2022.
260. Food Standards Australia New Zealand. 2020. Norovirus in food. <https://www.foodstandards.gov.au/consumer/safety/foodborne-illness/Pages/Norovirus.aspx> Accessed 25/05/2022.
261. Barrabeig I, Rovira A, Buesa J, Bartolomé R, Pintó R, *et al.* 2010. Foodborne norovirus outbreak: the role of an asymptomatic food handler. *BMC Infect Dis* **10**:269.
262. Glass RI, Parashar UD, Estes MK. 2009. Norovirus Gastroenteritis. *N Engl J Med* **361**:1776.
263. Graham DY, Jiang X, Tanaka T, Opekun AR, Madore HP, *et al.* 1994. Norwalk Virus Infection of Volunteers: New Insights Based on Improved Assays. *J Infect Dis* **170**:34.
264. Teunis PFM, Sukhrie FHA, Vennema H, Bogerman J, Beersma MFC, *et al.* 2015. Shedding of norovirus in symptomatic and asymptomatic infections. *Epidemiol Infect* **143**:1710.
265. Murata T, Katsushima N, Mizuta K, Muraki Y, Hongo S, *et al.* 2007. Prolonged Norovirus shedding in infants ≤ 6 months of age with gastroenteritis. *Pediatr Infect Dis J* **26**.
266. Avery RK, Lonze BE, Kraus ES, Marr KA, Montgomery RA. 2017. Severe chronic norovirus diarrheal disease in transplant recipients: Clinical features of an under-recognized syndrome. *Transpl Infect Dis* **19**:e12674.
267. Lopman BA, Reacher MH, Vipond IB, Sarangi J, Brown DWG. 2004. Clinical Manifestation of Norovirus Gastroenteritis in Health Care Settings. *Clin Infect Dis* **39**:318.
268. Mattner F, Sohr D, Heim A, Gastmeier P, Vennema H, *et al.* 2006. Risk groups for clinical complications of norovirus infections: an outbreak investigation. *Clin Microbiol Infect* **12**:69.
269. Schwartz S, Vergoulidou M, Schreier E, Lodenkemper C, Reinwald M, *et al.* 2011. Norovirus gastroenteritis causes severe and lethal complications after chemotherapy and hematopoietic stem cell transplantation. *Blood* **117**:5850.
270. Dolin R, Levy AG, Wyatt RG, Thornhill TS, Gardner JD. 1975. Viral gastroenteritis induced by the Hawaii agent: Jejunal histopathology and serologic response. *Am J Med* **59**:761.
271. Agus SG, Dolin R, Wyatt RG, Tousimis AJ, Northrup RS. 1973. Acute Infectious Nonbacterial Gastroenteritis: Intestinal Histopathology. *Ann Intern Med* **79**:18.
272. Blacklow NR, Dolin R, Fedson DS, Dupont H, Northrup RS, *et al.* 1972. Acute Infectious Nonbacterial Gastroenteritis: Etiology and Pathogenesis. *Ann Intern Med* **76**:993.
273. Meeroff JC, Schreiber DS, Trier JS, Blacklow NR. 1980. Abnormal gastric motor function in viral gastroenteritis. *Ann Intern Med* **92**:370.
274. Lindesmith L, Moe C, Marionneau S, Ruvoen N, Jiang X, *et al.* 2003. Human susceptibility and resistance to Norwalk virus infection. *Nat Med* **9**:548.
275. Rockx BHG, Vennema H, Hoebe CJPA, Duizer E, Koopmans MPG. 2005. Association of Histo-Blood Group Antigens and Susceptibility to Norovirus Infections. *J Infect Dis* **191**:749.
276. Hutson AM, Atmar RL, Graham DY, Estes MK. 2002. Norwalk Virus Infection and Disease Is Associated with ABO Histo-Blood Group Type. *J Infect Dis* **185**:1335.
277. Marionneau S, Ruvoën N, Le Moullac-Vaidye B, Clement M, Cailleau-Thomas A, *et al.* 2002. Norwalk virus binds to histo-blood group antigens present on gastroduodenal epithelial cells of secretor individuals. *Gastroenterology* **122**:1967.
278. Currier RL, Payne DC, Staat MA, Selvarangan R, Shirley SH, *et al.* 2015. Innate Susceptibility to Norovirus Infections Influenced by FUT2 Genotype in a United States Pediatric Population. *Clin Infect Dis* **60**:1631.

279. Asanaka M, Atmar Robert L, Ruvolo V, Crawford Sue E, Neill Frederick H, *et al.* 2005. Replication and packaging of Norwalk virus RNA in cultured mammalian cells. *Proceedings of the National Academy of Sciences* **102**:10327.
280. Greenberg HB, Valdesuso J, Kapikian AZ, Chanock RM, Wyatt RG, *et al.* 1979. Prevalence of antibody to the Norwalk virus in various countries. *Infect Immun* **26**:270.
281. Greenberg HR, Valdesuso J, Yolken RH, Gangarosa E, Gary W, *et al.* 1979. Role of Norwalk Virus in Outbreaks of Nonbacterial Gastroenteritis. *J Infect Dis* **139**:564.
282. Monroe SS, Glass RI, Noah N, Flewett TH, Caul EO, *et al.* 1991. Electron microscopic reporting of gastrointestinal viruses in the United Kingdom, 1985-1987. *J Med Virol* **33**:193.
283. Sekine S, Okada S, Hayashi Y, Ando T, Terayama T, *et al.* 1989. Prevalence of Small Round Structured Virus Infections in Acute Gastroenteritis Outbreaks in Tokyo. *Microbiol Immunol* **33**:207.
284. Noel JS, Fankhauser RL, Ando T, Monroe SS, Glass RI. 1999. Identification of a Distinct Common Strain of "Norwalk-like Viruses" Having a Global Distribution. *J Infect Dis* **179**:1334.
285. O'Brien SJ, Donaldson AL, Iturriza-Gomara M, Tam CC. 2016. Age-Specific Incidence Rates for Norovirus in the Community and Presenting to Primary Healthcare Facilities in the United Kingdom. *J Infect Dis* **213 Suppl 1**:S15.
286. Eden JS, Tanaka MM, Boni MF, Rawlinson WD, White PA. 2013. Recombination within the Pandemic Norovirus GII.4 Lineage. *J Virol* **87**:6270.
287. Tohma K, Lepore CJ, Ford-Siltz LA, Parra GI. 2017. Phylogenetic Analyses Suggest that Factors Other Than the Capsid Protein Play a Role in the Epidemic Potential of GII.2 Norovirus. *mSphere* **2**:e00187.
288. White PA, Hansman GS, Li A, Dable J, Isaacs M, *et al.* 2002. Norwalk-like virus 95/96-US strain is a major cause of gastroenteritis outbreaks in Australia. *J Med Virol* **68**:113.
289. Fankhauser RL, Noel JS, Monroe SS, Ando T, Glass RI. 1998. Molecular epidemiology of "Norwalk-like viruses" in outbreaks of gastroenteritis in the United States. *J Infect Dis* **178**:1571.
290. Lopman B, Vennema H, Kohli E, Pothier P, Sanchez A, *et al.* 2004. Increase in viral gastroenteritis outbreaks in Europe and epidemic spread of new norovirus variant. *Lancet* **363**:682.
291. Widdowson MA, Cramer EH, Hadley L, Bresee JS, Beard RS, *et al.* 2004. Outbreaks of acute gastroenteritis on cruise ships and on land: identification of a predominant circulating strain of norovirus-United States, 2002. *J Infect Dis* **190**:27.
292. Bull RA, Tu ETV, McIver CJ, Rawlinson WD, White PA. 2006. Emergence of a new norovirus genotype II.4 variant associated with global outbreaks of gastroenteritis. *J Clin Microbiol* **44**:327.
293. Eden JS, Bull RA, Tu E, McIver CJ, Lyon MJ, *et al.* 2010. Norovirus GII.4 variant 2006b caused epidemics of acute gastroenteritis in Australia during 2007 and 2008. *J Clin Virol* **49**:265.
294. Yen C, Wikswow ME, Lopman BA, Vinje J, Parashar UD, *et al.* 2011. Impact of an emergent norovirus variant in 2009 on norovirus outbreak activity in the United States. *Clin Infect Dis* **53**:568.
295. Eden JS, Hewitt J, Lim KL, Boni MF, Merif J, *et al.* 2014. The emergence and evolution of the novel epidemic norovirus GII.4 variant Sydney 2012. *Virology* **450-451**:106.
296. Kroneman A, Vennema H, Harris J, Reuter G, von Bonsdorff CH, *et al.* 2006. Increase in norovirus activity reported in Europe. *Euro Surveill* **11**:3093.
297. Ho ECM, Cheng PKC, Wong DA, Lau AWL, Lim WWL. 2006. Correlation of norovirus variants with epidemics of acute viral gastroenteritis in Hong Kong. *J Med Virol* **78**:1473.

298. Medici MC, Tummolo F, Martella V, Chezzi C, Arcangeletti MC, *et al.* 2014. Epidemiological and molecular features of norovirus infections in Italian children affected with acute gastroenteritis. *Epidemiol Infect* **142**:2326.
299. Tu ET, Bull RA, Greening GE, Hewitt J, Lyon MJ, *et al.* 2008. Epidemics of gastroenteritis during 2006 were associated with the spread of norovirus GII.4 variants 2006a and 2006b. *Clin Infect Dis* **46**:413.
300. van Beek J, de Graaf M, Al-Hello H, Allen DJ, Ambert-Balay K, *et al.* 2018. Molecular surveillance of norovirus, 2005–16: an epidemiological analysis of data collected from the NoroNet network. *Lancet Infect Dis* **18**:545.
301. van Beek J, Ambert-Balay K, Botteldoorn N, Eden JS, Fonager J, *et al.* 2013. Indications for worldwide increased norovirus activity associated with emergence of a new variant of genotype II.4, late 2012. *Euro Surveill* **18**:20345.
302. Lim KL, Hewitt J, Sitabkhan A, Eden JS, Lun J, *et al.* 2016. A Multi-Site Study of Norovirus Molecular Epidemiology in Australia and New Zealand, 2013-2014. *PLoS One* **11**:e0145254.
303. Lun JH, Hewitt J, Sitabkhan A, Eden JS, Enosi Tuipulotu D, *et al.* 2018. Emerging recombinant noroviruses identified by clinical and waste water screening. *Emerg Microbes Infect* **7**:50.
304. Bruggink LD, Triantafilou MJ, Marshall JA. 2018. The molecular epidemiology of norovirus outbreaks in Victoria, 2016. *Commun Dis Intell* **42**.
305. Matsushima Y, Ishikawa M, Shimizu T, Komane A, Kasuo S, *et al.* 2015. Genetic analyses of GII.17 norovirus strains in diarrheal disease outbreaks from December 2014 to March 2015 in Japan reveal a novel polymerase sequence and amino acid substitutions in the capsid region. *Euro Surveill* **20**.
306. Lu J, Sun L, Fang L, Yang F, Mo Y, *et al.* 2015. Gastroenteritis Outbreaks Caused by Norovirus GII.17, Guangdong Province, China, 2014-2015. *Emerg Infect Dis* **21**:1240.
307. Wangchuk S, Matsumoto T, Iha H, Ahmed K. 2017. Surveillance of norovirus among children with diarrhea in four major hospitals in Bhutan: Replacement of GII.21 by GII.3 as a dominant genotype. *PLoS One* **12**:e0184826.
308. Dove W, Cunliffe NA, Gondwe JS, Broadhead RL, Molyneux ME, *et al.* 2005. Detection and characterization of human caliciviruses in hospitalized children with acute gastroenteritis in Blantyre, Malawi. *J Med Virol* **77**:522.
309. Dey SK, Phathamavong O, Okitsu S, Mizuguchi M, Ohta Y, *et al.* 2010. Seasonal pattern and genotype distribution of norovirus infection in Japan. *Pediatr Infect Dis J* **29**.
310. Boon D, Mahar JE, Abente EJ, Kirkwood CD, Purcell RH, *et al.* 2011. Comparative evolution of GII.3 and GII.4 norovirus over a 31-year period. *J Virol* **85**:8656.
311. Chan MCW, Leung TF, Chung TWS, Kwok AK, Nelson EAS, *et al.* 2015. Virus Genotype Distribution and Virus Burden in Children and Adults Hospitalized for Norovirus Gastroenteritis, 2012–2014, Hong Kong. *Sci Rep* **5**:11507.
312. Niendorf S, Jacobsen S, Faber M, Eis-Hübinger AM, Hofmann J, *et al.* 2017. Steep rise in norovirus cases and emergence of a new recombinant strain GII.P16-GII.2, Germany, winter 2016. *Euro Surveill* **22**.
313. Matsushima Y, Shimizu T, Ishikawa M, Komane A, Okabe N, *et al.* 2016. Complete Genome Sequence of a Recombinant GII.P16-GII.4 Norovirus Detected in Kawasaki City, Japan, in 2016. *Genome announcements* **4**:e01099.
314. White PA, Netzler NE, Hansman GS. 2016. Foodborne viral pathogens. CRC Press.
315. Zhang M, Fu M, Hu Q. 2021. Advances in Human Norovirus Vaccine Research. *Vaccines* **9**.
316. Tan M. 2021. Norovirus Vaccines: Current Clinical Development and Challenges. *Pathogens* **10**:1641.

317. Netzler NE, Enosi Tuipulotu D, White PA. 2019. Norovirus antivirals: Where are we now? *Med Res Rev* **39**:860.
318. MacCannell T, Umscheid CA, Agarwal RK, Lee I, Kuntz G, *et al.* 2011. Guideline for the Prevention and Control of Norovirus Gastroenteritis Outbreaks in Healthcare Settings. *Infect Control Hosp Epidemiol* **32**:939.
319. Hall AJ, Vinjé J, Lopman B, Park GW, Yen C, *et al.* 2011. Updated Norovirus Outbreak Management and Disease Prevention Guidelines. *MMWR Recomm Rep* **60**:1.
320. Pieścik-Lech M, Shamir R, Guarino A, Szajewska H. 2013. Review article: the management of acute gastroenteritis in children. *Aliment Pharmacol Ther* **37**:289.
321. Kaufman SS, Green KY, Korba BE. 2014. Treatment of norovirus infections: Moving antivirals from the bench to the bedside. *Antiviral Res* **105**:80.
322. Hopper SM. 2010. A Practical Guide to Successful Rehydration. *Clin Pediatr Emerg Med* **11**:153.
323. Carter B, Fedorowicz Z. 2012. Antiemetic treatment for acute gastroenteritis in children: an updated Cochrane systematic review with meta-analysis and mixed treatment comparison in a Bayesian framework. *BMJ Open* **2**:e000622.
324. Cheng A. 2011. Emergency department use of oral ondansetron for acute gastroenteritis-related vomiting in infants and children. *Paediatr Child Health* **16**:177.
325. Lehert P, Chéron G, Calatayud GA, Cézard J-P, Castrellón PG, *et al.* 2011. Racecadotril for childhood gastroenteritis: an individual patient data meta-analysis. *Dig Liver Dis* **43**:707.
326. Ciccarelli S, Stolfi I, Caramia G. 2013. Management strategies in the treatment of neonatal and pediatric gastroenteritis. *Infection and drug resistance* **6**:133.
327. Estes MK, Ettayebi K, Tenge VR, Murakami K, Karandikar U, *et al.* 2019. Human Norovirus Cultivation in Nontransformed Stem Cell-Derived Human Intestinal Enteroid Cultures: Success and Challenges. *Viruses* **11**:638.
328. Parra GI, Bok K, Taylor R, Haynes JR, Sosnovtsev SV, *et al.* 2012. Immunogenicity and specificity of norovirus Consensus GII.4 virus-like particles in monovalent and bivalent vaccine formulations. *Vaccine* **30**:3580.
329. Bernstein DI, Atmar RL, Lyon GM, Treanor JJ, Chen WH, *et al.* 2014. Norovirus Vaccine Against Experimental Human GII.4 Virus Illness: A Challenge Study in Healthy Adults. *J Infect Dis* **211**:870.
330. Wang X, Ku Z, Dai W, Chen T, Ye X, *et al.* 2015. A bivalent virus-like particle based vaccine induces a balanced antibody response against both enterovirus 71 and norovirus in mice. *Vaccine* **33**:5779.
331. Kim L, Liebowitz D, Lin K, Kasperek K, Pasetti MF, *et al.* 2018. Safety and immunogenicity of an oral tablet norovirus vaccine, a phase I randomized, placebo-controlled trial. *JCI Insight* **3**.
332. Sherwood J, Mendelman PM, Lloyd E, Liu M, Boslego J, *et al.* 2020. Efficacy of an intramuscular bivalent norovirus GI. 1/GII. 4 virus-like particle vaccine candidate in healthy US adults. *Vaccine* **38**:6442.
333. Kocher J, Bui T, Giri-Rachman E, Wen K, Li G, *et al.* 2014. Intranasal P particle vaccine provided partial cross-variant protection against human GII. 4 norovirus diarrhea in gnotobiotic pigs. *J Virol* **88**:9728.
334. Tacket CO, Mason HS, Losonsky G, Estes MK, Levine MM, *et al.* 2000. Human immune responses to a novel Norwalk virus vaccine delivered in transgenic potatoes. *J Infect Dis* **182**:302.
335. Mathew LG, Herbst-Kralovetz MM, Mason HS. 2014. Norovirus Narita 104 virus-like particles expressed in *Nicotiana benthamiana* induce serum and mucosal immune responses. *Biomed Res Int* **2014**.

336. Tamminen K, Lappalainen S, Huhti L, Vesikari T, Blazevic V. 2013. Trivalent combination vaccine induces broad heterologous immune responses to norovirus and rotavirus in mice. *PLoS One* **8**:e70409.
337. Malm M, Tamminen K, Lappalainen S, Vesikari T, Blazevic V. 2016. Rotavirus recombinant VP6 nanotubes act as an immunomodulator and delivery vehicle for norovirus virus-like particles. *Journal of Immunology Research* **2016**.
338. Vesikari T, Saez-Llorens X, Blazevic V, Lopez P, Lopez E, *et al.* 2022. Immunogenicity of a bivalent virus-like particle norovirus vaccine in children from 1 to 8 years of age: A phase 2 randomized, double-blind study. *Vaccine* **40**:3588.
339. Rowe WP, Huebner RJ, Gilmore LK, Parrott RH, Ward TG. 1953. Isolation of a Cytopathogenic Agent from Human Adenoids Undergoing Spontaneous Degeneration in Tissue Culture. *Proc Soc Exp Biol Med* **84**:570.
340. D'Ambrosio E, Grosso ND, Chicca A, Midulla M. 1982. Neutralizing antibodies against 33 human adenoviruses in normal children in Rome. *J Hyg (Lond)* **89**:155.
341. Esposito S, Zampiero A, Bianchini S, Mori A, Scala A, *et al.* 2016. Epidemiology and Clinical Characteristics of Respiratory Infections Due to Adenovirus in Children Living in Milan, Italy, during 2013 and 2014. *PLoS One* **11**:e0152375.
342. Xie L, Zhang B, Xiao N, Zhang F, Zhao X, *et al.* 2019. Epidemiology of human adenovirus infection in children hospitalized with lower respiratory tract infections in Hunan, China. *J Med Virol* **91**:392.
343. Liu C, Xiao Y, Zhang J, Ren L, Li J, *et al.* 2015. Adenovirus infection in children with acute lower respiratory tract infections in Beijing, China, 2007 to 2012. *BMC Infect Dis* **15**:408.
344. Richter J, Panayiotou C, Tryfonos C, Koptides D, Koliou M, *et al.* 2016. Aetiology of Acute Respiratory Tract Infections in Hospitalised Children in Cyprus. *PLoS One* **11**:e0147041.
345. Yao Lh, Wang C, Wei Tl, Wang H, Ma Fl, *et al.* 2019. Human adenovirus among hospitalized children with respiratory tract infections in Beijing, China, 2017–2018. *Viol J* **16**:78.
346. Fischer TK, Rungoe C, Jensen CS, Breindahl M, Jørgensen TR, *et al.* 2011. The Burden of Rotavirus Disease in Denmark 2009–2010. *Pediatr Infect Dis J* **30**.
347. Portal TM, Reymão TKA, Quinderé Neto GA, Fiuza MKDC, Teixeira DM, *et al.* 2019. Detection and genotyping of enteric viruses in hospitalized children with acute gastroenteritis in Belém, Brazil: Occurrence of adenovirus viremia by species F, types 40/41. *J Med Virol* **91**:378.
348. Platts-Mills JA, Liu J, Rogawski ET, Kabir F, Lertsethtakarn P, *et al.* 2018. Use of quantitative molecular diagnostic methods to assess the aetiology, burden, and clinical characteristics of diarrhoea in children in low-resource settings: a reanalysis of the MAL-ED cohort study. *Lancet Glob Health* **6**:e1309.
349. Gu J, Su QQ, Zuo TT, Chen YB. 2021. Adenovirus diseases: a systematic review and meta-analysis of 228 case reports. *Infection* **49**:1.
350. Hess M, Blöcker H, Brandt P. 1997. The Complete Nucleotide Sequence of the Egg Drop Syndrome Virus: An Intermediate between Mastadenoviruses and Aviadenoviruses. *Virology* **238**:145.
351. Thomson D, Meers J, Harrach B. 2002. Molecular confirmation of an adenovirus in brushtail possums (*Trichosurus vulpecula*). *Virus Res* **83**:189.
352. Szivovics L, López P, Kopena R, Benkő M, Martín J, *et al.* 2016. Random Sampling of Squamate Reptiles in Spanish Natural Reserves Reveals the Presence of Novel Adenoviruses in Lacertids (Family Lacertidae) and Worm Lizards (Amphisbaenia). *PLoS One* **11**:e0159016.
353. Miller MM, Cornish TE, Creekmore TE, Fox K, Laegreid W, *et al.* 2017. Whole-genome sequences of *Odocoileus hemionus* deer adenovirus isolates from deer, moose and elk

- are highly conserved and support a new species in the genus Atadenovirus. *J Gen Virol* **98**:2320.
354. Kaján GL, Davison AJ, Palya V, Harrach B, Benkő M. 2012. Genome sequence of a waterfowl aviadenovirus, goose adenovirus 4. *J Gen Virol* **93**:2457.
 355. Das S, Fearnside K, Sarker S, Forwood JK, Raidal SR. 2017. A novel pathogenic aviadenovirus from red-bellied parrots (*Poicephalus rufiventris*) unveils deep recombination events among avian host lineages. *Virology* **502**:188.
 356. Kaján GL, Affranio I, Tóthné Bistyák A, Kecskeméti S, Benkő M. 2019. An emerging new fowl adenovirus genotype. *Heliyon* **5**:e01732.
 357. Benkő M, Élő P, Ursu K, Ahne W, LaPatra Scott E, *et al.* 2002. First Molecular Evidence for the Existence of Distinct Fish and Snake Adenoviruses. *J Virol* **76**:10056.
 358. Doszpoly A, Harrach B, LaPatra S, Benkő M. 2019. Unconventional gene arrangement and content revealed by full genome analysis of the white sturgeon adenovirus, the single member of the genus *Ichtadenovirus*. *Infect Genet Evol* **75**:103976.
 359. Hoppe E, Pauly M, Gillespie TR, Akoua-Koffi C, Hohmann G, *et al.* 2015. Multiple Cross-Species Transmission Events of Human Adenoviruses (HAdV) during Hominine Evolution. *Mol Biol Evol* **32**:2072.
 360. Balboni A, Tryland M, Mørk T, Killengreen ST, Fuglei E, *et al.* 2019. Unique genetic features of canine adenovirus type 1 (CAV-1) infecting red foxes (*Vulpes vulpes*) in northern Norway and arctic foxes (*Vulpes lagopus*) in Svalbard. *Vet Res Commun* **43**:67.
 361. Wernike K, Wylezich C, Höper D, Schneider J, Lurz PWW, *et al.* 2018. Widespread occurrence of squirrel adenovirus 1 in red and grey squirrels in Scotland detected by a novel real-time PCR assay. *Virus Res* **257**:113.
 362. Vidovszky MZ, Szeredi L, Doszpoly A, Harrach B, Hornyák Á. 2019. Isolation and complete genome sequence analysis of a novel ovine adenovirus type representing a possible new mastadenovirus species. *Arch Virol* **164**:2205.
 363. Standorf K, Cortés-Hinojosa G, Venn-Watson S, Rivera R, Archer LL, *et al.* 2018. Phylogenetic analysis of the genome of an enteritis-associated bottlenose dolphin mastadenovirus supports a clade infecting the Cetartiodactyla. *J Wildl Dis* **54**:112.
 364. Davison AJ, Wright KM, Harrach B. 2000. DNA sequence of frog adenovirus. *J Gen Virol* **81**:2431.
 365. Schumacher VL, Innis CJ, Garner MM, Risatti GR, Nordhausen RW, *et al.* 2012. Sulawesi tortoise adenovirus-1 in two impressed tortoises (*Manouria impressa*) and a Burmese star tortoise (*Geochelone platynota*). *J Zoo Wildl Med* **43**:501.
 366. Doszpoly A, Wellehan JFX, Childress AL, Tarján ZL, Kovács ER, *et al.* 2013. Partial characterization of a new adenovirus lineage discovered in testudinoid turtles. *Infect Genet Evol* **17**:106.
 367. Benkő M, Aoki K, Arnberg N, Davison AJ, Echavarría M, *et al.* 2022. ICTV Virus Taxonomy Profile: *Adenoviridae* 2022. *J Gen Virol* **103**.
 368. Adrian T, Wadell G, Hierholzer JC, Wigand R. 1986. DNA restriction analysis of adenovirus prototypes 1 to 41. *Arch Virol* **91**:277.
 369. Wadell G, Hammarskjöld M-L, Winberg G, Varsanyi TM, Sundell G. 1980. Genetic variability of adenoviruses. *Ann N Y Acad Sci* **354**:16.
 370. Sarantis H, Johnson G, Brown M, Petric M, Tellier R. 2004. Comprehensive Detection and Serotyping of Human Adenoviruses by PCR and Sequencing. *J Clin Microbiol* **42**:3963.
 371. Lu X, Erdman DD. 2006. Molecular typing of human adenoviruses by PCR and sequencing of a partial region of the hexon gene. *Arch Virol* **151**:1587.
 372. Allard A, Albinsson B, Wadell G. 2001. Rapid typing of human adenoviruses by a general PCR combined with restriction endonuclease analysis. *J Clin Microbiol* **39**:498.

373. Robinson CM, Singh G, Lee JY, Dehghan S, Rajaiya J, *et al.* 2013. Molecular evolution of human adenoviruses. *Sci Rep* **3**:1812.
374. Dehghan S, Seto J, Liu EB, Ismail AM, Madupu R, *et al.* 2019. A Zoonotic Adenoviral Human Pathogen Emerged through Genomic Recombination among Human and Nonhuman Simian Hosts. *J Virol* **93**:e00564.
375. Yoshitomi H, Sera N, Gonzalez G, Hanaoka N, Fujimoto T. 2017. First isolation of a new type of human adenovirus (genotype 79), species Human mastadenovirus B (B2) from sewage water in Japan. *J Med Virol* **89**:1192.
376. Ismail AM, Lee JS, Lee JY, Singh G, Dyer DW, *et al.* 2018. Adenoviromics: Mining the Human Adenovirus Species D Genome. *Front Microbiol* **9**.
377. Dhingra A, Hage E, Ganzenmueller T, Böttcher S, Hofmann J, *et al.* 2019. Molecular Evolution of Human Adenovirus (HAdV) Species C. *Sci Rep* **9**:1039.
378. Mao N, Zhu Z, Rivaller P, Chen M, Fan Q, *et al.* 2017. Whole genomic analysis of two potential recombinant strains within Human mastadenovirus species C previously found in Beijing, China. *Sci Rep* **7**:15380.
379. Rivaller P, Mao N, Zhu Z, Xu W. 2019. Recombination analysis of Human mastadenovirus C whole genomes. *Sci Rep* **9**:2182.
380. Kaján GL, Kajon AE, Pinto AC, Bartha D, Arnberg N. 2017. The complete genome sequence of human adenovirus 84, a highly recombinant new Human mastadenovirus D type with a unique fiber gene. *Virus Res* **242**:79.
381. Casas I, Avellon A, Mosquera M, Jabado O, Echevarria JE, *et al.* 2005. Molecular identification of adenoviruses in clinical samples by analyzing a partial hexon genomic region. *J Clin Microbiol* **43**:6176.
382. Kim J-S, Lee SK, Ko D-H, Hyun J, Kim H-S, *et al.* 2017. Associations of Adenovirus Genotypes in Korean Acute Gastroenteritis Patients with Respiratory Symptoms and Intussusception. *Biomed Res Int* **2017**:1602054.
383. Kumthip K, Khamrin P, Ushijima H, Maneekarn N. 2019. Enteric and non-enteric adenoviruses associated with acute gastroenteritis in pediatric patients in Thailand, 2011 to 2017. *PLoS One* **14**:e0220263.
384. Horne RW, Brenner S, Waterson AP, Wildy P. 1959. The icosahedral form of an adenovirus. *J Mol Biol* **1**:84.
385. Iltis JP, Daniels SB. 1977. Adenovirus of ring-necked pheasants: purification and partial characterization of marble spleen disease virus. *Infect Immun* **16**:701.
386. Crowther RA, Franklin RM. 1972. The structure of the groups of nine hexons from adenovirus. *J Mol Biol* **68**:181.
387. Reddy Vijay S, Natchiar SK, Stewart Phoebe L, Nemerow Glen R. 2010. Crystal Structure of Human Adenovirus at 3.5 Å Resolution. *Science* **329**:1071.
388. van Raaij MJ, Mitraki A, Lavigne G, Cusack S. 1999. A triple β -spiral in the adenovirus fibre shaft reveals a new structural motif for a fibrous protein. *Nature* **401**:935.
389. Zheng S, Ulasov IV, Han Y, Tyler MA, Zhu ZB, *et al.* 2007. Fiber-knob modifications enhance adenoviral tropism and gene transfer in malignant glioma. *J Gene Med* **9**:151.
390. Stevenson SC, Rollence M, White B, Weaver L, McClelland A. 1995. Human adenovirus serotypes 3 and 5 bind to two different cellular receptors via the fiber head domain. *J Virol* **69**:2850.
391. Belousova N, Krendelchtchikova V, Curiel DT, Krasnykh V. 2002. Modulation of Adenovirus Vector Tropism via Incorporation of Polypeptide Ligands into the Fiber Protein. *J Virol* **76**:8621.
392. Roelvink PW, Lizonova A, Lee JG, Li Y, Bergelson JM, *et al.* 1998. The coxsackievirus-adenovirus receptor protein can function as a cellular attachment protein for adenovirus serotypes from subgroups A, C, D, E, and F. *J Virol* **72**:7909.
393. Rafie K, Lenman A, Fuchs J, Rajan A, Arnberg N, *et al.* 2021. The structure of enteric human adenovirus 41 - A leading cause of diarrhea in children. *Sci Adv* **7**:eabe0974.

394. Stone D, Furthmann A, Sandig V, Lieber A. 2003. The complete nucleotide sequence, genome organization, and origin of human adenovirus type 11. *Virology* **309**:152.
395. Berciaud S, Rayne F, Kassab S, Jubert C, Faure-Della Corte M, *et al.* 2012. Adenovirus infections in Bordeaux University Hospital 2008–2010: Clinical and virological features. *J Clin Virol* **54**:302.
396. Teunis P, Schijven J, Rutjes S. 2016. A generalized dose-response relationship for adenovirus infection and illness by exposure pathway. *Epidemiol Infect* **144**:3461.
397. Lessler J, Reich NG, Brookmeyer R, Perl TM, Nelson KE, *et al.* 2009. Incubation periods of acute respiratory viral infections: a systematic review. *Lancet Infect Dis* **9**:291.
398. Wood DJ. 1988. Adenovirus gastroenteritis. *Br Med J (Clin Res Ed)* **296**:229.
399. Uhnoo I, Wadell G, Svensson L, Johansson ME. 1984. Importance of enteric adenoviruses 40 and 41 in acute gastroenteritis in infants and young children. *J Clin Microbiol* **20**:365.
400. Centers for Disease C, Prevention. 2013. Adenovirus-associated epidemic keratoconjunctivitis outbreaks--four states, 2008-2010. *MMWR Morb Mort Wkly Rep* **62**:637.
401. Artieda J, Piñeiro L, González MC, Muñoz MJ, Basterrechea M, *et al.* 2009. A swimming pool-related outbreak of pharyngoconjunctival fever in children due to adenovirus type 4, Gipuzkoa, Spain, 2008. *Euro Surveill* **14**:19125.
402. Crabtree KD, Gerba CP, Rose JB, Haas CN. 1997. Waterborne adenovirus: A risk assessment. *Water Sci Technol* **35**:1.
403. Echavarría M, Kolavic SA, Cersovsky S, Mitchell F, Sanchez JL, *et al.* 2000. Detection of adenoviruses (AdV) in culture-negative environmental samples by PCR during an AdV-associated respiratory disease outbreak. *J Clin Microbiol* **38**:2982.
404. Muller MP, Siddiqui N, Ivancic R, Wong D. 2018. Adenovirus-related epidemic keratoconjunctivitis outbreak at a hospital-affiliated ophthalmology clinic. *Am J Infect Control* **46**:581.
405. Ganime AC, Carvalho-Costa FA, Santos M, Costa Filho R, Leite JPG, *et al.* 2014. Viability of human adenovirus from hospital fomites. *J Med Virol* **86**:2065.
406. Jones MS, 2nd, Harrach B, Ganac RD, Gozum MM, Dela Cruz WP, *et al.* 2007. New adenovirus species found in a patient presenting with gastroenteritis. *J Virol* **81**:5978.
407. Portes SAR, Volotão EdM, Rocha MS, Rebelo MC, Xavier MdPTP, *et al.* 2016. A non-enteric adenovirus A12 gastroenteritis outbreak in Rio de Janeiro, Brazil. *Mem Inst Oswaldo Cruz* **111**:403.
408. Adrian T, Wigand R, Richter J. 1987. Gastroenteritis in infants, associated with a genome type of adenovirus 31 and with combined rotavirus and adenovirus 31 infection. *Eur J Pediatr* **146**:38.
409. Coleman KK, Robie ER, Abdelgadir A, Kozhumam AS, Binder RA, *et al.* 2021. Six Decades of Human Adenovirus Type 4 Infections Reviewed: Increasing Infections Among Civilians Are a Matter of Concern. *Clin Infect Dis* **73**:740.
410. Lin KH, Lin YC, Chen HL, Ke GM, Chiang CJ, *et al.* 2004. A two decade survey of respiratory adenovirus in Taiwan: The reemergence of adenovirus types 7 and 4. *J Med Virol* **73**:274.
411. Probst V, Datyner EK, Haddadin Z, Rankin DA, Hamdan L, *et al.* 2021. Human adenovirus species in children with acute respiratory illnesses. *J Clin Virol* **134**:104716.
412. Scott MK, Chommanard C, Lu X, Appelgate D, Grenz L, *et al.* 2016. Human Adenovirus Associated with Severe Respiratory Infection, Oregon, USA, 2013-2014. *Emerg Infect Dis* **22**:1044.
413. Koga S, Shindo K, Matsuya F, Hori T, Kanda S, *et al.* 1993. Acute hemorrhagic cystitis caused by adenovirus following renal transplantation: Review of the literature. *J Urol* **149**:838.

414. Mufson MA, Belshe RB. 1976. A Review of Adenoviruses in the Etiology of Acute Hemorrhagic Cystitis. *J Urol* **115**:191.
415. Wadell G, de Jong JC. 1980. Restriction endonucleases in identification of a genome type of adenovirus 19 associated with keratoconjunctivitis. *Infect Immun* **27**:292.
416. Fujimoto T, Matsushima Y, Shimizu H, Ishimaru Y, Kano A, *et al.* 2012. A molecular epidemiologic study of human adenovirus type 8 isolates causing epidemic keratoconjunctivitis in Kawasaki City, Japan in 2011. *Jpn J Infect Dis* **65**:260.
417. Aoki K, Tagawa Y. 2002. A Twenty-One Year Surveillance of Adenoviral Conjunctivitis in Sapporo, Japan. *Int Ophthalmol Clin* **42**.
418. Pauschinger M, Bowles NE, Fuentes-Garcia FJ, Pham V, Kühl U, *et al.* 1999. Detection of adenoviral genome in the myocardium of adult patients with idiopathic left ventricular dysfunction. *Circulation* **99**:1348.
419. Valdés O, Acosta B, Piñón A, Savón C, Goyenechea A, *et al.* 2008. First report on fatal myocarditis associated with adenovirus infection in Cuba. *J Med Virol* **80**:1756.
420. Ronan BA, Agrwal N, Carey EJ, De Petris G, Kusne S, *et al.* 2014. Fulminant hepatitis due to human adenovirus. *Infection* **42**:105.
421. Mena KD, Gerba CP. 2009. Waterborne Adenovirus, p 133-167. In Whitacre DM (ed), Rev Environ Contam Toxicol. Springer New York, New York, NY.
422. Bonadonna L, La Rosa G. 2019. A Review and Update on Waterborne Viral Diseases Associated with Swimming Pools. *Int J Environ Res Public Health* **16**:166.
423. Maunula L, Klemola P, Kauppinen A, Söderberg K, Nguyen T, *et al.* 2009. Enteric viruses in a large waterborne outbreak of acute gastroenteritis in Finland. *Food Environ Virol* **1**:31.
424. Laine J, Huovinen E, Virtanen MJ, Snellman M, Lumio J, *et al.* 2011. An extensive gastroenteritis outbreak after drinking-water contamination by sewage effluent, Finland. *Epidemiol Infect* **139**:1105.
425. Kosulin K, Geiger E, Vécsei A, Huber WD, Rauch M, *et al.* 2016. Persistence and reactivation of human adenoviruses in the gastrointestinal tract. *Clin Microbiol Infect* **22**:381.e1.
426. Magwalivha M, Wolfaardt M, Kiulia NM, van Zyl WB, Mwenda JM, *et al.* 2010. High prevalence of species D human adenoviruses in fecal specimens from Urban Kenyan children with diarrhea. *J Med Virol* **82**:77.
427. Grøndahl-Rosado RC, Yarovitsyna E, Trettenes E, Myrmel M, Robertson LJ. 2014. A One Year Study on the Concentrations of Norovirus and Enteric Adenoviruses in Wastewater and A Surface Drinking Water Source in Norway. *Food Environ Virol* **6**:232.
428. Ogorzaly L, Walczak C, Galloux M, Etienne S, Gassilloud B, *et al.* 2015. Human Adenovirus Diversity in Water Samples Using a Next-Generation Amplicon Sequencing Approach. *Food Environ Virol* **7**:112.
429. Fong TT, Phanikumar MS, Xagorarakis I, Rose JB. 2010. Quantitative detection of human adenoviruses in wastewater and combined sewer overflows influencing a Michigan river. *Appl Environ Microbiol* **76**:715.
430. van Heerden J, Ehlers MM, Grabow WOK. 2005. Detection and risk assessment of adenoviruses in swimming pool water. *J Appl Microbiol* **99**:1256.
431. Wyn-Jones AP, Carducci A, Cook N, D'Agostino M, Divizia M, *et al.* 2011. Surveillance of adenoviruses and noroviruses in European recreational waters. *Water Research* **45**:1025.
432. Prado T, de Castro Bruni A, Barbosa MRF, Garcia SC, de Jesus Melo AM, *et al.* 2019. Performance of wastewater reclamation systems in enteric virus removal. *Sci Total Environ* **678**:33.
433. Qiu Y, Li Q, Lee BE, Ruecker NJ, Neumann NF, *et al.* 2018. UV inactivation of human infectious viruses at two full-scale wastewater treatment plants in Canada. *Water Research* **147**:73.

434. Qiu Y, Lee BE, Neumann N, Ashbolt N, Craik S, *et al.* 2015. Assessment of human virus removal during municipal wastewater treatment in Edmonton, Canada. *J Appl Microbiol* **119**:1729.
435. Rigotto C, Hanley K, Rochelle PA, De Leon R, Barardi CRM, *et al.* 2011. Survival of Adenovirus Types 2 and 41 in Surface and Ground Waters Measured by a Plaque Assay. *Environ Sci Technol* **45**:4145.
436. Xie L, Yu XF, Sun Z, Yang XH, Huang RJ, *et al.* 2012. Two Adenovirus Serotype 3 Outbreaks Associated with Febrile Respiratory Disease and Pharyngoconjunctival Fever in Children under 15 Years of Age in Hangzhou, China, during 2011. *J Clin Microbiol* **50**:1879.
437. Wei S. 2016. An adenovirus outbreak associated with a swimming facility. *SM Tropical Medicine Journal* **1**:1007.
438. Li J, Lu X, Sun Y, Lin C, Li F, *et al.* 2018. A swimming pool-associated outbreak of pharyngoconjunctival fever caused by human adenovirus type 4 in Beijing, China. *Int J Infect Dis* **75**:89.
439. Tablan OC, Anderson LJ, Besser R, Bridges C, Hajjeh R. 2004. Guidelines for preventing health-care-associated pneumonia, 2003: recommendations of CDC and the Healthcare Infection Control Practices Advisory Committee. *MMWR Recomm Rep* **53**:1.
440. Rutala William A, Peacock Jeffrey E, Gergen Maria F, Sobsey Mark D, Weber David J. 2006. Efficacy of Hospital Germicides against Adenovirus 8, a Common Cause of Epidemic Keratoconjunctivitis in Health Care Facilities. *Antimicrob Agents Chemother* **50**:1419.
441. von Lilienfeld-Toal M, Berger A, Christopeit M, Hentrich M, Heussel CP, *et al.* 2016. Community acquired respiratory virus infections in cancer patients—Guideline on diagnosis and management by the Infectious Diseases Working Party of the German Society for haematology and Medical Oncology. *Eur J Cancer* **67**:200.
442. Yoo H, Gu SH, Jung J, Song DH, Yoon C, *et al.* 2017. Febrile Respiratory Illness Associated with Human Adenovirus Type 55 in South Korea Military, 2014-2016. *Emerg Infect Dis* **23**:1016.
443. Ljungman P, Ribaud P, Eyrich M, Matthes-Martin S, Einsele H, *et al.* 2003. Cidofovir for adenovirus infections after allogeneic hematopoietic stem cell transplantation: a survey by the Infectious Diseases Working Party of the European Group for Blood and Marrow Transplantation. *Bone Marrow Transplant* **31**:481.
444. Ison MG, Green M, the ASTIDCoP. 2009. Adenovirus in Solid Organ Transplant Recipients. *Am J Transplant* **9**:S161.
445. Lankester AC, Heemskerk B, Claas ECJ, Schilham MW, Beersma MFC, *et al.* 2004. Effect of Ribavirin on the Plasma Viral DNA Load in Patients with Disseminating Adenovirus Infection. *Clin Infect Dis* **38**:1521.
446. Hoke CH, Snyder CE. 2013. History of the restoration of adenovirus type 4 and type 7 vaccine, live oral (Adenovirus Vaccine) in the context of the Department of Defense acquisition system. *Vaccine* **31**:1623.
447. Top FHJ, Dudding BA, Russell PK, Buescher EL. 1971. Control of respiratory disease in recruits with types 4 and 7 adenovirus vaccines. *Am J Epidemiol* **94**:142.
448. Institute of Medicine. 2000. Urgent Attention Needed to Restore Lapsed Adenovirus Vaccine Availability: A Letter Report. The National Academies Press, Washington, DC.
449. Gray GC, Goswami PR, Malasig MD, Hawksworth AW, Trump DH, *et al.* 2000. Adult Adenovirus Infections: Loss of Orphaned Vaccines Precipitates Military Respiratory Disease Epidemics. *Clin Infect Dis* **31**:663.
450. Kolavic-Gray SA, Binn LN, Sanchez JL, Cersovsky SB, Polyak CS, *et al.* 2002. Large epidemic of adenovirus type 4 infection among military trainees: epidemiological, clinical, and laboratory studies. *Clin Infect Dis* **35**:808.

451. Potter RN, Cantrell JA, Mallak CT, Gaydos JC. 2012. Adenovirus-associated deaths in US military during postvaccination period, 1999-2010. *Emerg Infect Dis* **18**:507.
452. U.S. Food and Drug Administration. 2011. March 16, 2011 Approval Letter - Adenovirus Type 4 and Type 7 Vaccine, Live, Oral. 16 Mar 2011.
453. Radin JM, Hawksworth AW, Blair PJ, Faix DJ, Raman R, *et al.* 2014. Dramatic Decline of Respiratory Illness Among US Military Recruits After the Renewed Use of Adenovirus Vaccines. *Clin Infect Dis* **59**:962.
454. Peiris JSM, Jong MDd, Guan Y. 2007. Avian Influenza Virus (H5N1): a Threat to Human Health. *Clin Microbiol Rev* **20**:243.
455. Nishiura H, Omori R. 2010. An epidemiological analysis of the foot-and-mouth disease epidemic in Miyazaki, Japan, 2010. *Transbound Emerg Dis* **57**:396.
456. Sánchez-Cordón PJ, Montoya M, Reis AL, Dixon LK. 2018. African swine fever: A re-emerging viral disease threatening the global pig industry. *Vet J* **233**:41.
457. Heymann DL. 2004. The international response to the outbreak of SARS in 2003. *Philos Trans R Soc Lond B Biol Sci* **359**:1127.
458. Dwosh HA, Hong HH, Austgarden D, Herman S, Schabas R. 2003. Identification and containment of an outbreak of SARS in a community hospital. *CMAJ* **168**:1415.
459. Zumla A, Hui DS. 2014. Infection control and MERS-CoV in health-care workers. *Lancet* **383**:1869.
460. Park GE, Ko JH, Peck KR, Lee JY, Lee JY, *et al.* 2016. Control of an Outbreak of Middle East Respiratory Syndrome in a Tertiary Hospital in KoreaControl of an Outbreak of MERS in a Tertiary Hospital in Korea. *Ann Intern Med* **165**:87.
461. Weaver SC, Costa F, Garcia-Blanco MA, Ko AI, Ribeiro GS, *et al.* 2016. Zika virus: History, emergence, biology, and prospects for control. *Antiviral Res* **130**:69.
462. Cooper C, Fisher D, Gupta N, MaCauley R, Pessoa-Silva CL. 2016. Infection prevention and control of the Ebola outbreak in Liberia, 2014–2015: key challenges and successes. *BMC Med* **14**:2.
463. Scannell JW, Blanckley A, Boldon H, Warrington B. 2012. Diagnosing the decline in pharmaceutical R&D efficiency. *Nat Rev Drug Discov* **11**:191.
464. Taylor D. 2015. The Pharmaceutical Industry and the Future of Drug Development, p 1-33, Pharmaceuticals in the Environment. The Royal Society of Chemistry.
465. Chaudhuri S, Symons JA, Deval J. 2018. Innovation and trends in the development and approval of antiviral medicines: 1987–2017 and beyond. *Antiviral Res* **155**:76.
466. Prusoff WH, Lin TS, August EM, Wood TG, Marongiu ME. 1989. Approaches to antiviral drug development. *Yale J Biol Med* **62**:215.
467. Bauer DJ. 1985. A history of the discovery and clinical application of antiviral drugs. *Br Med Bull* **41**:309.
468. Elion GB. 1993. Acyclovir: Discovery, mechanism of action, and selectivity. *J Med Virol* **41**:2.
469. King DH. 1988. History, pharmacokinetics, and pharmacology of acyclovir. *J Am Acad Dermatol* **18**:176.
470. De Clercq E. 2008. The discovery of antiviral agents: Ten different compounds, ten different stories. *Med Res Rev* **28**:929.
471. Śledź P, Caflisch A. 2018. Protein structure-based drug design: from docking to molecular dynamics. *Curr Opin Struct Biol* **48**:93.
472. Caillet-Saguy C, Simister PC, Bressanelli S. 2011. An Objective Assessment of Conformational Variability in Complexes of Hepatitis C Virus Polymerase with Non-Nucleoside Inhibitors. *J Mol Biol* **414**:370.
473. Bauer L, Lyoo H, van der Schaar HM, Strating JRPM, van Kuppeveld FJM. 2017. Direct-acting antivirals and host-targeting strategies to combat enterovirus infections. *Curr Opin Virol* **24**:1.

474. Boldescu V, Behnam MAM, Vasilakis N, Klein CD. 2017. Broad-spectrum agents for flaviviral infections: dengue, Zika and beyond. *Nat Rev Drug Discov* **16**:565.
475. Mercorelli B, Palù G, Loregian A. 2018. Drug Repurposing for Viral Infectious Diseases: How Far Are We? *Trends Microbiol* **26**:865.
476. Julander JG, Siddharthan V, Evans J, Taylor R, Tolbert K, *et al.* 2017. Efficacy of the broad-spectrum antiviral compound BCX4430 against Zika virus in cell culture and in a mouse model. *Antiviral Res* **137**:14.
477. Siegel D, Hui HC, Doerffler E, Clarke MO, Chun K, *et al.* 2017. Discovery and Synthesis of a Phosphoramidate Prodrug of a Pyrrolo[2,1-f][triazin-4-amino] Adenine C-Nucleoside (GS-5734) for the Treatment of Ebola and Emerging Viruses. *J Med Chem* **60**:1648.
478. Delang L, Abdelnabi R, Neyts J. 2018. Favipiravir as a potential countermeasure against neglected and emerging RNA viruses. *Antiviral Res* **153**:85.
479. Jia H, Gong P. 2019. A structure-function diversity survey of the RNA-dependent RNA polymerases from the positive-strand RNA viruses. *Front Microbiol* **10**.
480. Kaptein SJF, Vincetti P, Crespan E, Rivera JIA, Costantino G, *et al.* 2018. Identification of Broad-Spectrum Dengue/Zika Virus Replication Inhibitors by Functionalization of Quinoline and 2,6-Diaminopurine Scaffolds. *ChemMedChem* **13**:1371.
481. Linden L, Vives-Adrián L, Selisko B, Ferrer-Orta C, Liu X, *et al.* 2015. The RNA Template Channel of the RNA-Dependent RNA Polymerase as a Target for Development of Antiviral Therapy of Multiple Genera within a Virus Family. *PLoS Pathog* **11**:e1004733.
482. Lani R, Hassandarvish P, Shu M-H, Phoon WH, Chu JH, *et al.* 2016. Antiviral activity of selected flavonoids against Chikungunya virus. *Antiviral Res* **133**:50.
483. Fumian TM, Tuipulotu DE, Netzler NE, Lun JH, Russo AG, *et al.* 2018. Potential Therapeutic Agents for Feline Calicivirus Infection. *Viruses* **10**:433.
484. Berman HM, Westbrook J, Feng Z, Gilliland G, Bhat TN, *et al.* 2000. The Protein Data Bank. *Nucleic Acids Res* **28**:235.
485. Sievers F, Wilm A, Dineen D, Gibson TJ, Karplus K, *et al.* 2011. Fast, scalable generation of high-quality protein multiple sequence alignments using Clustal Omega. *Mol Syst Biol* **7**:539.
486. Mastrangelo E, Pezzullo M, Tarantino D, Petazzi R, Germani F, *et al.* 2012. Structure-based inhibition of Norovirus RNA-dependent RNA polymerases. *J Mol Biol* **419**:198.
487. Croci R, Tarantino D, Milani M, Pezzullo M, Rohayem J, *et al.* 2014. PPNDs inhibits murine Norovirus RNA-dependent RNA-polymerase mimicking two RNA stacking bases. *FEBS Lett* **588**:1720.
488. Ng KK, Cherney MM, Vazquez AL, Machin A, Alonso JM, *et al.* 2002. Crystal structures of active and inactive conformations of a caliciviral RNA-dependent RNA polymerase. *J Biol Chem* **277**:1381.
489. Fullerton SW, Blaschke M, Coutard B, Gebhardt J, Gorbalenya A, *et al.* 2007. Structural and functional characterization of sapovirus RNA-dependent RNA polymerase. *J Virol* **81**:1858.
490. Brooks BR, Brucoleri RE, Olafson BD, States DJ, Swaminathan S, *et al.* 1983. CHARMM: A program for macromolecular energy, minimization, and dynamics calculations. *J Comput Chem* **4**:187.
491. Jones G, Willett P, Glen RC, Leach AR, Taylor R. 1997. Development and validation of a genetic algorithm for flexible docking. Edited by F. E. Cohen. *J Mol Biol* **267**:727.
492. Wolber G, Langer T. 2005. LigandScout: 3-D Pharmacophores Derived from Protein-Bound Ligands and Their Use as Virtual Screening Filters. *J Chem Inf Model* **45**:160.
493. Drwal M. 2013. Design of novel inhibitors of DNA topoisomerases using computer-aided methods. Doctor of Philosophy. University of New South Wales, Sydney, Australia.

494. Kurogi Y, Guner OF. 2001. Pharmacophore modeling and three-dimensional database searching for drug design using catalyst. *Curr Med Chem* **8**:1035.
495. Néron B, Ménager H, Maufrais C, Joly N, Maupetit J, *et al.* 2009. MobyLe: a new full web bioinformatics framework. *Bioinformatics* **25**:3005.
496. Alland C, Moreews F, Boens D, Carpentier M, Chiusa S, *et al.* 2005. RPBS: a web resource for structural bioinformatics. *Nucleic Acids Res* **33**:W44.
497. Lun JH. 2014. A study of norovirus: molecular epidemiology and potential antiviral development. Bachelor of Science (Honours). University of New South Wales, Sydney, Australia.
498. Russo A. 2016. Investigating viruses of Aedes mosquitoes: Diversity, endogenisation, and antiviral development. Bachelor of Advanced Science (Honours). University of New South Wales, Sydney, Australia.
499. Eltahla AA, Lackovic K, Marquis C, Eden JS, White PA. 2013. A fluorescence-based high-throughput screen to identify small compound inhibitors of the genotype 3a hepatitis C virus RNA polymerase. *J Biomol Screen* **18**:1027.
500. Eltahla AA, Lim KL, Eden JS, Kelly AG, Mackenzie JM, *et al.* 2014. Nonnucleoside inhibitors of norovirus RNA polymerase: scaffolds for rational drug design. *Antimicrob Agents Chemother* **58**:3115.
501. Esser-Nobis K, Harak C, Schult P, Kusov Y, Lohmann V. 2015. Novel perspectives for hepatitis A virus therapy revealed by comparative analysis of hepatitis C virus and hepatitis A virus RNA replication. *Hepatology (Baltimore, Md)* **62**:397.
502. Jones DM, Domingues P, Targett-Adams P, McLauchlan J. 2010. Comparison of U2OS and Huh-7 cells for identifying host factors that affect hepatitis C virus RNA replication. *J Gen Virol* **91**:2238.
503. Julander JG, Demarest JF, Taylor R, Gowen BB, Walling DM, *et al.* 2021. An update on the progress of galidesivir (BCX4430), a broad-spectrum antiviral. *Antiviral Res* **195**:105180.
504. Venkataraman S, Prasad BVLS, Selvarajan R. 2018. RNA Dependent RNA Polymerases: Insights from Structure, Function and Evolution. *Viruses* **10**:76.
505. Lee J-H, Alam I, Han KR, Cho S, Shin S, *et al.* 2011. Crystal structures of murine norovirus-1 RNA-dependent RNA polymerase. *J Gen Virol* **92**:1607.
506. Ferrer-Orta C, Arias A, Pérez-Luque R, Escarmís C, Domingo E, *et al.* 2007. Sequential structures provide insights into the fidelity of RNA replication. *Proc Natl Acad Sci U S A* **104**:9463.
507. Bruenn JA. 2003. A structural and primary sequence comparison of the viral RNA-dependent RNA polymerases. *Nucleic Acids Res* **31**:1821.
508. Vendeville S, Lin TI, Hu L, Tahri A, McGowan D, *et al.* 2012. Finger loop inhibitors of the HCV NS5b polymerase. Part II. Optimization of tetracyclic indole-based macrocycle leading to the discovery of TMC647055. *Bioorg Med Chem Lett* **22**:4437.
509. Tropsha A. 2010. Best Practices for QSAR Model Development, Validation, and Exploitation. *Mol Inform* **29**:476.
510. Anderson AC. 2003. The Process of Structure-Based Drug Design. *Chem Biol* **10**:787.
511. Lipinski CA, Lombardo F, Dominy BW, Feeney PJ. 1997. Experimental and computational approaches to estimate solubility and permeability in drug discovery and development settings. *Adv Drug Deliv Rev* **23**:3.
512. Baell JB, Nissink JWM. 2018. Seven Year Itch: Pan-Assay Interference Compounds (PAIS) in 2017-Utility and Limitations. *ACS Chem Biol* **13**:36.
513. Dalton KP, Nicieza I, Abrantes J, Esteves PJ, Parra F. 2014. Spread of new variant RHDV in domestic rabbits on the Iberian Peninsula. *Vet Microbiol* **169**:67.
514. Almeras T, Schreiber P, Fournel S, Martin V, Nicolas CS, *et al.* 2017. Comparative efficacy of the Leucofeligen™ FeLV/RCP and Purevax™ RCP FeLV vaccines against infection with circulating feline Calicivirus. *BMC Vet Res* **13**:300.

515. Monath TP. 2005. Yellow fever vaccine. *Expert Rev Vaccines* **4**:553.
516. Heinz FX, Stiasny K, Holzmann H, Grgic-Vitek M, Kriz B, *et al.* 2013. Vaccination and tick-borne encephalitis, central Europe. *Emerg Infect Dis* **19**:69.
517. World Health Organisation. 2016. Yellow fever situation report. World Health Organisation, Geneva. 28 Oct 2016.
518. Zell R, Delwart E, Gorbalenya AE, Hovi T, King AMQ, *et al.* 2017. ICTV Virus Taxonomy Profile: *Picornaviridae*. *J Gen Virol* **98**:2421.
519. Tapparel C, Siegrist F, Petty TJ, Kaiser L. 2013. Picornavirus and enterovirus diversity with associated human diseases. *Infect Genet Evol* **14**:282.
520. Thorne N, Auld DS, Inglese J. 2010. Apparent activity in high-throughput screening: origins of compound-dependent assay interference. *Curr Opin Chem Biol* **14**:315.
521. Gangwal RP, Damre MV, Das NR, Sharma SS, Sangamwar AT. 2015. Biological evaluation and structural insights for design of subtype-selective peroxisome proliferator activated receptor- α (PPAR- α) agonists. *Bioorg Med Chem Lett* **25**:270.
522. Duval C, Müller M, Kersten S. 2007. PPAR α and dyslipidemia. *Biochim Biophys Acta* **1771**:961.
523. Fuentes E, Guzmán-Jofre L, Moore-Carrasco R, Palomo I. 2013. Role of PPARs in inflammatory processes associated with metabolic syndrome (Review). *Mol Med Rep* **8**:1611.
524. Muhlestein JB, May HT, Jensen JR, Horne BD, Lanman RB, *et al.* 2006. The Reduction of Inflammatory Biomarkers by Statin, Fibrate, and Combination Therapy Among Diabetic Patients With Mixed Dyslipidemia: The DIACOR (Diabetes and Combined Lipid Therapy Regimen) Study. *J Am Coll Cardiol* **48**:396.
525. Kersten S. 2014. Integrated physiology and systems biology of PPAR α . *Molecular Metabolism* **3**:354.
526. Jordan TX, Randall G. 2016. Flavivirus modulation of cellular metabolism. *Curr Opin Virol* **19**:7.
527. Rasheed S, Yan JS, Lau A, Chan AS. 2008. HIV Replication Enhances Production of Free Fatty Acids, Low Density Lipoproteins and Many Key Proteins Involved in Lipid Metabolism: A Proteomics Study. *PLoS One* **3**:e3003.
528. Sumbria D, Berber E, Mathayan M, Rouse BT. 2021. Virus Infections and Host Metabolism—Can We Manage the Interactions? *Front Immunol* **11**.
529. Ketter E, Randall G. 2019. Virus Impact on Lipids and Membranes. *Annu Rev Virol* **6**:319.
530. Sehgal N, Kumawat KL, Basu A, Ravindranath V. 2012. Fenofibrate Reduces Mortality and Precludes Neurological Deficits in Survivors in Murine Model of Japanese Encephalitis Viral Infection. *PLoS One* **7**:e35427.
531. Skolnik PR, Rabbi MF, Mathys J-M, Greenberg AS. 2002. Stimulation of Peroxisome Proliferator-Activated Receptors α and γ Blocks HIV-1 Replication and TNF α Production in Acutely Infected Primary Blood Cells, Chronically Infected U1 Cells, and Alveolar Macrophages From HIV-Infected Subjects. *J Acquir Immune Defic Syndr* **31**:1.
532. You J, Hou S, Malik-Soni N, Xu Z, Kumar A, *et al.* 2015. Flavivirus Infection Impairs Peroxisome Biogenesis and Early Antiviral Signaling. *J Virol* **89**:12349.
533. Hughes JP, Rees S, Kalindjian SB, Philpott KL. 2011. Principles of early drug discovery. *Br J Pharmacol* **162**:1239.
534. Pires SM, Fischer-Walker CL, Lanata CF, Devleesschauwer B, Hall AJ, *et al.* 2015. Aetiology-Specific Estimates of the Global and Regional Incidence and Mortality of Diarrhoeal Diseases Commonly Transmitted through Food. *PLoS One* **10**:e0142927.
535. Lai CC, Wang YH, Wu CY, Hung CH, Jiang DDS, *et al.* 2013. A norovirus outbreak in a nursing home: Norovirus shedding time associated with age. *J Clin Virol* **56**:96.

536. Hasing ME, Lee BE, Qiu Y, Xia M, Pabbaraju K, *et al.* 2019. Changes in norovirus genotype diversity in gastroenteritis outbreaks in Alberta, Canada: 2012–2018. *BMC Infect Dis* **19**:177.
537. Cannon JL, Barclay L, Collins NR, Wikswo ME, Castro CJ, *et al.* 2017. Genetic and Epidemiologic Trends of Norovirus Outbreaks in the United States from 2013 to 2016 Demonstrated Emergence of Novel GII.4 Recombinant Viruses. *J Clin Microbiol* **55**:2208.
538. Martella V, Medici MC, De Grazia S, Tummolo F, Calderaro A, *et al.* 2013. Evidence for Recombination between Pandemic GII.4 Norovirus Strains New Orleans 2009 and Sydney 2012. *J Clin Microbiol* **51**:3855.
539. Ruis C, Roy S, Brown JR, Allen DJ, Goldstein RA, *et al.* 2017. The emerging GII.P16-GII.4 Sydney 2012 norovirus lineage is circulating worldwide, arose by late-2014 and contains polymerase changes that may increase virus transmission. *PLoS One* **12**:e0179572.
540. CaliciNet. 2021. CaliciNet Data Table, *on* Centers for Disease Control and Prevention. <https://www.cdc.gov/norovirus/reporting/calicinet/data.html> Accessed 02/09/2017, 26/06/2018, 11/01/2019, 11/04/2020, 18/05/2020, 18/11/2021.
541. Bidalot M, Théry L, Kaplon J, De Rougemont A, Ambert-Balay K. 2017. Emergence of new recombinant noroviruses GII.P16-GII.4 and GII.P16-GII.2, France, winter 2016 to 2017. *Euro Surveill* **22**:30508.
542. Medici MC, Tummolo F, Martella V, De Conto F, Arcangeletti MC, *et al.* 2018. Emergence of novel recombinant GII. P16_GII. 2 and GII. P16_GII. 4 Sydney 2012 norovirus strains in Italy, winter 2016/2017. *New Microbiol* **41**:71.
543. Barreira DMPG, Fumian TM, Tonini MAL, Volpini LPB, Santos RP, *et al.* 2017. Detection and molecular characterization of the novel recombinant norovirus GII.P16-GII.4 Sydney in southeastern Brazil in 2016. *PLoS One* **12**:e0189504.
544. Degiuseppe JI, Barclay L, Gomes KA, Costantini V, Vinjé J, *et al.* 2020. Molecular epidemiology of norovirus outbreaks in Argentina, 2013-2018. *J Med Virol* **92**:1330.
545. Choi YS, Koo ES, Kim MS, Choi JD, Shin Y, *et al.* 2017. Re-emergence of a GII.4 Norovirus Sydney 2012 Variant Equipped with GII.P16 RdRp and Its Predominance over Novel Variants of GII.17 in South Korea in 2016. *Food Environ Virol* **9**:168.
546. Thanusuwannasak T, Puenpa J, Chuchaona W, Vongpunsawad S, Poovorawan Y. 2018. Emergence of multiple norovirus strains in Thailand, 2015–2017. *Infect Genet Evol* **61**:108.
547. Thongprachum A, Okitsu S, Khamrin P, Maneekarn N, Hayakawa S, *et al.* 2017. Emergence of norovirus GII.2 and its novel recombination during the gastroenteritis outbreak in Japanese children in mid-2016. *Infect Genet Evol* **51**:86.
548. Ao Y, Cong X, Jin M, Sun X, Wei X, *et al.* 2018. Genetic Analysis of Reemerging GII.P16-GII.2 Noroviruses in 2016–2017 in China. *J Infect Dis* **218**:133.
549. Kwok K, Niendorf S, Lee N, Hung T-N, Chan L-Y, *et al.* 2017. Increased Detection of Emergent Recombinant Norovirus GII.P16-GII.2 Strains in Young Adults, Hong Kong, China, 2016-2017. *Emerg Infect Dis* **23**:1852.
550. Lu J, Fang L, Sun L, Zeng H, Li Y, *et al.* 2017. Association of GII.P16-GII.2 Recombinant Norovirus Strain with Increased Norovirus Outbreaks, Guangdong, China, 2016. *Emerg Infect Dis* **23**:1188.
551. Sarmiento SK, de Andrade JdSR, Miagostovich MP, Fumian TM. 2021. Virological and Epidemiological Features of Norovirus Infections in Brazil, 2017–2018. *Viruses* **13**:1724.
552. Niendorf S, Faber M, Tröger A, Hackler J, Jacobsen S. 2020. Diversity of noroviruses throughout outbreaks in Germany 2018. *Viruses* **12**:1157.
553. Prevost B, Lucas FS, Goncalves A, Richard F, Moulin L, *et al.* 2015. Large scale survey of enteric viruses in river and waste water underlines the health status of the local population. *Environ Int* **79**:42.

554. Greay TL, Gofton AW, Zahedi A, Paparini A, Linge KL, *et al.* 2019. Evaluation of 16S next-generation sequencing of hypervariable region 4 in wastewater samples: An unsuitable approach for bacterial enteric pathogen identification. *Sci Total Environ* **670**:1111.
555. Miura T, Lhomme S, Le Saux J-C, Le Mehaute P, Guillois Y, *et al.* 2016. Detection of Hepatitis E Virus in Sewage After an Outbreak on a French Island. *Food Environ Virol* **8**:194.
556. Greening GE, Hewitt J, Rivera-Aban M, Croucher D. 2012. Molecular epidemiology of norovirus gastroenteritis outbreaks in New Zealand from 2002–2009. *J Med Virol* **84**:1449.
557. Kojima S, Kageyama T, Fukushi S, Hoshino FB, Shinohara M, *et al.* 2002. Genogroup-specific PCR primers for detection of Norwalk-like viruses. *J Virol Methods* **100**:107.
558. Richards GP, Watson MA, Fankhauser RL, Monroe SS. 2004. Genogroup I and II noroviruses detected in stool samples by real-time reverse transcription-PCR using highly degenerate universal primers. *Appl Environ Microbiol* **70**:7179.
559. Anderson AD, Heryford AG, Sarisky JP, Higgins C, Monroe SS, *et al.* 2003. A Waterborne Outbreak of Norwalk-Like Virus among Snowmobilers—Wyoming, 2001. *J Infect Dis* **187**:303.
560. Tu E. 2008. Molecular epidemiology and detection of norovirus. Doctor of Philosophy. University of New South Wales, Sydney, Australia.
561. Kimura M. 1980. A simple method for estimating evolutionary rates of base substitutions through comparative studies of nucleotide sequences. *J Mol Evol* **16**:111.
562. Kroneman A, Vennema H, Deforche K, v d Avoort H, Peñaranda S, *et al.* 2011. An automated genotyping tool for enteroviruses and noroviruses. *J Clin Virol* **51**:121.
563. Guévremont E, Brassard J, Houde A, Simard C, Trottier Y-L. 2006. Development of an extraction and concentration procedure and comparison of RT-PCR primer systems for the detection of hepatitis A virus and norovirus GII in green onions. *J Virol Methods* **134**:130.
564. Fu J, Ai J, Jin M, Jiang C, Zhang J, *et al.* 2015. Emergence of a new GII.17 norovirus variant in patients with acute gastroenteritis in Jiangsu, China, September 2014 to March 2015. *Euro Surveill* **20**:21157.
565. Ao Y, Wang J, Ling H, He Y, Dong X, *et al.* 2017. Norovirus GII.P16/GII.2-Associated Gastroenteritis, China, 2016. *Emerg Infect Dis* **23**:1172.
566. Fang Y, Dong Z, Liu Y, Wang W, Hou M, *et al.* 2021. Molecular epidemiology and genetic diversity of norovirus among hospitalized children with acute gastroenteritis in Tianjin, China, 2018–2020. *BMC Infect Dis* **21**:682.
567. Cao R-R, Ma X-Z, Li W-Y, Wang B-N, Yang Y, *et al.* 2021. Epidemiology of norovirus gastroenteritis in hospitalized children under five years old in western China, 2015–2019. *J Microbiol Immunol Infect* **54**:918.
568. Mahar JE, Bok K, Green KY, Kirkwood CD. 2013. The importance of intergenic recombination in norovirus GII.3 evolution. *J Virol* **87**:3687.
569. Saito M, Goel-Apaza S, Espetia S, Velasquez D, Cabrera L, *et al.* 2014. Multiple Norovirus Infections in a Birth Cohort in a Peruvian Periurban Community. *Clin Infect Dis* **58**:483.
570. Sakon N, Yamazaki K, Nakata K, Kanbayashi D, Yoda T, *et al.* 2014. Impact of Genotype-Specific Herd Immunity on the Circulatory Dynamism of Norovirus: A 10-Year Longitudinal Study of Viral Acute Gastroenteritis. *J Infect Dis* **211**:879.
571. Parrino TA, Schreiber DS, Trier JS, Kapikian AZ, Blacklow NR. 1977. Clinical Immunity in Acute Gastroenteritis Caused by Norwalk Agent. *N Engl J Med* **297**:86.
572. Simmons K, Gambhir M, Leon J, Lopman B. 2013. Duration of immunity to norovirus gastroenteritis. *Emerg Infect Dis* **19**:1260.

573. Bucardo F, Reyes Y, Becker-Dreps S, Bowman N, Gruber JF, *et al.* 2017. Pediatric norovirus GII.4 infections in Nicaragua, 1999–2015. *Infect Genet Evol* **55**:305.
574. Kishimoto K, Bun S, Shin J-h, Takada D, Morishita T, *et al.* 2021. Early impact of school closure and social distancing for COVID-19 on the number of inpatients with childhood non-COVID-19 acute infections in Japan. *Eur J Pediatr*.
575. Angoulvant F, Ouldali N, Yang DD, Filser M, Gajdos V, *et al.* 2020. COVID-19 pandemic: Impact caused by school closure and national lockdown on pediatric visits and admissions for viral and non-viral infections, a time series analysis. *Clin Infect Dis*:ciaa710.
576. NoroSTAT. 2021. NoroSTAT Data Table, on Centers for Disease Control and Prevention. <https://www.cdc.gov/norovirus/reporting/norostat/data.html> Accessed 07/05/2021.
577. Eigner U, Verstraeten T, Weil J. 2021. Decrease in norovirus infections in Germany following COVID-19 containment measures. *J Infect* **82**:276.
578. Bruggink LD, Garcia-Clapes A, Tran T, Druce JD, Thorley BR. 2021. Decreased incidence of enterovirus and norovirus infections during the COVID-19 pandemic, Victoria, Australia, 2020. *Commun Dis Intell* **45**.
579. Ahmed SM, Lopman BA, Levy K. 2013. A Systematic Review and Meta-Analysis of the Global Seasonality of Norovirus. *PLoS One* **8**:e75922.
580. Liu LT, Kuo TY, Wu CY, Liao WT, Hall AJ, *et al.* 2017. Recombinant GII.P16-GII.2 Norovirus, Taiwan, 2016. *Emerg Infect Dis* **23**:1180.
581. Cannon JL, Bonifacio J, Bucardo F, Buesa J, Bruggink L, *et al.* 2021. Global Trends in Norovirus Genotype Distribution among Children with Acute Gastroenteritis. *Emerg Infect Dis* **27**:1438.
582. Friesema IHM, de Boer RF, Duizer E, Kortbeek LM, Notermans DW, *et al.* 2012. Etiology of acute gastroenteritis in children requiring hospitalization in the Netherlands. *Eur J Clin Microbiol Infect Dis* **31**:405.
583. Nicholson MR, Van Horn GT, Tang YW, Vinjé J, Payne DC, *et al.* 2016. Using multiplex molecular testing to determine the etiology of acute gastroenteritis in children. *J Pediatr* **176**:50.
584. Khare R, Espy MJ, Cebelinski E, Boxrud D, Sloan LM, *et al.* 2014. Comparative Evaluation of Two Commercial Multiplex Panels for Detection of Gastrointestinal Pathogens by Use of Clinical Stool Specimens. *J Clin Microbiol* **52**:3667.
585. Binnicker MJ, Kraft CS. 2015. Multiplex Molecular Panels for Diagnosis of Gastrointestinal Infection: Performance, Result Interpretation, and Cost-Effectiveness. *J Clin Microbiol* **53**:3723.
586. Sciandra I, Piccioni L, Coltella L, Ranno S, Giannelli G, *et al.* 2020. Comparative analysis of 2 commercial molecular tests for the detection of gastroenteric viruses on stool samples. *Diagn Microbiol Infect Dis* **96**:114893.
587. Francesco MAD, Lorenzin G, Meini A, Schumacher RF, Caruso A, *et al.* 2021. Nonenteric Adenoviruses Associated with Gastroenteritis in Hospitalized Children. *Microbiol Spectr* **9**:e00300.
588. Qiu FZ, Shen XX, Li GX, Zhao L, Chen C, *et al.* 2018. Adenovirus associated with acute diarrhea: a case-control study. *BMC Infect Dis* **18**:450.
589. Gelaw A, Pietsch C, Liebert UG. 2019. Genetic diversity of human adenovirus and human astrovirus in children with acute gastroenteritis in Northwest Ethiopia. *Arch Virol* **164**:2985.
590. Liu L, Qian Y, Zhang Y, Deng J, Jia L, *et al.* 2014. Adenoviruses Associated with Acute Diarrhea in Children in Beijing, China. *PLoS One* **9**:e88791.
591. Lun JH, Crosbie ND, White PA. 2019. Genetic diversity and quantification of human mastadenoviruses in wastewater from Sydney and Melbourne, Australia. *Sci Total Environ* **675**:305.

592. Primo D, Pacheco GT, Timenetsky MdCST, Luchs A. 2018. Surveillance and molecular characterization of human adenovirus in patients with acute gastroenteritis in the era of rotavirus vaccine, Brazil, 2012–2017. *J Clin Virol* **109**:35.
593. Li L, Phan TG, Nguyen TA, Kim KS, Seo JK, *et al.* 2005. Molecular epidemiology of adenovirus infection among pediatric population with diarrhea in Asia. *Microbiol Immunol* **49**:121.
594. Chhabra P, Samoilovich E, Yermalovich M, Chernyshova L, Gheorghita S, *et al.* 2014. Viral gastroenteritis in rotavirus negative hospitalized children <5 years of age from the independent states of the former Soviet Union. *Infect Genet Evol* **28**:283.
595. Grimwood K, Carzino R, Barnes GL, Bishop RF. 1995. Patients with enteric adenovirus gastroenteritis admitted to an Australian pediatric teaching hospital from 1981 to 1992. *J Clin Microbiol* **33**:131.
596. Mücke MM, Zeuzem S. 2022. The recent outbreak of acute severe hepatitis in children of unknown origin – what is known so far. *J Hepatol*.
597. Cevik M, Rasmussen AL, Bogoch II, Kindrachuk J. 2022. Acute hepatitis of unknown origin in children. *BMJ* **377**:o1197.
598. World Health Organisation. 2022. Acute hepatitis of unknown aetiology in children - Multi-country. 27 May 2022.
599. European Centre for Disease Prevention and Control. 2022. Increase in severe acute hepatitis cases of unknown aetiology in children. 28 Apr 2022.
600. Liu L, Qian Y, Zhang Y, Zhao L, Jia L, *et al.* 2016. Epidemiological aspects of rotavirus and adenovirus in hospitalized children with diarrhea: a 5-year survey in Beijing. *BMC Infect Dis* **16**:508.
601. Tamerius J, Nelson MI, Zhou SZ, Viboud C, Miller MA, *et al.* 2011. Global influenza seasonality: reconciling patterns across temperate and tropical regions. *Environ Health Perspect* **119**:439.
602. Iturriza-Gómara M, Jere KC, Hungerford D, Bar-Zeev N, Shioda K, *et al.* 2019. Etiology of Diarrhea Among Hospitalized Children in Blantyre, Malawi, Following Rotavirus Vaccine Introduction: A Case-Control Study. *J Infect Dis* **220**:213.
603. Kotloff KL, Nataro JP, Blackwelder WC, Nasrin D, Farag TH, *et al.* 2013. Burden and aetiology of diarrhoeal disease in infants and young children in developing countries (the Global Enteric Multicenter Study, GEMS): a prospective, case-control study. *Lancet* **382**:209.
604. van Dongen JAP, Rouers EDM, Schuurman R, Bonten MJM, Bruijning-Verhagen P, *et al.* 2021. Acute Gastroenteritis Disease Burden in Infants With Medical Risk Conditions in the Netherlands. *Pediatr Infect Dis J* **40**:300.
605. Quee FA, de Hoog MLA, Schuurman R, Bruijning-Verhagen P. 2020. Community burden and transmission of acute gastroenteritis caused by norovirus and rotavirus in the Netherlands (RotaFam): a prospective household-based cohort study. *Lancet Infect Dis* **20**:598.
606. de Jong JC, Kapsenberg JG, Muzerie CJ, Wermenbol AG, Kidd AH, *et al.* 1983. Candidate adenoviruses 40 and 41: Fastidious adenoviruses from human infant stool. *J Med Virol* **11**:215.
607. Jarecki-Khan K, Tzipori SR, Unicomb LE. 1993. Enteric adenovirus infection among infants with diarrhea in rural Bangladesh. *J Clin Microbiol* **31**:484.
608. de Jong JC, Bijlsma K, Wermenbol AG, Verweij-Uijterwaal MW, van der Avoort HG, *et al.* 1993. Detection, typing, and subtyping of enteric adenoviruses 40 and 41 from fecal samples and observation of changing incidences of infections with these types and subtypes. *J Clin Microbiol* **31**:1562.
609. Brown M. 1990. Laboratory identification of adenoviruses associated with gastroenteritis in Canada from 1983 to 1986. *J Clin Microbiol* **28**:1525.

610. Willcocks MM, Carter MJ, Laidler FR, Madeley CR. 1988. Restriction enzyme analysis of faecal adenoviruses in Newcastle upon Tyne. *Epidemiol Infect* **101**:445.
611. Scott-Taylor TH, Hammond GW. 1995. Local succession of adenovirus strains in pediatric gastroenteritis. *J Med Virol* **45**:331.
612. Shinozaki T, Araki K, Fujita Y, Kobayashi M, Tajima T, *et al.* 1991. Epidemiology of enteric adenoviruses 40 and 41 in acute gastroenteritis in infants and young children in the Tokyo area. *Scand J Infect Dis* **23**:543.
613. Iaconelli M, Valdazo-González B, Equestre M, Ciccaglione AR, Marcantonio C, *et al.* 2017. Molecular characterization of human adenoviruses in urban wastewaters using next generation and Sanger sequencing. *Water Research* **121**:240.
614. Fernandez-Cassi X, Timoneda N, Martínez-Puchol S, Rusiñol M, Rodríguez-Manzano J, *et al.* 2018. Metagenomics for the study of viruses in urban sewage as a tool for public health surveillance. *Sci Total Environ* **618**:870.
615. Martínez-Puchol S, Rusiñol M, Fernández-Cassi X, Timoneda N, Itarte M, *et al.* 2020. Characterisation of the sewage virome: comparison of NGS tools and occurrence of significant pathogens. *Sci Total Environ* **713**:136604.
616. Kaas L, Ogorzaly L, Lecellier G, Berteaux-Lecellier V, Cauchie H-M, *et al.* 2019. Detection of Human Enteric Viruses in French Polynesian Wastewaters, Environmental Waters and Giant Clams. *Food Environ Virol* **11**:52.
617. Chitambar S, Gopalkrishna V, Chhabra P, Patil P, Verma H, *et al.* 2012. Diversity in the Enteric Viruses Detected in Outbreaks of Gastroenteritis from Mumbai, Western India. *Int J Environ Res Public Health* **9**:895.
618. Matsushima Y, Shimizu H, Phan TG, Ushijima H. 2011. Genomic characterization of a novel human adenovirus type 31 recombinant in the hexon gene. *J Gen Virol* **92**:2770.
619. Pabbaraju K, Tellier R, Pang XL, Xie J, Lee BE, *et al.* 2020. A Clinical Epidemiology and Molecular Attribution Evaluation of Adenoviruses in Pediatric Acute Gastroenteritis: a Case-Control Study. *J Clin Microbiol* **59**:e02287.
620. Akihara S, Phan TG, Nguyen TA, Hansman G, Okitsu S, *et al.* 2005. Existence of multiple outbreaks of viral gastroenteritis among infants in a day care center in Japan. *Arch Virol* **150**:2061.
621. La Rosa G, Della Libera S, Petricca S, Iaconelli M, Donia D, *et al.* 2015. Genetic Diversity of Human Adenovirus in Children with Acute Gastroenteritis, Albania, 2013–2015. *Biomed Res Int* **2015**:142912.
622. Fox JP, Hall CE, Cooney MK. 1977. The Seattle Virus Watch. VII. Observations of adenovirus infections. *Am J Epidemiol* **105**:362.
623. Roy S, Calcedo R, Medina-Jaszek A, Keough M, Peng H, *et al.* 2011. Adenoviruses in Lymphocytes of the Human Gastro-Intestinal Tract. *PLoS One* **6**:e24859.
624. Rovida F, Campanini G, Sarasini A, Adzasehoun KMG, Piralla A, *et al.* 2013. Comparison of immunologic and molecular assays for the diagnosis of gastrointestinal viral infections. *Diagn Microbiol Infect Dis* **75**:110.
625. Gray JJ, Kohli E, Ruggeri FM, Vennema H, Sánchez-Fauquier A, *et al.* 2007. European Multicenter Evaluation of Commercial Enzyme Immunoassays for Detecting Norovirus Antigen in Fecal Samples. *Clin Vaccine Immunol* **14**:1349.
626. van Maarseveen NM, Wessels E, de Brouwer CS, Vossen ACTM, Claas ECJ. 2010. Diagnosis of viral gastroenteritis by simultaneous detection of Adenovirus group F, Astrovirus, Rotavirus group A, Norovirus genogroups I and II, and Sapovirus in two internally controlled multiplex real-time PCR assays. *J Clin Virol* **49**:205.
627. Mijatovic-Rustempasic S, Esona MD, Williams AL, Bowen MD. 2016. Sensitive and specific nested PCR assay for detection of rotavirus A in samples with a low viral load. *J Virol Methods* **236**:41.
628. Echavarría M. 2008. Adenoviruses in immunocompromised hosts. *Clin Microbiol Rev* **21**:704.

629. Chakrabarti S, Collingham KE, Fegan CD, Milligan DW. 1999. Fulminant adenovirus hepatitis following unrelated bone marrow transplantation: failure of intravenous ribavirin therapy. *Bone Marrow Transplant* **23**:1209.
630. Johnson PR, Yin JA, Morris DJ, Desai M, Cinkotai KI, *et al.* 1990. Fulminant hepatic necrosis caused by adenovirus type 5 following bone marrow transplantation. *Bone Marrow Transplant* **5**:345.
631. Munoz RE, Piedra PA, Demmler GJ. 1998. Disseminated adenovirus disease in immunocompromised and immunocompetent children. *Clin Infect Dis* **27**:1194.
632. Marie R, Stéphanie M-J, Catherine S, Régis Peffault de L, Christèle F, *et al.* 2007. Disseminated adenovirus infections after allogeneic hematopoietic stem cell transplantation: incidence, risk factors and outcome. *Haematologica* **92**:1254.
633. Mynarek M, Ganzenmueller T, Mueller-Heine A, Mielke C, Gonnermann A, *et al.* 2014. Patient, Virus, and Treatment-Related Risk Factors in Pediatric Adenovirus Infection after Stem Cell Transplantation: Results of a Routine Monitoring Program. *Biol Blood Marrow Transplant* **20**:250.
634. Bordigoni P, Carret AS, Venard V, Witz F, Le Faou A. 2001. Treatment of Adenovirus Infections in Patients Undergoing Allogeneic Hematopoietic Stem Cell Transplantation. *Clin Infect Dis* **32**:1290.
635. Lion T, Baumgartinger R, Watzinger F, Matthes-Martin S, Suda M, *et al.* 2003. Molecular monitoring of adenovirus in peripheral blood after allogeneic bone marrow transplantation permits early diagnosis of disseminated disease. *Blood* **102**:1114.
636. Rocholl C, Gerber K, Daly J, Pavia AT, Byington CL. 2004. Adenoviral Infections in Children: The Impact of Rapid Diagnosis. *Pediatrics* **113**:e51.
637. Ozbay Hoşnut F, Canan O, Ozçay F, Bilezikçi B. 2008. Adenovirus infection as possible cause of acute liver failure in a healthy child: a case report. *Turk J Gastroenterol* **19**:281.
638. Matoq A, Salahuddin A. 2016. Acute hepatitis and pancytopenia in healthy infant with adenovirus. *Case Rep Pediatr* **2016**:8648190.
639. European Centre for Disease Prevention and Control. 2022. Guidance for diagnostic testing of cases with severe acute hepatitis of unknown aetiology in children. 25 May 2022.
640. Akello JO, Kamgang R, Barbani MT, Suter-Riniker F, Aebi C, *et al.* 2021. Genomic analyses of human adenoviruses unravel novel recombinant genotypes associated with severe infections in pediatric patients. *Sci Rep* **11**:24038.
641. Madisch I, Hofmayer S, Moritz C, Grintzalis A, Hainmueller J, *et al.* 2007. Phylogenetic analysis and structural predictions of human adenovirus penton proteins as a basis for tissue-specific adenovirus vector design. *J Virol* **81**:8270.
642. Medema G, Heijnen L, Elsinga G, Italiaander R, Brouwer A. 2020. Presence of SARS-Coronavirus-2 RNA in Sewage and Correlation with Reported COVID-19 Prevalence in the Early Stage of the Epidemic in The Netherlands. *Environ Sci Technol Lett*:acs.estlett.0c00357.
643. Randazzo W, Truchado P, Cuevas-Ferrando E, Simón P, Allende A, *et al.* 2020. SARS-CoV-2 RNA in wastewater anticipated COVID-19 occurrence in a low prevalence area. *Water Research* **181**:115942.
644. World Health Organisation. 2021. Hepatitis A fact sheet. 2 Jun 2022.
645. Shearer FM, Moyes CL, Pigott DM, Brady OJ, Marinho F, *et al.* 2017. Global yellow fever vaccination coverage from 1970 to 2016: an adjusted retrospective analysis. *Lancet Infect Dis* **17**:1209.
646. Nwachukwu WE, Yusuff H, Nwangwu U, Okon A, Ogunniyi A, *et al.* 2020. The response to re-emergence of yellow fever in Nigeria, 2017. *Int J Infect Dis* **92**:189.
647. Martinez JP, Sasse F, Brönstrup M, Diez J, Meyerhans A. 2015. Antiviral drug discovery: broad-spectrum drugs from nature. *Nat Prod Rep* **32**:29.

648. Dreiman GHS, Bictash M, Fish PV, Griffin L, Svensson F. 2021. Changing the HTS Paradigm: AI-Driven Iterative Screening for Hit Finding. *SLAS Discov* **26**:257.
649. Shun TY, Lazo JS, Sharlow ER, Johnston PA. 2011. Identifying Actives from HTS Data Sets: Practical Approaches for the Selection of an Appropriate HTS Data-Processing Method and Quality Control Review. *J Biomol Screen* **16**:1.
650. Dahlin JL, Walters MA. 2016. How to Triage PAINS-Full Research. *Assay drug dev technol* **14**:168.
651. Dahlin JL, Nissink JWM, Strasser JM, Francis S, Higgins L, *et al.* 2015. PAINS in the assay: chemical mechanisms of assay interference and promiscuous enzymatic inhibition observed during a sulfhydryl-scavenging HTS. *J Med Chem* **58**:2091.
652. Godoy AS, Lima GMA, Oliveira KIZ, Torres NU, Maluf FV, *et al.* 2017. Crystal structure of Zika virus NS5 RNA-dependent RNA polymerase. *Nat Commun* **8**:14764.
653. Klema VJ, Ye M, Hindupur A, Teramoto T, Gottipati K, *et al.* 2016. Dengue virus nonstructural protein 5 (NS5) assembles into a dimer with a unique methyltransferase and polymerase interface. *PLoS Pathog* **12**:e1005451.
654. Choi KH, Groarke JM, Young DC, Kuhn RJ, Smith JL, *et al.* 2004. The structure of the RNA-dependent RNA polymerase from bovine viral diarrhea virus establishes the role of GTP in *de novo* initiation. *Proc Natl Acad Sci U S A* **101**:4425.
655. Dubankova A, Boura E. 2019. Structure of the yellow fever NS5 protein reveals conserved drug targets shared among flaviviruses. *Antiviral Res* **169**:104536.
656. Ferrer-Orta C, Sierra M, Agudo R, Higuera IdI, Arias A, *et al.* 2010. Structure of Foot-and-Mouth Disease Virus Mutant Polymerases with Reduced Sensitivity to Ribavirin. *J Virol* **84**:6188.
657. Chen C, Wang Y, Shan C, Sun Y, Xu P, *et al.* 2013. Crystal Structure of Enterovirus 71 RNA-Dependent RNA Polymerase Complexed with Its Protein Primer VPg: Implication for a trans Mechanism of VPg Uridylation. *J Virol* **87**:5755.
658. Love RA, Maegley KA, Yu X, Ferre RA, Lingardo LK, *et al.* 2004. The crystal structure of the RNA-dependent RNA polymerase from human rhinovirus: A dual function target for common cold antiviral therapy. *Structure* **12**:1533.
659. Thompson AA, Albertini RA, Peersen OB. 2007. Stabilization of Poliovirus Polymerase by NTP Binding and Fingers–Thumb Interactions. *J Mol Biol* **366**:1459.
660. Jumper J, Evans R, Pritzel A, Green T, Figurnov M, *et al.* 2021. Highly accurate protein structure prediction with AlphaFold. *Nature* **596**:583.
661. Debbink K, Lindesmith LC, Donaldson EF, Costantini V, Beltramello M, *et al.* 2013. Emergence of New Pandemic GII.4 Sydney Norovirus Strain Correlates With Escape From Herd Immunity. *J Infect Dis* **208**:1877.
662. Kent SJ, Fernandez CS, Jane Dale C, Davenport MP. 2005. Reversion of immune escape HIV variants upon transmission: insights into effective viral immunity. *Trends Microbiol* **13**:243.
663. Bailey Justin R, Laskey S, Wasilewski Lisa N, Munshaw S, Fanning Liam J, *et al.* 2012. Constraints on Viral Evolution during Chronic Hepatitis C Virus Infection Arising from a Common-Source Exposure. *J Virol* **86**:12582.
664. Botosso VF, Zanotto PMdA, Ueda M, Arruda E, Gilio AE, *et al.* 2009. Positive Selection Results in Frequent Reversible Amino Acid Replacements in the G Protein Gene of Human Respiratory Syncytial Virus. *PLoS Pathog* **5**:e1000254.
665. Fryer HR, Frater J, Duda A, Roberts MG, The STI, *et al.* 2010. Modelling the Evolution and Spread of HIV Immune Escape Mutants. *PLoS Pathog* **6**:e1001196.
666. Wagner A. 2014. A genotype network reveals homoplastic cycles of convergent evolution in influenza A (H3N2) haemagglutinin. *Proc Biol Sci* **281**:20132763.
667. Lemon SM, Binn LN, Marchwicki R, Murphy PC, Ping L-H, *et al.* 1990. *In vivo* replication and reversion to wild type of a neutralization-resistant antigenic variant of hepatitis A virus. *J Infect Dis* **161**:7.

668. Leslie A, Pfafferott K, Chetty P, Draenert R, Addo M, *et al.* 2004. HIV evolution: CTL escape mutation and reversion after transmission. *Nat Med* **10**:282.
669. Bull RA, Eden JS, Rawlinson WD, White PA. 2010. Rapid Evolution of Pandemic Noroviruses of the GII.4 Lineage. *PLoS Pathog* **6**:e1000831.
670. Arias A, Thorne L, Ghurburrun E, Bailey D, Goodfellow I, *et al.* 2016. Norovirus Polymerase Fidelity Contributes to Viral Transmission *In Vivo*. *mSphere* **1**:e00279.
671. Chan MCW, Lee N, Hung T-N, Kwok K, Cheung K, *et al.* 2015. Rapid emergence and predominance of a broadly recognizing and fast-evolving norovirus GII.17 variant in late 2014. *Nat Commun* **6**:10061.
672. Zhu X, He Y, Wei X, Kong X, Zhang Q, *et al.* 2021. Molecular Epidemiological Characteristics of Gastroenteritis Outbreaks Caused by Norovirus GII.4 Sydney [P31] Strains - China, October 2016-December 2020. *China CDC Wkly* **3**:1127.
673. He Y, Jin M, Chen K, Zhang H, Yang H, *et al.* 2016. Gastroenteritis Outbreaks Associated with the Emergence of the New GII.4 Sydney Norovirus Variant during the Epidemic of 2012/13 in Shenzhen City, China. *PLoS One* **11**:e0165880.
674. Han J, Ji L, Shen Y, Wu X, Xu D, *et al.* 2015. Emergence and predominance of norovirus GII.17 in Huzhou, China, 2014–2015. *Virology* **12**:139.
675. Fu J, Ai J, Bao C, Zhang J, Wu Q, *et al.* 2021. Evolution of the GII.3[P12] Norovirus from 2010 to 2019 in Jiangsu, China. *Gut Pathog* **13**:34.
676. Boonchan M, Guntapong R, Sripirom N, Ruchusatsawat K, Singchai P, *et al.* 2018. The dynamics of norovirus genotypes and genetic analysis of a novel recombinant GII.P12-GII.3 among infants and children in Bangkok, Thailand between 2014 and 2016. *Infect Genet Evol* **60**:133.
677. Huang P, Farkas T, Marionneau S, Zhong W, Ruvoën-Clouet N, *et al.* 2003. Noroviruses Bind to Human ABO, Lewis, and Secretor Histo-Blood Group Antigens: Identification of 4 Distinct Strain-Specific Patterns. *J Infect Dis* **188**:19.
678. Parra GI, Squires RB, Karangwa CK, Johnson JA, Lepore CJ, *et al.* 2017. Static and Evolving Norovirus Genotypes: Implications for Epidemiology and Immunity. *PLoS Pathog* **13**:e1006136.
679. Benschop KS, Albert J, Anton A, Andrés C, Aranzamendi M, *et al.* 2021. Re-emergence of enterovirus D68 in Europe after easing the COVID-19 lockdown, September 2021. *Euro Surveill* **26**:2100998.
680. van Summeren J, Meijer A, Aspelund G, Casalegno JS, Erna G, *et al.* 2021. Low levels of respiratory syncytial virus activity in Europe during the 2020/21 season: what can we expect in the coming summer and autumn/winter? *Euro Surveill* **26**:2100639.
681. Eden JS, Sikazwe C, Xie R, Deng YM, Sullivan SG, *et al.* 2022. Off-season RSV epidemics in Australia after easing of COVID-19 restrictions. *Nat Commun* **13**:2884.
682. Larrauri A, Prosenc Trilar K. 2021. Preparing for an influenza season 2021/22 with a likely co-circulation of influenza virus and SARS-CoV-2. *Euro Surveill* **26**:2100975.
683. Burki TK. 2021. Circulation of influenza, RSV, and SARS-CoV-2: an uncertain season ahead. *Lancet Respir Med* **9**:e103.
684. Bolinger B, Sims S, Swadling L, O'Hara G, de Lara C, *et al.* 2015. Adenoviral Vector Vaccination Induces a Conserved Program of CD8+ T Cell Memory Differentiation in Mouse and Man. *Cell Rep* **13**:1578.
685. Lasaro MO, Ertl HCJ. 2009. New insights on adenovirus as vaccine vectors. *Mol Ther* **17**:1333.
686. Majhen D, Calderon H, Chandra N, Fajardo CA, Rajan A, *et al.* 2014. Adenovirus-Based Vaccines for Fighting Infectious Diseases and Cancer: Progress in the Field. *Hum Gene Ther* **25**:301.
687. Chang J. 2021. Adenovirus Vectors: Excellent Tools for Vaccine Development. *Immune Netw* **21**:e6.

688. Fitzgerald JC, Gao G-P, Reyes-Sandoval A, Pavlakis GN, Xiang ZQ, *et al.* 2003. A Simian Replication-Defective Adenoviral Recombinant Vaccine to HIV-1 Gag. *J Immunol* **170**:1416.
689. Chirmule N, Propert KJ, Magosin SA, Qian Y, Qian R, *et al.* 1999. Immune responses to adenovirus and adeno-associated virus in humans. *Gene Ther* **6**:1574.
690. Buchbinder SP, Mehrotra DV, Duerr A, Fitzgerald DW, Mogg R, *et al.* 2008. Efficacy assessment of a cell-mediated immunity HIV-1 vaccine (the Step Study): a double-blind, randomised, placebo-controlled, test-of-concept trial. *Lancet* **372**:1881.
691. Zhu FC, Li YH, Guan XH, Hou LH, Wang WJ, *et al.* 2020. Safety, tolerability, and immunogenicity of a recombinant adenovirus type-5 vectored COVID-19 vaccine: a dose-escalation, open-label, non-randomised, first-in-human trial. *Lancet* **395**:1845.
692. Zhu FC, Guan XH, Li YH, Huang JY, Jiang T, *et al.* 2020. Immunogenicity and safety of a recombinant adenovirus type-5-vectored COVID-19 vaccine in healthy adults aged 18 years or older: a randomised, double-blind, placebo-controlled, phase 2 trial. *Lancet* **396**:479.
693. Li JX, Hou LH, Meng FY, Wu SP, Hu YM, *et al.* 2017. Immunity duration of a recombinant adenovirus type-5 vector-based Ebola vaccine and a homologous prime-boost immunisation in healthy adults in China: final report of a randomised, double-blind, placebo-controlled, phase 1 trial. *Lancet Glob Health* **5**:e324.
694. Xiang Z, Li Y, Cun A, Yang W, Ellenberg S, *et al.* 2006. Chimpanzee adenovirus antibodies in humans, sub-Saharan Africa. *Emerg Infect Dis* **12**:1596.
695. Metzgar D, Osuna M, Yingst S, Rakha M, Earhart K, *et al.* 2005. PCR Analysis of Egyptian Respiratory Adenovirus Isolates, Including Identification of Species, Serotypes, and Coinfections. *J Clin Microbiol* **43**:5743.